ROBUSTNESS PROPERTIES OF NONLINEAR PROCESS CONTROL AND IMPLICATIONS FOR THE DESIGN AND CONTROL OF A PACKED BED REACTOR

Dissertation by

Francis J. Doyle III

In Partial Fulfillment of the Requirements

for the Degree of

Doctor of Philosophy

California Institute of Technology

Division of Chemistry & Chemical Engineering

Pasadena, California

1991

(Defended 22 May 1991)

To my parents for all their love and suppport.

"Nothing in the world can take the place of persistence.
Talent will not; nothing is more common than unsuccessful men with talent.
Genius will not; unrewarded genius is almost a proverb.
Education will not; the world is full of educated derelicts.
Persistence and determination alone are omnipotent."

Calvin Coolidge

Acknowledgements

There are a number of individuals who have, in one way or another, contributed to this endeavor and to them I would like to express my sincere gratitude.

My Ph.D. advisor, Manfred Morari, allowed me considerable freedom in conducting this research, and the opportunity to attend a number of conferences and workshops during the course of this work. For this I am very grateful. His demanding standards and sense of perfection have clearly had a very positive effect on this thesis. I would also like to acknowledge his financial support through partial funding from the Department of Energy, National Science Foundation, Shell Development Company, and E.I DuPont deNemours & Co.

I wish to also express my appreciation to my co-advisor, John Doyle, for his role in this project. John is a constant source of brilliant ideas, if only I were able to write them down as quickly as he fired them off in our meetings. I also wish to express my gratitude to John for his appreciation of my extracurricular activities.

I want to thank George Gavalas, who always made me work for my signatures on the progress reports; and my other committee members, Athanasios Sideris and Joel Burdick, for their role on my thesis committee.

My B.S.E. advisor, Roy Jackson, and my C.P.G.S. advisor, Alan Hayhurst, both have had a tremendous influence on my eventual career path. I can only hope to be half the role model to my students as they were to me.

There are two individuals who were involved in the research program at Caltech at various times during this thesis, and whose impact on the resultant work is tremendous. They are Andy Packard for his help with μ theory; and Hector Budman for his help with the packed bed reactor project. I greatly value the technical collaboration with these guys and the friendship which grew from that.

Special thanks to the "Texan trio" with whom I shared office space over the years; Pete, Tyler, and Doug. I will certainly miss our "chalkboard problem du jour" (not to mention the huge Lone Star Republic flag!). I was very lucky to have gotten to know many of the Morari students over the years (Evanghelos Zafiriou, Sigurd Skogestad, Richard Colberg, Chris Webb, Tony Skjellum, Lionel Laroche, Jay Lee, Marc Gelormino, Richard Braatz, Nik Bekiaris, to name a few), and I look forward to continued interactions with them.

My extracurricular thanks go first, of course, to the co-founding fathers of 217 St. Francis St.; Eric, Matt, and Chuck. Ever present at poolside and parties in San Gabriel were John and Tammy, and their friendship is greatly treasured. Thanks also to the second generation Franciscans, Rob and Tyler, for carrying the torch. Thanks to Jerry, dude, for showing me the world of Joshua Tree, rock climbing, and truly abominable puns. Though there are few of them left in the country, I want to thank all of the nanny crowd for some great memories (especially Toga Party, 1988). My thanks go out to my very close friends from Churchill, Jim and Stephen, whose friendship has been unwavering over the time and distance which separates us.

I was fortunate to have played softball for several years with the Divergent Graduates (including two championship seasons!) and I want to thank my many teammates for the fond memories: Val, Todd, Dane, Jorge, Brent, Jacky, Chaitan, Tony, Tony, Pete, Julie, Dave, Sarah, John, Tammy, Andy, Jerry, Eric, Bob, Marsha, Pete, Linda, Lou, Marianne, Matt, Susan, Roger, Doug, Clair, Diana.

I am grateful for the sailing opportunities provided by my skippers at the Newport Harbor Yacht Club, David Team and Nina Neilsen. Though my sailing activities were not appreciated by all, I know that the occasional regatta helped preserve my sanity. In defense, I call on Roy Jackson's recollection of the following quote from G.I. Taylor: "When my brain gets tired, I go sailing."

Speaking of Newport Beach, I want to thank the girls on 41st Street; Kelli, Tracy, and Diana. Diana, I know that you only came along in the middle of this degree, but I feel as if your presence has had a lifetime of impact. Thank you for your patience and support through these last few difficult months. I truly look forward to finding out what a lifetime of your company is like.

Last, and far from least, I want to thank my parents and the rest of the Doyle clan. Your love and support over the years helped pull me through the troughs and valleys in my work. I am really looking forward to my upcoming year in Delaware and the chance to grow closer with all of you.

ROBUSTNESS PROPERTIES OF NONLINEAR PROCESS CONTROL AND IMPLICATIONS FOR THE DESIGN AND CONTROL OF A PACKED BED REACTOR

Francis J. Doyle III

Abstract

The robustness properties of nonlinear process control are studied with particular emphasis on applications to the design and control of a catalytic fixed bed reactor.

Analysis tools are developed to determine the stability and performance of nonlinear dynamical systems. The results are based upon new extensions of the structured singular value to a class of nonlinear and time-varying systems. Conic sectors are utilized in approximating the static nonlinearities present and an algorithm is developed for optimal conic sector calculation.

The synthesis tools of differential geometry are studied with respect to their closed loop robust performance properties. New results in approximate linearization are contrasted with exact linearization and linear control. It is shown that the approximate linearization technique is superior with respect to disturbance handling, optimization of the resultant transformations, and range of applicability.

Nonlinear approaches for the control of a packed bed reactor are investigated. In particular, the differential geometric technique of input-output linearization is found to yield superior closed-loop performance over regions of open-loop parametric sensitivity. The synthesis of a linearizing controller for this nonlinear distributed parameter system involves a two-tier approach. In the first stage, a low order nonlinear model is developed for the reactor. This is accomplished by treating the active transport

mechanisms in the bed as a nonlinear wave which propagates through the bed in response to changes in the operating conditions. The resultant lumped parameter model facilitates the design of the input-output linearizing controller in the second tier of this scheme. The implementational hurdles for this approach are identified and comparisons are drawn on the strengths of this approach over robust linear control for the reactor.

Practical guidelines are developed for the design of packed bed reactors. The criteria result from requirements on the radial temperature profile, temperature sensitivity, and acceptable pressure drop. The stabilizing effects of feedback control for industrial fixed bed catalytic reactors are addressed. Simulations support the result that violation of the proposed criteria leads to unacceptable closed-loop performance.

In conclusion, general guidelines are constructed from a series of case studies on the proper selection of linear versus "linearizing" control. The relative performance is measured by the region of attraction, magnitude of manipulated variable action, and sensitivity to input disturbances. The work represents the first objective evaluation of the strengths and limitations of input-output linearization compared to linear control.

Nomenclature

A	Area $[L]$
Bi	Biot Number $\frac{h_w D}{2k_e}$
C	Cone Center
C_p	Specific Heat $[\frac{L^2}{t^2 T}]$
c	Concentration
D	Tube Diameter $[L]$
E	Activation Energy $[\frac{ML^2}{t^2}]$
F	Flow Rate $[\frac{M}{t}]$
G	Superficial Mass Flow Velocity $[\frac{M}{L^2 t}]$
H	Specific Enthalpy $[\frac{L^2}{t^2}]$
h	Heat Transfer Coefficient $[\frac{M}{t^3 T}]$
h_v	Normalized Heat Transfer Coefficient $\frac{hA}{V}$ $[\frac{M}{t^3 TL}]$
k_0	Rate Constant
k_{eff}	Effective Thermal Conductivity $[\frac{ML}{t^3 T}]$
k_e	Radial Thermal Conductivity $[\frac{ML}{t^3 T}]$
L	Reactor Length $[L]$
n	Reaction Order
N	$\frac{h_v e^{E/RT_w}}{C_p c_0 k_0}$
P	Pressure $[\frac{M}{Lt^2}]$
Pr	Prandtl Number $\frac{C_p/mu}{k}$
Q_f	Feed Stream Flow Rate
r	Reaction Rate
R	Gas Constant or Dilution/Recycle Factor or Cone Radius
Re	Reynolds Number $\frac{\rho VD}{\mu}$
S	$\frac{\Delta T_{ad}}{\Theta}$ or Cone Radius
T	Temperature $[T]$
t	Time $[t]$
U	Heat Transfer Coefficient
u	Manipulated Variable
v_s	Space Velocity $[\frac{M}{L^3 t}]$
V	Volume $[L^3]$
x	Fractional Conversion or Dimensionless Temperature
x_a	$\frac{C_A}{C_{Af}}$
x_b	$\frac{C_B}{C_{Af}}$
x_c	$\frac{C_C}{C_{Af}}$
y	System Output or Dimensionless Concentration
Δ	Difference

ϵ	Fractional Void Space
γ	$\frac{E}{rT_w}$
λ	Flow Coefficient for Heat Transfer
λ_i	Purity of i
μ	Viscosity $[\frac{M}{Lt}]$
ψ	Catalyst Particle Shape Factor
ρ	Density $[\frac{M}{L^3}]$
Θ	$\frac{RT_w^2}{E}$ $[T]$
τ	Residence Time, Time Lag $[t]$

Subscripts

0	Initial or Nominal
ad	Adiabatic
b	Bulk
c	Coolant
eff	Effective
eq	Equilibrium
f	Fluid
max	Maximum
min	Minimum
p	Particle
r	Radial
w	Wall

Superscripts

*	Solid
~	Deviation Variable
^	Approximate

Abbreviations

AL	Approximate Linearization
DPS	Distributed Parameter System
GSL	Global State Linearization
IOL	Input-Output Linearization
LMLC	Linear Model, Linear Control

LPS	Lumped Parameter System
MP	Minimum Phase
NMP	Nonminimum Phase
NLMLC	Nonlinear Model, Linear Control
NLMNLC	Nonlinear Model, Nonlinear Control
QAL	Quadratic Approximate Linearization
TI	Time-Invariant
TV	Time-Varying

Contents

List of Figures

List of Tables

Chapter 1

Introduction

Chemical reaction systems display a rich array of nonlinear dynamical behavior, from simple stability, bifurcations, limit cycles, chaos, to pathological instability. In contrast, the tools of feedback control theory, which have been used for the regulation of these systems, have primarily been restricted to linear methods. The objective of this thesis is the development of practical tools for the study of nonlinear dynamical systems from which an effective and objective analysis on the merits of nonlinear control can be accomplished.

1.1 Motivation

1.1.1 Nonlinear Process Control

Chemical process systems are inherently nonlinear. Indeed, no real physical system conforms to precisely linear dynamical behavior. This idea was expressed, perhaps, most eloquently by the physicist Enrico Fermi:

> "It does not say in the Bible that all the laws of nature are expressible linearly!" [35]

There are a number of well-known mechanisms which contribute to the nonlinear behavior observed in process systems:

- **Reaction Kinetics** – Rate expressions for chemical reactors often have a polynomial or fractional dependence on the concentration of the reacting species. The dependence of reaction rates on temperature is usually exponential, in accordance with the Arrhenius law. These expressions are further complicated in heterogeneous systems with catalytic rate mechanisms.

- **Thermodynamics** – The equilibrium relationships in multiphase, multicomponent systems are highly nonlinear. This is manifested, for example, in the relative volatility of two species in a distillation column.

- **Transport Phenomena** – The nonlinear nature of the equations of continuity, motion, and energy is clearly manifested in the dependence of such parameters as the mass transfer coefficient, drag coefficient, and heat transfer coefficient on the flow rate (Reynolds number).

Control approaches for these processes have relied primarily on linear designs which are based upon first-order approximations of the actual physical systems. These approaches are inherently conservative as performance is sacrificed in order to guarantee stability for a much larger class of models than merely the single first-order approximation. This tradeoff is characterized in the "robustness" of the controller [67] and reflects the fact that the simple linear model is an inaccurate description of the true system.

Clearly, more accurate models are required; furthermore, more efficient utilization of these models in the control synthesis is demanded. A logical progression involves the incorporation of well characterized system nonlinearities into the control algorithm, yielding a nonlinear controller. A promising approach for such a technique is provided in the area of differential geometry. These approaches will be reviewed in the subsequent chapters and, using the new tools presented in this thesis, an objective evaluation of their applicability to practical industrial process systems is carried out.

It is emphasized that these approaches represent an *alternative* to traditional linear methods, and not an absolute *complement* to these methods as the word *nonlinear* might imply. This distinction has been pointed out in other contexts:

> The mathematician Stanislaw remarked that to call the study ... "nonlinear science" was like calling zoology "the study of nonelephant animals." [35]

These nonlinear methods of feedback linearization must be considered as a *competitive* approach to linear control. An objective comparison of the two is carried out in this thesis.

1.1.2 Packed Bed Reactor

The packed bed reactor is a key unit operation in the chemical process industry. It is characterized by highly nonlinear, heterogeneous kinetics and its distributed nature leads to an (ideal) model consisting of partial differential equations. Its utility as a target application for the present work is evident.

A primary shortcoming of many previous studies in nonlinear process control is the limit of scope to primarily theoretical and academic issues. In the area of differential geometric control methods, the emphasis in research has been on very simple reaction systems for which low-order, lumped parameter models were readily derived. The value of such studies is important to the advancement of nonlinear control theory. However, their ultimate practical utility to the chemical process industry is limited. To date, only one industrial application of such techniques has been reported [58].

The packed bed reactor represents a practically useful system, although its ideal model does not readily admit solutions for feedback linearization. This has prompted, in the present work, the development of appropriate models which both accurately describe the complicated fixed bed dynamics and are suitable for the application of feedback linearizing control. This approach to deriving a reduced-order nonlinear

model for the packed bed reactor represents an attractive technique for modeling a variety of process systems. Thus, the reactor case study serves as a demonstration of a general technique for robust nonlinear model-based control design.

The industrial utility of the packed bed reactor does not sufficiently justify the practical value of theoretical studies on reactor design and control. As in the case of nonlinear control, there have been a number of very useful academic studies which have served to further the theoretical understanding of reactor fundamentals. However, some of the key practical issues have often been overlooked, thus limiting their overall value. Among these considerations are the multitubular variations in the reactor and the limited set of measurements available for control purposes. This present study addresses these issues and provides useful guidelines for the design and control of packed bed reactors.

1.2 Previous Work

1.2.1 Nonlinear Control Theory

Early work in nonlinear control theory was primarily limited to analysis results dating from the work of Lyapunov [60] on the stability of autonomous differential equations. The key results for closed-loop systems are largely attributed to Zames [95] and Popov [77] in which they addressed the stability of linear dynamical systems which are perturbed by memoryless, norm-bounded, nonlinear perturbations. The question of model/plant mismatch was addressed by Doyle [18] in a similar framework in which model uncertainty is formulated as a structured, norm-bounded, linear perturbation on a nominal model. The present work addresses nonlinear systems in this same framework using the Small Gain Theorem developed by Zames [95] and extensions of the structured singular value. The result is a conservative bound on the attainable performance levels in a system.

Outside the area of differential geometry, nonlinear control synthesis research pro-

ceeded as a natural extension of several successful linear approaches. Economou and Morari [26] extend the linear design approach of Internal Model Control to the nonlinear setting. They present a numerical algorithm for calculating the inverse operator of a nonlinear plant which is used in the control law. Nonlinear Model Predictive Control is another approach which extends the ideas of linear Model Predictive Control to the case of a nonlinear plant [9]. A nonlinear optimization problem is set up in the time domain to calculate the value of the control action which minimizes the performance objective over a time horizon. However, global convergence of the nonlinear optimization is not guaranteed and rigorous performance/stability results are not available.

The nonlinear synthesis problem in differential geometry dates back to the work by Poincare [76] in which he studied the problem of transforming an autonomous nonlinear system by a change of coordinates into a simpler or normal form. The first rigorous results for controlled systems are mainly attributed to Hunt, Su and Meyer [43] who showed the equivalence of a nonlinear system and a linear controllable system through state transformations and nonlinear feedback. A similar result by Krener [56] showed how the work of Poincare could be used to calculate an approximate linearization. By allowing higher order remainder terms in the transformed system, the restrictions on problems which admit a solution are somewhat relaxed. One shortcoming of both state linearization approaches is the fact that the "linearized" portion of the original system is the state dynamics and *not* the input-output mapping. This was addressed by Kravaris [52] who showed that a linear input-output linearizing controller could be derived for a nonlinear system by calculating a realization of the system inverse. The restriction imposed is that the original system is invertible (minimum phase). An approximate approach for input-output linearization has recently been introduced by Hauser [39]. As with Krener's approach, a relaxed set of requirements on the transformed system allows the treatment of a much larger set of problems. The appeal to

these control approaches is that differential geometry provides tools which are natural extensions of the linear algebraic tools used in optimal linear control.

The pioneer work by Hunt, Su, and Meyer [43] paved the way for application studies in the areas of robotics, aircraft control, biomedical engineering, and process control (see [44], [54], [83] and references contained therein). The process control applications have been largely limited to simple lumped parameter systems such as flow control in a tank or a continuous stirred tank reactor. In addition, with the exception of severely restrictive matching condition methods [12], [55], there has been minimal work done to address the robustness properties of these closed-loop systems. A third weakness of the application work for process systems is the lack of an objective evaluation of the strengths of these approaches over traditional linear approaches. The present work addresses these concerns by the definition of meaningful robust performance objectives and through application studies on a complex process system.

1.2.2 Packed Bed Reactor

The design and control of packed bed reactors have been the subjects of a number of theoretical and experimental studies. A comprehensive survey of the academic and industrial efforts in these areas is provided in [46].

Packed bed reactor modeling approaches for control studies have relied on approximating the distributed parameter system by a set of ordinary differential equations. Typical approaches to this problem have included the techniques of orthogonal collocation and finite differences. The drawback to this approach is the relatively large number of dynamic variables which result. In particular, the differential geometric approaches described above require models of size less than about 10 ordinary differential equations or the resulting Lie Algebraic calculations are intractable.

An alternative approach for low-order modeling of distributed parameter systems

was put forth by Gilles and co-workers in the early 1980s [32], [33], [34]. This approach involved the modeling of concentration and temperature profiles as nonlinear waves which propagate through the medium in response to changes in operating conditions. The intuitive appeal to this approach is the identification of a small set (typically 2 to 6) of key dynamical variables for the system resulting in low-order lumped parameter models. A survey of these techniques was recently published [67] in which a broad range of chemical engineering applications were discussed. This so-called wave propagation approach was modified for use in the present study.

Theoretical studies on packed bed reactor stability have focused on describing conditions of parametric sensitivity where small perturbations in the operating conditions lead to huge excursions in the reactor temperature [68], [69], [70], [78], [89]. These studies involved the formulation of differential sensitivities for describing conditions of runaway behavior. Experimental validation of these results has been published in [8], [30]. However, the direct implications of this sensitivity theory for practical reactor design are not apparent.

The stabilization of sensitive reactor behavior can be accomplished in a CSTR by application of simple proportional feedback control [4]. Theoretically, the same stabilization theory can be invoked for a packed bed reactor and safe closed-loop operation can be attained in a region of open-loop sensitivity (see, *e.g.*, [80]). A number of experimental studies have also focused on the stabilizing effects of feedback control in a *single* tube reactor [38], [41], [64], [85]. However, these studies have largely ignored some of the key industrial issues such as multitubular variations and availability of measurement signals for control purposes.

1.3 Thesis Overview

In chapter 2, a novel condition for nonlinear robust performance is presented. The approach utilizes new extensions of the structured singular value and conic sector bounds

of nonlinear operators to result in an upper bound for the attainable performance level in a nonlinear system. The approach is demonstrated through application to a continuous stirred tank reactor. The resulting tools provide a systematic approach to the calculation of stability and performance properties for a general nonlinear system.

In chapter 3, the differential geometric techniques of exact and approximate state linearization are studied as candidate approaches for chemical reactor control. The approaches are compared with respect to disturbance handling, optimization of the resultant nonlinear transformations, and the restrictions on application. It is shown that the relaxed restrictions and type of coordinate transformation for approximate linearization results in superior performance. These ideas are demonstrated through simulations involving two non-involutive reaction systems. The tools of chapter 2 are employed in calculating robust performance properties for two additional reaction systems under closed-loop approximate linearization and linear control.

In chapter 4, a nonlinear controller is derived for a packed bed reactor. The approach involves two steps: (i) first the development of a reduced-order nonlinear model, and (ii) the synthesis of an input-output linearizing feedback controller. In addition, the implementational issues for the "linearizing" controller are addressed. The resulting scheme is compared to standard linear approaches for packed bed reactor control. This work represents the first application of differential geometric techniques to packed bed reactor control.

In chapter 5, simple guidelines are presented for the design of industrial packed bed reactors. Requirements on the radial temperature profile, temperature sensitivity, and pressure drop are translated into criteria involving the practical design parameters of length and diameter. The stabilizing effect of feedback control for practical packed bed reactors is addressed. It is demonstrated by simulation that violation of the proposed criteria leads to unacceptable closed-loop performance in an industrial reactor.

In chapter 6, an objective comparison of nonlinear "linearizing" versus linear con-

trol is presented. A series of case studies involving physical and some purely mathematical systems reveals the strengths and limitations of the novel design technique of input-output linearization. Consideration is given to region of attraction, penalties on the actuator movement, and sensitivity to input disturbances. The work represents the first objective evaluation of these "linearizing" techniques and suggests guidelines for the judicious selection of "linearizing" over linear control.

A summary of the contributions of this thesis and recommendations for further work are presented in chapter 7.

Appendix A contains a discussion of ℓ^1-optimal control as an alternative to the H_∞ formulation for structured uncertainty analysis. Comments on the relative merits of the two approaches are made in the context of the present work.

Appendix B contains data from the Caltech methanation reactor which is used to fit the wave-propagation model introduced in chapter 4 to an actual system.

Chapter 2

Tools for Nonlinear Analysis - Motivated by CSTR Example

Abstract

A design methodology is presented for the analysis and synthesis of robust linear controllers for a nonlinear continuous stirred tank reactor. Operating regions are defined in the phase plane in which the maintenance of robust stability and the achievement of robust performance levels are guaranteed. The results are based upon new extensions of the structured singular value theory to a class of nonlinear and time-varying systems. Comparisons are drawn between these results and previous Lyapunov-function approaches to stability analysis, and extensions are proposed for the application of this methodology to more complex schemes. This chapter provides insight into a novel condition for nonlinear robust performance and the first application of recent advances in control theory to a chemical process.

2.1 Introduction

Chemical reactor stability analysis can be traced back to the classic three-part treatise by Aris [4,5,6] in which a systematic study of the complex behavior exhibited by a well-agitated continuous reactor was undertaken. They utilized the concept of *linearization* to evaluate the merits of various control schemes in stabilizing the open-loop system. The present work is also concerned with the stabilization of regions in the phase

plane. A *nonlinear* approach is proposed, however.

There has been considerable interest in nonlinear control theory over the past decade, particularly in the area of process control. This can be partially attributed to the inherently nonlinear nature of chemical processes. The complex dynamics which can evolve from these systems are revealed in the simple example of a single first-order reaction carried out in a stirred tank. This system is known to exhibit bifurcations to multiple steady states and periodic limit cycles [86]. Traditionally, linear methods have been used to design controllers for these nonlinear processes. The control schemes which were proposed include "conservative" linear controllers and linear controllers with gain schedules. These methods are based on a first-order approximation of the actual system at a single point and a discrete set of operating points, respectively. Consequently, these techniques cannot account for large perturbations or operation away from the steady state operating curve. In addition, linear model-based techniques have been used in the analysis of control schemes for such processes. Robustness properties have been calculated with respect to linear perturbations acting on a nominal linear model.

In recent years, various design methods have been proposed which utilize more accurate nonlinear models. A precise treatment of model nonlinearities has emerged with the new differential geometric techniques of linearization [44]. These methods have been applied to the aforementioned CSTR problem to obtain exact state linearization [42], exact input/output linearization [55], and state linearization with disturbance rejection [13]. The controller synthesis involves two steps: first, a state feedback transformation to a new coordinate system in which the transformed variables exhibit linear dynamics; and second, a controller design for the resultant linear system. The major shortcoming of these techniques is their lack of robustness guarantees; in particular, *robust performance*, that is the maintenance of desired performance levels in the face of model uncertainty, cannot be assured. In fact, even

nominal performance cannot be assessed quantitatively for these schemes.

For the case of linear model-plant mismatch, i.e., linear model with linear time-invariant perturbation, model uncertainty has been handled most efficiently by the structured singular value (SSV) approach [19]. Using this method, necessary and sufficient conditions are calculated which guarantee stability and performance levels for the perturbed nominal system. This technique has been applied to a complex chemical reactor model [61]. New advances in SSV theory [71] allow the application of the results to a class of time-varying and nonlinear models. These models include the class of dynamical systems with cone-bounded nonlinearities. The focus of the present work is the application of this new technique to the calculation of margins of robust stability and robust performance for a nonlinear CSTR model.

The treatment of the reactor problem in this work parallels the approach of linear optimal control theory in as much as a systematic procedure is outlined for the design of robust control systems. The design approach will entail the following steps:

(i) identification of system variables (inputs, outputs, manipulated variables);

(ii) selection of overall control objectives;

(iii) modeling of the nonlinear system, in particular, formulation in the general framework for SSV treatment;

(iv) synthesis and/or analysis of a controller using nonlinear SSV.

The objective of this chapter is the presentation of a systematic design procedure for nonlinear systems which guarantees the achievement of stability and performance levels over a wide operating range. With the exception of a conference paper by Smith and Doyle [84], there have been no published accounts of the application of these advances to practical control systems. Although the treatment will be developed for the generic class of systems with cone-bounded nonlinearities, it will be motivated

by the specific application to a first order exothermic reaction carried out in a CSTR. A short description of the reactor problem is given in section 2.2. In section 2.3, the structured singular value is re-introduced and the recent developments for nonlinear perturbations are reviewed. The controller design methodology is outlined in section 2.4, with the CSTR problem serving as a case study. A discussion of actual simulations and performance characteristics for the controlled CSTR can be found in section 2.5. The further potential of this method is discussed in the concluding section.

2.2 The CSTR Problem Formulation

2.2.1 The Physical System

The mass and energy balances for a CSTR with first order, irreversible, exothermic kinetics ($A \rightarrow B$) are given by [86]:

$$\frac{dC_A}{dt} = \frac{Q_f}{V}(C_{AF} - C_A) - k_0 C_A e^{-E_a/RT} \tag{2.1}$$

$$\frac{dT}{dt} = \frac{Q_f}{V}(T_F - T) - \frac{k_0 C_A}{Cp}(-\Delta H)e^{-E_a/RT} - \frac{UA_h}{VCp}(T - T_c) \tag{2.2}$$

This simple model has two state variables (reactant concentration, reactor temperature) and one manipulated variable (cooling water temperature). Various control objectives are possible, with the reactant concentration being a likely candidate for regulation. In addition, it is possible to consider perturbations in the feed temperature as an unmeasured disturbance entering the second state equation. Using the dimensionless quantities defined in Table 2.1, the normalized model is given by:

$$\dot{x}_1 = -x_1 + \mathcal{D}a(1 - x_1)e^{\frac{x_2}{1+x_2/\gamma}} \tag{2.3}$$

$$\dot{x}_2 = -x_2 + \mathbf{B}\mathcal{D}a(1 - x_1)e^{\frac{x_2}{1+x_2/\gamma}} - \beta(x_2 - x_c) + \beta u + d \tag{2.4}$$

The pertinent dynamical information for the open-loop reactor can be summa-

Table 2.1 Dimensionless Variables for CSTR Model	
x_1	$(C_{Af} - C_A)/C_A$
x_2	$(T - T_{f_0})/T_{f_0}\gamma$
x_c	$(T_{c_0} - T_{f_0})/T_{f_0}\gamma$
d	$(T_f - T_{f_0})/T_{f_0}\gamma$
u	$(T_c - T_{c_0})/T_{f_0}\gamma$
$\mathcal{D}a$	$\frac{V}{Q_f}k_0 e^{-\gamma}$
$\mathbf{B}$	$-\Delta H C_{Af}/C_p T_{f_0}\gamma$
β	$UA_h/Q_f C_p$
γ	Ea/RT_{f_0}

rized in a phase plot with axes representing the two state variables. Two plots are particularly insightful for this analysis: first, a phase portrait for the uncontrolled system; and second, a plot of the stable and unstable portions of the operating curve for fixed values of the manipulated variable. Two example plots for a particularly pathological set of parameter values ($\mathbf{B} = 22.0, \beta = 3.0, \mathcal{D}a = 0.082, \gamma \rightarrow \infty, u = 0$) are shown in Figures 2.1 and 2.2. In this case the uncontrolled system has three steady states (one stable, two unstable) and an attracting limit cycle.

2.2.2 Previous CSTR Nonlinear Control Approaches

Recent advances in differential geometry have led to a number of useful, so-called "linearization" techniques which have been applied to CSTR control. One approach [43] involves coordinate transformations on the state and input variables to transform the nonlinear system to a controllable linear system. Another approach [52] utilizes an input transformation by state feedback to obtain, in the new coordinates, a linear input/output map. These ambitious approaches suffer from a number of weaknesses. The class of systems which yield solutions to state linearization is limited to involutive systems and input/output linearization requires minimum phase systems. Typical chemical reactor problems violate one or the other of these con-

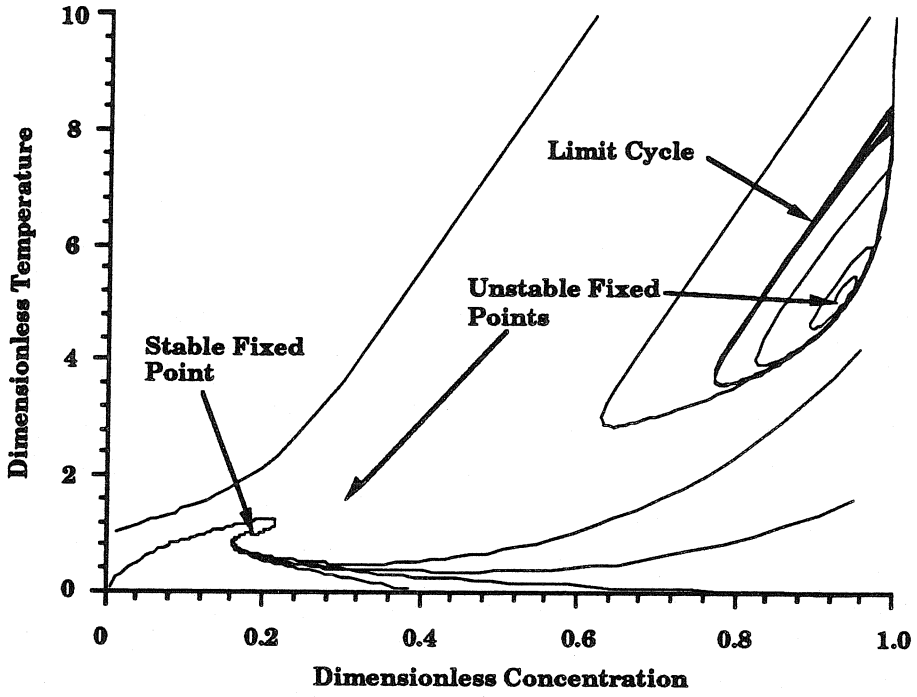

Figure 2.1. Phase Portrait

ditions [54]. In addition, these methods require a knowledge of the state variables, information which is not always available. This requirement is difficult to meet with an observer since there is no separation principle to guarantee stability for the combined controller-observer nonlinear system. In [13], additional shortcomings of these methods are outlined with respect to disturbance handling, constraints and modeling errors. They propose an IMC-based method for handling the first two problems.

A major weakness of the aforementioned techniques is the lack of robust performance guarantees. There are a few results, using numerical Lyapunov functions, which guarantee robust stability for certain unmodeled dynamics [55]. However, work has been done which suggests that these linearization techniques can be very sensitive to model error [2]. Furthermore, due to the "pseudo" transformed variables, it is not

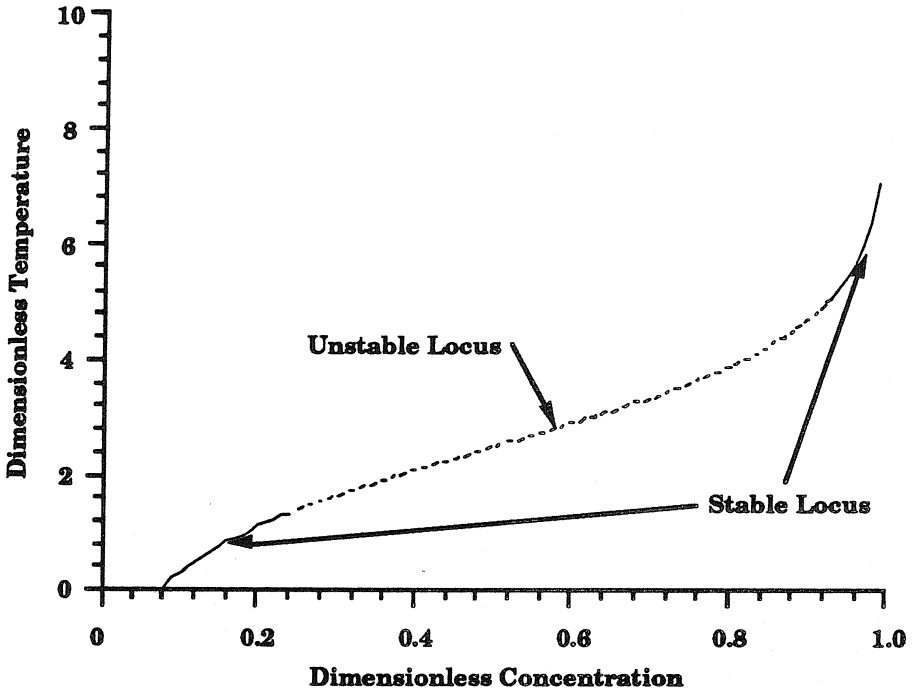

Figure 2.2. System Operating Curve

a straightforward procedure to specify traditional performance criteria on the input, output, and state variables for a given problem.

The results presented in this chapter provide a complementary approach to the previous CSTR nonlinear control techniques by outlining a new technique for analyzing the robustness properties of nonlinear systems. The present work focuses on fairly simple linear controllers but the theory is sufficiently general as to include a wide variety of nonlinear plants *and* nonlinear controllers. The strength of these new methods is the development of a technique, albeit sufficient, for the evaluation of performance for uncertain nonlinear systems.

2.3 Structured Singular Value Concepts

2.3.1 The General Framework

We will employ a general dynamical system description which establishes the relationship between the inputs, states and outputs. Elements which may comprise the system include a nominal plant, a feedback controller, and an uncertainty block. The latter element is used to represent a family of plants which can be arrived at by perturbing the nominal plant. The input v represents setpoints, disturbances and noise, the output e represents error signals. In this framework, the control analysis problem focuses on two key questions: first, is the system stable for all perturbations in some prescribed set (robust stability); and second, does the error e remain in a desired bounded set for all perturbations and inputs in some appropriate sets (robust performance). We will develop a general framework within which conditions for robust stability and robust performance can be expressed mathematically.

The usual Euclidean norm or 2-norm will be used to calculate the norm of vectors in $\mathcal{C}^n$ or $\mathcal{R}^n$. For vector signals $e(t)$ this norm is defined to be: $\|e(t)\|^2 = \int_{-\infty}^{\infty} e^T(t)e(t)dt$. The operator norm induced by the 2-norm is:

$$\sup_{\substack{v\neq 0 \\ v\in\mathcal{L}_2}} \frac{\|Gv\|}{\|v\|} = \sup_{\omega} \bar{\sigma}(G(j\omega)) \triangleq \|G\|_\infty \tag{2.5}$$

where $\mathcal{L}_2$ is the space of functions with bounded 2-norm.

An understanding of uncertainty descriptions can be gained by considering the nominal time-invariant, linear system $G(s)$:

$$\begin{aligned} \dot{x} &= Ax + Bv \\ e &= Cx + Dv \end{aligned} \tag{2.6}$$

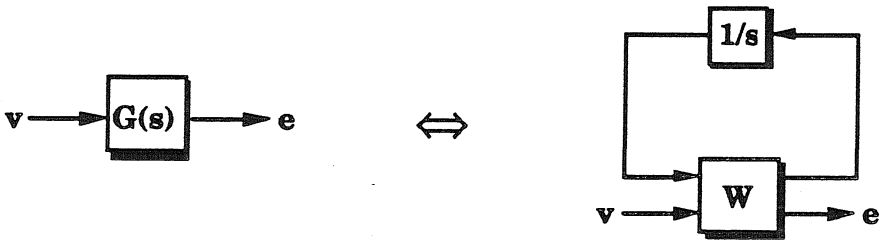

Figure 2.3. General Framework (Nominal)

This system leads to a state-space realization which can be defined by the matrix W:

$$\begin{pmatrix} \dot{x} \\ e \end{pmatrix} = \begin{pmatrix} A & B \\ C & D \end{pmatrix} \begin{pmatrix} x \\ v \end{pmatrix} = W \begin{pmatrix} x \\ v \end{pmatrix} \tag{2.7}$$

It can be seen from Figure 2.3 that $G(s)$ can be obtained by closing the top loop on W with an integrator block s^{-1}, leading to the *linear fractional transformation* (LFT) for the transfer function:

$$e = G(s)v = F_u(W, \frac{1}{s})v = [D + C\frac{1}{s}(I - A\frac{1}{s})^{-1}B]v \tag{2.8}$$

where the subscript u refers to the fact that the *upper* loop has been closed. For this example, the stability of $G(s)$ depends obviously on the invertibility of $(sI - A)$, or equivalently, on the location of the eigenvalues of A.

As an illustration of this general description, consider a structured perturbation on the nominal system leading to a new transfer function $G_\Delta(s)$ defined by:

$$\begin{aligned} \dot{x} &= (A + \textstyle\sum_{i=1}^{k} \delta_i A_i)x + Bv \\ e &= Cx + Dv \end{aligned} \tag{2.9}$$

Here, the scalar parameters δ_i represent the uncertainty for this system. Again, an LFT can be constructed for this perturbed system with an appropriate state-space

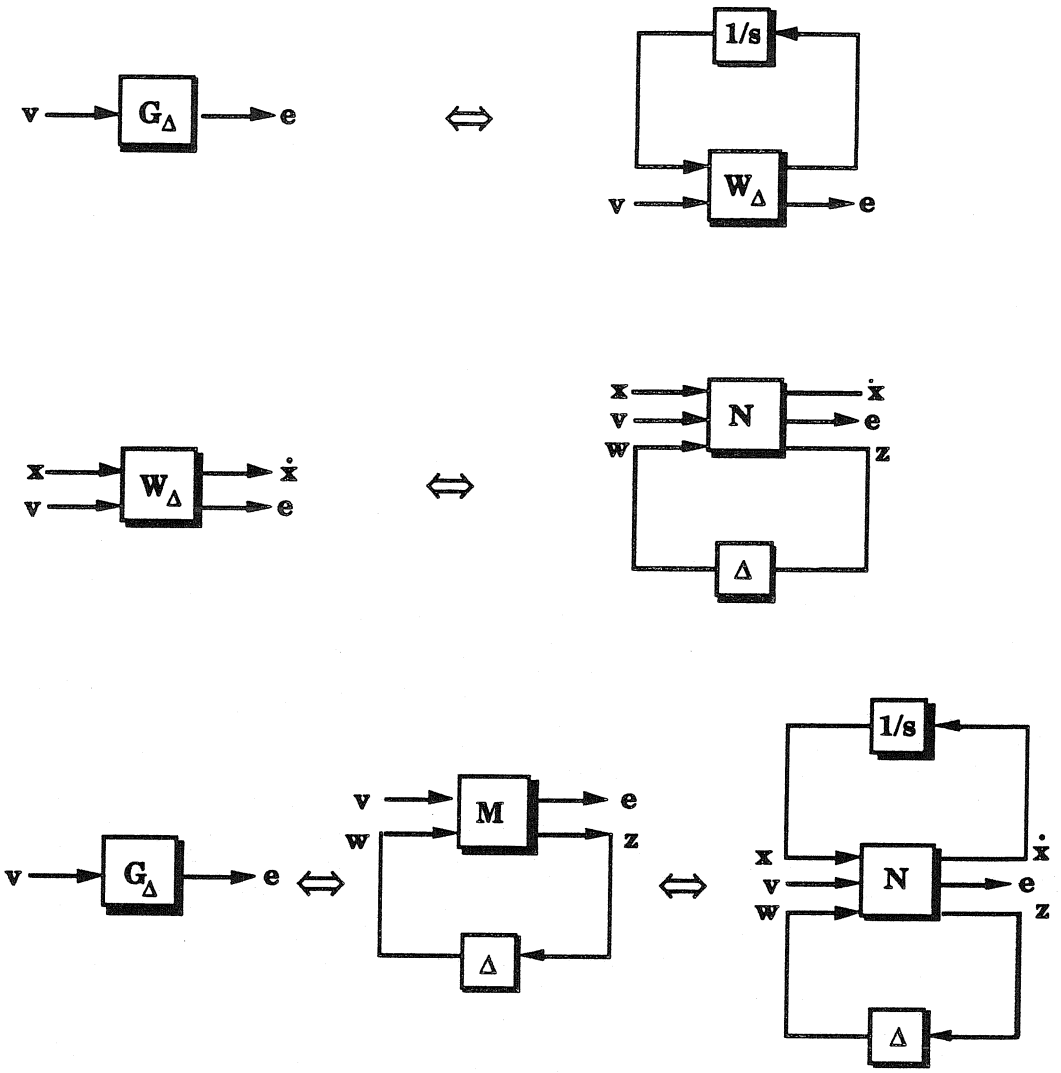

Figure 2.4. General Framework (Perturbed)

matrix W_Δ:

$$W_\Delta \triangleq \begin{pmatrix} A + \sum_{i=1}^{k} \delta_i A_i & B \\ C & D \end{pmatrix} \tag{2.10}$$

From the block diagram in Figure 2.4, the perturbed LFT is given by:

$$e = F_u(W_\Delta, \frac{1}{s})v \tag{2.11}$$

It is desirable to isolate the uncertainty elements from the overall transfer function

G_Δ. Stepwise, this proceeds as illustrated in Figure 2.4. First, the matrix W_Δ is rewritten as a feedback connection of a matrix N and an uncertainty block Δ. The matrix N is an algebraic function of the elements of W_Δ but is independent of the uncertainty elements δ_i. The block Δ is composed of k diagonal scalar-times-identity blocks with dimensions equal to the rank of the A_i matrices. For example, if all the A_i have full rank then

$$N = \begin{pmatrix} A & B & I & I & \dots & I \\ C & D & 0 & 0 & \dots & 0 \\ A_1 & 0 & & & & 0 \\ A_2 & 0 & & & & 0 \\ \vdots & \vdots & & & & \vdots \\ A_k & 0 & 0 & 0 & & 0 \end{pmatrix} \tag{2.12}$$

The structure of the uncertainty block is a key feature of this representation and will be exploited in the following sections. Note that in general, the uncertainty block will be a linear operator in the set

$$\mathbf{\Delta} := \{\mathrm{diag}[\delta_1 I_{r_1}, \dots, \delta_m I_{r_m}, \Delta_1, \dots, \Delta_n]\} \tag{2.13}$$

where depending on the problem the δ_i, Δ_j will be restricted to certain classes. We define the bounded subset:

$$B\mathbf{\Delta} := \{\Delta \in \mathbf{\Delta} | \bar{\sigma}(\Delta) \leq 1\} \tag{2.14}$$

Note that the LFT representation for W_Δ is given by

$$W_\Delta = F_\ell(N, \Delta) \tag{2.15}$$

where ℓ refers to the fact that the *lower* loop is closed. Finally, a general LFT for $G_\Delta(s)$ can be given by:

$$G_\Delta(s) = F_\ell(F_u(N, \frac{1}{s}), \Delta) \tag{2.16}$$

and defining $M \triangleq F_u(N, \frac{1}{s})$ (see Figure 2.4):

$$G_\Delta(s) = F_\ell(M, \Delta) \tag{2.17}$$

Thus, the so-called "$M - \Delta$ structure" is constructed. This mapping from $\begin{pmatrix} v \\ w \end{pmatrix}$ to $\begin{pmatrix} e \\ z \end{pmatrix}$ can be appropriately partitioned:

$$\begin{pmatrix} e \\ z \end{pmatrix} = \begin{pmatrix} M_{11} & M_{12} \\ M_{21} & M_{22} \end{pmatrix} \begin{pmatrix} v \\ w \end{pmatrix} \tag{2.18}$$

Thus, for $w = \Delta z$, the general LFT for G_Δ is given by:

$$F_\ell(M, \Delta) \triangleq M_{11} + M_{12}\Delta(I - M_{22}\Delta)^{-1}M_{21} \tag{2.19}$$

The previously mentioned concepts of robust stability and robust performance can be defined in this LFT framework. Robust stability requires that $F_\ell(M, \Delta)$ remain stable for all $\Delta \in B\mathbf{\Delta}$. Robust performance requires that a norm bound on the mapping from input v to output e is met for all perturbations.

Filters can be designed which "shape" the input signal class into the expected set of inputs, and similarly weight the outputs (by frequency) according to the specified performance criteria. All of these "performance and uncertainty weights" are usually absorbed into the structure M. Then the appropriate robust performance condition is:

$$\|F_\ell(M, \Delta)\|_\infty < 1 \qquad \forall \quad \Delta \in B\mathbf{\Delta} \tag{2.20}$$

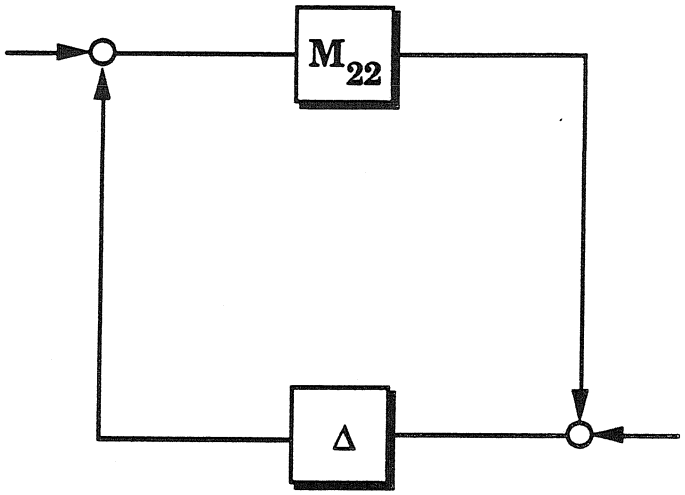

Figure 2.5. Well-posedness Loop

2.3.2 Benefit of Constant D Scalings

Considering the system in Figure 2.4, it is clear that the input-output system is well-posed if and only if the $(I - M_{22}\Delta)$ term in Equation 2.19 is invertible and the perturbed system is stable if the operator $(I - M_{22}\Delta)^{-1}$ is stable. The term "well-posed" indicates that for each input v there are unique vectors w, z and e which satisfy the closed-loop equations. M describes the nominal closed-loop system; therefore we will assume that M is stable. The robust stability condition can be reformulated by considering the loop in Figure 2.5. An application of the small gain theorem then gives a sufficient condition for stability [95]:

$$\sup_{\omega} \bar{\sigma}(M_{22}) < \gamma \quad (\gamma > 0) \qquad \forall \Delta \in \frac{1}{\gamma} B\mathbf{\Delta} \tag{2.21}$$

where $\frac{1}{\gamma} B\mathbf{\Delta}$ is the subset of $\mathbf{\Delta}$ with $\bar{\sigma}(\Delta) \leq \frac{1}{\gamma}$.

Consider the class of matrices, D, which *commute* with the perturbation block Δ.

Table 2.2 Commuting $D - \Delta$ Pairs	
Uncertainty (Δ)	Scaling (D)
TI, full block, complex	Frequency-varying, scalar-times-identity
TI, scalar-times-identity, complex	Frequency-varying, full block
TV, full block, complex	Constant, scalar-times-identity
TV, scalar-times-identity, complex	Constant, full block

Definition 2.1 *If D and Δ commute, then by definition*

$$D\Delta D^{-1} = \Delta \tag{2.22}$$

A listing of appropriate D, Δ commuting pairs is given in Table 2.2.

If Equation 2.22 holds, then for any operator M_{22}, the two diagrams in Figure 2.6 are equivalent to each other and to the structure in Figure 2.5.

Now, application of the Small Gain Theorem to Figure 2.6 guarantees the stability of the loop for all stable and time-varying Δ which also satisfy:

$$\bar{\sigma}(\Delta) < \frac{1}{\|DM_{22}D^{-1}\|_\infty} \tag{2.23}$$

This equation shows that conservatism can be minimized by considering

$$\inf_{D \in \mathcal{D}} \|DM_{22}D^{-1}\|_\infty \tag{2.24}$$

where $\mathcal{D}$ defines an appropriate commuting set for the Δ in Equation 2.13:

$$\mathcal{D} \triangleq \left\{ \text{diag}[D_1, \ldots, D_m, d_1 I_{k_1}, \ldots, d_n I_{k_n}] \,|\, D_i \in C^{r_i \times r_i} \text{ is invertible, } d_i \neq 0 \right\} \tag{2.25}$$

The D scale which achieves or gets arbitrarily close to the infimum in Equation 2.24 is referred to as the *optimal D scale* since it maximizes the bound that can

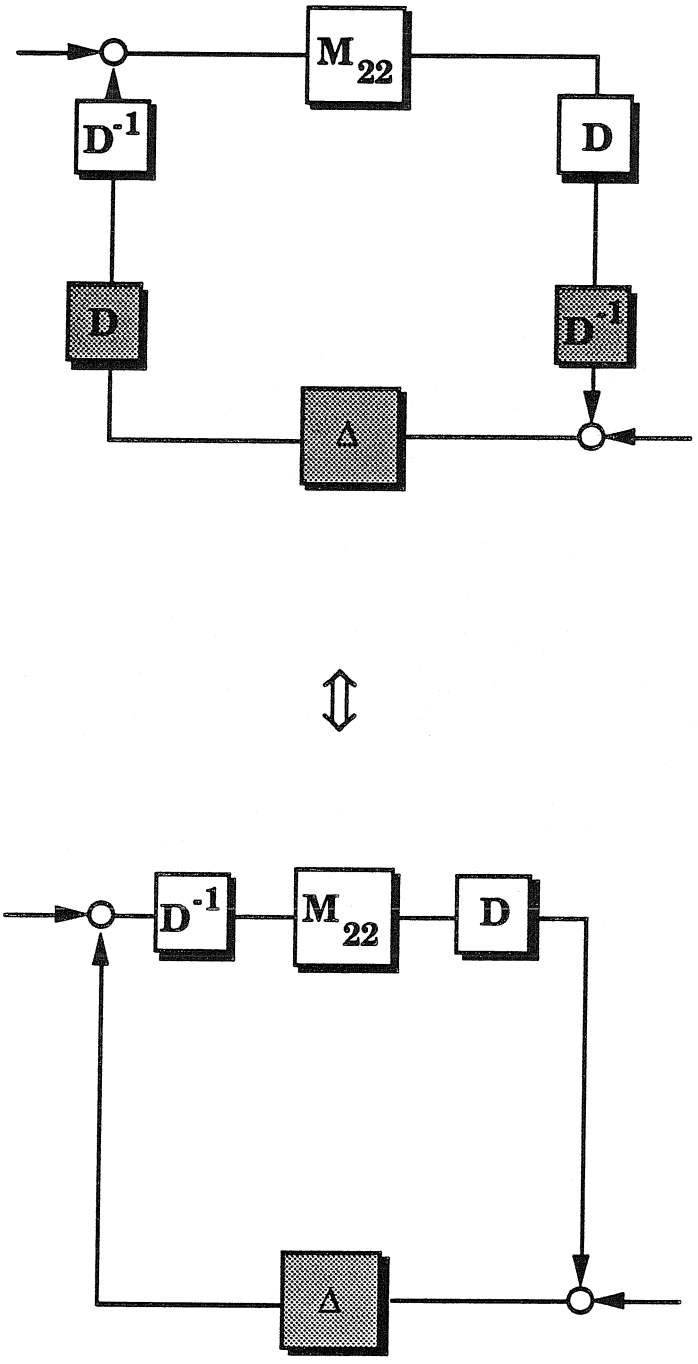

Figure 2.6. Equivalent Scaled Loops for Robust Stability

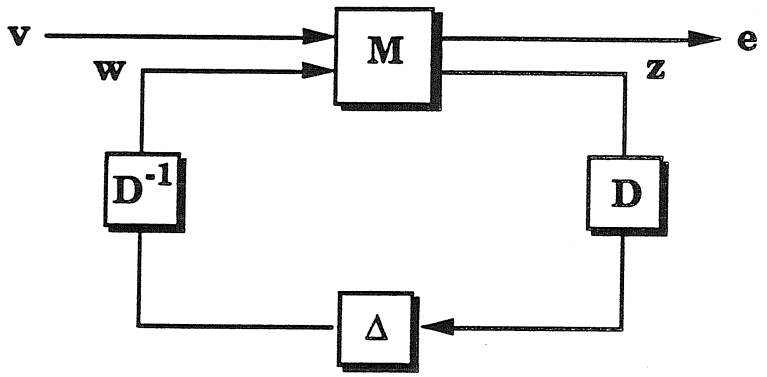

Figure 2.7. D Scalings for Robust Performance

be obtained with this method.

Given these D scales, it is possible to formulate a less conservative condition for robust stability than that proposed in the previous subsection.

Theorem 2.1 *(Robust Stability; Time-Varying, Complex Δ)*

The system $F_\ell(M, \Delta)$ is stable for all time-varying $\Delta \in B\mathbf{\Delta}$ if

$$\inf_{D} \sup_{\omega} \bar{\sigma}(DM_{22}D^{-1}) < 1 \tag{2.26}$$

where D is appropriately constructed as in Table 2.2.

Proof 2.1 *Follows directly from Small Gain Theorem [95].*

The details for deriving the robust performance criterion can be seen by examining Figure 2.7. Absorbing the D scales into the M block yields the transformed matrix:

$$\begin{pmatrix} I & 0 \\ 0 & D \end{pmatrix} \begin{pmatrix} M_{11} & M_{12} \\ M_{21} & M_{22} \end{pmatrix} \begin{pmatrix} I & 0 \\ 0 & D^{-1} \end{pmatrix} \tag{2.27}$$

Just as for robust stability, a less conservative condition then Equation 2.20 can be derived for robust performance:

Theorem 2.2 *(Robust Performance; Time-Varying, Complex Δ)*

$F_\ell(M,\Delta)$ is stable and $\|F_\ell(M,\Delta)\|_\infty < 1 \quad \forall\Delta \in B\mathbf{\Delta}$ if

$$\inf_D \sup_\omega \bar{\sigma}\left[\begin{pmatrix} I & 0 \\ 0 & D \end{pmatrix} M \begin{pmatrix} I & 0 \\ 0 & D^{-1} \end{pmatrix}\right] = \beta < 1 \tag{2.28}$$

where D is appropriately constructed as in Table 2.2.

Proof 2.2 *The condition of the theorem implies (see Figure 2.7): $\|z\|^2 + \|e\|^2 \leq \beta^2(\|v\|^2 + \|w\|^2)$. Furthermore, from Equation 2.22 and $\bar{\sigma}(\Delta) \leq 1$: $\|z\|^2 \geq \|w\|^2$. Thus $\|e\|^2 \leq \beta^2\|v\|^2$ and $\|F_\ell(M,\Delta)\|_\infty < 1$*

In order to use Theorems 2.1 and 2.2, a procedure has to be found for finding the optimal D's which are required on the LHS of the inequalities 2.26 and 2.28. The following two sections establish an equivalent minimization problem which is easier to solve.

2.3.3 Connection to Lyapunov Approach

The following section outlines the robust stability and robust performance results in the time domain. The motivation for this analysis is twofold: first, the usual Lyapunov results for stability can be clearly represented in the time domain; and second, the actual calculations involved for the scaled singular values are computationally more attractive in the time domain.

In order to provide a clear exposition, the calculations will be carried out for discrete systems. In the z-domain, the robustness results are considerably simpler than the corresponding results in the Laplace domain. The equivalence of these results can be demonstrated by constructing a norm-preserving bilinear transformation which maps the unit disk to the right half plane. For example, consider the transfer function which has the continuous realization (A, B, C, D). Its equivalent discrete realization

is given by

$$\begin{pmatrix} \tilde{A} & \tilde{B} \\ \tilde{C} & \tilde{D} \end{pmatrix} = \begin{pmatrix} (I+A)(I-A)^{-1} & \sqrt{2}(I-A)^{-1}B \\ \sqrt{2}C(I-A)^{-1} & D+C(I-A)^{-1}B \end{pmatrix} \tag{2.29}$$

where the transformation $s = (1-z)/(1+z)$ is used.

Consider the linear difference equation

$$x_{k+1} = F_\ell(\tilde{N}, \Delta_k)x_k \tag{2.30}$$

where $x_k \in \mathcal{C}^n$, $\tilde{N} \in \mathcal{C}^{(n+m)\times(n+m)}$ and for each k, Δ_k is an element of the prescribed uncertainty set $\mathbf{\Delta}$. The stability of this system for a prescribed set of Δ_k is to be investigated. The assumptions on Δ_k are:

i) $\bar{\sigma}(\Delta_k) \leq 1$

ii) Δ_k varies with k

The time-varying nature of Δ_k invalidates spectral radius arguments which do not guarantee that x_k decreases for all k. However, the following sufficient condition does yield exponential stability:

$$\max_{\Delta_k \in B\mathbf{\Delta}} \bar{\sigma}(F_\ell(\tilde{N}, \Delta_k)) < 1 \tag{2.31}$$

This condition guarantees that the operator $F_\ell(\tilde{N}, \Delta_k)$ is a contraction. This conservative result can be strengthened by searching for a single quadratic Lyapunov function, x^*Px, for the entire set of operators contained in $\{F_\ell(\tilde{N}, \Delta_k) | \Delta_k \in B\mathbf{\Delta}\}$. A necessary and sufficient condition for the existence of such a function is given by:

$$\max_{\Delta_k \in B\mathbf{\Delta}} \bar{\sigma}(TF_\ell(\tilde{N}, \Delta_k)T^{-1}) < 1 \quad \text{for some } T \in \mathcal{C}^{n\times n}, \text{ invertible} \tag{2.32}$$

This result is equivalent to the usual discrete Lyapunov matrix equation

$$F^*PF - P < -Q \qquad Q \text{ positive definite} \tag{2.33}$$

where $F = F_\ell(\tilde{N}, \Delta_k)$. In other words, $P = T^*T$ is a suitable Lyapunov function and equivalently, given P satisfying Equation 2.33, then $T = P^{\frac{1}{2}}$ satisfies Equation 2.32. Equation 2.32 can be rewritten as:

$$\max_{\Delta_k \in B\Delta} \bar{\sigma}(F_\ell(\tilde{N}_T, \Delta_k)) < 1 \quad \text{for some } T \in \mathcal{C}^{n\times n}, \text{ invertible} \tag{2.34}$$

where

$$\tilde{N}_T \triangleq \begin{pmatrix} T & 0 \\ 0 & I \end{pmatrix} \begin{pmatrix} \tilde{N}_{11} & \tilde{N}_{12} \\ \tilde{N}_{21} & \tilde{N}_{22} \end{pmatrix} \begin{pmatrix} T^{-1} & 0 \\ 0 & I \end{pmatrix} \tag{2.35}$$

By comparing Equations 2.26 and 2.35, it is clear that the Lyapunov approach involves a type of scaling not unlike the optimal D scales. In this case, the "scaling" consists of a coordinate transformation T on the state variable. It is possible to reformulate Equation 2.34 by incorporating the appropriate D scales in Figure 2.8. Now, a sufficient condition for the existence of a Lyapunov function is given by

$$\inf_{T,D_2} \bar{\sigma} \left[\begin{pmatrix} T & 0 \\ 0 & D_2 \end{pmatrix} \begin{pmatrix} \tilde{N}_{11} & \tilde{N}_{12} \\ \tilde{N}_{21} & \tilde{N}_{22} \end{pmatrix} \begin{pmatrix} T^{-1} & 0 \\ 0 & D_2^{-1} \end{pmatrix} \right] = \beta < 1 \tag{2.36}$$

where D_2 commutes with Δ_k and $T \in C^{n\times n}$, invertible. To see this, note that Equation 2.36 implies

$$\|\tilde{x}_{k+1}\|^2 + \|z_k\|^2 \leq \beta^2 \left(\|\tilde{x}_k\|^2 + \|w_k\|^2 \right) \tag{2.37}$$

(where the $\tilde{}$ denotes the transformed states). The restriction on Δ_k implies that

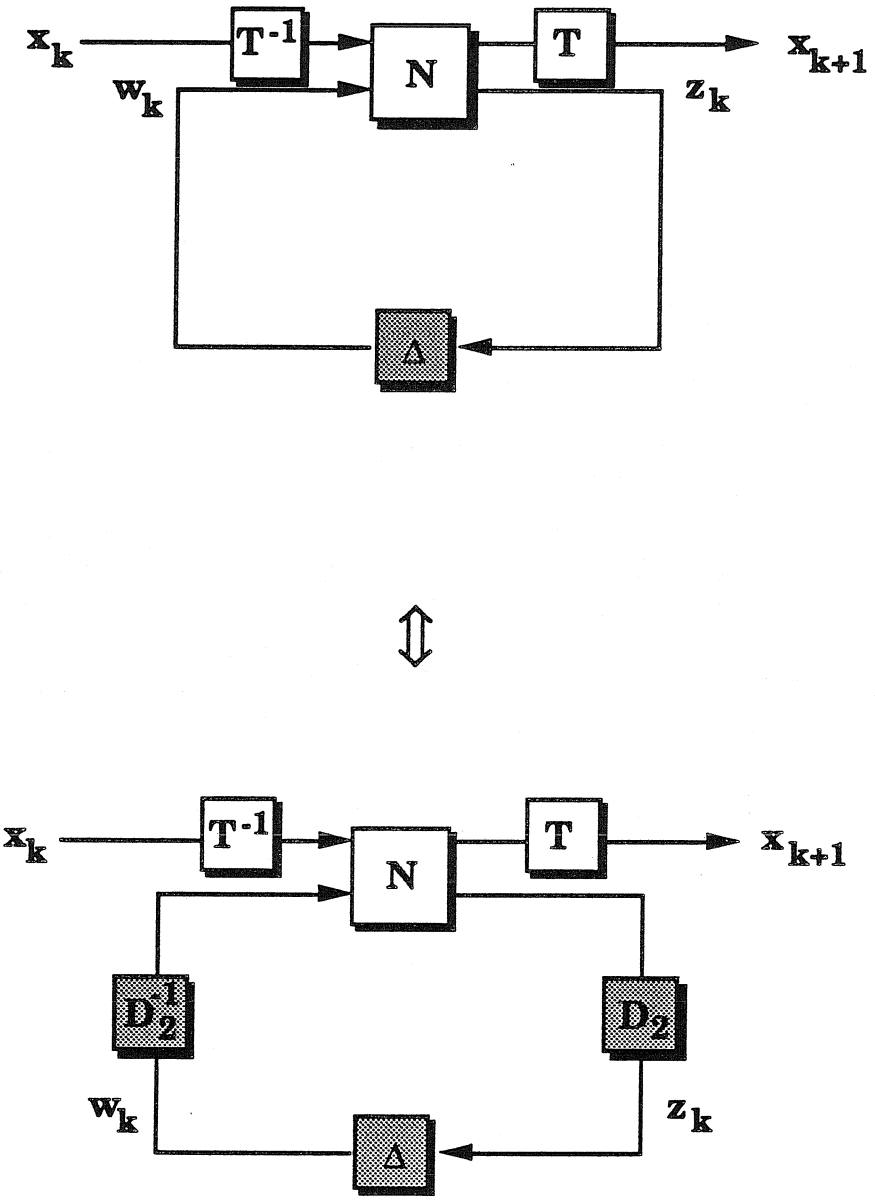

Figure 2.8. Equivalent Scaled and Transformed Loops for Robust Stability

$\|w_k\| \leq \|z_k\|$. Combining these facts we obtain:

$$\|\tilde{x}_{k+1}\|^2 \leq \beta^2 \|\tilde{x}_k\|^2 \tag{2.38}$$

But this is exactly what we are trying to obtain in Equation 2.32. This proves the sufficiency direction. For a limited, special class of uncertainties, Equation 2.36 is also necessary for the existence of a single quadratic Lyapunov function [71]. For readers familiar with structured singular value theory, this class constitutes precisely those problems for which the structured singular value is equal to its upper bound. A complete description of these uncertainty structures is given in [72].

It can be verified that the uncertainty description used in the subsequent reactor analysis is a member of this set. Consequently, the stability results for the reactor problem are completely equivalent to quadratic Lyapunov function stability results. The advantage of this technique is that a systematic method is proposed to search for the optimal scalings and transformations.

The robust performance results follow quite naturally from the above calculations. Consider the full system

$$\begin{pmatrix} x_{k+1} \\ e_k \\ z_k \end{pmatrix} = \begin{pmatrix} N_{11} & N_{12} & N_{13} \\ N_{21} & N_{22} & N_{23} \\ N_{31} & N_{32} & N_{33} \end{pmatrix} \begin{pmatrix} x_k \\ v_k \\ w_k \end{pmatrix} \tag{2.39}$$

where the uncertainty is fed back from z_k to w_k through the perturbation block Δ_k. The objective is the achievement of gain less than 1 across the v to e path for all perturbations in the set Δ_k. Consider the equivalent structures in Figure 2.9, where once again the proper scaling matrices have been introduced. Robust performance

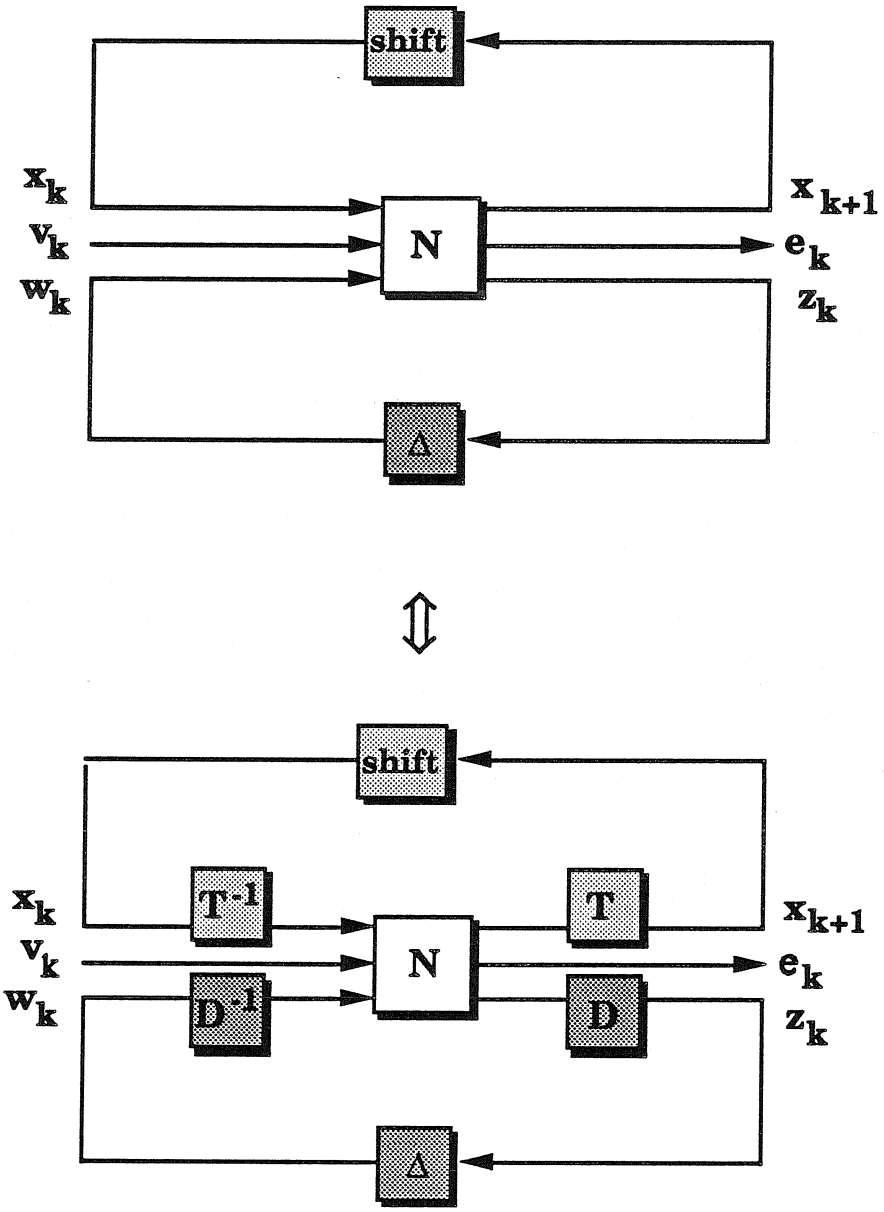

Figure 2.9. Equivalent Scaled and Transformed Loops for Robust Performance

can be guaranteed if

$$\inf_{T,D} \bar{\sigma} \left[\begin{pmatrix} T & 0 & 0 \\ 0 & I & 0 \\ 0 & 0 & D \end{pmatrix} N \begin{pmatrix} T^{-1} & 0 & 0 \\ 0 & I & 0 \\ 0 & 0 & D^{-1} \end{pmatrix} \right] = \beta < 1 \quad \forall \Delta_k \in B\Delta \tag{2.40}$$

To see this, examine the inequality implied by Equation 2.40:

$$\|\tilde{x}_{k+1}\|^2 + \|e_k\|^2 + \|z_k\|^2 \leq \beta^2(\|\tilde{x}_k\|^2 + \|v_k\|^2 + \|w_k\|^2) \tag{2.41}$$

The bound on Δ_k gives $\|w_k\|^2 \leq \|z_k\|^2$ yielding:

$$\|\tilde{x}_{k+1}\|^2 + \|e_k\|^2 \leq \beta^2(\|\tilde{x}_k\|^2 + \|v_k\|^2) \tag{2.42}$$

Summing over k from 0 to τ gives

$$\|\tilde{x}_{\tau+1}\|^2 + \|e\|_\tau^2 + (1-\beta^2)\|\tilde{x}\|_\tau^2 \leq \beta^2\|v\|_\tau^2 + \|\tilde{x}_0\|^2 \tag{2.43}$$

where the τ-norm ($\|x\|_\tau^2 = \sum_{k=0}^{\tau} \|x_k\|^2$) becomes the usual Euclidean norm in the limit as τ goes to infinity. Defining ℓ_2 as the set of 2-norm bounded discrete signals and given that $v \in \ell_2$, we can see from Equation 2.43 that $x \in \ell_2$ and $e \in \ell_2$. This implies that $\|\tilde{x}_{\tau+1}\|$ goes to zero as τ goes to infinity. If we further assume that $\tilde{x}_0 = 0$, then we arrive at the desired robust performance result:

$$\text{if } x_0 = 0 \text{ and } \{v_k\}_{k=0}^{\infty} \in \ell_2 \text{ then } \|e\| \leq \beta\|v\|$$

An entirely analogous argument can be used to interpret the result given in Equation 2.40 in terms of the so-called power norm. For vector signals $e(t)$ the power norm is defined by: $\|e(t)\|_P^2 = \lim_{\tau\to\infty} \int_{-\tau}^{\tau} \frac{1}{2\tau} e^T(t)e(t)dt$. Strictly speaking, the power norm does not satisfy all the properties of a norm. However, the class of bounded power signals is of practical interest. The argument proceeds from Equation 2.42, but now

the summation must be carried out with division by τ. In this case the $P\tau$-norm ($\|x\|_{P\tau}^2 = \sum_{k=0}^{\tau} \frac{1}{\tau}\|x_k\|^2$) becomes the power norm in the limit as τ goes to infinity. A notable difference in the calculations is that the $\tilde{x}_0$ term (finite) divided by τ goes to zero, which not unexpectedly leads to a result which is independent of the initial conditions. Defining ℓ_P as the the set of power-norm-bounded discrete signals and using the fact that $v \in \ell_P$ combined with Equation 2.43 implies that $x \in \ell_P$ and $e \in \ell_P$. This yields an alternative performance result:

$$\text{if } \{v_k\}_{k=0}^{\infty} \in \ell_P \text{ then } \|e\|_P \leq \beta\|v\|_P$$

Thus, the performance results obtained by this method are applicable to problems with bounded energy inputs and outputs and to problems with bounded power inputs and outputs. For completeness it should be noted that the induced power norm for a stable operator with power-norm-bounded inputs is the infinity norm.

In summary, the results given by Equation 2.36 and Equation 2.40 give time domain conditions which guarantee robust stability and robust performance, and are sufficient for the existence of a quadratic Lyapunov function. For certain uncertainty structures an equivalence can be shown. The primary objective of this section has been the derivation of these time domain results which are computationally simpler than the earlier frequency domain results. The minimum-maximum calculations given by Equation 2.26 and Equation 2.28 have been reduced to single infimum calculations in the time domain (Equation 2.36 and Equation 2.40).

2.3.4 Computation of Optimal Constant Ds

The unifying connection between the continuous frequency domain results of Section 2.3.2 and the discrete time domain results of Section 2.3.3 can be given by the following theorem:

Theorem 2.3 *Optimal D Scalings*

Let $\begin{pmatrix} A & B \\ C & D \end{pmatrix} \in \mathcal{R}^{(n+m)\times(n+m)}$ *be given, with all eigenvalues of* A *in the open left half plane. Let* $\mathcal{D}$ *be some set of scaling matrices.*

Then $\exists \mathbf{D} \in \mathcal{D}$ *such that*

$$\sup_{\omega} \bar{\sigma}\left(\mathbf{D}(C(j\omega I - A)^{-1}B + D)\mathbf{D}^{-1}\right) < 1 \tag{2.44}$$

iff $\exists T \in \mathcal{C}^{n\times n}$ *invertible,* $\mathbf{D} \in \mathcal{D}$ *such that*

$$\bar{\sigma}\left[\begin{pmatrix} T & 0 \\ 0 & \mathbf{D} \end{pmatrix}\begin{pmatrix} (I+A)(IA)^{-1} & \sqrt{2}(I-A)^{-1}B \\ \sqrt{2}(I-A)^{-1}C & D+(I-A)^{-1}B \end{pmatrix}\begin{pmatrix} T^{-1} & 0 \\ 0 & \mathbf{D}^{-1} \end{pmatrix}\right] < 1 \tag{2.45}$$

Proof 2.3 *Follows below.*

This result shows that constant D scalings can be found if and only if the state space test can be made. The latter minimization can be reformulated as a convex, nondifferentiable optimization, and as such, has been computationally successful [10]. The sufficiency direction will be proved as the logic fits within the framework of the previous calculations. For the necessity direction, the reader is referred to [72].

Using the block diagram in Figure 2.10, we can obtain the following inequality from Equation 2.45:

$$\|z\|^2 + \|a\|^2 < \|w\|^2 + \|b\|^2 \tag{2.46}$$

Operation by $e^{i\theta}I$ preserves norm, so $\|b\| = \|a\|$ and thus $\|z\| < \|w\|$. Noting that the T matrices commute with the diagonal $e^{i\theta}I$, we can define the following discrete transfer function from w to z:

$$T_{wz}(e^{i\theta}I) = \mathbf{D}[\tilde{D} + \tilde{C}z(I - \tilde{A}z)^{-1}\tilde{B}]\mathbf{D}^{-1} \tag{2.47}$$

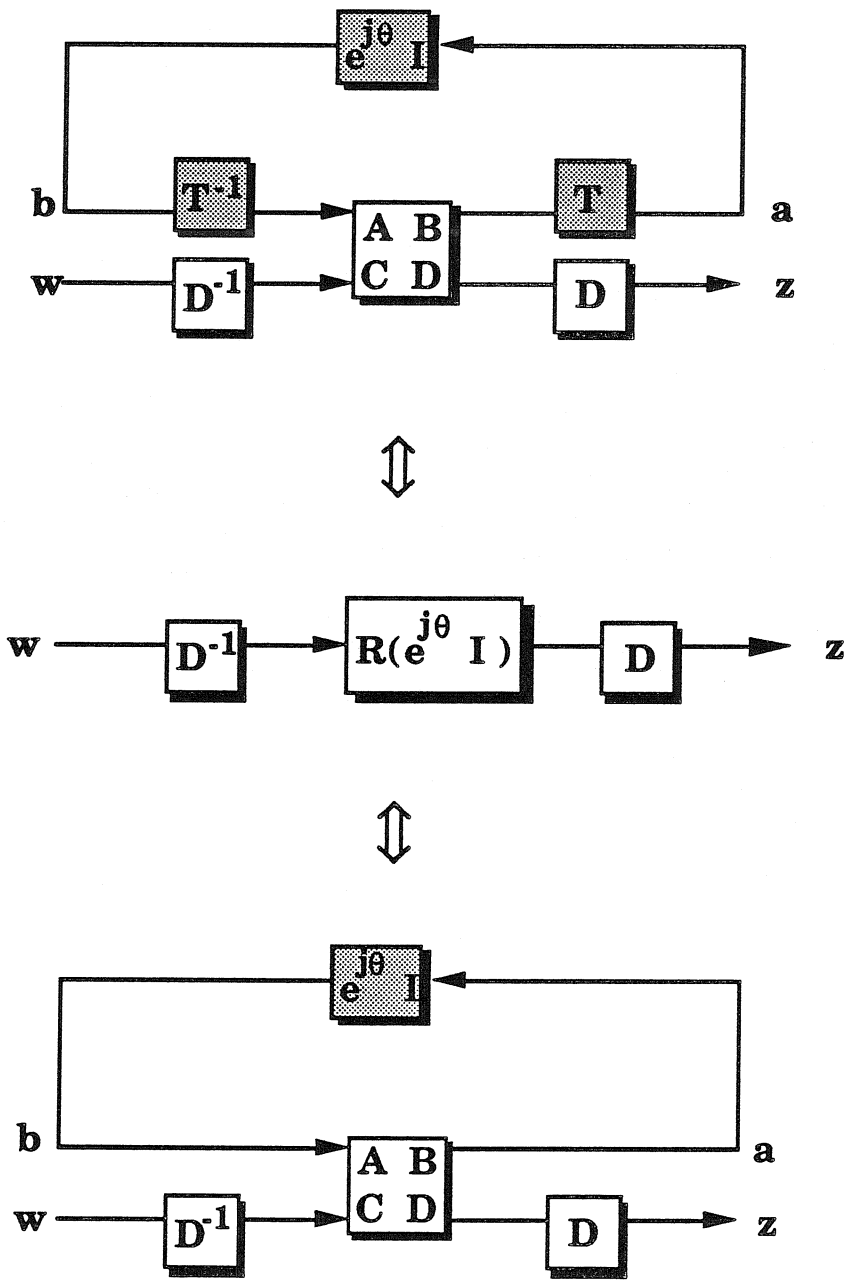

Figure 2.10. Equivalent Transformed Discrete Systems

where $\tilde{A}, \tilde{B}, \tilde{C}, \tilde{D}$ are the discrete state space elements given in Equation 2.45. Since $\|z\| < \|w\|$ then

$$\bar{\sigma}(\mathbf{D}T_{wz}(e^{i\theta}I)\mathbf{D}^{-1}) < 1 \quad \forall\theta \tag{2.48}$$

or equivalently,

$$\|\mathbf{D}T_{wz}(e^{i\theta}I)\mathbf{D}^{-1}\|_{\infty} < 1 \tag{2.49}$$

But this is equivalent to Equation 2.44, where (A, B, C, D) is the continuous state space representation of $T_{wz}(s)$.

2.3.5 Scaling and Performance Degradation

The potential difficulty of the theorems 2.1 and 2.2 is the dependence of the results on the specified perturbation bounds. Results with greater flexibility can be derived by introducing a scaling factor $\gamma(< 1)$ into the robust stability result of theorem 2.1. The Small Gain Theorem allows for a scaling on M_{22} provided that Δ is scaled by the inverse of γ. Thus, the requirement stated in theorem 2.1 becomes $\inf_D \sup_\omega \bar{\sigma}(D\gamma M_{22}D^{-1}) < 1 \quad \forall\bar{\sigma}(\Delta) \leq \gamma$. Theorem 2.2 already reveals the relationship between the achievable performance and the maximum singular value of the closed loop. If the error signal is scaled by $\alpha(< 1)$ until β is just less than 1, then the achievable performance level is $1/\alpha$. This can be seen clearly in Figure 2.11, where the scalings α and γ are depicted. In this manner it is possible to analyze the effect of perturbation size on performance level:

Theorem 2.4 *(Performance Degradation; Time-Varying, Complex Δ)*

Consider $M: \begin{pmatrix} v \\ w \end{pmatrix} \rightarrow \begin{pmatrix} e \\ z \end{pmatrix}$ *such that* $e = F_\ell(M, \Delta)v$ *and* $\Delta \in B\mathbf{\Delta}$.

Let $\inf_{D_1} \bar{\sigma}(D_1\gamma M_{22}D_1^{-1}) < 1$.

Define $\alpha_\gamma = \max_{\alpha>0}\{\alpha | \inf_{D_2} \sup_\omega \bar{\sigma}(D_2 M_\alpha D_2^{-1}) < 1\}$

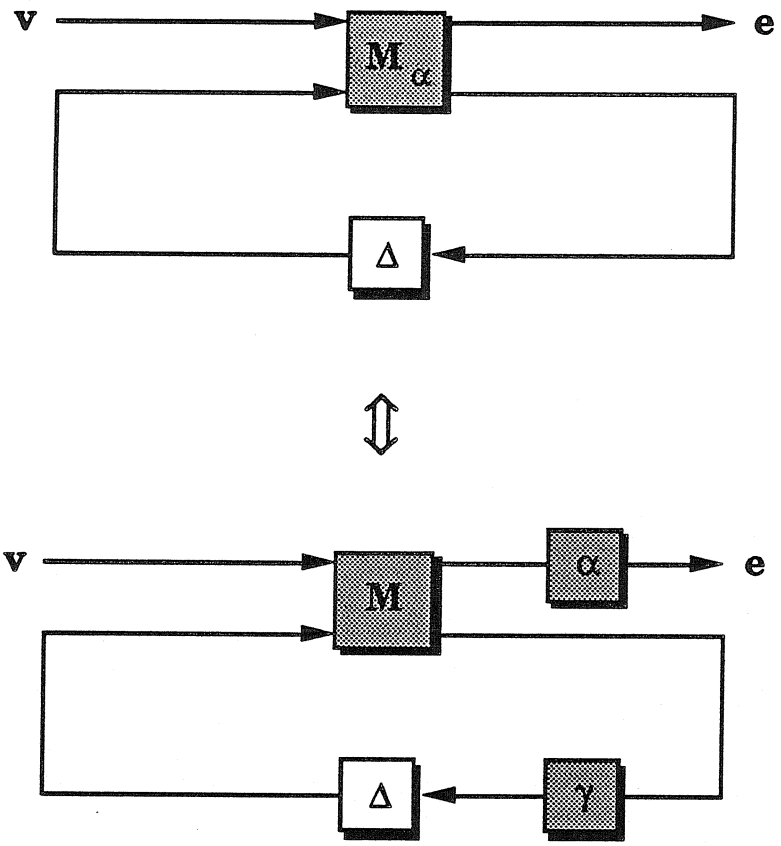

Figure 2.11. Scalings for Performance Degradation

$$\textit{where } M_\alpha = \begin{pmatrix} \alpha M_{11} & \alpha M_{12} \\ \gamma M_{21} & \gamma M_{22} \end{pmatrix}$$

$$\textit{then } \inf_{D_2} \sup_{\Delta \in \gamma B\Delta} \bar{\sigma}(D_2 M D_2^{-1}) = \tfrac{1}{\alpha\gamma}$$

Proof 2.4 *Follows from above discussion.*

A final remark should be made concerning the results of the previous sections. For the special case of linear time-invariant perturbations, there exist necessary and sufficient conditions for robust stability and robust performance. The results involve a test on the so-called structured singular value, for which the D-scaled maximum singular value is an upper bound. The reader is referred to [18] for further details. In addition, theoretical results have recently been obtained for the case of real perturbations [11], [94]. This method shares some of the computationally attractive features

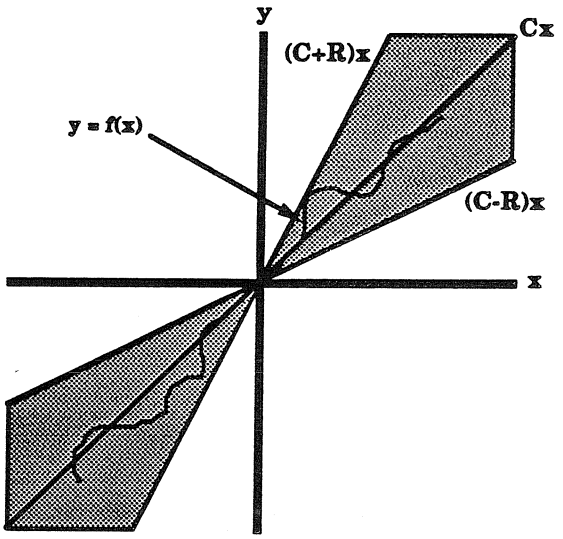

Figure 2.12. Conic Sector (C,R)

of the previously discussed problems.

2.3.6 Conic-Sector Bounded Nonlinearities

In this section, a class of nonlinear systems is described which fits into the previously described $M - \Delta$ structure. A conic sector can be interpreted as the bounds on a linear approximation to a nonlinear or time-varying operator. Rigorously speaking, a conic sector is defined as

$$\text{Cone}(C, R) \equiv \{(x, y) | \|y - Cx\| \leq \|Rx\|\} \tag{2.50}$$

where (x, y) is the input-output pair for a general nonlinear operator, $y = f(x)$, (see Figure 2.12). (This is a simplistic representation and will be expanded in the next chapter to include correlations between the outputs.) Evidently, a nonlinear operator enveloped tightly by a conic sector is most accurately approximated (linearly) by the cone center C. In general, the cone center will not coincide with the plant described by the Jacobian of the nonlinear model evaluated at an operating point. The model suggested by the cone formulation is more sensitive to variations in the nonlinearities

over the operating range. Further research is being conducted to assess the value of this linear approximation over the standard Taylor series approximation for certain control applications.

Note that because we have replaced a potentially highly nonlinear operator by a function consisting of two linear time-invariant operators, the cost of this simplification is increased conservatism. The cone (C, R) describes many input-output pairs, some of which may yield worse performance than the original operator.

It should be clear that there exists a direct correspondence between a nonlinear cone-bounded operator and a time-varying gain. From the conic sector definition, the plant can be interpreted as being equal to the nominal value (C) which is perturbed by a time varying gain of magnitude R. R and C are absorbed into the system to arrive at the general structure in Figure 2.4, where now Δ is a time-varying gain of norm 1. It should be noted that in a strict sense, constant Ds do not commute with cone-bounded nonlinearities in the sense that Equation 2.22 is not satisfied. However, the similarity transformation on Δ by constant Ds does remain within the original cone bound on Δ. Thus, the necessary norm inequalities given in Theorems 2.1 and 2.2 still hold.

A final calculation should clarify the connection between general conic-sector-bounded nonlinear dynamics and the conventional state space uncertainty structure. Consider the nonlinear system

$$\begin{aligned} \dot{x} &= f(x) + bu \\ y &= cx \end{aligned} \tag{2.51}$$

where $y, u \in \mathcal{R}^1$. Assume that f is inside the cone (A_0, A_1) where A_1 has rank 1. Introduce the time-varying scalar parameter Δ_1 which can take on values between -1

and 1 and the system in Equation 2.51 becomes

$$\begin{aligned} \dot{x} &= A_0 x + \Delta_1 A_1 x + bu \\ y &= cx \end{aligned} \tag{2.52}$$

or:

$$\begin{pmatrix} \dot{x} \\ y \end{pmatrix} = \left[\begin{pmatrix} A_0 & b \\ c & 0 \end{pmatrix} + \Delta_1 \begin{pmatrix} A_1 & 0 \\ 0 & 0 \end{pmatrix} \right] \begin{pmatrix} x \\ u \end{pmatrix} \tag{2.53}$$

Factor the A_1 term in to two vectors (by singular value decomposition for higher order problems):

$$A_1 = a_1 \cdot b_1^T \tag{2.54}$$

Then the plant is given by $F_u(N, \Delta_1)$ where

$$N = \begin{pmatrix} A & b & a_1 \\ c & 0 & 0 \\ b_1 & 0 & 0 \end{pmatrix} \tag{2.55}$$

The details of the construction of interconnection structures for more general uncertainty descriptions can be found in [67].

2.4 Controller Design for a Nonlinear CSTR Model

The case study under consideration is regulation of outlet reactant concentration, which is assumed to be measured. Coolant temperature is the manipulated variable; input saturations will not be considered. The control objective will be the accurate tracking of step changes in the concentration set point. Two sets of parameter values will be investigated, one which was introduced in section 2.2. The other ($\mathbf{B} = 1.0, \beta = 0.3, \gamma = 20.0, \mathcal{D}a = 0.072$) yields an open-loop system with a single stable steady state for all fixed values of the input. In each of the two cases, the goal of the controller analysis will be the construction of an operating range or "window" in the phase

plane over which certain robustness properties are guaranteed.

2.4.1 Uncertainty Characterization

In section 2.3 it was shown that for conic-sector-bounded nonlinearities, it is possible to formulate a structured uncertainty interconnection structure. In this subsection we show how the CSTR dynamics can be treated as a time-varying linear operator. First, the dynamics are represented in deviation variables so that the origin is a fixed point. Note that a cone-bounded operator must satisfy this property. Consequently, the nominal or center plants are limited to points along the fixed-point operating curve. The equations are:

$$\begin{aligned}
\dot{\tilde{x}}_1 &= \tilde{f}_1 = -\tilde{x}_1 - x_{10} + \mathcal{D}a(1 - \tilde{x}_1 - x_{10})e^{\frac{\tilde{x}_2 + x_{20}}{1+(\tilde{x}_2+x_{20})/\gamma}} \\
\dot{\tilde{x}}_2 &= \tilde{f}_2 - \beta u = -\tilde{x}_2 - x_{20} + \mathbf{B}\mathcal{D}a(1 - \tilde{x}_1 - x_{10})e^{\frac{\tilde{x}_2 + x_{20}}{1+(\tilde{x}_2+x_{20})/\gamma}} \\
&\quad -\beta(\tilde{x}_2 + x_{20}) - \beta(\tilde{u} + u_0)
\end{aligned} \tag{2.56}$$

The nonlinearity in these equations is solely a function of the state variables and therefore would be equivalent to uncertainty in the state-space A matrix, provided that $\tilde{f}_1, \tilde{f}_2$ can be shown to be conic-sector bounded.

Two physical insights should be observed here. First, the dimensionless concentration (or conversion), x_1, is physically limited to positive values less than or equal to 1. Second, the exponential term reaches an asymptotic value of e^{γ} for large temperature, x_2, and equals 1 when the reactor temperature approaches the inlet temperature. The physics of the problem already impose some useful bounds on the state variables. For the purposes of this study, we will impose bounds on the state variables which define an operating window in the phase-plane. Consider the nominal point (x_{10}, x_{20}), a window width (x_{1r}, x_{2r}), and a plot of $\tilde{f}_1$ and $\tilde{f}_2$ (Figure 2.13). A simple calculation

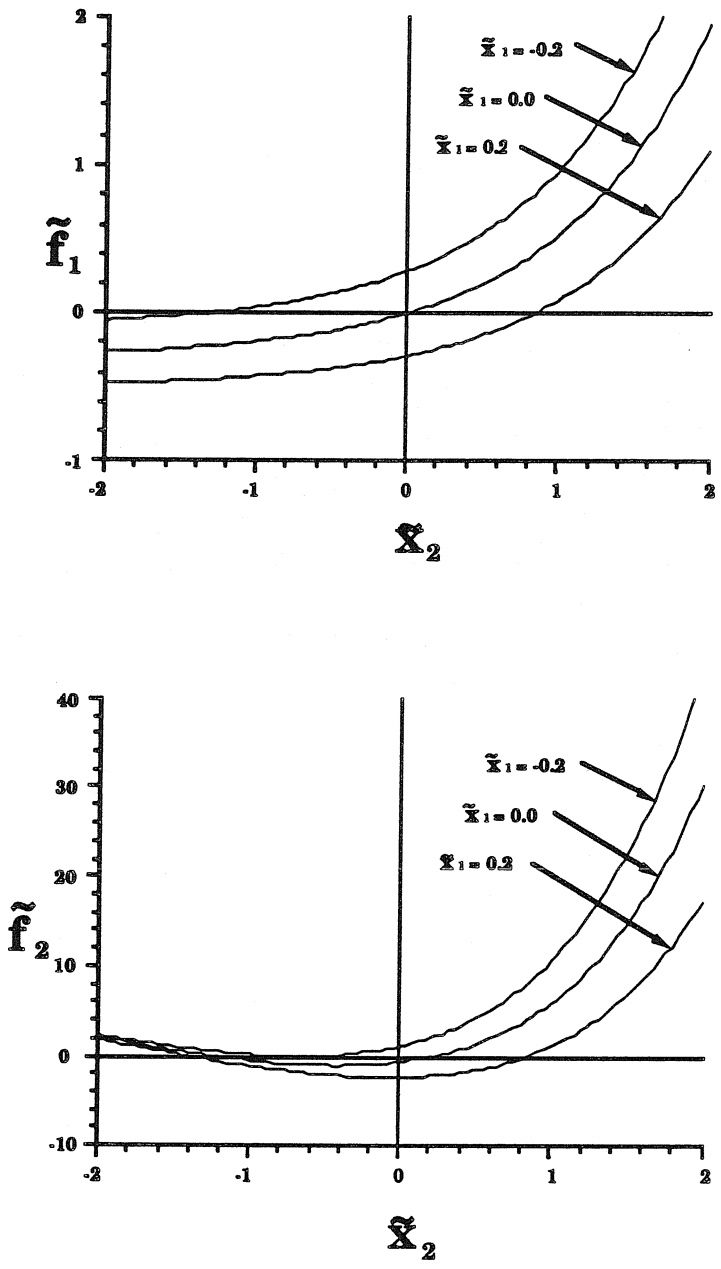

Figure 2.13. Contour Plots of Nonlinearity

reveals that the following bounds are valid

$$\begin{pmatrix} \tilde{f}_1 \\ \tilde{f}_2 \end{pmatrix} = \begin{pmatrix} \gamma_{11} & \gamma_{12} \\ \gamma_{21} & \gamma_{22} \end{pmatrix} \begin{pmatrix} \tilde{x}_1 \\ \tilde{x}_2 \end{pmatrix} \tag{2.57}$$

where

$$\begin{aligned}
-1 - \mathcal{D}ae^{\frac{x_{20}-x_{2r}}{1+(x_{20}-x_{2r})/\gamma}} &\leq \gamma_{11} \leq -1 - \mathcal{D}ae^{\frac{x_{20}+x_{2r}}{1+(x_{20}+x_{2r})/\gamma}} \\
\gamma_{12LB} &\leq \gamma_{12} \leq \gamma_{12UB} \\
\gamma_{12LB} &= \tfrac{-1}{x_{2r}}\mathcal{D}a(1 - x_{10} - x_{1r})(e^{\frac{x_{20}}{1+x_{20}/\gamma}} - e^{\frac{x_{20}-x_{2r}}{1+(x_{20}-x_{2r})/\gamma}}) \\
\gamma_{12UB} &= \tfrac{1}{x_{2r}}\mathcal{D}a(1 - x_{10} + x_{1r})(e^{\frac{x_{20}+x_{2r}}{1+(x_{20}+x_{2r})/\gamma}} - e^{\frac{x_{20}}{1+x_{20}/\gamma}}) \\
\gamma_{11} &= C_{11} \pm R_{11} \\
\gamma_{12} &= C_{12} \pm R_{12} \\
\gamma_{21} &= \mathbf{B}(C_{11} + 1) \pm \mathbf{B}R_{11} = C_{21} \pm R_{21} \\
\gamma_{22} &= (-1 - \beta + \mathbf{B}C_{12}) \pm \mathbf{B}R_{12} = C_{22} \pm R_{22}
\end{aligned} \tag{2.58}$$

where C and R are derived in a straightforward manner from the upper and lower bounds above. Utilizing these bounds, it is possible to formulate a cone for the nonlinearities which consists of two independent uncertain gains. Intuitively, this accounts for both the exponential temperature dependence of the reaction rate and the coupling between the concentration and temperature in the rate expression. Our final plant description is given by

$$G_\Delta : \begin{pmatrix} \dot{x} \\ y \end{pmatrix} = \left[\begin{pmatrix} A & B \\ C & O \end{pmatrix} + \Delta_1 \begin{pmatrix} A_1 & 0 \\ 0 & 0 \end{pmatrix} + \Delta_2 \begin{pmatrix} A_2 & 0 \\ 0 & 0 \end{pmatrix} \right] \begin{pmatrix} x \\ u \end{pmatrix} \tag{2.59}$$

where

$$\begin{aligned}
A &= \begin{pmatrix} C_{11} & C_{12} \\ C_{21} & C_{22} \end{pmatrix}; \quad A_1 = \begin{pmatrix} R_{11} & 0 \\ R_{12} & 0 \end{pmatrix}; \\
A_2 &= \begin{pmatrix} 0 & R_{21} \\ 0 & R_{22} \end{pmatrix}; \quad B = \begin{pmatrix} 0 \\ \beta \end{pmatrix}; \qquad C = [1 \quad 0]
\end{aligned} \tag{2.60}$$

and is in the general structure of Figure 2.4 for structured singular value analysis.

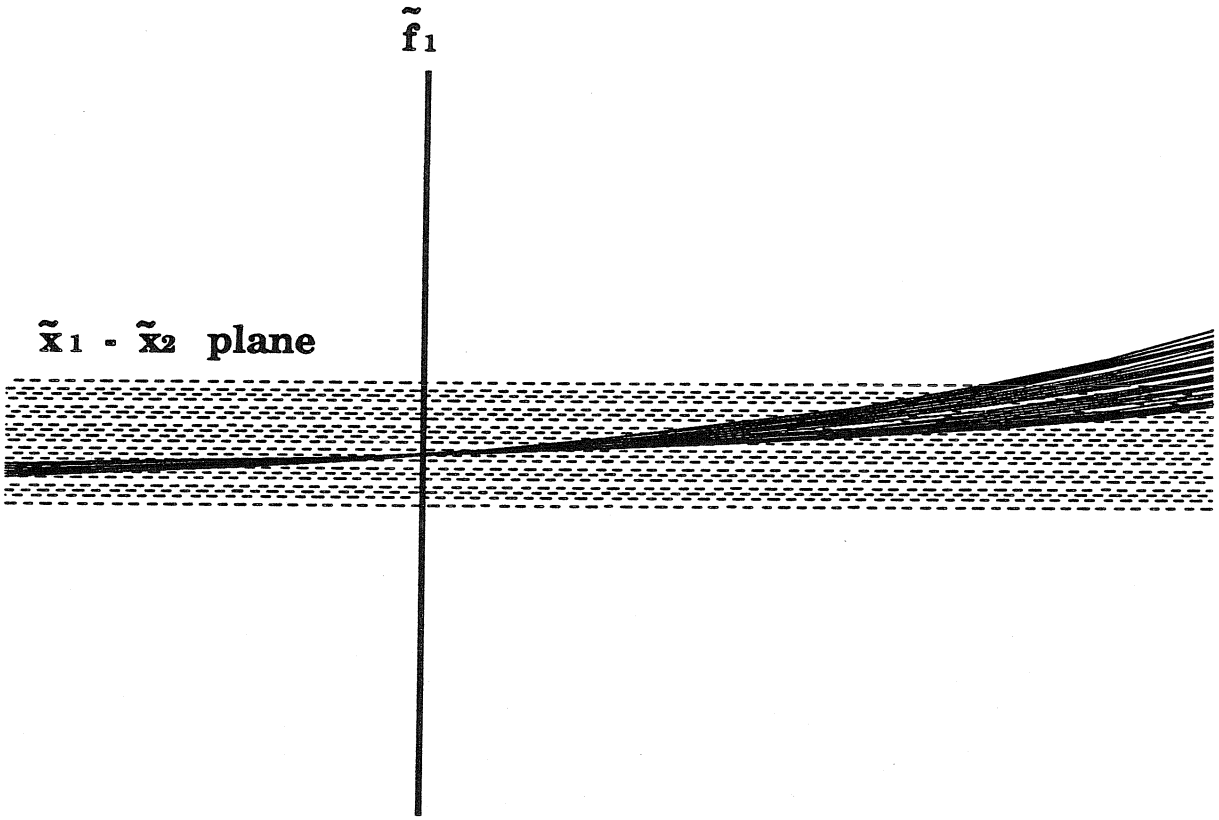

Figure 2.14. Three-Dimensional Plot of Nonlinearity

Actually, a deeper analysis of the problem reveals that it is possible to formulate a tighter conic-sector bound with only one uncertain gain. This is due to the linear dependence of the rate expression on the concentration. This can be seen in a three-dimensional plot, (Figure 2.14), where with the proper perspective on the $\tilde{x}_1 - \tilde{x}_2$ plane, the nonlinearity falls within a well-defined "bow-tie" region. The nonlinearity is bounded by two planes, both perpendicular to the plane of observation in the figure.

Now the plant description is given by

$$G_\Delta : \begin{pmatrix} \dot{x} \\ y \end{pmatrix} = \left[\begin{pmatrix} \tilde{A} & B \\ C & O \end{pmatrix} + \Delta_1 \begin{pmatrix} \tilde{A}_1 & 0 \\ 0 & 0 \end{pmatrix} \right] \begin{pmatrix} x \\ u \end{pmatrix} \tag{2.61}$$

where

$$\tilde{A} = \begin{pmatrix} \tilde{C}_{11} & \tilde{C}_{12} \\ \tilde{C}_{21} & \tilde{C}_{22} \end{pmatrix}; \quad \tilde{A}_1 = \begin{pmatrix} \tilde{R}_{11} & \tilde{R}_{12} \\ \tilde{R}_{21} & \tilde{R}_{22} \end{pmatrix}; \quad B = \begin{pmatrix} 0 \\ \beta \end{pmatrix}; \quad C = [1 \quad 0] \tag{2.62}$$

and $\tilde{A}, \tilde{A}_1$ are easily calculated from Equation 2.58 and basic trigonometric manipulations.

A formal numerical procedure for calculating these uncertainty structures and selecting the optimal uncertainty formulation is presented in the next chapter.

The calculations in the following sections are based upon an uncertainty description consisting of two independent uncertain complex gains.

2.4.2 H_2-Optimal Controller Design

A convenient choice of control objective is the minimization of the integral square error (ISE) or the 2-norm of the error for a specific input (e.g., a step input). Following the IMC procedure [67], one can readily derive the H_2-optimal controller. The family of plants under consideration for the CSTR consists of second order, minimum phase systems which may have 0 or 1 unstable pole. The procedure requires a nominal linear plant, which will be taken to be the center of the cone defined by the chosen operating window. If this model is designated as $P_m(s)$, then the controller is given by:

$$C_{IMC}(s) = P_m^{-1}(s)F(s) \tag{2.63}$$

Here $F(s)$ is a low-pass filter which renders the controller proper, allows for asymptotic tracking properties, and provides robustness. For stable systems $F(s)$ is given by $(\lambda s + 1)^{-2}$, while for unstable systems the filter structure is more complicated

$$F(s) = \frac{(s - p_1)(s - p_2)(a_0 s + 1)}{(\lambda s + 1)^3 - a_0 s - 1}; \quad a_0 = \frac{((\lambda p_1 + 1)^3 - 1)}{p_1} \tag{2.64}$$

where p_1 is the unstable pole and p_2 the stable one.

The filter time constant affects the speed of the closed-loop response and can be increased (detuned) to achieve robust stability at the expense of reduced performance ($\lambda = 0$ is H_2-optimal).

2.4.3 H_∞-Optimal Controller Design

For the unstable operating condition, we will consider, as an alternative to the H_2-optimal control objective, the minimization of the error for a set of inputs of bounded two-norm. This class includes steps, pulses and narrow-band signals of various frequencies. As mentioned in section 2.3.1, the operator norm induced by the two-norm is the infinity norm. Consequently, this optimization entails a minimization of the infinity-norm of the weighted sensitivity operator. The appropriate weight is chosen to reflect the expected inputs and the desired performance. A reasonable selection is the inverse of the nominal closed-loop sensitivity function weighted by a scalar gain (< 1). A transfer function of the form $\frac{as}{bs+1}$ closely follows the nominal sensitivity and also "pushes" for zero error at steady state.

The aforementioned weights can be used in analyzing the closed-loop system (with weights absorbed) for robustness properties. An H_∞-optimal method can be used to find the controller, K, which solves:

$$\|F_\ell(M, \Delta)\|_\infty \leq 1 \tag{2.65}$$

where M represents the weighted closed-loop sensitivity function. The optimal K is found by a search over all stabilizing K's and scaling D's so that the quantity

$$\|DF_\ell(M, \Delta)D^{-1}\|_\infty \tag{2.66}$$

is minimized. For this problem, since only constant D's commute properly, it is

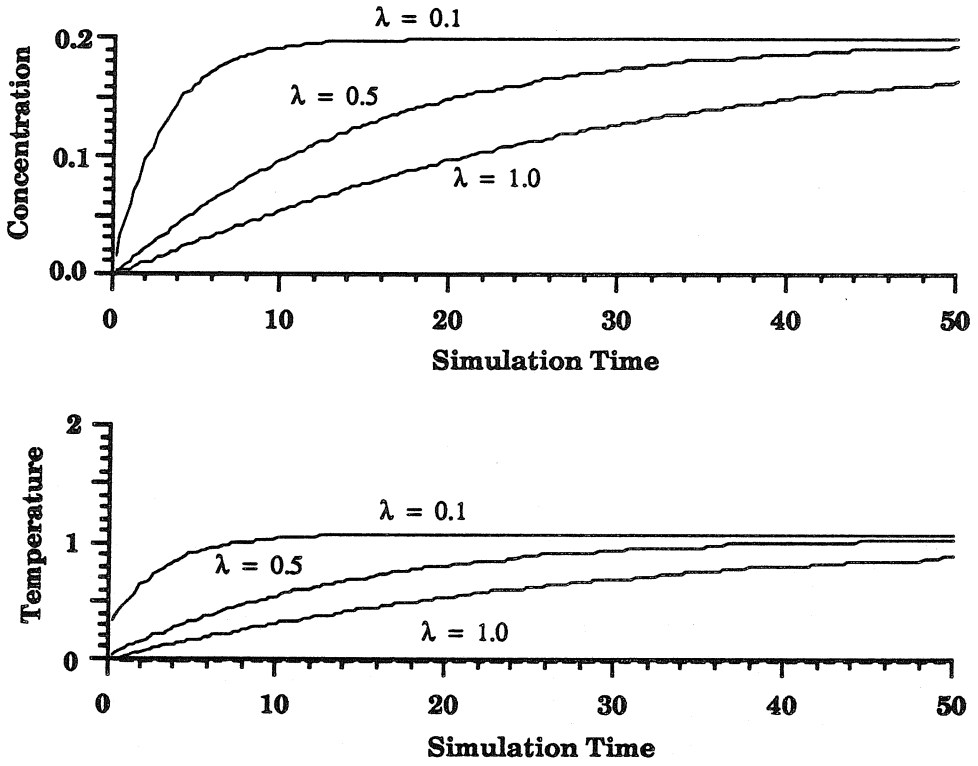

Figure 2.15. IMC Simulation

straightforward to set up a grid and search for the optimal scaled H_∞-solution.

2.5 Computational Results

2.5.1 Single, Stable Steady State ($x_{10} = 0.3, x_{20} = 1.96$; uncontrolled)

$[\mathbf{B} = 1.0, \beta = 0.3, \gamma = 20.0, \mathcal{D}a = 0.072]$

For this case study, a relatively mild operating condition was considered with the expectation that robustness properties can be established for a large window in the phase plane. The operating window is defined to be: $|x_1 - 0.3| \leq 0.3, |x_2 - 1.96| \leq 1.96$. Throughout this window the open-loop poles along the operating curve vary from -1.1 to -1.8.

An IMC controller was designed for this stable system and the simulation results are shown in Figure 2.15. In this plot, the concentration and temperature profiles are

given for a setpoint change of magnitude 0.2 in the concentration for various values of the filter parameter λ. The role played by this tuning parameter is evident, although a prediction of the transient response is only possible in a local neighborhood of the operating point where the linear model is valid. It can be seen in Figure 2.15 that the initial speed of response varies inversely with the magnitude of λ (as expected). Balancing the tradeoff between fast response and bounded initial transients, a value of $\lambda = 0.1$ was selected for the IMC controller.

An analysis of the robust stability of the closed-loop system yields a scaled maximum singular value of 0.9 for the IMC controller. Thus, stability is assured throughout the entire operating window and could in fact be extended to include a region approximately 10% larger. An analytical performance evaluation of the controller is shown in the performance degradation plots of Figure 2.16. Presented here is a plot of the attainable performance level measured by the infinity-norm versus the magnitude of the perturbation (Δ). The intercept of the curve at the y-axis represents the nominal performance (zero perturbation) while perturbation magnitude corresponding to the vertical asymptote represents the SSV for robust stability (no performance). Another interpretation of the x-axis is the necessary reduction factor for the window to achieve a given performance level. An important point to note is that these performance bounds are only guaranteed when the system states remain with the described operating window. An additional curve is included in this plot. It represents the necessary and sufficient condition for robust performance with time-invariant perturbations. The distance between the two curves indicates both the sufficiency of the time-varying result and the additional constraint that time-varying perturbations place on performance levels above those imposed by time-invariant perturbations. Thus, if the two curves lie close together, then the time-varying result is not particularly conservative.

A final plot is given to substantiate the claim that the chosen operating window is

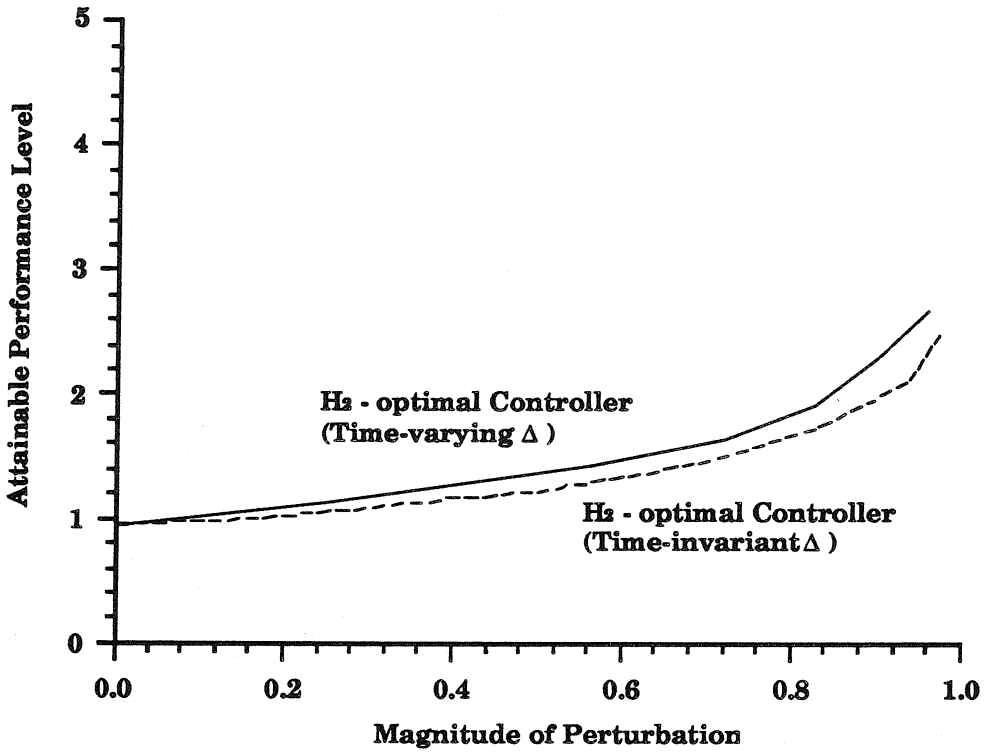

Figure 2.16. Performance Degradation Curve (Stable Case)

physically meaningful. In Figure 2.17, the transient responses of the system to various setpoint changes and step disturbances are given in the $x_1 - x_2$ phase plane. It can be seen that, for these examples, the system trajectories remain within the operating window, thus validating the assumptions required for the robustness results.

2.5.2 Multiple Steady States (uncontrolled) [B $= 22.0, \beta = 3.0, \mathcal{D}a = 0.082, \gamma \to \infty$]

The second case study presents a more formidable control challenge. Consequently, both H_2 and H_∞-optimal controllers have been designed for this case study. For the chosen parameter values, the open-loop dynamics are somewhat pathological as

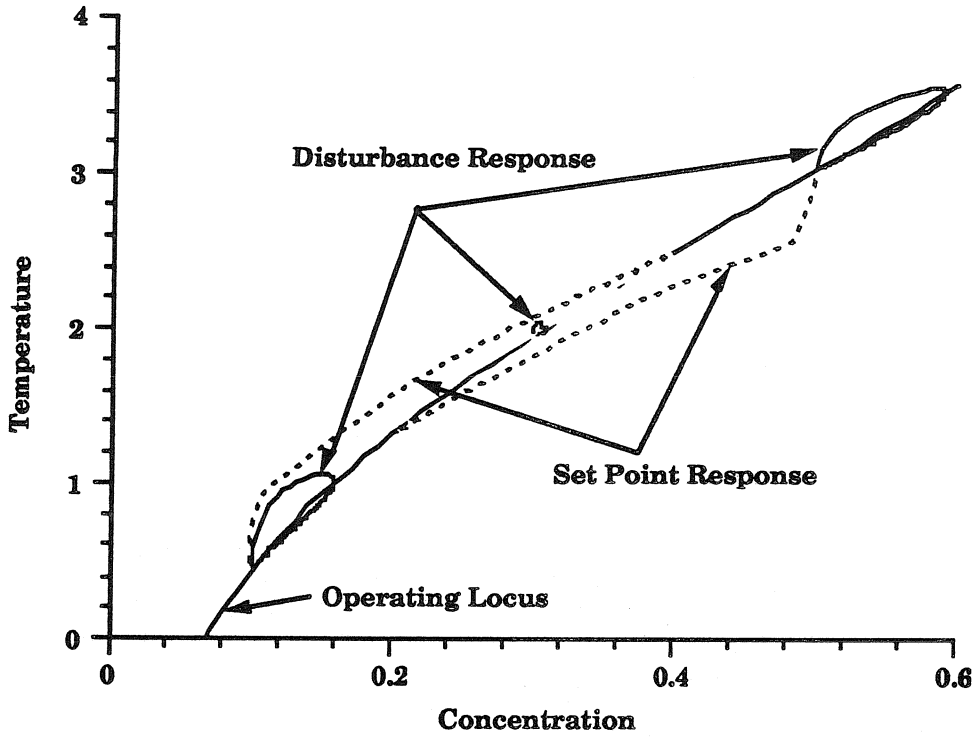

Figure 2.17. Trajectories in Operating Window (Stable Case)

evidenced in Figure 2.1. In this case, the control objective is the construction of a window about the open-loop operating point ($x_1 = 0.305, x_2 = 1.677, u = 0$). The chosen operating region is: $|x_1 - 0.305| \leq 0.2, |x_2 - 1.677| \leq 1.677$. The open-loop poles along the operating curve in this window range from $(1.4 \pm 0.35i)$ to $(-0.54, 5.5)$. This window also encompasses the stable uncontrolled fixed point $x_1 = 0.184, x_2 = 1.014$.

Following the design approach of the previous subsection, an IMC controller is constructed and the tuning parameter is chosen to be $\lambda = 0.1$. Using an output performance weight of $(\frac{s+0.5}{1.9s})$, an H_∞-optimal controller was designed to achieve the infimum in theorem 2.2. A comparison of the transient response of the CSTR system implemented with the two controllers can be seen in Figure 2.18.

Robust stability analysis yields scaled maximum singular values of 0.9 for the IMC controller and 1.1 for the H_∞-optimal controller. In this case, the H_2-optimal closed

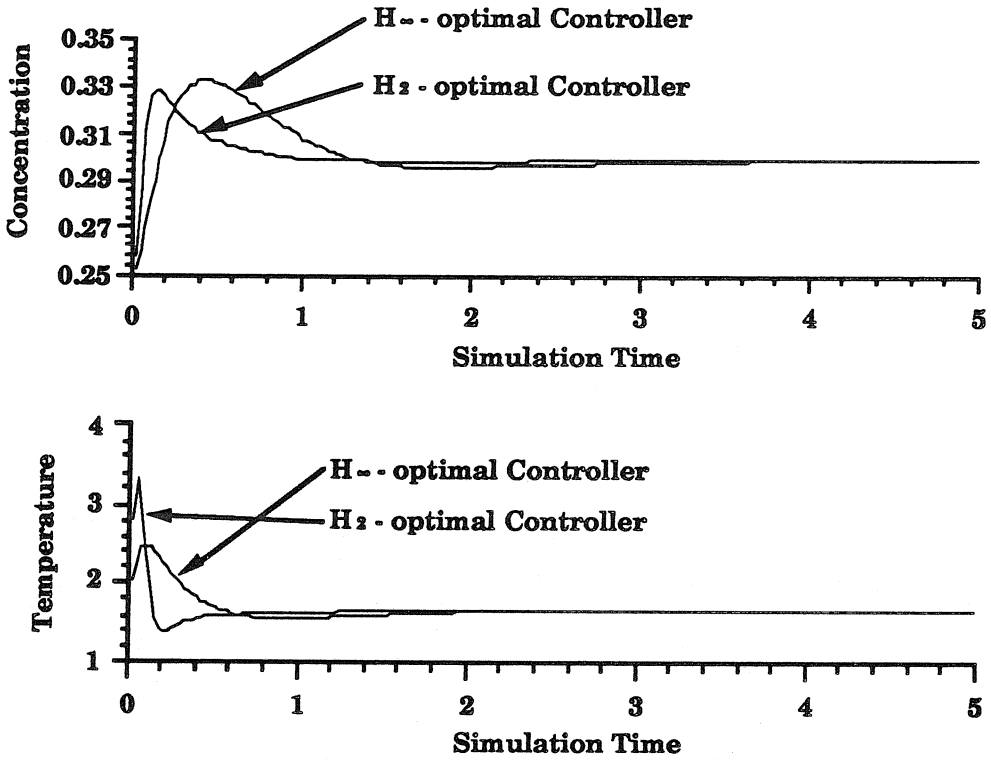

Figure 2.18. H_2 and H_∞ Optimal Simulations (Unstable Case)

loop has guaranteed stability throughout the phase window but the H_∞-optimal controller yields a stable closed loop throughout a region approximately 10% smaller than the chosen window.

The performance degradation curves for these two controllers are given in Figure 2.19. The achievable performance levels are not as low as for the first case study, which is not surprising given the range of uncertainty for the latter, more pathological case. It can be seen that for this sufficiency measure, the H_∞-optimal controller gives a better performance guarantee. It is important to realize that since the analysis results are only sufficient, a comparison of relative performance levels for the two controllers is meaningless. Only upper bounds on guaranteed performance can be inferred. Included in the same figure are the corresponding necessary and sufficient performance degradation curves for time-invariant perturbations. Finally, the transient responses in the phase plane, shown in Figure 2.20, validate the utility of the

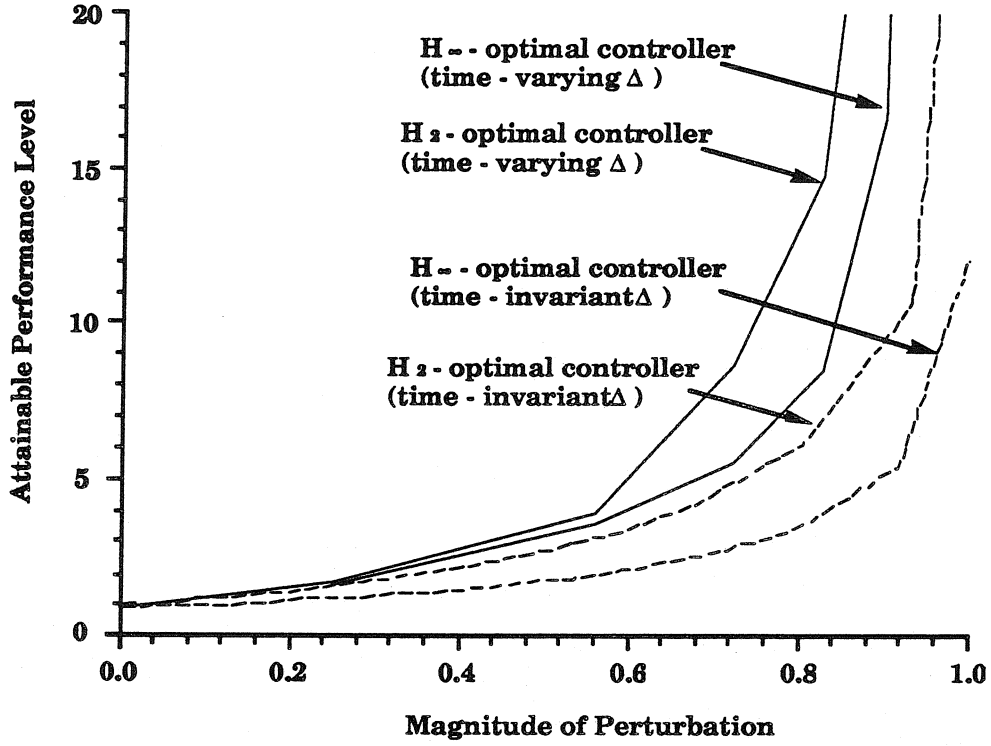

Figure 2.19. Performance Degradation Curve (Unstable Case)

chosen window for a range of operating conditions.

State space realizations of the controllers used in the preceding sections can be found in Table 2.3.

2.5.3 Interpretation of Results

For purposes of comparison, several quadratic Lyapunov functions are calculated for the specific nonlinearities which describe the CSTR system. Using the standard techniques described in [74], regions of attraction are constructed for the open-loop CSTR system, that is areas from which no trajectories can escape. Thus, this stability analysis is for an unforced (zero-input) system. These regions are depicted in Figure 2.21.

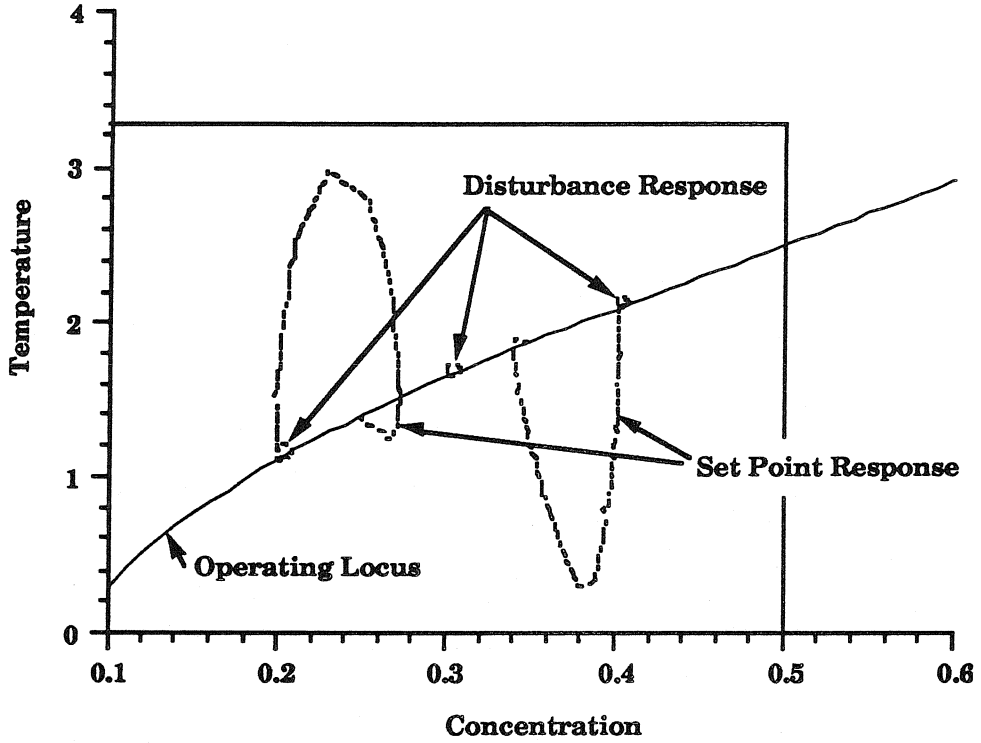

Figure 2.20. Trajectories in Operating Window (Unstable Case)

Also shown in this diagram is the ellipse defined by the Lyapunov function x^*T^*Tx (Equation 2.32) corresponding to the optimal D-scalings which were computed for the open-loop time-varying uncertainty description. The D-scalings are 2-by-2 matrices which give the general orientation and shape of the ellipse; the radius is determined by inscribing the ellipse in the operating window. The ellipse cannot exceed the calculated window since this would violate the conic-sector bound and thus invalidate the stability results. In other words, there is no stability guarantee for trajectories originating outside the operating window. The large disparity in size between the specific regions of attraction for the nonlinearity and the ellipse for the cone can be readily explained by the fact that the cone contains many nonlinearities. The latter region corresponds to the worst case nonlinearity in the cone, which is evidently more pathological than the specific nonlinearity under consideration. This point is elucidated by considering that the cone encompasses not only the nonlinear effects,

Table 2.3 Controllers for Simulations

H_2-optimal Controller, Stable Operating Condition:

$7.489E-2$	1	0
$-1.5035E0$	$-2.008E1$	1
0	$-1.795E3$	$1.0E2$

H_2-optimal Controller, Unstable Operating Condition:

6.749	1	0	0
$-5.298E-1$	$-5.072E-2$	1	0
0	$-1.020E0$	$-3.670E1$	1
$-1.223E-11$	$-1.819E-12$	$-1.868E4$	$5.446E2$

H_∞-optimal Controller, Unstable Operating Condition:

$-2.658E1$	$8.549E-1$	$-7.510E-17$	$-2.462E1$
$-3.928E4$	$-3.569E3$	$2.597E4$	$-4.493E2$
0	0	0	1
$-1.294E4$	$-1.194E3$	$8.658E3$	0

but also covers model uncertainty, which alters the nonlinear curves lying within the cone. Thus, the critical nonlinearity can be interpreted as the worst case unmodeled dynamics which fit within the cone.

Another interesting comparison is illustrated in Figure 2.22. Here the operating windows and respective regions of attraction are depicted for the open- and closed-loop (H_2-optimal) systems obtained from the two different conic-sector descriptions given in section 2.4.1. For closed-loop systems, the computation of the quadratic Lyapunov function is somewhat involved since the D-scalings are typically of dimension 4 or 5. These higher-order "ellipsoids" are projected onto the $x_1 - x_2$ plane to yield bounds on the possible trajectories. Consistent with intuition, the closed-loop

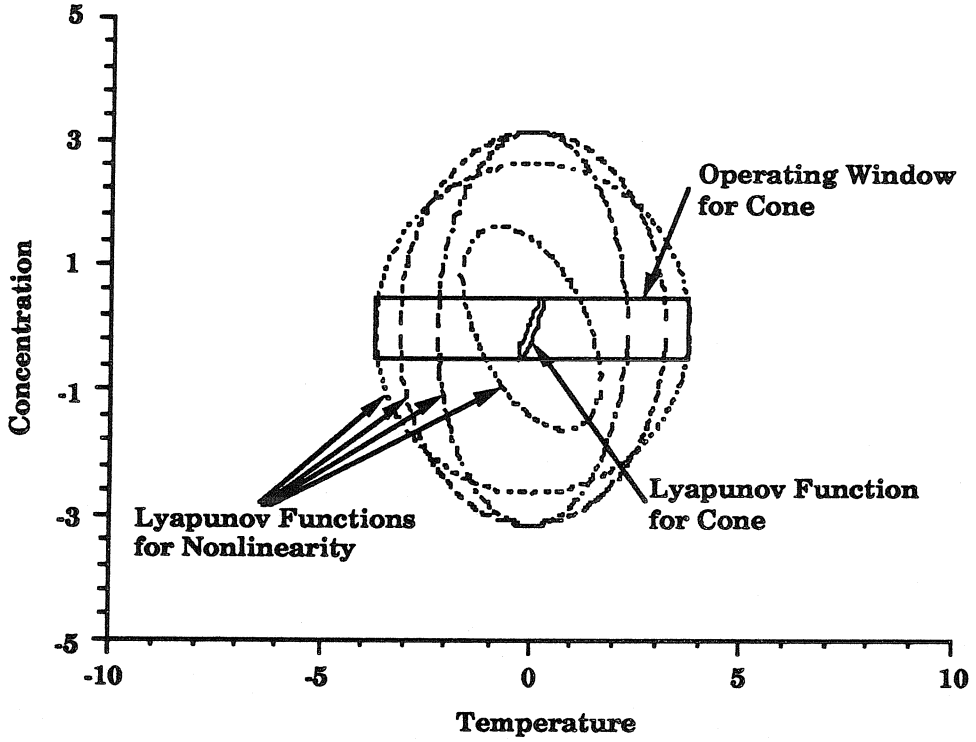

Figure 2.21. Lyapunov Regions of Attraction

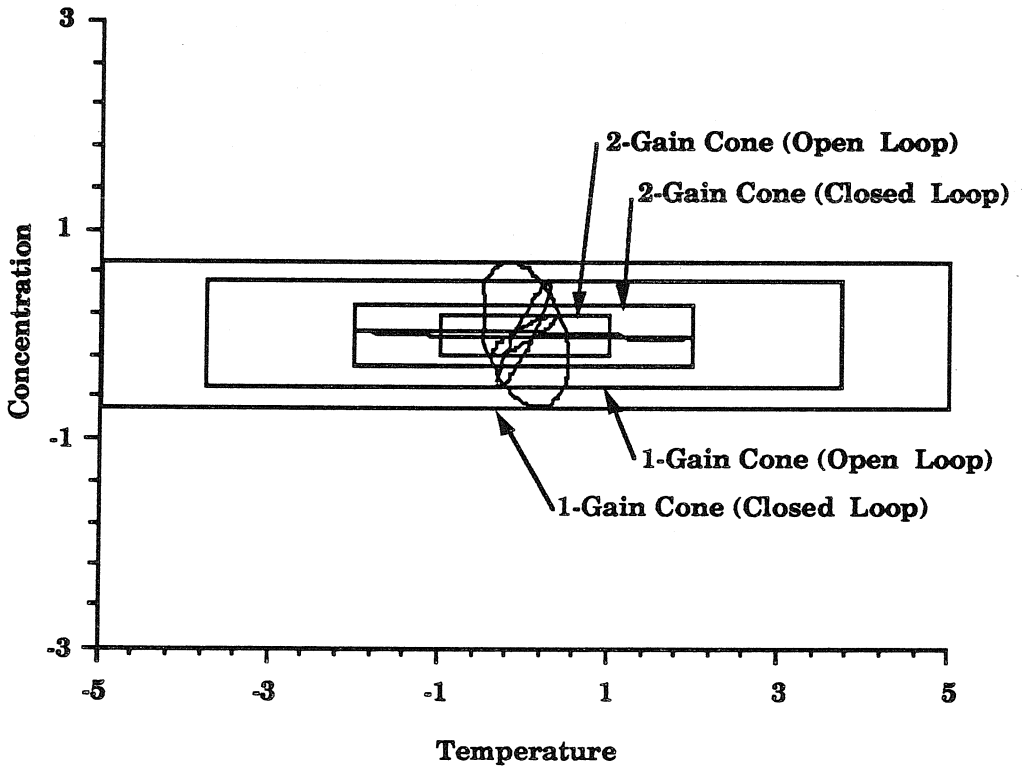

Figure 2.22. Windows and Regions of Attraction for Various Cones

regions in Figure 2.22 are significantly larger than the open-loop areas, indicating the stabilizing effect of feedback control. The second observation revealed in this figure is the superiority of a single uncertain gain conic-sector description compared to one with two uncertain gains. Evidently the conic-sector formulation is critical for these computations. A final observation can be made regarding the orientation of the ellipses and their subsequent total area. There appears to be no connection between a maximal region of attraction and the computation of optimal D-scalings for the structured singular value.

The robust performance results obtained for the nonlinear or time-varying system require further consideration. Unlike linear time-invariant systems, a linear time-varying operator will not preserve the frequency of the input signal. Consequently, the design of an output performance weight for time-varying systems cannot assume any correspondence between inputs and outputs of a particular frequency. The input weights still retain their function of shaping a bounded ball of signals into the appropriate input set. The output performance weight can be designed to attenuate signals of a specified frequency range without regard to the input frequency content. Thus the design of performance weights for both linear time-invariant and linear time-varying systems are qualitatively similar.

With respect to the operating windows, the robust performance results indicate that input signals of bounded power or bounded energy produce outputs of bounded power or energy, respectively, *provided that* these input signals produce states which remain in the defined window. As stated before, this can be compared to the standard linearization results which yield bounded input-bounded output results in an ambiguous region "over which the linear model is valid." Our method explicitly defines the region over which the robustness properties are guaranteed.

Stronger results for guaranteeing the system's state bounds are possible using the structured singular value. In particular, one can define an operating window

which yields bounded trajectories, thus validating the proposed uncertainty structure (conic-sector bounds). The details of this result will be described in the next chapter.

2.6 Conclusions

A practical problem is presented which demonstrates the utility of the new extensions of the structured singular value to nonlinear systems. While robust control of the closed-loop system over the entire phase plane is too ambitious for these potentially pathological systems, it is demonstrated that closed-loop systems can be obtained with linear controllers which are robustly stable over a significantly large portion of the phase plane. The new results allow us to evaluate robust performance as a function of the size of the operating window.

These results suggest the potential for application of these techniques to more complex systems such as packed bed reactors. This is investigated in more detail in chapter 4. An examination of the simple plug flow model for a fixed-bed reactor which incorporates only external heat and mass transfer limitations [70] reveals the same type of nonlinearities as those in the simple CSTR model. The structured uncertainty formulation lends itself readily to analysis of model uncertainty, and coupled with the nonlinear extensions, could be used to evaluate robustness properties with regard to nonlinear model errors. The authors envision the application of these results to complicated systems comprised of a variety of uncertainty elements; real and complex, time-varying and time invariant.

While conservatism is inherent in the analysis of time-varying systems, the presented technique shows a computationally attractive method for quadratic Lyapunov function construction. It should be possible to reduce the values of the structured singular values by considering real variations in Δ (as opposed to complex). The physical system considered in this chapter would be more accurately described by real perturbations, and work is underway to develop software to handle this class of

problem. Additional conservatism is introduced by the formulation of conic-sector bounds on the nonlinearities. Careful and clever modeling is required to minimize the cone size to limit the uncertainties introduced in this design step.

The presented calculations in the H_∞ setting are inherently conservative because of the Small Gain Theorem. Recent results have suggested an alternative approach, ℓ^1-optimal control. In this setting, it is possible to derive necessary and sufficient results for norm-bounded nonlinear perturbations interconnected with a nominal linear plant. A comparative discussion of this approach is found in appendix A.

Note

Versions of this chapter originally appeared in [23] and [25].

Chapter 3

Tools for Nonlinear Control Synthesis - Exact and Approximate Linearizations

Abstract

The robustness properties of exact and approximate linearization are studied in the context of chemical reactor control. The relative merits of the two techniques are investigated in terms of the disturbance handling, optimization of the nonlinear transformations, and restrictions on application. With these properties as measures, the approximate linearization represents a significantly superior approach. The robustness properties are further investigated using extensions of structured singular value theory to nonlinear systems. The uncertainty structure is formulated using conic-sector bounds, and an algorithm for computing optimal conic sectors is presented. The results are supported by a series of case studies involving both involutive and non-involutive chemical reactor systems.

3.1 Introduction

There has been considerable interest in the application of differential geometry to the control of nonlinear process systems over the past five years. The inherently nonlinear nature of chemical process dynamics and the pathological behavior which can evolve from these systems have motivated the application of these techniques to process control. Two of the more popular approaches, state linearization and

input-output linearization, have received considerable attention. With a few notable exceptions [12], the issues of unmeasured disturbances and unmodeled dynamics in these frameworks have not been properly emphasized. In this chapter, we propose a general methodology to address these issues.

The analysis tools employed in this research are extensions of the structured singular value (SSV) to nonlinear systems [25], [71]. Utilizing the conic-sector approximation of a nonlinear operator, it is possible to represent a nonlinear system as a nominal LTI plant perturbed by a bounded nonlinear operator. The SSV results for nonlinear perturbations are only sufficient and thus conservative. Therefore, the primary objective in this design scheme is the minimization of the size of the nonlinear perturbations. This is accomplished by two means. First, the nonlinear nature of the plant is minimized by means of exact or approximate linearization via state transformation and feedback [43], [56]. Second, a tight characterization of the resultant nonlinearity is achieved with an optimization program. Thus, we arrive at a nearly "linear" plant description which can then be handled with standard robust linear control theory.

The usual Euclidean norm or 2-norm will be used to calculate the norm of vectors in $\mathcal{C}^n$ or $\mathcal{R}^n$. For vector signals $e(t)$, this norm is defined to be: $\|e(t)\|^2 = \int_{-\infty}^{\infty} e^T(t)e(t)dt$. The operator norm induced by the 2-norm is

$$\sup_{\substack{v\neq 0 \\ v\in\mathcal{L}_2}} \frac{\|Gv\|}{\|v\|} = \sup_{\omega} \bar{\sigma}(G(j\omega)) \triangleq \|G\|_\infty \tag{3.1}$$

where $\mathcal{L}_2$ is the space of functions with bounded 2-norm. This is also the operator norm induced by the power norm defined to be: $\|e(t)\|_P^2 = \lim_{\tau\to\infty} \int_{-\tau}^{\tau} \frac{1}{2\tau} e^T(t)e(t)dt$. The Frobenius norm for matrices in $\mathcal{C}^{n\times n}$ is given by $\|A\|_F = \left[\sum_i \sum_j |a_{ij}|^2\right]^{\frac{1}{2}}$. The superscript notation, $f^{(\rho)}(x)$, will be used to represent a polynomial function of order ρ in the argument.

The following Lie Algebraic definitions and notation will be utilized in the rest of this thesis. We define the vector fields f and g on $\Re^n$ which are functions of $x \in \Re^n$. The scalar field h on $\Re^n$ maps the state vector $x \in \Re^n$ in $\Re$. The differential operator L_f is defined as:

$$L_f \equiv f_1 \frac{\partial}{\partial x_1} + \cdots + f_n \frac{\partial}{\partial x_n} \tag{3.2}$$

Using this operator, we define two types of Lie derivatives associated with these vector fields. The first is the *Lie Derivative* or directional derivative of a function with respect to a vector field:

$$L_f(h) \equiv \langle dh, f \rangle \equiv f_1 \frac{\partial h}{\partial x_1} + \cdots + f_n \frac{\partial h}{\partial x_n} \tag{3.3}$$

Another useful quantity is the Lie derivative of a vector field with respect to a vector field, denoted the *Lie Bracket* (or commutator or Poisson bracket). It is defined as follows:

$$[f, g] \equiv \frac{\partial g}{\partial x} f - \frac{\partial f}{\partial x} g \tag{3.4}$$

The following recursive notation will be employed for successive Lie Brackets:

$$\begin{aligned} ad_f^0(g) &\equiv g \\ ad_f^1(g) &\equiv [f, g] \\ &\vdots \\ ad_f^k(g) &\equiv [f, ad_f^{k-1}(g)] \end{aligned} \tag{3.5}$$

Having set up the notation, one can now formally define the property of involutivity which will be referred to throughout the following chapters.

Definition 3.1 *The linearly independent vector fields $g_1(x), g_2(x), \cdots, g_n(x)$ are* **involutive** *if the Lie Bracket of any two members of the set is expressible as a linear*

combination of the members of the set.

3.2 Feedback Linearization

The standard nonlinear control problem focuses on control-linear systems of the form:

$$\dot{x} = f(x) + g(x)u \tag{3.6}$$

In addition, the more general dynamical system (including disturbance effects) is described by

$$\dot{x} = f(x) + g(x)u + d(x,t) \tag{3.7}$$

where $x \in \Re^n$, $u \in \Re^m$ and $d \in \Re^n$. Here, $d(x,t)$ may represent external disturbances as well as unmodeled dynamics; the key point is that it is unmeasured. The standard state feedback linearization problem can be stated as follows: when does there exist an invertible coordinate transformation which, when coupled with the appropriate nonlinear feedback, results in a linear controllable system in the new coordinates? The answer to this question involves the following state and input transformations

$$z = T(x) \tag{3.8}$$

$$u = \alpha(x) + (I + \beta(x))v \tag{3.9}$$

and is provided by the following theorems:

Theorem 3.1 *Global State Linearization (GSL)*

The nonlinear system 3.6 can be transformed with a nonlinear change of coordinates (3.8) and nonlinear feedback (3.9) into the linear system

$$\dot{z} = \begin{pmatrix} 0 & 1 \\ 0 & 0 \end{pmatrix} z + \begin{pmatrix} 0 \\ 1 \end{pmatrix} v \tag{3.10}$$

where (A, B) is in Brunovsky companion form iff

1. $[g, \ldots, ad_f^{n-1} g]$ *span* $\Re^n$
2. $[g, \ldots, ad_f^{n-2} g]$ *is involutive*

Proof 3.1 *See [43]*

Comment

(1) is a standard controllability condition. (2) is an integrability condition which arises from application of the Frobenius theorem to the integration of the nonlinear change of coordinates.

Theorem 3.2 *Approximate Linearization (AL)*

The nonlinear system 3.6 can be transformed with a nonlinear change of coordinates (3.8) and nonlinear feedback 3.9 into the linear system

$$\dot{z} = Fz + Gv + O^{\rho+1}(z, v) \tag{3.11}$$

where (F, G) represent the Jacobian matrices corresponding to the system (3.6) iff

1. *span* $[g, \ldots, ad_f^{n-1} g]$ *has order* ρ *local basis*
2. $[g, \ldots, ad_f^{n-2} g]$ *is order* ρ *involutive*

Proof 3.2 *See [56]*

Comments

Note the relaxation of the requirements as compared to GSL. Now, for instance, the involutivity condition need only be solved to within order ρ terms. This will considerably widen the class of linearizable systems.

These theorems describe the necessary and sufficient conditions for accomplishing the transformation of our original system (Equation 3.6) into a linear (or within order ρ linear) system. The intuitive appeal of this approach is readily apparent. The nonlinearities in the system are directly treated by "bending" the coordinates. Standard optimal linear control is employed on the resulting linear system. The control problem is effectively decoupled into two stages: (i) removal of the nonlinearity; (ii) linear control design to match specifications (robustness, performance, etc.).

We consider now a more detailed comparative analysis of the Global State Linearization [43] (GSL) technique and the Approximate Linearization (AL) technique developed by Krener and co-workers [48], [56]. Using the following features as measures, the AL represents a *significantly* superior linearization approach:

- Transformed Coordinate System
- Disturbance Effects
- Involutivity Restrictions
- Optimization of Possible Transformations

These issues will now be discussed in more detail.

3.2.1 Transformed Coordinate System

GSL transforms a second order system of the form in Equation 3.7 into the following dynamical system:

$$\dot{z} = \begin{pmatrix} 0 & 1 \\ 0 & 0 \end{pmatrix} z + \begin{pmatrix} 0 \\ 1 \end{pmatrix} v + [\frac{\partial T}{\partial x} d(x,t)]_{x=T^{-1}(z)} \tag{3.12}$$

Although the resultant nominal state dynamics are linear, they are in Brunovsky canonical form in which many of the states have lost their physical significance. For process systems in which the states are typically temperatures and concentrations, the transformed variables may represent unmeasurable quantities or highly nonlinear functions of the measurable variables. Another problem with the so-called "global" techniques is the fact that the state transformation $T(x)$ is only a local diffeomorphism, and therefore, these techniques can only be applied over finite regions of the phase space.

AL also handles systems of the form in Equation 3.7, but for convenience we will represent the nominal system as a series expansion of the terms in Equation 3.6:

$$\dot{x} = Fx + f^{(2)}(x) + \cdots + f^{(\rho)}(x) + \left(G + g^{(1)}(x) + \cdots + g^{(\rho-1)}(x)\right) u + O^{(\rho+1)}(x,u)$$

The following structure is imposed upon the state transformation:

$$z = x - \phi^{(\rho)}(x) \tag{3.13}$$

The resultant dynamical system is linear in the state dynamics up through order ρ terms:

$$\dot{z} = Fz + Gv + [\frac{\partial T}{\partial x} d(x,t)]_{x=T^{-1}(z)} + O^{\rho+1}(z,v) \tag{3.14}$$

The particular choice of state transformation in Equation 3.13 and input transformation (Equation 3.9) leads to first order terms F and G which are identical to the respective terms in the first order approximation of the original dynamical system. Mathematically, we say that the new variables z have ρth-order contact with the original variables x. This is contrasted with the GSL in which the transformed coordinates have only zero order contact with the original variables (higher derivatives do not match). The implications for control design are obvious. Optimal linear con-

trollers can be calculated for the first order approximation of the original system and then application to the AL system is direct. For the GSL approach, the desired first order dynamics in x must be translated to the new coordinate system, z, before the corresponding linear control law can be calculated.

3.2.2 Effect of Disturbances and Unmodeled Dynamics

A related weakness of the GSL technique is revealed by the impact of disturbances and unmodeled dynamics in the transformed coordinates. These terms are incorporated into the new coordinate system after pre-multiplication by the Jacobian of the state transformation. Thus, even simple linear disturbances are transformed by GSL into potentially pathological operators in the linearized coordinate system. Simple perturbations in d may dramatically affect the already critically stable nominal system (open loop).

This is contrasted with the AL approach in which the transformation Jacobian matrix has zero-order terms equal to identity. The higher order terms are simple polynomials in x. Just as with the transformed coordinate system, the disturbances and unmodeled dynamics have ρ-th order contact with the original variables. Thus, to first order, these two perturbations are the same in both coordinate systems (x and z). In effect, this minimizes the "nonlinear" nature of the disturbances.

3.2.3 Involutivity Restrictions

A restriction on the nonlinear systems which admit GSL solutions is an involutivity condition, the computation of which becomes quite difficult for large order systems. Typical chemical engineering processes, particularly complex reaction systems, violate this constraint. A precise understanding of the interpretation of involutivity for process dynamical systems is not possible. However, a number of properties have been identified which lead to non-involutive systems. These include:

1. Recycle reaction systems.

2. Second and higher order reactions for nonisothermal CSTRs.

3. Reaction systems with optima involving sign changes in the system gain.

In contrast, the AL approach requires only that the system be "approximately involutive" or order-ρ involutive (Theorem 3.2). This is a milder constraint in the sense that it allows an order ρ remainder term, whereas GSL requires zero remainder.

3.2.4 Optimization of Possible Transformation

One of the real strengths of the AL approach lies in its flexibility to "optimize" the resultant solution. Consider the mapping from the transformations (ϕ, α, β) to the functions (f, g). For AL, one can represent this mapping in terms of the polynomial coefficients of the various polynomial functions. (A straightforward interpretation is not possible for the GSL.) If this mapping has a non-trivial kernel, then a parametrized family of solutions results. The parameters are selected to minimize the "size" of α, β and ϕ. If the magnitude of ϕ is minimized, then the mapping from x to z becomes closer to identity. Similarly, minimizing α and β yields a mapping from u to v that is close to identity. Thus the linearization is accomplished with *minimal* nonlinear "distortion" of the original system.

Similarly, if the map is deficient in rank, then a linearization solution is not possible (*i.e.*, the system is not ρ-order involutive). In this case, one can search over the space of solutions $(\hat{f}, \hat{g})$ which *are* linearizable. An optimization is done to minimize the "distance" between (f, g) and $(\hat{f}, \hat{g})$. The reader is referred to [48] for the optimization algorithm and a discussion of the relevant metrics used to define the various sizes and distances.

In effect, the constraint in Theorem 3.1 is removed. This will be demonstrated with two non-involutive examples in the next sections. This systematic procedure for

finding the "closest" linearizable system reveals the flexibility of the AL approach.

3.2.5 Summary

It has been shown in Equations 3.12 and 3.14 how the so-called linearization techniques actually result in nonlinear systems when the effects of disturbances and unmodeled dynamics are accounted for. This is represented in Figure 3.1 where the shaded blocks are nonlinear operators. At the center of this structure are the input transformation, nonlinear plant, and state transformation. The effect of unmodeled dynamics and disturbances on the stability of the open-loop transformed system is clear. Δ_1 represents the difference between the true nonlinear dynamics and the assumed nominal *linear* model. The linear model here is taken as the "linearized" system in z coordinates (GSL, AL) or as the Jacobian (classical linearization) of the original system in x coordinates (linear control). For instance, the Quadratic Approximate Linearization scheme (QAL), $\rho = 2$, has a Δ_1 term to represent order 3 and higher effects. Δ_2 represents the nonlinear effect of the disturbance acting through the Jacobian of the transformation. Finally, Δ_3 represents the nonlinearity associated with the actual coordinate transformation itself and its effect upon the set-point signal.

Consider the case of unmeasured disturbances which enter linearly into the original system (Equation 3.7). The resulting uncertainty formulation yields an uncertainty structure with magnitudes described in Table 3.1. In the linear control case, the disturbance effects remain linear (Δ_1) in the unchanged coordinate system, but the original nonlinear system has a potentially large discrepancy between the model and its Jacobian (Δ_2). In the case of GSL, the nonlinear dynamics are completely cancelled (Δ_1), but the linear disturbance becomes nonlinearly transformed in the new coordinates (Δ_2). Finally, for AL, the nonlinear dynamics are approximately cancelled (Δ_1) and the linear disturbance remains approximately linear (Δ_2). Clearly,

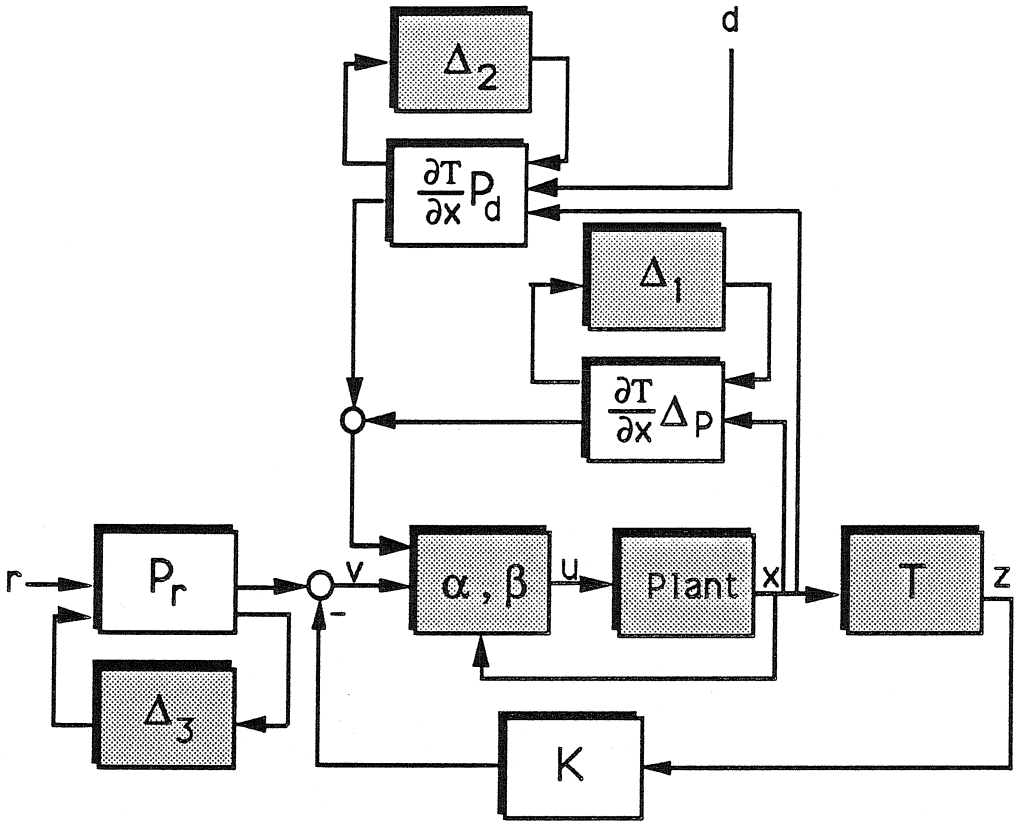

Figure 3.1. General Linearization Uncertainty Structure

the AL approach strikes an overall balance in reducing the nonlinearity in the system

Table 3.1 Relative Magnitude of Uncertainty Elements

Control Action	Δ_1 **Nonlinear Dynamics**	Δ_2 **Nonlinear Disturbances**
Linear	Large	Zero
GSL	Zero	Possibly Large
AL	Approximately Zero	Approximately Zero

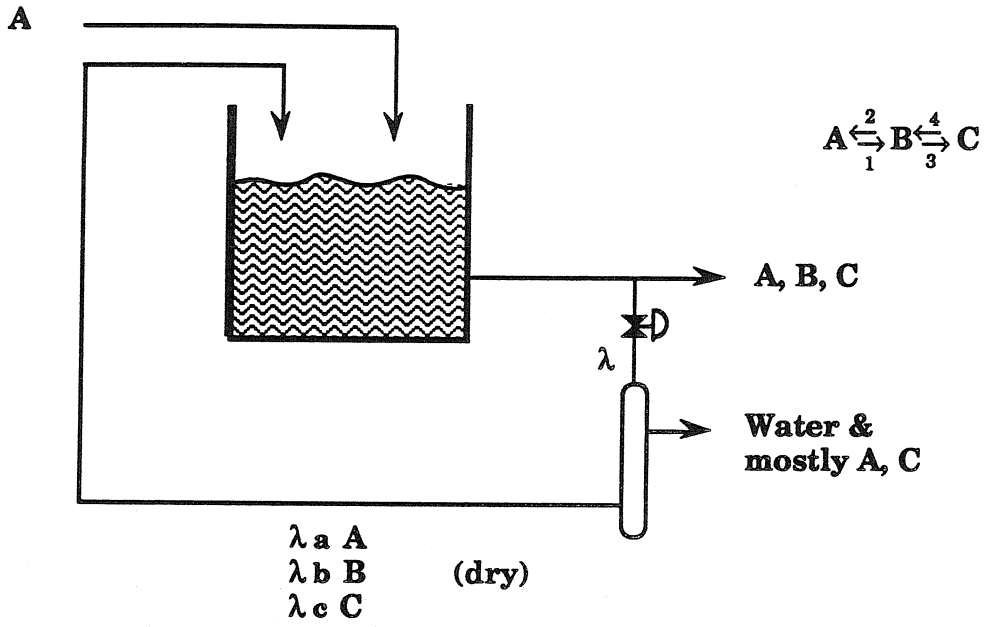

Figure 3.2. Non-Involutive Reaction System (Example #1)

dynamics and the impact of the disturbance.

The preceding four sections have clearly enumerated the incentives for using Approximate Linearization. This overall practicality motivates its use in the present design. In addition, there are extensions of this technique to systems in which the outputs are nonlinear functions of the states. Although they are not explored here, they represent an attractive framework for pursuing input-output linearization.

3.2.6 Example #1: Non-Involutive System

Consider a continuous stirred tank reactor (CSTR) in which the following isothermal, liquid-phase chemical reactions take place (Figure 3.2):

$$A \overset{1,2}{\rightleftharpoons} B \overset{3,4}{\rightleftharpoons} C \tag{3.15}$$

Schematically, the reactor system is described in Figure 3.2. The following rate expressions hold: $r_1 = k_1 C_A, r_2 = k_2 C_B^2, r_3 = k_3 C_B^2$ and $r_4 = k_4 C_C$. Regulation of

the concentration of C (desired output) will be accomplished by manipulating the flow rate (λ) of a feedback stream consisting primarily of component B (fraction = λ_b), which has been separated from the aqueous solution by a drying process. Mass balances for the system are given by the following differential equations:

$$\begin{aligned} V\dot{C}_A &= FC_{AF} - Vk_1C_A + Vk_2C_B^2 - FC_A + \lambda_a FC_A\lambda \\ V\dot{C}_B &= Vk_1C_A - Vk_2C_B^2 - Vk_3C_B^2 - FC_B + \lambda_b FC_B\lambda \\ V\dot{C}_C &= Vk_3C_B^2 - FC_C + \lambda_c FC_C\lambda \end{aligned} \tag{3.16}$$

The following choice of physical parameters ($\frac{F}{V} = 1.0, k_1 = 3.0, k_2 = 0.5, k_3 = 1.0, k_4 = 2.0, \lambda_a = 0.1, \lambda_b = 0.75, \lambda_c = 0.15, C_{AF} = 1.0$) and operating point ($u = \lambda = 0.5, x_{a0} = 0.33, x_{b0} = 0.79, x_{c0} = 0.21$) lead to the normalized dimensionless mass balances:

$$\begin{aligned} \dot{\tilde{x}} = &\begin{pmatrix} -3.95 & .790 & 0.0 \\ 3.0 & 2.994 & 2.0 \\ 0.0 & 1.580 & -2.925 \end{pmatrix} \tilde{x} + \begin{pmatrix} .033 \\ .592 \\ .032 \end{pmatrix} \tilde{u} \\ &+ \begin{pmatrix} .5\tilde{x}_b^2 \\ -1.5\tilde{x}_b^2 \\ 1.0\tilde{x}_b^2 \end{pmatrix} + \begin{pmatrix} 0.1 & 0.0 & 0.0 \\ 0.0 & 0.75 & 0.0 \\ 0.0 & 0.0 & 0.15 \end{pmatrix} \begin{pmatrix} \tilde{x}_a \\ \tilde{x}_b \\ \tilde{x}_c \end{pmatrix} \tilde{u} \end{aligned} \tag{3.17}$$

Note that this system is second order and is in control-linear form. However, it is straightforward to show that this system is not involutive (unless $\lambda_a = \lambda_b = \lambda_c$). Using the MATLAB software for QAL [48] (see Acknowledgements), one sees that

the following plant is in fact involutive:

$$\dot{\hat{\tilde{x}}} = \begin{pmatrix} -3.95 & .790 & 0.0 \\ 3.0 & 2.994 & 2.0 \\ 0.0 & 1.580 & -2.925 \end{pmatrix} \hat{\tilde{x}} + \begin{pmatrix} .033 \\ .592 \\ .032 \end{pmatrix} \hat{\tilde{u}}$$

$$+ \begin{pmatrix} -.00058\hat{\tilde{x}}_a\hat{\tilde{x}}_b & .490\hat{\tilde{x}}_b^2 & -.00056\hat{\tilde{x}}_b\hat{\tilde{x}}_c \\ & -1.5\hat{\tilde{x}}_b^2 & \\ .00027\hat{\tilde{x}}_a\hat{\tilde{x}}_b & 1.005\hat{\tilde{x}}_b^2 & .00026\hat{\tilde{x}}_b\hat{\tilde{x}}_c \end{pmatrix} \tag{3.18}$$

$$+ \begin{pmatrix} 0.112 & -0.012 & 0.027 \\ -.00039 & 0.750 & -.00086 \\ -.0052 & 0.011 & 0.138 \end{pmatrix} \begin{pmatrix} \hat{\tilde{x}}_a \\ \hat{\tilde{x}}_b \\ \hat{\tilde{x}}_c \end{pmatrix} \hat{\tilde{u}}$$

The remarkable closeness of the two systems is attributable to a remainder term which satisfies the approximate involutivity condition for system 3.18. The following simulation results confirm that when the QAL for 3.18 is applied to 3.17, the resultant closed loop exhibits less nonlinear behavior than the original nonlinear plant with simple linear control. The subsequent simulations employ the QAL for the system in Equation 3.18, which are given by the state transformation $z = x - \phi(x)$ where

$$-\phi_1 = 0.07577\tilde{x}_1^2 - 21.68\tilde{x}_1\tilde{x}_2 - 0.991\tilde{x}_1\tilde{x}_3 + 0.07904\tilde{x}_2^2 - 0.0158\tilde{x}_2\tilde{x}_3 + 0.1636\tilde{x}_3^2$$

$$-\phi_2 = -1.290\tilde{x}_1^2 - 1.367\tilde{x}_1\tilde{x}_2 + 3.9925\tilde{x}_1\tilde{x}_3 + 0.5225\tilde{x}_2^2 - 0.2640\tilde{x}_2\tilde{x}_3 + 0.4220\tilde{x}_3^2$$

$$-\phi_3 = 0.384\tilde{x}_1^2 - 0.02033\tilde{x}_1\tilde{x}_2 - 1.554\tilde{x}_1\tilde{x}_3 + 0.05586\tilde{x}_2^2 - 0.1632\tilde{x}_2\tilde{x}_3 + 0.1173\tilde{x}_3^2 \tag{3.19}$$

and nonlinear feedback $\tilde{u} = \alpha + (I + \beta)\tilde{v}$ where:

$$\begin{aligned} \alpha &= 2.082\tilde{x}_1^2 + 22.78\tilde{x}_1\tilde{x}_2 - 21.84\tilde{x}_1\tilde{x}_3 \\ &\quad -8.289\tilde{x}_2^2 + 8.519\tilde{x}_2\tilde{x}_3 - 0.08154\tilde{x}_3^2 \\ \beta &= -1.297\tilde{x}_1 + 2.22\tilde{x}_2 - 0.08721\tilde{x}_3 \end{aligned} \tag{3.20}$$

In the following simulations, three closed-loop systems will be compared:

1. Linear Model with Linear Controller (LMLC). This represents a linear approximation of the true nonlinear system controlled by an optimal linear controller. It will serve as a benchmark for comparison of the next two systems.

2. Nonlinear system with Linear Controller (NLMLC). This is the true system with an optimal linear controller.

3. Nonlinear system with Nonlinear Controller (NLMNLC). This is the true system with quadratic approximate linearization (QAL).

The linear feedback law is a quadratic optimal regulator designed with identity weighting matrices on the states and inputs. The resulting controller gains are:

$$K = [0.1317, 0.2032, 0.1363] \tag{3.21}$$

The closed-loop eigenvalues are:

$$\lambda_i = (-5.6184, -3.4890, -0.8910) \tag{3.22}$$

Three simulation studies are depicted in Figures 3.3, 3.4, and 3.5. In the graphs, the various curves representing the closed-loop systems correspond to LMLC (solid), NLMLC (dash - dot), and NLMNLC (dashed).

In the first case (Figure 3.3), the system is started from nonzero initial conditions $(0.25, 0.0, 0.0)$ and the objective is to return to this equilibrium as quickly as possible. From this figure one can see that the nonlinear control law shows a faster speed of response and smaller overshoot as the states return to their equilibrium value of $(0.0, 0.0, 0.0)$. This is accomplished at the expense of somewhat excessive manipulated variable action.

The second simulation (Figure 3.4) shows the response of the system to a step disturbance (magnitude 0.25) in the input. The objective here is a minimal perturbation or offset from the equilibrium value. Here it is seen that the nonlinear dynamics are cancelled and the offset for the NLMNLC system is roughly equal to the offset predicted by the linear system (LMLC). However, the linearly controlled nonlinear system (NLMLC) exhibits greater nonlinear offset in response to the disturbance.

The final simulation (Figure 3.5) also reveals the ability of the nonlinear controller to mitigate nonlinear effects. In this case, a sinusoidal input $(0.4 \sin t)$ is applied. Again, it is observed that the NLMNLC yields nearly linear behavior (as measured by LMLC), in contrast to the NLMLC case. The achievement of this dynamic behavior is accomplished by the highly nonlinear control action shown in the figure.

3.2.7 Example #2: Non-Involutive System

Consider a pair of continuous stirred tank reactors (CSTRs) in which the following autocatalytic, isothermal, liquid-phase chemical reactions take place:

$$A \xrightarrow{1} B \tag{3.23}$$

Schematically, the reactor system is described in Figure 3.6. The following rate expression holds: $r_1 = kC_AC_B$. Regulation of the concentration of B (desired output) will be accomplished by manipulating the concentration of A fed into the first tank,

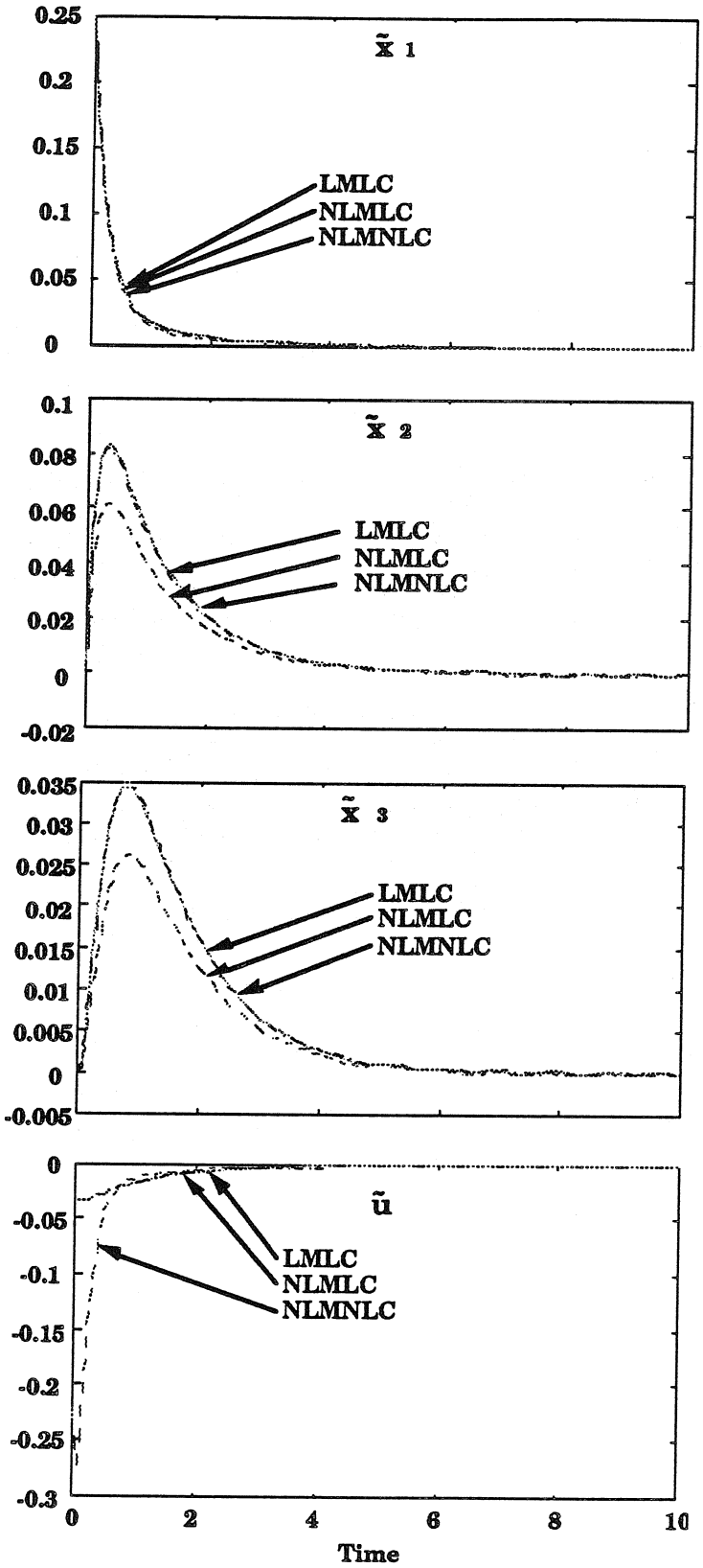

Figure 3.3. Closed-Loop Response (Example #1, Nonzero Initial Conditions)

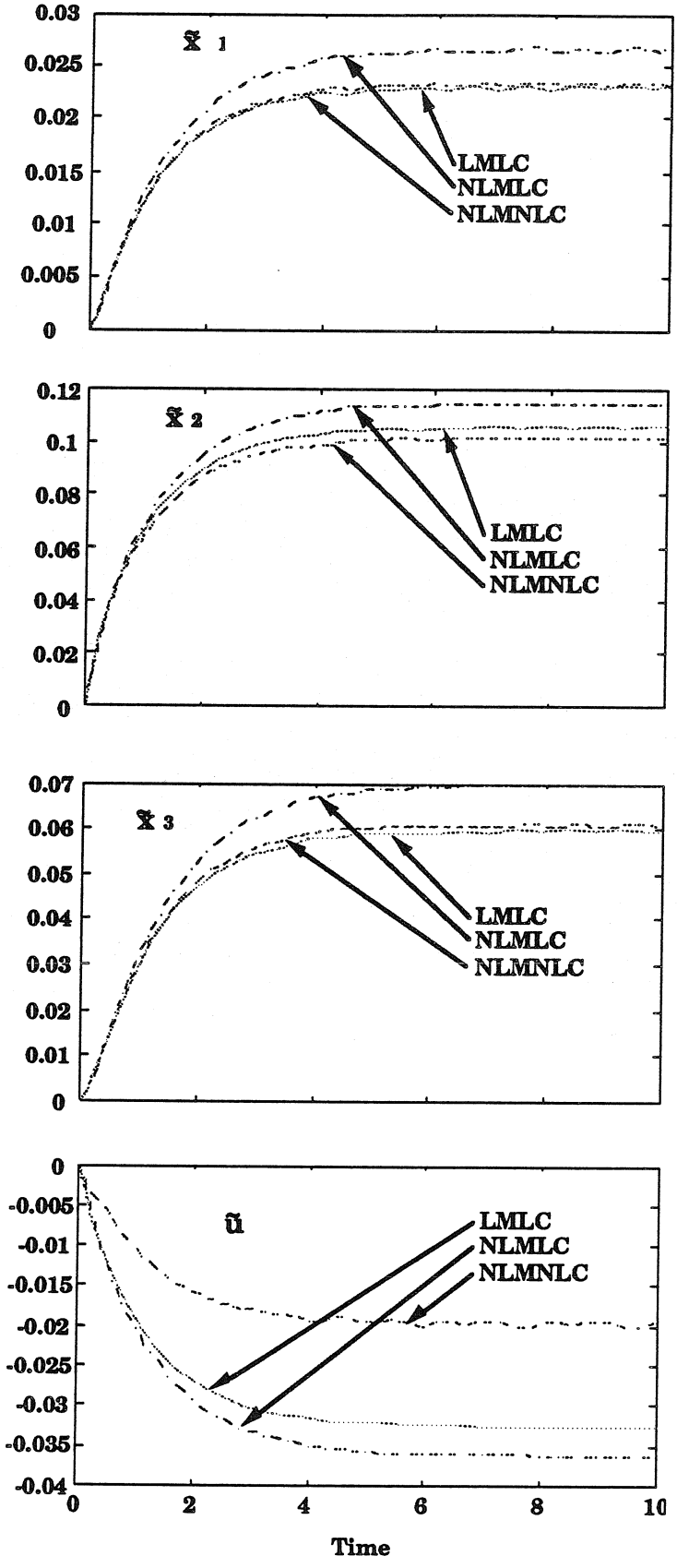

Figure 3.4. Closed-Loop Response (Example #1, Step Disturbance)

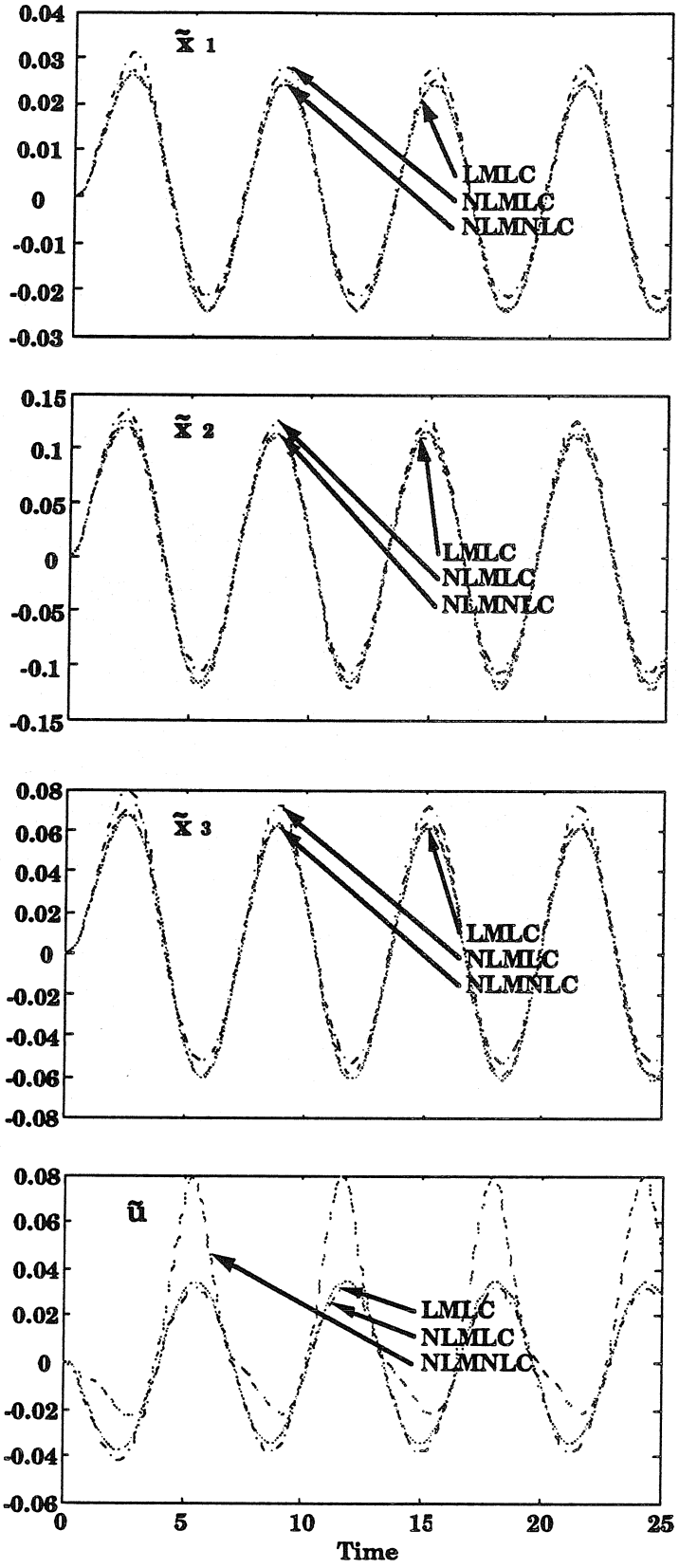

Figure 3.5. Closed-Loop Response (Example #1, Sinusoidal Disturbance)

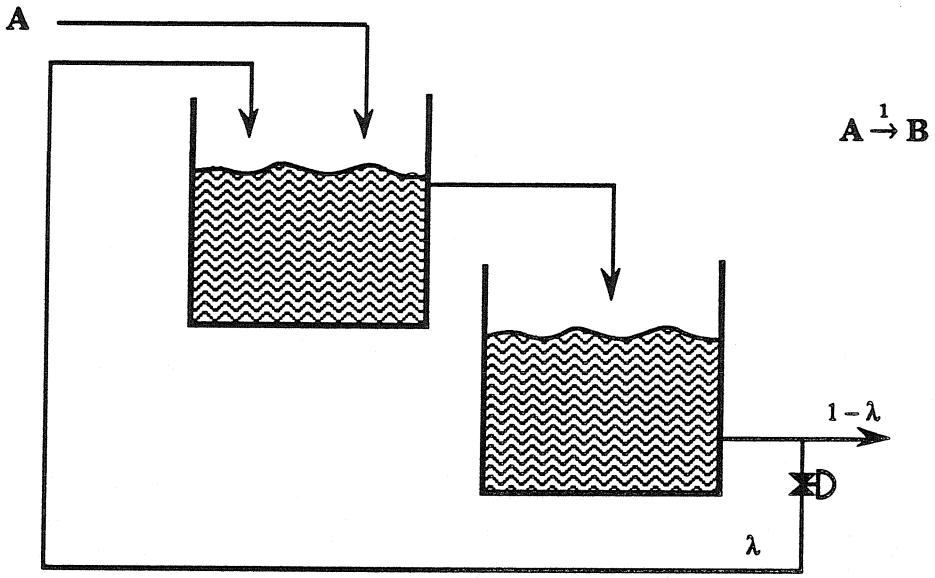

Figure 3.6. Non-involutive Reaction System (#2)

and the amount of recycle from the second tank back to the first tank. Mass balances for the system are given by the following differential equations:

$$\begin{aligned} V\dot{C}_{A1} &= FC_{AF} - VkC_{A1}C_{B1} - F(1+\lambda)C_{A1} + F\lambda C_{A2} \\ V\dot{C}_{B1} &= VkC_{A1}C_{B1} - F(1+\lambda)C_{B1} + F\lambda C_{B2} \\ V\dot{C}_{A2} &= -VkC_{A2}C_{B2} + F(1+\lambda)C_{A1} - F(1+\lambda)C_{A2} \\ V\dot{C}_{B2} &= VkC_{A2}C_{B2} + F(1+\lambda)C_{B1} - F(1+\lambda)C_{B2} \end{aligned} \tag{3.24}$$

The following choice of physical parameters ($k = 1.1, \frac{V}{F} = 1.0$) and operating point ($u_{10} = \lambda = 1.0, u_{20} = C_{AF} = 0.1, x_{10} = 0.798, x_{20} = 0.202, x_{30} = 0.550, x_{40} = 0.450$)

leads to the normalized dimensionless mass balances:

$$\dot{\tilde{x}} = \begin{pmatrix} -1.3225 & -0.8775 & 0.1 & 0.0 \\ 0.2225 & -0.2225 & 0.0 & 0.1 \\ 1.1 & 0.0 & -1.5948 & -0.6052 \\ 0.0 & 1.1 & 0.4948 & -0.4948 \end{pmatrix} \tilde{x} + \begin{pmatrix} -0.2475 & 1 \\ 0.2475 & 0 \\ 0.2475 & 0 \\ -0.2475 & 0 \end{pmatrix} \tilde{u}$$

$$+ \begin{pmatrix} -1.1\tilde{x}_1\tilde{x}_2 \\ 1.1\tilde{x}_1\tilde{x}_2 \\ -1.1\tilde{x}_3\tilde{x}_4 \\ 1.1\tilde{x}_3\tilde{x}_4 \end{pmatrix} + \begin{pmatrix} -1.0 & 0.0 & 1.0 & 0.0 \\ 0.0 & -1.0 & 0.0 & 1.0 \\ 1.0 & 0.0 & -1.0 & 0.0 \\ 0.0 & 1.0 & 0.0 & -1.0 \end{pmatrix} \begin{pmatrix} \tilde{x}_1 \\ \tilde{x}_2 \\ \tilde{x}_3 \\ \tilde{x}_4 \end{pmatrix} \tilde{u}_1 \tag{3.25}$$

Note that this system is second order and is in control-linear form. However, it is straightforward to show that this system is not involutive. Using the MATLAB software for QAL, one sees that the following plant is in fact involutive:

$$\dot{\hat{\tilde{x}}} = \begin{pmatrix} -1.3225 & -0.8775 & 0.1 & 0.0 \\ 0.2225 & -0.2225 & 0.0 & 0.1 \\ 1.1 & 0.0 & -1.5948 & -0.6052 \\ 0.0 & 1.1 & 0.4948 & -0.4948 \end{pmatrix} \hat{\tilde{x}} + \begin{pmatrix} -0.2475 & 1 \\ 0.2475 & 0 \\ 0.2475 & 0 \\ -0.2475 & 0 \end{pmatrix} \hat{\tilde{u}}$$

$$+ \begin{pmatrix} -1.1\hat{\tilde{x}}_1\hat{\tilde{x}}_2 \\ 1.1\hat{\tilde{x}}_1\hat{\tilde{x}}_2 \\ -1.1\hat{\tilde{x}}_3\hat{\tilde{x}}_4 \\ 1.1\hat{\tilde{x}}_3\hat{\tilde{x}}_4 \end{pmatrix} + \begin{pmatrix} -1.0 & 0.0 & 1.0 & 0.0 \\ 0.2677 & -1.0 & 0.0 & 1.0 \\ 0.4645 & 0.0 & -1.0 & 0.0 \\ -0.2677 & 1.0 & 0.0 & -1.0 \end{pmatrix} \begin{pmatrix} \hat{\tilde{x}}_1 \\ \hat{\tilde{x}}_2 \\ \hat{\tilde{x}}_3 \\ \hat{\tilde{x}}_4 \end{pmatrix} \hat{\tilde{u}}_1 \tag{3.26}$$

$$+ \begin{pmatrix} 0.4645 & 0.0 & -1.0 & 0.0 \\ -0.2677 & 1.0 & 0.0 & -1.0 \\ 0.0 & 0.0 & 0.0 & 0.0 \\ 0.0663 & -0.0663 & -0.0663 & 0.0663 \end{pmatrix} \begin{pmatrix} \hat{\tilde{x}}_1 \\ \hat{\tilde{x}}_2 \\ \hat{\tilde{x}}_3 \\ \hat{\tilde{x}}_4 \end{pmatrix} \hat{\tilde{u}}_2$$

It can be seen that the presence of additional remainder terms in Equation 3.26 satisfies the approximate involutivity condition. The following simulation results confirm that when the QAL for 3.26 is applied to 3.25, the resultant closed loop exhibits less nonlinear behavior than the original nonlinear plant with simple linear control.

The state and input transformations which solve the QAL problem for the system in Equation 3.26 are used in the subsequent closed-loop simulations. They consist of the following change of coordinates:

$$
\begin{aligned}
-\phi_1 &= \tilde{x}_1 0.4013\tilde{x}_1^2 + 2.278\tilde{x}_1\tilde{x}_2 + 0.8375\tilde{x}_1\tilde{x}_3 - 0.07577\tilde{x}_1\tilde{x}_4 + 1.661\tilde{x}_2^2 \\
&\quad -0.3834\tilde{x}_2\tilde{x}_3 - 2.366\tilde{x}_2\tilde{x}_4 - 0.002917\tilde{x}_3^2 - 0.2301\tilde{x}_3\tilde{x}_4 + 0.6091\tilde{x}_4^2 \\
-\phi_2 &= \tilde{x}_2 + 0.0227\tilde{x}_1^2 + 0.5873\tilde{x}_1\tilde{x}_2 + 0.2752\tilde{x}_1\tilde{x}_3 + 0.4748\tilde{x}_1\tilde{x}_4 + 0.6304\tilde{x}_2^2 \\
&\quad -0.558\tilde{x}_2\tilde{x}_3 - 0.04539\tilde{x}_2\tilde{x}_4 - 0.07592\tilde{x}_3^2 + 0.3749\tilde{x}_3\tilde{x}_4 - 0.2046\tilde{x}_4^2 \\
-\phi_3 &= \tilde{x}_3 + 0.1221\tilde{x}_1^2 + 0.3885\tilde{x}_1\tilde{x}_2 + 0.07641\tilde{x}_1\tilde{x}_3 + 0.6736\tilde{x}_1\tilde{x}_4 - 1.602\tilde{x}_2^2 \\
&\quad +2.775\tilde{x}_2\tilde{x}_3 + 3.061\tilde{x}_2\tilde{x}_4 - 0.3357\tilde{x}_3^2 - 0.6528\tilde{x}_3\tilde{x}_4 + 1.285\tilde{x}_4^2 \\
-\phi_4 &= \tilde{x}_4 - 0.0227\tilde{x}_1^2 - 0.5873\tilde{x}_1\tilde{x}_2 + 0.2752\tilde{x}_1\tilde{x}_3 - 0.4748\tilde{x}_1\tilde{x}_4 - 0.6119\tilde{x}_2^2 \\
&\quad +0.865\tilde{x}_2\tilde{x}_3 + 0.3906\tilde{x}_2\tilde{x}_4 + 0.3059\tilde{x}_3^2 + 0.3921\tilde{x}_3\tilde{x}_4 + 0.7607\tilde{x}_4^2
\end{aligned}
\tag{3.27}
$$

and nonlinear feedback $\tilde{u} = \alpha + (I + \beta)\tilde{v}$ where:

$$\begin{aligned}
\alpha_1 &= 1.899\tilde{x}_1^2 + 0.09872\tilde{x}_1\tilde{x}_2 - 3.847\tilde{x}_1\tilde{x}_3 - 1.61\tilde{x}_1\tilde{x}_4 - 4.097\tilde{x}_2^2 \\
&\quad +4.427\tilde{x}_2\tilde{x}_3 + 0.4322\tilde{x}_2\tilde{x}_4 + 1.65\tilde{x}_3^2 - 3.26\tilde{x}_3\tilde{x}_4 - 1.56\tilde{x}_4^2 \\
\alpha_2 &= 2.426\tilde{x}_1^2 - 0.1675\tilde{x}_1\tilde{x}_2 - 2.263\tilde{x}_1\tilde{x}_3 - 1.07\tilde{x}_1\tilde{x}_4 - 3.444\tilde{x}_2^2 \\
&\quad -1.412\tilde{x}_2\tilde{x}_3 + 0.3\tilde{x}_2\tilde{x}_4 + 0.3506\tilde{x}_3^2 + 0.3244\tilde{x}_3\tilde{x}_4 - 0.3165\tilde{x}_4^2 \\
\beta_{11} &= 1.4243\tilde{x}_1 - 3.879\tilde{x}_2 - 1.36\tilde{x}_3 + 4.304\tilde{x}_4 \\
\beta_{12} &= 0.341\tilde{x}_1 - 0.2109\tilde{x}_2 + 0.4167\tilde{x}_3 + 0.1399\tilde{x}_4 \\
\beta_{21} &=).4512\tilde{x}_1 + 2.105\tilde{x}_2 + 0.8442\tilde{x}_3 + 2.186\tilde{x}_4 \\
\beta_{22} &= -0.691\tilde{x}_1 + 2.799\tilde{x}_2 + 1.046\tilde{x}_3 + 0.4653\tilde{x}_4
\end{aligned} \tag{3.28}$$

As before, the following simulations will be compared:

1. Linear Model with Linear Controller (LMLC).
2. Nonlinear system with Linear Controller (NLMLC).
3. Nonlinear system with Nonlinear Controller (NLMNLC).

The expectation is that effective "linearization" by QAL will result in similar behavior between the LMLC system and NLMNLC system. The linear feedback law is a quadratic optimal regulator designed with identity weighting matrices on the states

and inputs. The resulting controller gains are:

$$K = \begin{pmatrix} 0.0169 & 0.8176 & 0.0938 & 0.1031 \\ 0.5268 & 0.6117 & 0.1813 & 0.1978 \end{pmatrix} \tag{3.29}$$

The closed-loop eigenvalues are:

$$\lambda_i = (-1.3371 \pm 0.1214i, -1.2415, -0.4416) \tag{3.30}$$

The three simulation studies are depicted in Figures 3.7, 3.8, and 3.9. In the graphs, the curves representing the closed-loop systems correspond to LMLC (solid), NLMLC (dash – dot), and NLMNLC (dashed).

In the first case (Figure 3.7), the system is started from nonzero initial conditions $(0.25, 0.0, 0.0, 0.0)$ and the control action works to restore equilibrium at $(0.0, 0.0, 0.0)$. From this figure one can see that the nonlinear control law shows a faster speed of response and smaller overshoot as the states return to their equilibrium value.

The second simulation (Figure 3.8) shows the response of the system to a step disturbance (magnitude -0.2) in the second input. The objective here is a minimization of the transients away from the equilibrium value. Here it is seen that the nonlinear dynamics are cancelled and the offset for the NLMNLC system is roughly equal to the offset predicted by the linear system (LMLC). However, the linearly controlled nonlinear system (NLMLC) exhibits greater nonlinear offset in response to the disturbance.

The final simulation (Figure 3.9) also reveals the ability of the nonlinear controller to cancel nonlinear effects. In this case, a sinusoidal input $(0.1 \sin t)$ is applied to the first input. Again, it is observed that the NLMNLC yields nearly linear behavior (as exhibited by LMLC), in contrast to the NLMLC case.

These two case studies demonstrate the strength of the QAL approach with respect to broad applicability. The two nonlinear non-involutive examples cannot be

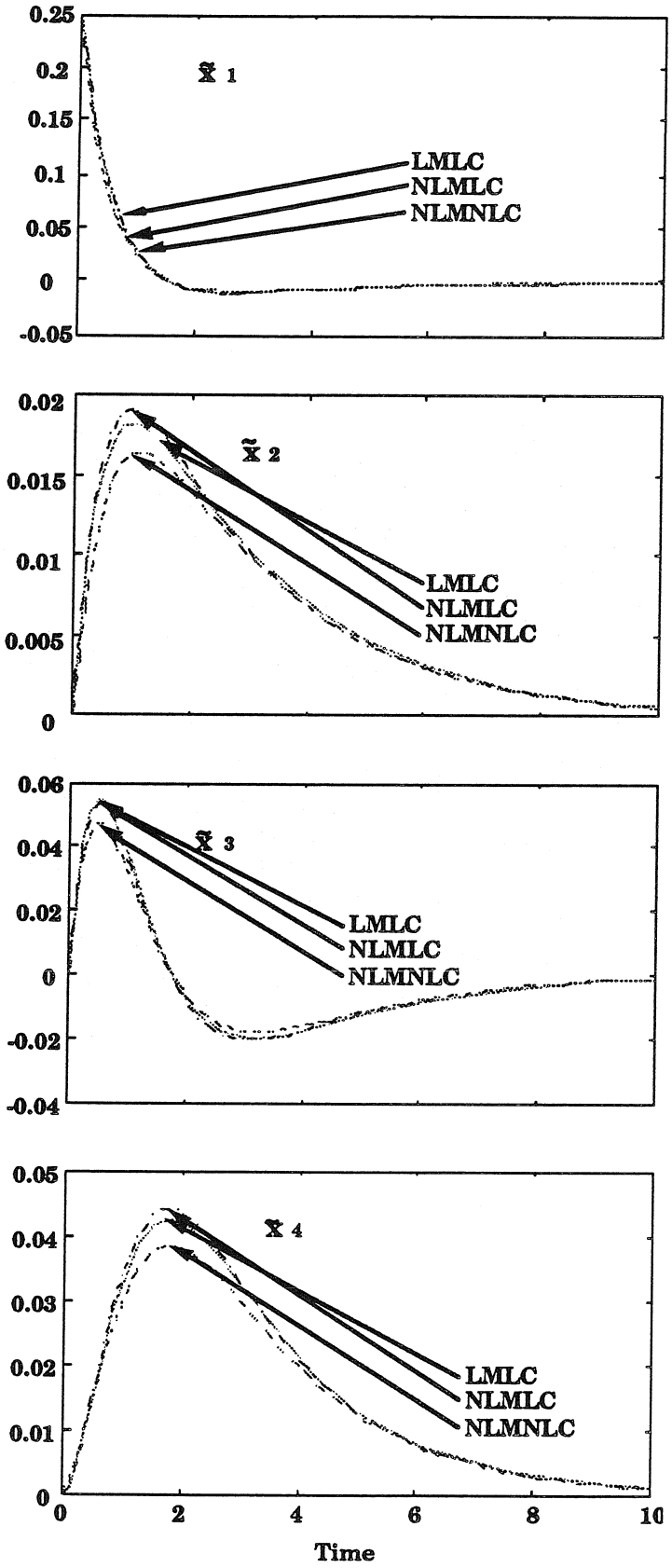

Figure 3.7. Closed-Loop Response (Example #2, Nonzero Initial Conditions)

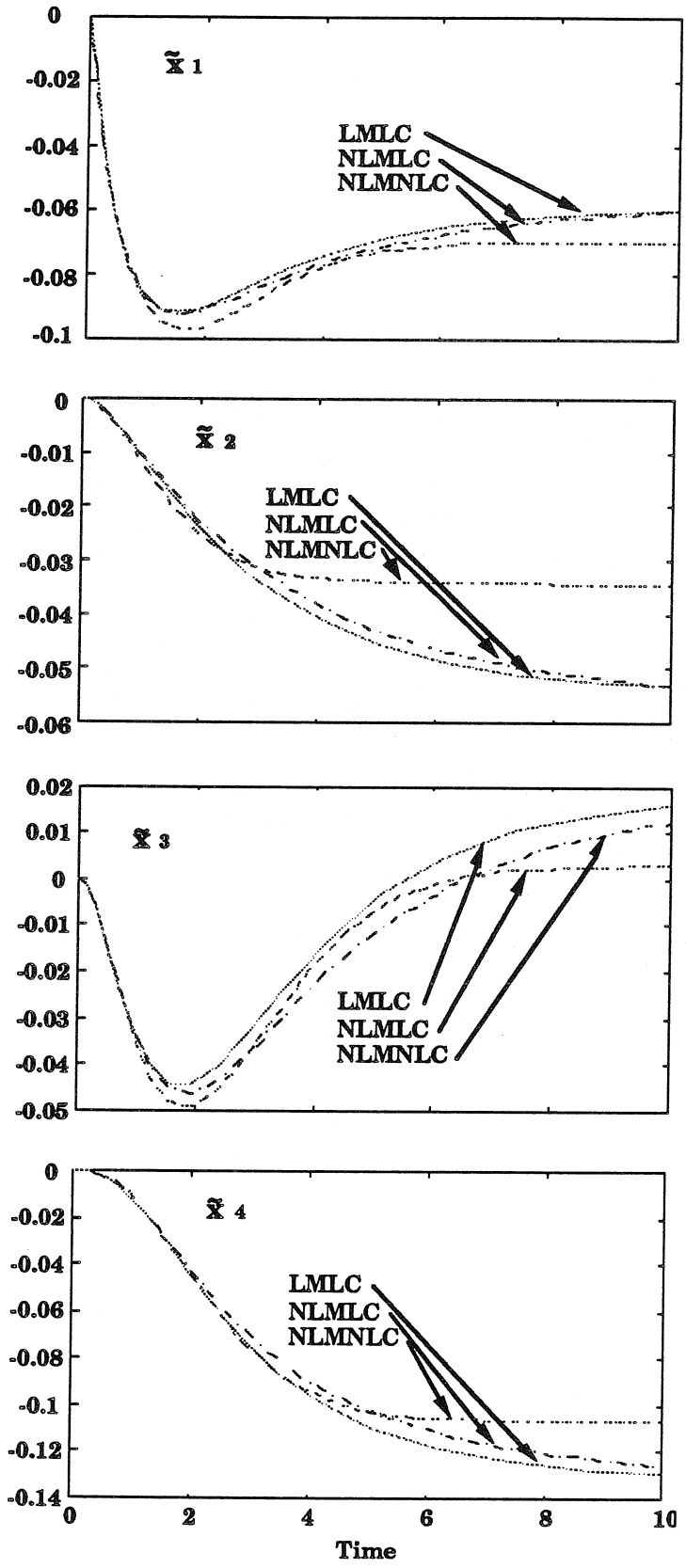

Figure 3.8. Closed-Loop Response Example #2, Step Disturbance)

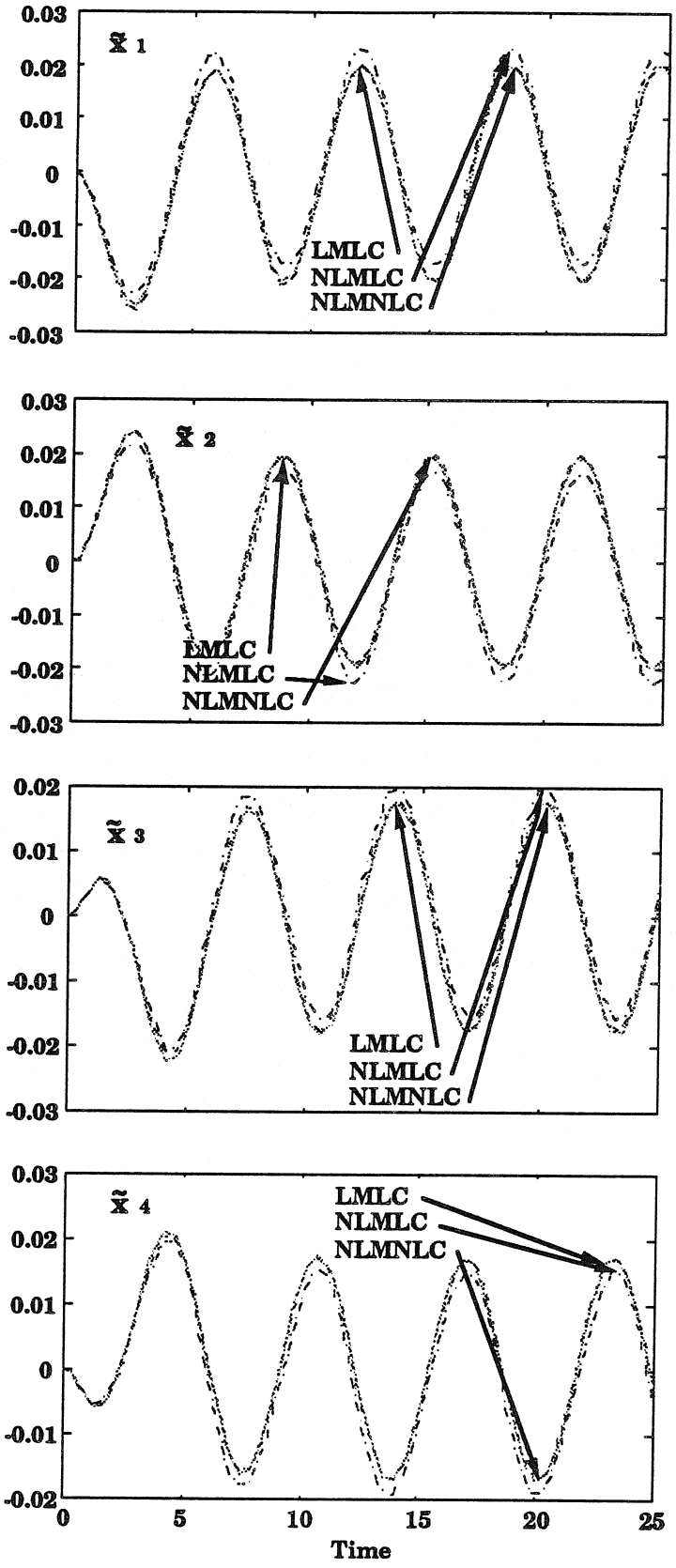

Figure 3.9. Closed-Loop Response (Example #2, Sinusoidal Disturbance)

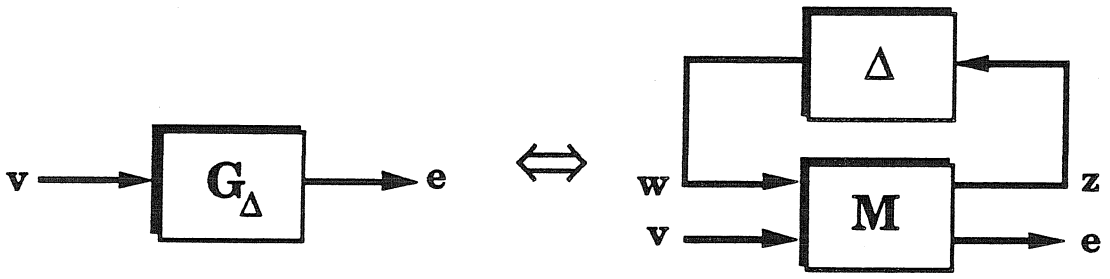

Figure 3.10. M – Δ Structure

controlled by GSL. However, a QAL controller was synthesized in each case and simulations illustrate the improved performance of QAL over linear control.

In the following sections, a more detailed analysis of the robustness properties of the differential geometric approaches is carried out using structured singular value (SSV) theory in combination with conic-sector approximations of nonlinear operators.

3.3 Structured Singular Value Concepts

3.3.1 General Framework

Reviewing the notation from the previous chapter, the general framework is depicted in Figure 3.10, where M(s) is a linear time invariant operator and Δ is a nonlinear operator with the following block structure:

$$\Delta \triangleq \{\text{diag}[\delta_1 I_{r_1}, \ldots, \delta_m I_{r_m}, \Delta_1, \ldots, \Delta_n]\} \tag{3.31}$$

This structure can be arrived at from any interconnection of linear blocks and nonlinear perturbations, Δ. In the diagram, the input v represents set points, disturbances and noise, the output e represents error signals. In this framework, the control analysis problem focuses on two key questions : first, is the system stable for all perturbations in some prescribed set (robust stability); and second, does the error remain in a desired bounded set for all perturbations and inputs in some appropriate sets (robust

performance).

Practically speaking, this approach will be applied to plants with input signals of bounded energy or bounded power, and the results guarantee that the outputs are also bounded in energy or power, respectively. For the class of bounded-energy signals, mild smoothness conditions guarantee that the signal goes to zero asymptotically. It should be noted that the class of input signals can be broadened by the inclusion of weights which are incorporated into the nominal plant M. This can be used, for example, to include steps in the input class. Similarly, the output signals can be weighted to incorporate performance criteria.

3.3.2 Stability and Performance Results

In this section, the robustness results of the last chapter are briefly summarized. Consider again Figure 3.10 and an appropriate partitioning of M:

$$\begin{pmatrix} e \\ z \end{pmatrix} = \begin{pmatrix} M_{11} & M_{12} \\ M_{21} & M_{22} \end{pmatrix} \begin{pmatrix} v \\ w \end{pmatrix} \tag{3.32}$$

Connecting the loop between z and w yields the linear fractional transformation (LFT) representation for the overall operator, G_Δ :

$$e = F_\ell(M, \Delta)v \triangleq [M_{11} + M_{12}\Delta(I - M_{22}\Delta)^{-1}M_{21}]v \tag{3.33}$$

Since it is required that the nonlinearities are conic-sector bounded, it is without loss of generality that Δ is restricted to the class of bounded operators:

$$B\mathbf{\Delta} := \{\Delta \in \mathbf{\Delta} | \Delta \in \text{Cone}(0, \text{I}, \text{I})\} \tag{3.34}$$

We forgo formally defining the cone notation until the next section. It suffices to say that the operators in this class have well-behaved bounded properties. The Small

Gain Theorem can be used to arrive at sufficient conditions for robust stability and performance (RS) and (RP):

$$\begin{aligned} RS: &\quad \|M_{22}\|_\infty = \beta_{RS} \qquad (\beta_{RS} < 1) \\ RP: &\quad \|F_\ell(M,\Delta)\|_\infty = \beta_{RP} \quad (\beta_{RP} < 1) \text{ for all } \Delta \in B\mathbf{\Delta} \end{aligned} \tag{3.35}$$

These conservative conditions can be improved by the introduction of constant scaling matrices which commute with the perturbation block Δ. In this context, commutivity is defined to be:

$$\|D\Delta D^{-1}\|_\infty \leq \|\Delta\|_\infty \tag{3.36}$$

For the uncertainty structure given in Equation 3.31, one appropriately structured commuting set is:

$$\begin{aligned} \mathcal{D} \triangleq \{&\text{diag}[D_1,\ldots,D_m,d_1I_{k_1},\ldots,d_nI_{k_n}] \\ &|D_i \in C^{r_i\times r_i} \text{ is invertible}, d_i \neq 0\} \end{aligned} \tag{3.37}$$

Incorporating these scaling matrices, we can arrive at less conservative conditions for robust stability (RS') and robust performance (RP'):

$$\begin{aligned} RS': &\quad \|DM_{22}D^{-1}\|_\infty = \beta_{RS'} \quad (\beta_{RS'} < 1) \\ RP': &\quad \|F_\ell\left(\left[\begin{pmatrix} I & 0 \\ 0 & D \end{pmatrix} M \begin{pmatrix} I & 0 \\ 0 & D^{-1} \end{pmatrix}\right],\Delta\right)\|_\infty = \beta_{RP'} \\ &(\beta_{RP'} < 1) \text{ for all } \Delta \in B\mathbf{\Delta} \end{aligned} \tag{3.38}$$

In [25], the motivation was presented for carrying out the SSV calculations in the time domain because of the computational attractiveness of the resulting calculations. Consider now the discrete map $N(z)$, which is calculated from $M(s)$ with the norm-preserving bilinear transformation, $s = \frac{1-z}{1+z}$, mapping the unit disk to the right half

plane. The map is appropriately partitioned

$$\begin{pmatrix} x_{k+1} \\ e_k \\ z_k \end{pmatrix} = \begin{pmatrix} N_{11} & N_{12} & N_{13} \\ N_{21} & N_{22} & N_{23} \\ N_{31} & N_{32} & N_{33} \end{pmatrix} \begin{pmatrix} x_k \\ v_k \\ w_k \end{pmatrix} \tag{3.39}$$

where $w_k = \Delta(k, z_k)$ and for each k, Δ is an element of the prescribed uncertainty set $B\mathbf{\Delta}$. Now a coordinate transformation, $\hat{T}$, is introduced as a scaling on the state variables. In an analogous manner to the commuting D scales, the coordinate transformation reduces the conservatism of the time domain result.

Theorem 3.3 *Robust Performance*

Given a system N and block structure Δ. Suppose Δ is inside cone(0,I,I). If there are appropriately partitioned constant scaling matrices $\hat{T}$ and D such that

$$\bar{\sigma}\left(\begin{pmatrix} \hat{T} & 0 & 0 \\ 0 & I & 0 \\ 0 & 0 & D \end{pmatrix} N \begin{pmatrix} \hat{T}^{-1} & 0 & 0 \\ 0 & I & 0 \\ 0 & 0 & D^{-1} \end{pmatrix}\right) = \beta < 1$$

then the uncertain system

$$\begin{pmatrix} x_{k+1} \\ e_k \\ z_k \end{pmatrix} = \begin{pmatrix} N_{11} & N_{12} & N_{13} \\ N_{21} & N_{22} & N_{23} \\ N_{31} & N_{32} & N_{33} \end{pmatrix} \begin{pmatrix} x_k \\ v_k \\ w_k \end{pmatrix}$$

$$w_k = \Delta(k, z_k)$$

is zero-input exponentially stable and if $x_0 = 0$ and $\{v_k\}_{k=0}^{\infty} \in \ell_2$, then $\|e\|_{\ell_2} \leq \beta \|v\|_{\ell_2}$.

Proof 3.3 *See [25].*

3.3.3 State-Bounded Result

For this study, it is necessary to impose bounds on the state variables to guarantee the invertibility of the linearizing transformations as well as to facilitate the calculation of conic-sector bounds. The region will consist of a scaled unit hypersphere which becomes a hyperellipsoid in the original variables.

The SSV yields performance results with the norm of an error signal being bounded by a norm on the input signal. If we select as an error signal x_s, the scaled states, then we can calculate an upper bound for x_s as a function of the inputs and the initial conditions. This particular value of the SSV will be denoted β_{BS}.

Theorem 3.4 *State Bound*

If the conditions of Theorem 3.3 are satisfied when the system state, x_s, are selected as the output, e, then the following bounds on the states hold:

$$\|x_s\|^2 \leq \alpha^2\|v\|^2 + \gamma^2\|x_{s0}\|^2 \leq 1 \tag{3.40}$$

where:

$$\begin{aligned} \alpha &= \beta_{BS}^2 \\ \gamma &= \bar{\sigma}^2(\hat{T}) \end{aligned}$$

and $\hat{T}$ is the state transformation used in Theorem 3.3.

Proof 3.4 *Theorem 3.3 results in:*

$$\|e\|_{\ell_2}^2 + (1-\beta^2)\|\hat{T}x_{cl}\|_{\ell_2}^2 \leq \beta^2\|v\|_{\ell_2}^2 + \|\hat{T}x_{cl0}\|_{\ell_2}^2 \tag{3.41}$$

Unwrapping the state transformation yields:

$$\|e\|_{\ell_2}^2 + \underline{\sigma}^2(\hat{T})(1-\beta^2)\|x_{cl}\|_{\ell_2}^2 \leq \beta^2\|v\|_{\ell_2}^2 + \bar{\sigma}^2(\hat{T})\|x_{cl0}\|_{\ell_2}^2 \tag{3.42}$$

Selecting the output, e, to be the plant states, x_s, and choosing zero initial conditions for the controller yields:

$$\|x_s\|_{\ell_2}^2 + \underline{\sigma}^2(\hat{T})(1-\beta^2)\|x_{cl}\|_{\ell_2}^2 \leq \beta^2\|v\|_{\ell_2}^2 + \bar{\sigma}^2(\hat{T})\|x_{s0}\|_{\ell_2}^2 \tag{3.43}$$

Which implies:

$$\|x_s\|_{\ell_2}^2 \leq \beta^2\|v\|_{\ell_2}^2 + \bar{\sigma}^2(\hat{T})\|x_{s0}\|_{\ell_2}^2 \tag{3.44}$$

For a given k, the following holds: $\|x_{sk}\|^2 \leq \sum_{k=1}^{\infty}\|x_{sk}\|^2 = \|x_s\|_{\ell_2}^2$. Thus the bounds hold but are somewhat conservative.

3.4 Conic-Sector-Bounded Nonlinearities

3.4.1 General Description

In this section, the class of nonlinear operators which are to be considered is formally defined. It is required that the operator $y = N(x)$ be inside a *conic sector* or *cone.* The simple definition for a conic sector introduced in chapter 2 is expanded as follows:

Definition 3.2 *The conic sector Cone(C,R,S) describes the bounds on a static, nonlinear, input-output mapping ($y = f(x)$), which satisfies:*

$$\text{Cone(C, R, S)} \triangleq \{(x,y) | y = Cx + S\Delta(Rx), \|\Delta(x)\| \leq \|x\|\} \tag{3.45}$$

For $y \in \Re^p, x \in \Re^n$ and a square Δ structure of size d, then $S \in \Re^{p\times d}, R \in \Re^{d\times n}$ and $C \in \Re^{p\times n}$. The cone described in chapter 2 now corresponds to:

$$\text{Cone(C, R, I)} \triangleq \{(x,y) | \|y - Cx\| \leq \|Rx\|\} \tag{3.46}$$

In simplest terms, the cone center C represents the best linear approximation of the nonlinear operator over the range of interest. The radii R and S give some measure of the error associated with this representation. A key point to note is that the Cone(C,R,S) contains many different operators, some of which may be considerably more pathological than the original nonlinear operator.

In terms of LFTs, the conic sector has a convenient representation which lends itself naturally to SSV analysis

$$\text{Cone(C, R, S)} = F_u(M_c, \hat{\Delta}) \text{ where } M_c = \begin{pmatrix} 0 & R \\ S & C \end{pmatrix} \tag{3.47}$$

and $\hat{\Delta}$ is inside the Cone(0,I,I). This shows quite clearly how the nominal plant Cx is perturbed via the terms R and S. A minimization of these two factors yields the least "uncertain" or most linear system. The term R accounts for the interactions between the inputs to the operator, and the term S takes into account the coupling between the outputs of the system. For example, a perfectly diagonal map such as $y_i = f_i(x)$ for $i = 1, p$, can be described by a cone with a diagonal R term and a diagonal Δ structure with p uncertain gains (the diagonal S term can be absorbed through the Δ block into the R term).

3.4.2 Optimal Cones

The objective of a minimally conservative paradigm is to reduce the effect of the $S\Delta R$ term in the conic-sector description of our nonlinear plant. This is determined by two factors:

- The overall magnitude of R and S.
- The complexity of the Δ structure.

The balancing of these two factors to yield the least conservative SSV calculation is a formidable task involving an elaborate iterative scheme. A simple algorithm is proposed here to arrive at a sub-optimal solution to this problem (though not necessarily the global optimum).

In general, the maximum (sensible) Δ is a diagonal matrix containing np independent gains. This assumes completely independent gains for each input-output matching in the mapping of N. At the other extreme, the simplest nonlinear operator could be described with a single uncertain gain. This is true in the conic-sector representation for the dynamics of a simple CSTR [25]. Simpler Δ structures are more attractive from a computational perspective and, in fact, the SSV is equal to its computable upper bound for some simple structures in the case where Δ is linear (but possibly time-varying) [72].

For a fixed Δ structure, a simple geometric argument will be made for the definition of a minimally conservative cone. Consider the case of a scalar nonlinear operator ($S = 1$). In Table 3.2 is shown the geometric interpretation of various conic sectors. In order to minimize the region inside the cone, one can minimize the hyperdimensional angle (or sum of such quantities), which defines the region. It can be shown that this is equivalent to a minimization of the Frobenius norm of the matrix R. This result can also be derived from the fact that the Frobenius norm is an upper bound for the infinity norm. Using the conic sector definition (Equation 3.45) we get:

$$\frac{\|S\Delta(Rx)\|}{\|x\|^2} \leq \frac{\|S\|\|\Delta(Rx)\|}{\|x\|^2} \leq \frac{\|S\|\|Rx\|}{\|x\|^2} \leq \|S\|_F\|R\|_F \qquad (3.48)$$

Three possibly distinct solutions to the conic-sector minimization problem can be envisioned corresponding to three Δ structures.

Table 3.2 Conic-Sector Regions - Geometric Interpretation		
d	**n**	**Region**
1	1	2 Flat Slices
1	2	2 Infinitely Deep Slices
2	2	2 Square Based Pyramids

Definition 3.3 *The* **Feasible** *solution to the nonlinear conic-sector bound minimizes the Frobenius norm of the product of the cone radii S, R, corresponding to the smallest* Δ *structure which can envelop the nonlinear operator.*

Definition 3.4 *The* **Full** *solution to the nonlinear conic-sector bound minimizes the Frobenius norm of the product of the cone radii S, R, corresponding to the largest sensible* Δ *structure (np independent gains).*

As the size of the Δ structure increases, the Frobenius norm must necessarily decrease (*i.e.*, the smaller feasible structures are all subsets of a larger structure).

Definition 3.5 *The* **Global Optimal** *solution to the nonlinear conic-sector bound minimizes the upper bound on the Structured Singular Value (SSV) corresponding to the uncertainty structure associated with the cone (C,R,S).*

As the first two are the limiting cases, the *Global Optimal* solution must lie between them. The tradeoff between simple Δ structure and small Frobenius norm is balanced at this point.

3.4.3 Numerical Calculations

A nonlinear program (NLP) is set up to calculate the solution which minimizes the Frobenius norm for a given Δ structure. The program requires q data points consisting of an input vector x and corresponding output vector y. As most of the nonlinearities for this study are monotonic and constrained to a finite region in x, it was often sufficient to calculate the data points along the boundary of the hyper-ellipsoid. The general scheme of the NLP is to minimize the Frobenius norm with the constraint that the data lie inside the calculated conic sector. Obviously, the larger the value of q, the more accurate the calculated conic sector and the greater the computational complexity of the NLP. For the case where the d sub-blocks of Δ are scalar, the NLP can be written

$$\begin{aligned}
&\text{Min } \eta \\
&\left(\sqrt{\textstyle\sum_{i=1}^{p}\sum_{j=1}^{d} S_{ij}^2}\right)\left(\sqrt{\textstyle\sum_{i=1}^{d}\sum_{j=1}^{n} R_{ij}^2}\right) = \eta \\
k = 1,q \begin{cases}
\sum_{i=1}^{n} C_{1i}x_{ik} + \sum_{i=1}^{d}\left[S_{1i}\left(\sum_{j=1}^{n} R_{ij}x_{jk}\right)\delta_{ik}\right] &= y_{1k} \\
\vdots & \\
\sum_{i=1}^{n} C_{pi}x_{ik} + \sum_{i=1}^{d}\left[S_{pi}\left(\sum_{j=1}^{n} R_{ij}x_{jk}\right)\delta_{ik}\right] &= y_{pk} \\
|\delta_{1k}| &\leq 1 \\
\vdots & \\
|\delta_{dk}| &\leq 1
\end{cases}
\end{aligned}$$

where $\{(y_{1k},\ldots,y_{pk}),(x_{1k},\ldots,x_{nk})\}$ are the given data points $(k = 1,q)$. The total number of variables is $(1 + dn + dp + pn + dq)$ and the total number of constraints is $(1 + pq + dq)$. It is important to note that the above algorithm can be used to find the linear bounds on an arbitrary polynomial approximation (cone center) to the nonlinear function. The additional variables introduced appear linearly in the equality constraint equations ($y = C_1x + C_2x^2 + \cdots$). For example, consider a quadratic cone center which approximates an operator with two inputs and one output. As there is

only a single output, there is no need for an S matrix, and the equality constraints in the NLP become:

$$C_{11}x_{1k}^2 + C_{12}x_{1k}x_{2k} + C_{22}x_{2k}^2$$
$$+ [\delta_{1k}(R_{11}x_{1k} + R_{12}x_{2k}) + \delta_{2k}(R_{21}x_{1k} + R_{22}x_{2k})] = y_{1k}$$

This approach will be used in conjunction with the QAL scheme.

3.4.4 Design Procedure

The overall design procedure is indicated by the flowchart in Figure 3.11. First, a reasonable region of operation is selected over which the selected control law is valid (no singularities in the nonlinear control algorithm). Next, a second order approximation is introduced for the cone center in the numerical algorithm of Section 3.4.3. Using the QAL software, the approximate involutivity condition is verified. In the event that this property is not satisfied, the "nearest" involutive second order plant is found. The result at this stage is a representation of the closed-loop linearized plant and the Δ_1 term which is required to represent the third and higher order terms neglected in the approximate linearization. Next we consider the impact of disturbances on the nonlinear closed-loop system. The nonlinear cone center and radii for this additional nonlinearity is calculated and the resultant system is evaluated against theorem 3.4. Violation of this theorem suggests two alternatives. First, the magnitude of the disturbance can be reduced in an effort to satisfy the originally formulated state bounds. Otherwise, the region of operation (state bounds) must shrink until theorem 3.4 is satisfied. If the state bounds shrink to zero, the robust performance for the nonlinear system approaches the nominal performance for its linear approximation (Jacobian). Using this as a lower bound, the region is increased and, as more nonlinearity is introduced, the resulting performance degradation is observed.

Once the state bounds have been verified, the uncertainty formulation based upon the conic-sector description is validated. Now the standard robust performance analysis can be performed upon the closed-loop system.

3.5 Example #3: Nonlinear Exothermic CSTR with First Order Kinetics

3.5.1 CSTR Model

The dimensionless mass and energy balances for a CSTR (see Figure 3.12) with first order, irreversible, exothermic kinetics ($A \rightarrow B$) are given by

$$\begin{aligned} \dot{\tilde{x}}_1 &= \tilde{f}_1 = -\tilde{x}_1 - x_{10} + \mathcal{D}a(1 - \tilde{x}_1 - x_{10})e^{\frac{\tilde{x}_2 + x_{20}}{1+(\tilde{x}_2+x_{20})/\gamma}} \\ \dot{\tilde{x}}_2 &= \tilde{f}_2 - \beta u + d = -\tilde{x}_2 - x_{20} - \beta(\tilde{u} + u_0) + d \\ &\quad + \mathbf{B}\mathcal{D}a(1 - \tilde{x}_1 - x_{10})e^{\frac{\tilde{x}_2 + x_{20}}{1+(\tilde{x}_2+x_{20})/\gamma}} - \beta(\tilde{x}_2 + x_{20}) \end{aligned} \tag{3.49}$$

using the dimensionless quantities defined in Table 2.1. This simple model has two state variables (reactant concentration, reactor temperature). The control problem focuses on the SISO regulation of the reactor temperature by manipulating the cooling water temperature while subjected to disturbances in the feed-stream temperature. The values of the dimensionless parameters are [12]: $\mathcal{D}a = 0.072, \mathbf{B} = 8, \beta = 0.3, \gamma = 20$ and $x_c = 0.0$. These conditions lead to multiple steady states and operation is chosen at the unstable point ($u_0 = -0.20, x_{10} = 0.5, x_{20} = 3.03$).

3.5.2 Linearizing Transformations and Uncertainty Description

We consider three controller synthesis techniques (GSL, QAL and simple linear (P, PI)), as well as two disturbance classes (bounded energy and steps). The GSL results have been published elsewhere [12],[42]; we merely summarize here. The state and

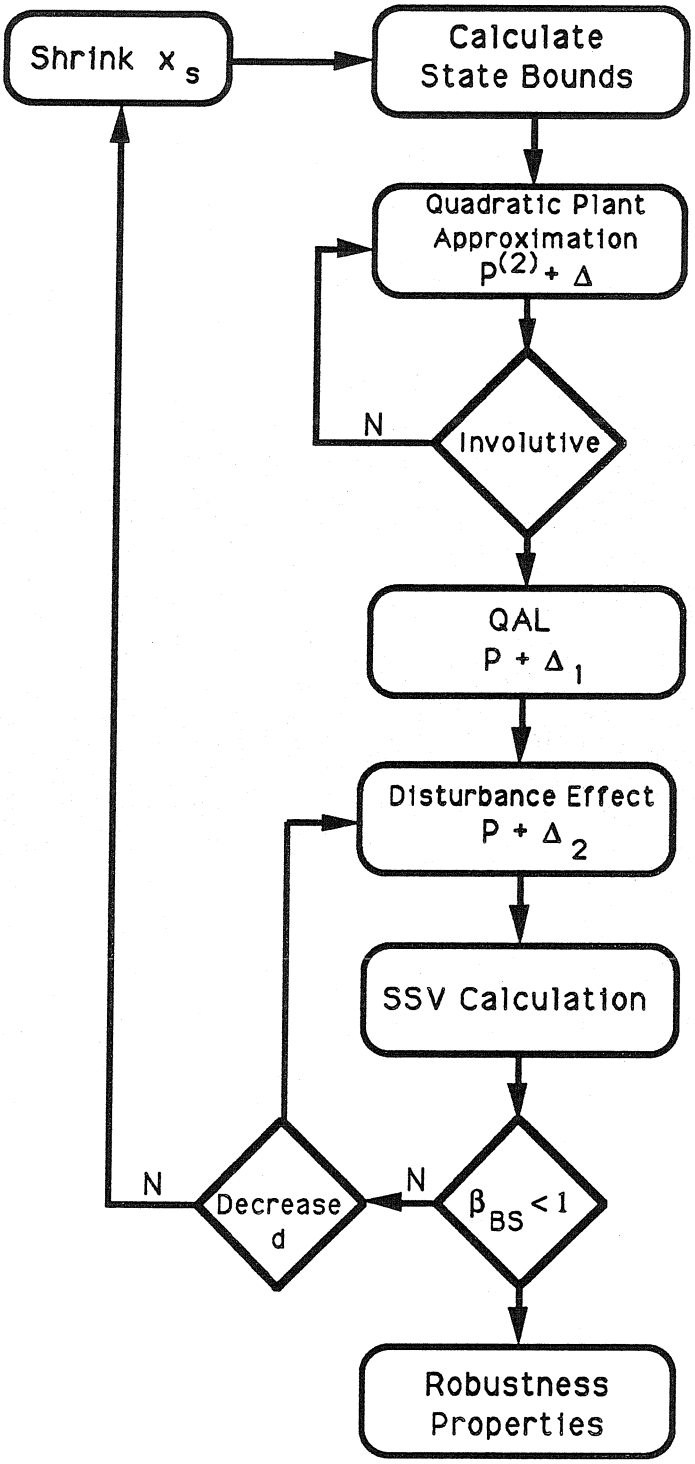

Figure 3.11. Design Flowchart

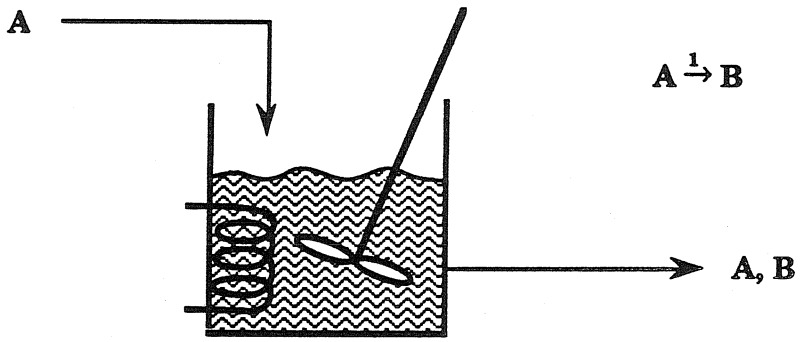

Figure 3.12. Example #3 – Exothermic CSTR

input transformations

$$\begin{aligned} z_1 = \quad & T_1(x) = \quad x_1 - x_{10} \\ z_2 = \quad & T_2(x) = \quad \tilde{f}_1(x_1 - x_{10}) \\ \alpha(x) = \quad & < dT_2, f > \\ \beta(x) = \quad & < dT_2, g > -I \end{aligned} \tag{3.50}$$

yield, in transformed coordinates, the dynamical system

$$\dot{z} = \begin{pmatrix} 0 & 1 \\ 0 & 0 \end{pmatrix} z + \begin{pmatrix} 0 \\ 1 \end{pmatrix} v + \begin{pmatrix} 0 \\ \dfrac{(z_2+z_1+x_{10})d}{\left[1+\dfrac{1}{\frac{\gamma}{\ln\frac{z_2+z_1+x_{10}}{Da(1-z_1-x_{10})}}-1}\right]^2} \end{pmatrix} \tag{3.51}$$

It is clear to see the constraints imposed by inverting $T_2(x)$ in Equation 3.50. For general problems, this inherent limitation restricts the application of state linearization techniques to local regions in the phase space. For the purpose of this study, we consider the region of interest to be the interior of the ellipse:

$$\frac{z_1^2}{.08^2} + \frac{z_2^2}{.55^2} = 1 \tag{3.52}$$

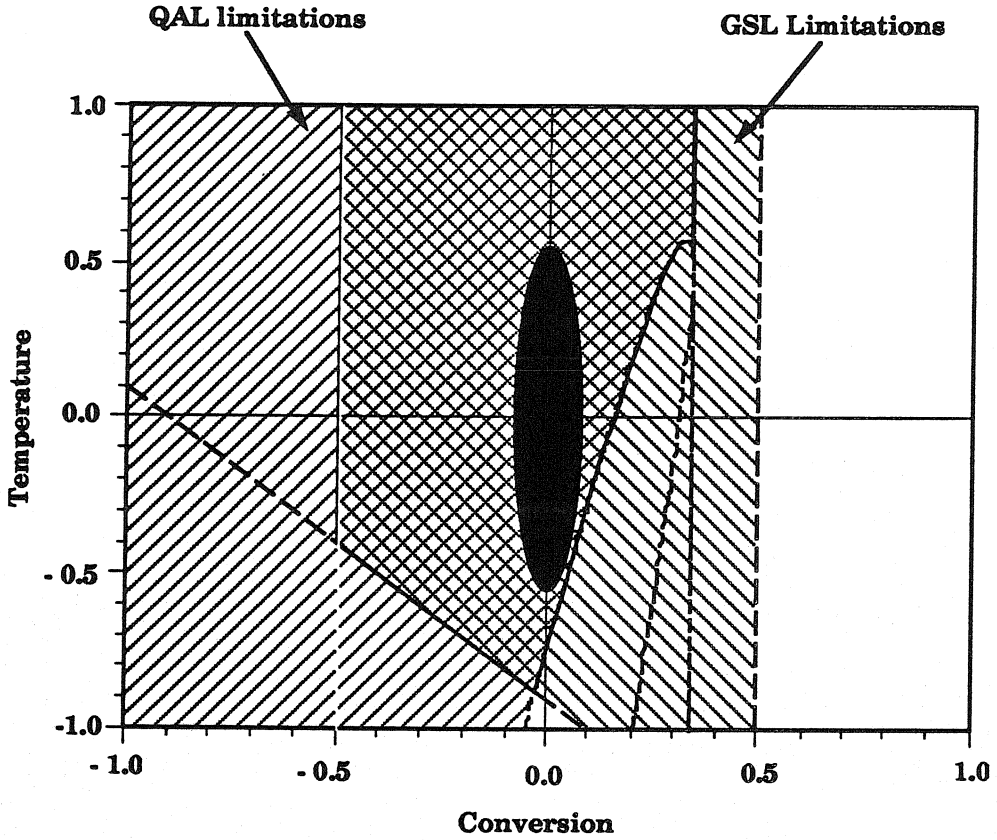

Figure 3.13. Region of Operation (Example #3)

for QAL. This corresponds roughly to a circle of radius 0.1 in the z domain for GSL. This region and the constraints on it are depicted in Figure 3.13.

For the QAL, it is necessary to calculate a nominal quadratic plant. Using the NLP described in the previous section, it is found that the *second* order plant with the tightest conic sector over the region of interest (Equation 3.52) is given by:

$$\begin{aligned} \dot{\tilde{x}}_1 &= -2\tilde{x}_1 + .381\tilde{x}_2 + .020\tilde{x}_1^2 - .761\tilde{x}_1\tilde{x}_2 + .127\tilde{x}_2^2 \\ \dot{\tilde{x}}_2 &= -8\tilde{x}_1 + 1.75\tilde{x}_2 + .320\tilde{x}_1^2 - 6.09\tilde{x}_1\tilde{x}_2 + 1.02\tilde{x}_2^2 + 0.3\tilde{u} \end{aligned} \tag{3.53}$$

The uncertainty is characterized by a single uncertain gain with radii: $S = (1 \quad 8)^T, R = (0 \quad 0.0067)$. This can be compared with the tightest conic sector

associated with a *first* order approximation of the nonlinear plant

$$\dot{\tilde{x}} = \begin{pmatrix} -2 & 0.377 \\ -8 & 1.718 \end{pmatrix} \tilde{x} + \begin{pmatrix} 1 \\ 0.3 \end{pmatrix} \tilde{u} \tag{3.54}$$

and its associated uncertainty radii: $S = (1 \quad 8)^T, R = (0 \quad 0.104)$. Using the objective in our NLP as a measure, the quadratic approximation reduces the nonlinear uncertainty by a factor of 15. The second order system in Equation 3.53 yields an exact quadratic linearization with the following state and input transformations :

$$\begin{aligned} z_1 = T_1(x) = \quad & \tilde{x}_1 \quad -0.7388\tilde{x}_1^2 \\ z_2 = T_2(x) = \quad & \tilde{x}_2 \quad +3.9320\tilde{x}_1^2 - 3.4751\tilde{x}_1\tilde{x}_2 + 0.3333\tilde{x}_2^2 \\ \alpha(x) = \quad & \quad -1.3304\tilde{x}_1^2 - 4.9235\tilde{x}_1\tilde{x}_2 + 0.9311\tilde{x}_2^2 \\ \beta(x) = \quad & \quad -3.4751\tilde{x}_1 + 0.6667\tilde{x}_2 \end{aligned} \tag{3.55}$$

Just as in the case of GSL, the state transformations derived for QAL are not globally invertible and the loci of singularity are shown in Figure 3.13. These loci correspond to values of z which result in complex values for x.

The transformed coordinates yield the same linear approximation

$$\dot{z} = \begin{pmatrix} -2 & 0.3808 \\ -8 & 1.7467 \end{pmatrix} z + \begin{pmatrix} 0 \\ 0.3 \end{pmatrix} v + \left[\frac{\partial T}{\partial x} \begin{pmatrix} 0 \\ d \end{pmatrix} \right]_{x=T^{-1}(z)} + \Delta P \tag{3.56}$$

where the Jacobian is calculated from Equation 3.55. The other term in this equation, ΔP, accounts for both the error in approximating the nonlinear plant by a second order system and also for the order three and higher terms inherent in the QAL.

In summary for the disturbance problem, the GSL scheme requires a single uncertainty block to represent the nonlinear effect of the disturbance. This block is optimally modeled with two uncertain nonlinear gains. The QAL technique requires an uncertainty block for both the nonlinear disturbance effect and the plant model-

Table 3.3 Uncertainty Description (Example #3)		
Method	**Δ structure**	$\|S\|_F \|R\|_F$
GSL	$\begin{pmatrix} \delta_1 & 0 \\ 0 & \delta_2 \end{pmatrix}$	0.29
QAL	$\begin{pmatrix} \delta_1 & 0 & 0 \\ 0 & \delta_2 & 0 \\ 0 & 0 & \delta_3 \end{pmatrix}$	0.61
Linear	(δ_1)	1.10

ing error. In this case, the optimal uncertainty description has three nonlinear gains. Finally, the simple linear control approach requires a single uncertain gain to represent the error inherent in the first order approximation. The structure of the various uncertainty blocks and the magnitude of their radii are listed in Table 3.3. It should be pointed out that conclusions about the various schemes based on these data alone should be drawn carefully. The schemes represent rather different coordinate systems as well as uncertainty structures.

3.5.3 Analysis of Stability Properties

We restrict our attention in this chapter to a particular performance criterion - namely the bounding of the states while the plant is subjected to two classes of disturbances. In the first case, we consider bounded inputs of bounded energy (*e.g.*, decaying sinusoids). In the second case, we consider the class of inputs of bounded energy passed through the filter $\frac{1}{s}$ (*e.g.*, steps).

Bounded-Energy Disturbances

In this case it is sufficient to consider simple proportional control in the outer loop of Figure 3.1. No integral action is required for feed temperature disturbances of bounded energy to guarantee zero offset. The controller gains $[1.35, 2.12]$, as found in [12], are used for the GSL, and the gains $[-16.9, 6.23]$ yield the same closed-loop poles for the QAL (and the simple linear approach). To simplify the comparison, all three systems are required to have the same closed-loop dynamics in the *transformed* variables. A more realistic comparison might involve calculating a controller to give the same dynamics in the original variables, but as shown in section 3.1, this is not easily done for the GSL.

The analysis procedure involves varying the magnitude of d and calculating a corresponding value of β_{BS}. Then we can use Equation 3.40 to calculate a bound on the initial state. For the general robust performance problem, one can use this approach to calculate the tradeoff between initial condition and input magnitude effects on the computed performance guarantee. For the state bound problem, the tradeoff curves are plotted in Figure 3.14. Recall that this approach yields sufficient results, so the curves in this diagram represent a lower bound on the tolerable disturbance and initial condition magnitudes which give rise to bounded states. An additional point is given in the diagram to show an actual simulation in which the states escape the bound in Equation 3.52. This represents an upper bound on the tolerable disturbance magnitude (zero initial condition), and the proximity of the points along the y-axis shows the promise of this technique.

In Figure 3.15, we depict the various state bounds as they are mapped into the true $x_1 - x_2$ coordinate system. As expected, the QAL contour shows minimal deformation of the original ellipse as compared to the GSL contour. It is evident from this figure that a precise comparison of the results is not possible. Each result guarantees stability over a different region in the phase space. Included in this diagram is the

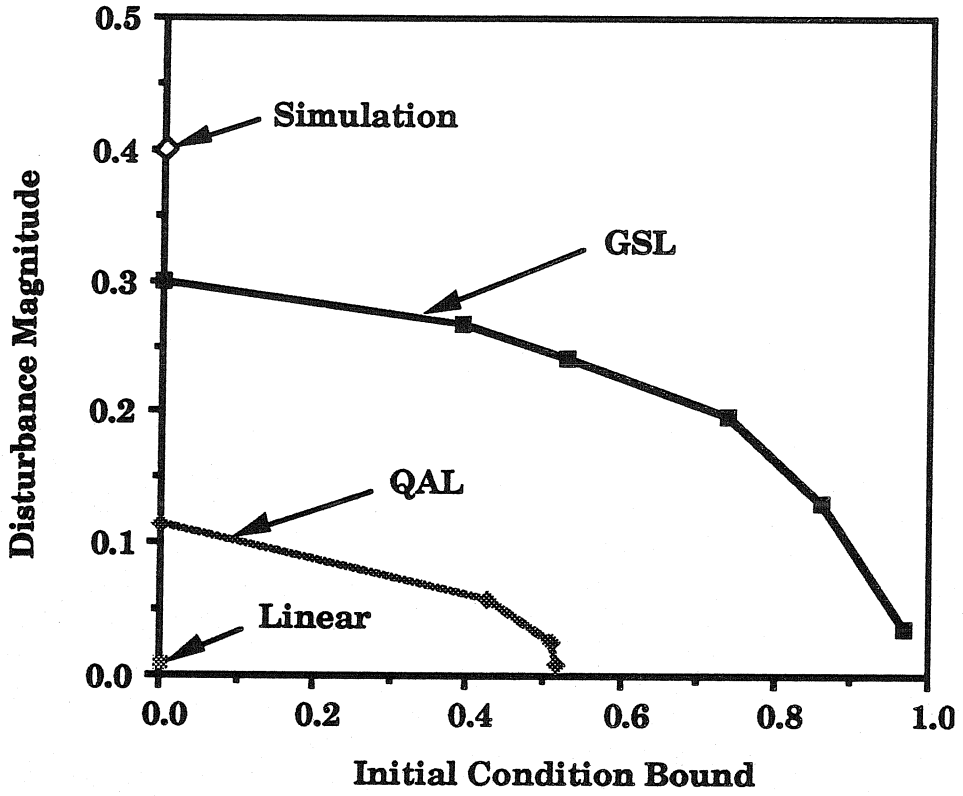

Figure 3.14. Bounds for Which Closed-Loop Stability is Guaranteed (Example #3, Bounded $\mathcal{L}_2$ Signals)

phase portrait of the response of the simple linear system to the input disturbance $0.3\,e^{-.25t}\,sin(.5t)$. The response of the QAL and GSL are virtually identical to the depicted response for this input. This indicates that Table 3.3 is a reasonable measure of the conservatism inherent in analyzing the three approaches in the SSV framework.

Step Inputs

The above procedure is repeated for persistent step disturbances with PI control in the outer loop for asymptotic tracking. The controller gains are $[4.93, 3.93]$ for the GSL and the error in z_1 is integrated with $\tau_I = 0.422$. For the QAL (and linear) schemes, the gains which yield the same closed-loop poles are $[-17.27, 12.25]$ and $\tau_I = 0.0482$. The GSL approach suffers from the weakness that only z_1 represents a

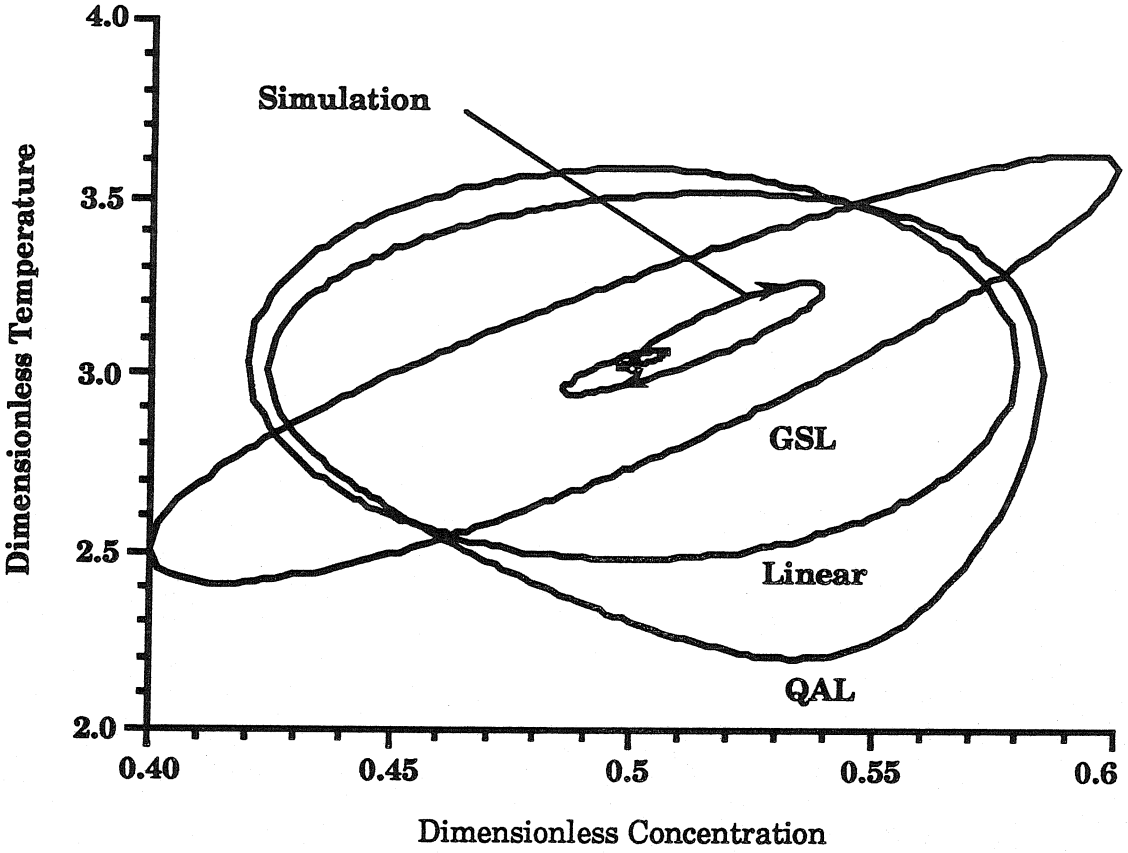

Figure 3.15. Bounds on State Trajectories (Example #3)

physically meaningful quantity to integrate. This is opposed to the flexibility inherent in the QAL scheme to integrate a reasonable estimate of x_2. The tradeoff between disturbance bounds and initial condition magnitudes is shown in Figure 3.16.

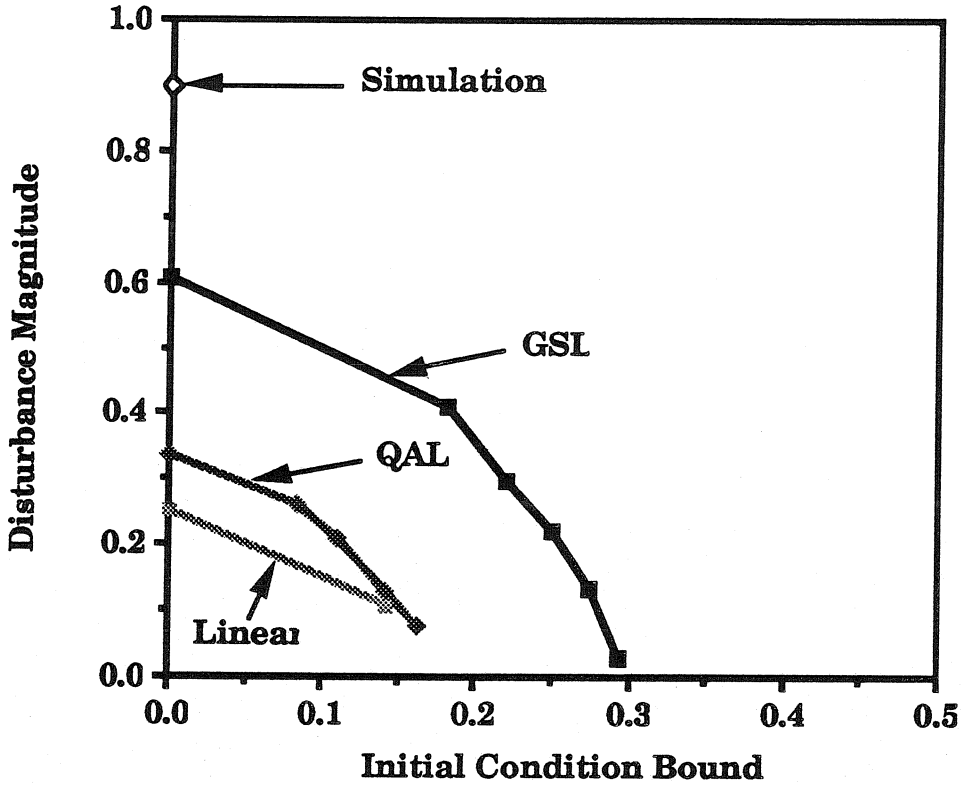

Figure 3.16. Bounds for Which Closed-Loop Stability is Guaranteed (Example #3, Step-like Signals)

3.6 Example #4: Nonlinear Isothermal CSTR with Van de Vusse Kinetics

3.6.1 CSTR Model

The dimensionless mass balances for a CSTR with isothermal Van de Vusse kinetics [87] (Figure 3.17) are given by

$$\begin{aligned} \dot{x}_1 &= -k_1 x_1 - k_3 x_1^2 + u(x_{10} - x_1) \\ \dot{x}_2 &= k_1 x_1 - k_2 x_2 + u(-x_2) + d \\ y &= x_2 \end{aligned} \tag{3.57}$$

using the dimensionless quantities defined in Table 3.4. This simple model has two

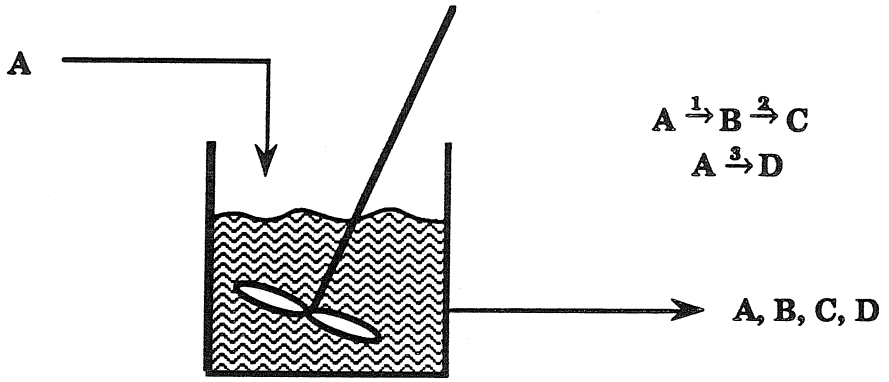

Figure 3.17. Example #4 – Van de Vusse Reaction

Table 3.4 Dimensionless Variables for Example #4	
x_1	$x_{10}\frac{C_A}{C_{A0}}$
x_2	$x_{10}\frac{C_B}{C_{A0}}$
d	$x_{10}\frac{C_{B0}}{C_{A0}}$
u	$\frac{F}{V}$

state variables corresponding to the two chemical species. The control problem focuses on the SISO regulation of the concentration of B by manipulating the inlet flowrate of A (dilution rate) while subjected to disturbances from a side stream containing B. The values of the dimensionless parameters are: $x_{10} = 5.0, k_1 = 0.5, k_2 = 3.0, k_3 = 0.5$. These conditions allow operation at the following point: $(u_0 = -1.0, x_{10} = 2.0, x_{20} = 0.25)$.

3.6.2 Linearizing Transformations and Uncertainty Description

We consider three controller synthesis techniques (GSL, QAL and simple linear (P, PI)). The GSL approach results in the following state and input transformations :

$$z_1 = \quad T_1(x) = \quad \text{function of } \frac{x_2}{x_{10} - x_1}$$

$$z_2 = \quad T_2(x) = \quad L_f(z_1)$$

$$\begin{aligned} \alpha(x) = &\quad < dT_2, f > \\ \beta(x) = &\quad < dT_2, g > -I \end{aligned} \tag{3.58}$$

In this example, we find that the new states (z_1, z_2) have very complicated dependence on the original states (x_1, x_2) and yield a dynamical system for which it is difficult to translate our original control objectives (on the concentration of B). One approach around this is to satisfy the GSL conditions for one of the states but retain our output (x_2) in the resultant linearized dynamics. This leads to the so-called input-output linearization (IOL) [54]. A detailed discussion of this approach is postponed until chapter 4. It is sufficient to point out that this method requires a minimum phase system. It can be easily shown that the system described above also violates this condition.

Consequently, the only meaningful approach is to consider QAL. The second order system in Equation 3.57 yields an exact quadratic linearization with the following state and input transformations :

$$\begin{aligned} \tilde{z}_1 = T_1(\tilde{x}) = &\quad \tilde{x}_1 \quad -0.09376\tilde{x}_1^2 - 0.5225\tilde{x}_1\tilde{x}_2 - 0.1529\tilde{x}_2^2 \\ \tilde{z}_2 = T_2(\tilde{x}) = &\quad \tilde{x}_2 \quad +0.02532\tilde{x}_1^2 + 0.1303\tilde{x}_1\tilde{x}_2 + 0.03345\tilde{x}_2^2 \\ \alpha(\tilde{x}) = &\quad -0.1444\tilde{x}_1^2 + 0.6457\tilde{x}_1\tilde{x}_2 + 0.2294\tilde{x}_2^2 \\ \beta(\tilde{x}) = &\quad -0.4773\tilde{x}_1 - 0.4970\tilde{x}_2 \end{aligned} \tag{3.59}$$

As before, there are constraints imposed by inverting the transformations in Equation 3.59. For the purpose of this study, we consider the region of interest to be the interior of the ellipse:

$$\frac{z_1^2}{.27^2} + \frac{z_2^2}{.05^2} = 1 \tag{3.60}$$

The nonlinear transformations are invertible over the entire physical range of the variables (zero concentration - full conversion). In the transformed coordinates the

Table 3.5 Uncertainty Description (Example #4)

Method	Δ structure	$\|S\|_F\|R\|_F$
QAL	$\begin{pmatrix} \delta_1 & 0 & 0 & 0 & 0 \\ 0 & \delta_2 & 0 & 0 & 0 \\ 0 & 0 & \delta_3 & 0 & 0 \\ 0 & 0 & 0 & \delta_4 & 0 \\ 0 & 0 & 0 & 0 & \delta_5 \end{pmatrix}$	2.67
Linear	$\begin{pmatrix} \delta_1 & 0 & 0 \\ 0 & \delta_2 & 0 \\ 0 & 0 & \delta_3 \end{pmatrix}$	1.14

dynamics are given by

$$\dot{z} = \begin{pmatrix} -3.5 & 0.0 \\ -0.5 & -4.0 \end{pmatrix} z + \begin{pmatrix} 3 \\ -0.25 \end{pmatrix} v + \left[\frac{\partial T}{\partial x} \begin{pmatrix} 0 \\ d \end{pmatrix} \right]_{x=T^{-1}(z)} + \Delta P \tag{3.61}$$

where the Jacobian is calculated from Equation 3.59. The quadratic transformation is also invertible over the region defined in Equation 3.60. The other term in this equation, ΔP, accounts for both the error in approximating the nonlinear plant by a second order system and also for the order 3 and higher terms inherent in the QAL. It can be calculated from the following equation which is obtained by subtracting the linear resulting plant from the transformed nonlinear original system:

$$\begin{aligned} \Delta P = & \left(\tfrac{\partial T}{\partial x} \left[f(x) + g(x)\alpha(x) \right] |_{x=T^{-1}(z)} \right) + \left(\tfrac{\partial T}{\partial x} \left[g(x)(I + \beta(x)) \right] |_{x=T^{-1}(z)} \right) v \\ & - \left[\begin{pmatrix} -3.5 & 0.0 \\ -0.5 & -4.0 \end{pmatrix} z + \begin{pmatrix} 3 \\ -0.25 \end{pmatrix} v \right] \end{aligned} \tag{3.62}$$

The tightest uncertainty formulation for these two closed-loop systems (QAL and

linear), including disturbances, is outlined in Table 3.5. QAL requires five independent nonlinear gains for enveloping the nonlinear remainder terms and the linearly controlled reactor required three independent nonlinear gains to cover its nonlinear elements. The product of the Frobenius norm of the radii for QAL is more than twice as large as the product of the Frobenius norm for the linear case. This is in part due to the number of gains in the QAL structure, and in part due to the resultant transformations which have not been normalized over the relatively skewed ellipse in Equation 3.60. As mentioned in the previous case study, it is not advised to draw comparative observations from the results in this table. The SSV calculations are conservative and represent upper bounds for attainable performance levels. In fact, as the simulations in the next section will demonstrate, the QAL scheme demonstrates superior robust stability properties over linear control for the Van de Vusse reactions in a CSTR.

3.6.3 Analysis of Stability Properties

Bounded-Energy Disturbances

The linear control synthesis scheme for the linearly controlled system and the outer loop for QAL are identical due to the equivalent Jacobian approximations in each case. As can be verified from Equation 3.61, the reaction system possesses a right half plane zero and is therefore minimum phase. The IMC approach is used to synthesize a linear controller with a first order filter (time constant = 0.1).

The design procedure outlined in Figure 3.11 results in the tradeoff curves depicted in Figure 3.18. This figure suggests that the linearly controlled system can handle much larger disturbances over a wider range in the state variables than the QAL controlled system. The trends in this figure follow logically from the uncertainty formulation in Table 3.5. However, it is emphasized that these results are only upper bounds.

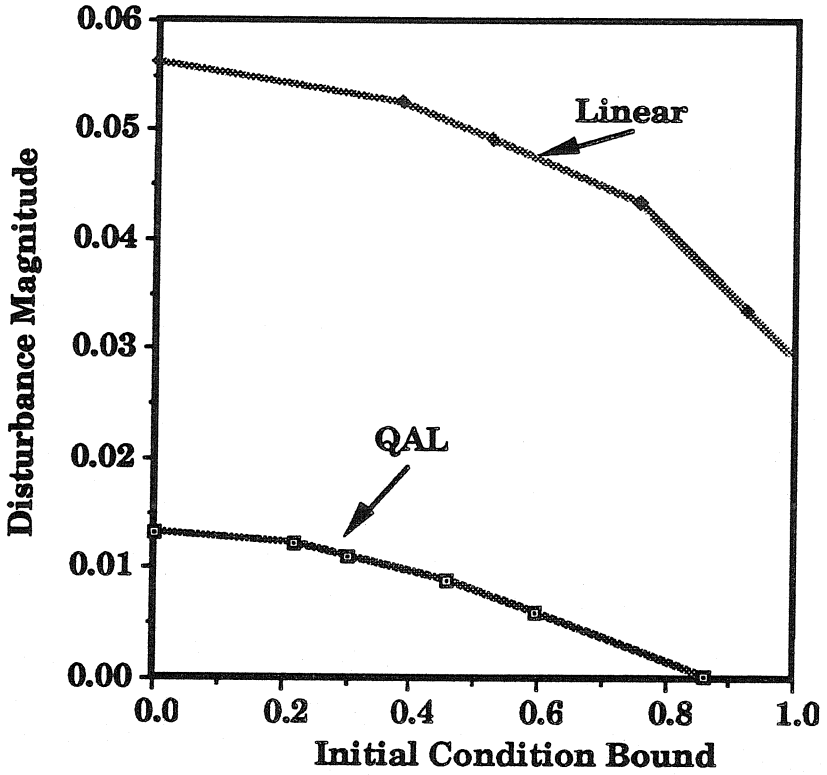

Figure 3.18. Bounds for Which Closed-Loop Stability is Guaranteed (Example #4, Bounded $\mathcal{L}_2$ Signals)

Despite the results from the SSV analysis, QAL for a quadratic, highly nonlinear system is expected to yield vastly superior robustness results over the linearly controlled system. (Highly nonlinear refers to the presence of nonlinear $f(x)$ and $g(x)$ in the state dynamics for the reactor.) These claims will be investigated through closed-loop simulations.

Simulation

In Figure 3.19 are shown the responses of the closed-loop reactor system to an impulse disturbance in the concentration of species A (equivalently consider nonzero initial conditions for x_1). The top two graphs show the response of C_A and C_B (in normalized, deviation variables) for both QAL (solid line) and IMC linear control (dashed line) to a 10% perturbation in C_A. The results are virtually indistinguish-

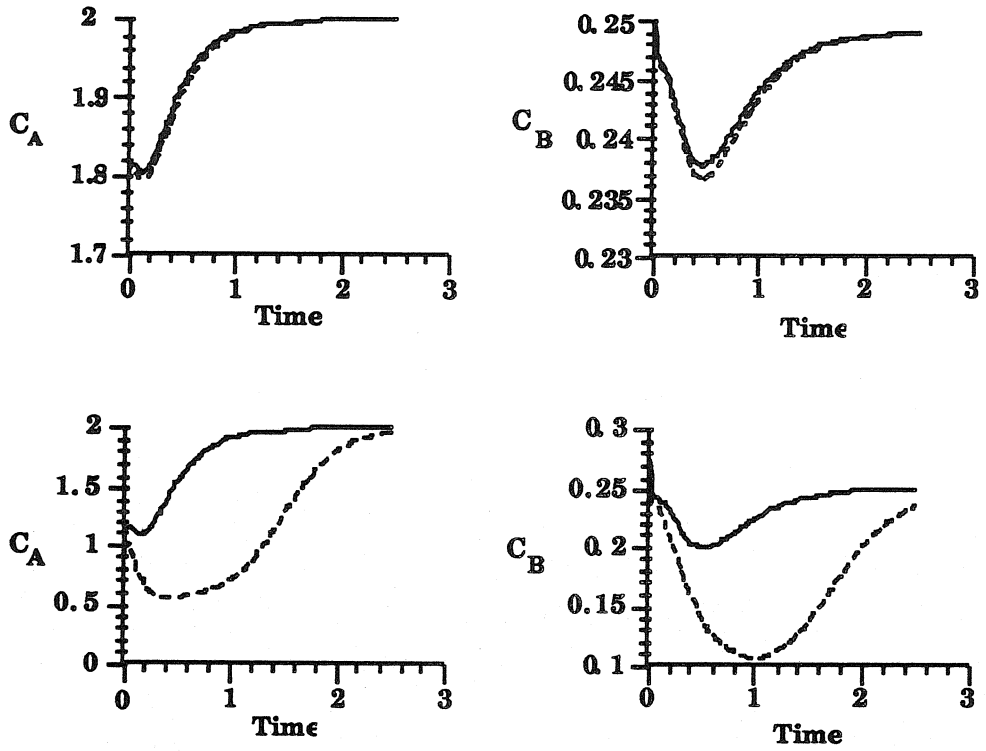

Figure 3.19. Disturbance Response (Example #4, Linear (dashed), QAL (solid))

able over this small range. Note that this range is completely covered by the ellipse in Equation 3.60. This indicates that the results in Table 3.5 are very conservative.

The lower two graphs in Figure 3.19 show the same reactor variables when subjected to a larger (45%) perturbation in C_A. Now the nonlinear dynamics are clearly manifested in the linearly controlled system. In fact, a slightly larger perturbation (50%) will drive the linearly controlled system unstable. This is in direct contrast to the QAL scheme, which behaves qualitatively the same in each case: its response is scaled linearly. To understand this effect more clearly, consider the curves in Figures 3.20 and 3.21.

Shown here are the values of the output, C_B, and the manipulated variable, u, from the last simulation. The curves represent the linear controller (NLMLC), QAL (NLMNLC), and an additional curve is added to show the response of the ideal linear model (Jacobian) under linear control (LMLC). Now the "linearizing" ability of QAL

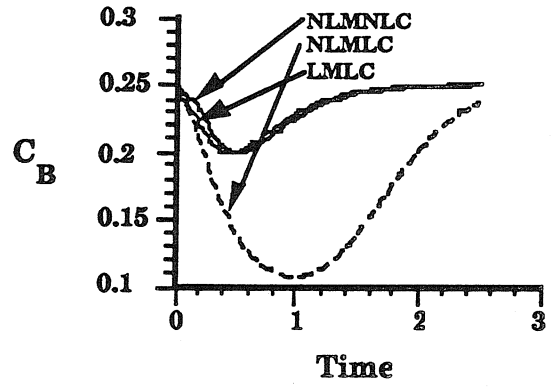

Figure 3.20. Disturbance Response (Example #4)

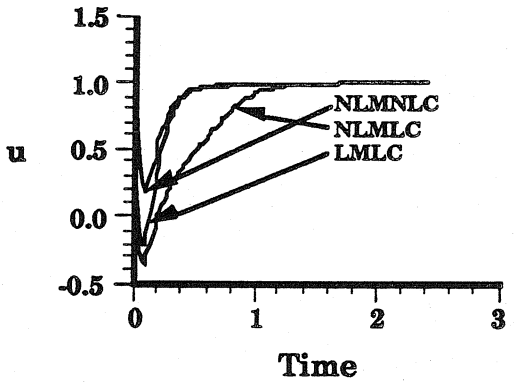

Figure 3.21. Disturbance Response (Example #4)

is evident. The output for QAL in Figure 3.20 tracks the linear output exactly. This is accomplished at the expense of the relatively aggressive control action illustrated in Figure 3.21.

A few concluding comments regarding this example are in order:

- Simulations confirm the superior performance of QAL over linear control for this reactor.
- Results from SSV theory predict a vastly superior performance for the linearly controlled system.

This example clearly emphasizes the need for continued research in the formulation of minimally conservative criteria for the calculation of robustness properties for a

nonlinear system. The positive result demonstrated in this example is the tremendous improvement in system performance attained when second order nonlinear effects are directly treated.

3.7 Conclusion

In this chapter, we have revealed the theoretical concepts which demonstrate that the Quadratic Approximate Linearization is a more practical linearization scheme than the Global State Linearization. The presence of external disturbances and unmodeled dynamics is manifested in relatively minimal nonlinear behavior in the QAL scheme. In addition, the broad applicability of this technique and potential for systematic optimization of the resultant solution further motivate its use. Through several case studies, the relative merit of QAL over both GSL and linear control is clearly demonstrated.

An additional contribution developed in this chapter is a formal algorithm for calculating minimally conservative conic-sector bounds for a general nonlinear operator. The result is expressed in the form of an nonlinear optimization and several examples involving its application are illustrated. New extensions of the structured singular value are used in conjunction with the uncertainty structures resulting from these conic-sector bounds to calculate bounds on the robustness properties of several chemical reaction systems. Performance specifications are derived over physically significant operating regions in the reactors. Unfortunately, the conclusions drawn for a single system with different controllers (GSL, QAL, and linear) indicate that the results are fairly conservative and not appropriate for absolute comparisons.

In the final case study, the application of QAL to a highly nonlinear quadratic system resulted in vastly superior performance over linear control. This demonstrates the utility in a nonlinear approach which directly handles successively higher order terms in a series approximation of a true system. The software for Ternary Approx-

imate Linearization (TAL) is currently being released and future work in this area will center on an investigation of the incremental improvement in TAL over QAL for certain classes of process systems.

Acknowledgements

The author wishes to thank Sinan Karahan for providing a preliminary version of the MATLAB software for Approximate Linearization.

Chapter 4

Implications of Nonlinear Control for a Packed Bed Reactor

Abstract

A nonlinear controller design for a packed bed reactor is presented. The scheme employs a two-tier approach in which first, a low-order nonlinear model is developed and, subsequently, a feedback linearizing control law is synthesized. The reduced-order model treats transport mechanisms in the reactor as a nonlinear wave which propagates through the bed. Application of input-output "linearizing" control yields mild linear dynamics over a range of operating conditions which lead to parametrically sensitive (open-loop) reactor behavior. The practical issues of implementing the resultant digital, implicit, nonlinear control law on an actual system are addressed. Analytical tools are employed, along with closed-loop simulations, to illustrate the robustness properties of the nonlinear controller. In addition, the relative strengths of this approach over traditional linear control are identified.

4.1 Introduction

Packed bed reactor control and modeling have been an active area for both academic and industrial research. For the most part, previous approaches have focused on models described by large-order linear systems of ordinary differential equations (ODEs) which approximate the partial differential equations (PDEs) for the mass and en-

ergy balances in the reactor. These models, in turn, are employed in a model-based framework, such as model predictive control or internal model control, to synthesize a controller. For a survey of the academic and industrial efforts towards this goal, the interested reader is referred to [46].

While traditional approaches toward packed bed reactor control have sought to maintain the cooling jacket temperature at its optimal steady-state value, more recent studies have suggested that periodic control can lead to higher yields [27]. By exploiting the excitation of intermediates on the catalyst, these highly nonlinear and heterogeneous kinetics are optimized.

Recently there has been considerable interest in nonlinear approaches to controlling other chemical process systems, notably the differential geometric techniques of feedback linearization. These schemes use measurements of the system's dynamic states in the construction of a nonlinear inverse for the process. Effectively, this yields a linear dynamical system which can be treated with the rich array of linear control tools. Previous studies have investigated the application of these techniques to lumped parameter models of CSTRs [12] [42], bioreactors [47], and polymerization reactors [17]. In the area of distributed parameter systems (DPS), recent work has described the application of these techniques to a distillation column [63]. However, there have been no reported results of application of these techniques to complex, distributed parameter reaction systems like packed bed reactors.

In this chapter, a nonlinear control methodology for a fixed bed catalytic reactor is developed. There were a number of restrictions and constraints encountered in applying these techniques to a packed bed reactor, particularly with regard to the type of reactor model employed. The control synthesis techniques require relatively low-order nonlinear lumped parameter models. This has lead to the formulation of a two-tier approach for the controller design:

- Develop an accurate low-order nonlinear reactor model.

- Synthesize a feedback linearizing control law for the reactor.

In addition, there are many practical issues which arise in the application of these techniques to complex practical systems. These include sampling effects for digital control implementation and the treatment of implicit nonlinear control laws.

Finally, there are some fundamental analytical questions which must be addressed concerning the effectiveness of nonlinear control. This issue is often overlooked in feedback linearization studies. The proposed algorithm is evaluated against traditional linear approaches to process control.

In summary, the primary contributions of this chapter are:

- The development of an accurate low-order nonlinear model for a packed bed reactor.
- The synthesis of feedback linearizing control for the packed bed reactor.
- The identification of practical issues of implementing feedback linearizing control for a practical system.
- The analysis of the comparative merits of nonlinear versus linear control for the packed bed reactor.

Although the differential geometric techniques have been largely restricted in study to academic examples in the literature, an industrial application has been reported recently in France [58]. Here, the targeted process is a 42-tray depropanizer and the results suggest strong improvements when nonlinear control is chosen to replace the existing linear approach. It is anticipated that future studies, such as the one presented in this work, will help to elucidate the potential advantages for nonlinear control of chemical process units and may, in turn, lead to further industrial implementation of such control techniques.

4.1.1 Notation

A brief review of some of the technical terms and concepts used in the field of differential geometry is presented. The first-order approximation (Jacobian) of a nonlinear system will be referred to as the *classical linearization* in contrast to the nonlinear control scheme known as *feedback linearization.* Let $x \in \Re^n$, and f, g, and h be real analytic vector functions of x. The following differential operator, so-called the *Lie* derivative or directional derivative, is defined as the following:

$$L_f \doteq f_1 \frac{\partial}{\partial x_1} + \cdots + f_n \frac{\partial}{\partial x_n} \tag{4.1}$$

where f_i is the i^{th} component of f.

4.2 Reactor Model Development

4.2.1 Previous Approaches

The mass and energy balances for a tubular catalytic reactor with an exothermic reaction are given by the following coupled nonlinear PDEs (homogeneous model):

$$\begin{gathered} u\frac{\partial c}{\partial z} = r(c,T)(1-\epsilon) \\ c(t,0) = c_0(t) \\ (\rho C_p)^* \frac{\partial T}{\partial t} + u\rho C_p \frac{\partial T}{\partial z} - \bar{\lambda}\frac{\partial^2 T}{\partial t^2} + \frac{4h}{D}(T - T_w) = (-\Delta H_r) r(c,T)(1-\epsilon) \\ T(t,0) = T_0(t) \\ (\frac{\partial T}{\partial z})_\ell = 0 \end{gathered} \tag{4.2}$$

The expression $r(c,T)$ represents the reaction rate term, which is generally determined experimentally and may be a complicated nonlinear function of c and T as well as other operating conditions (*e.g.* deactivation effects).

For control purposes, a system of (possibly nonlinear) ODEs is required. Hence it

is necessary to approximate the distributed parameter system (DPS) given in Equation 4.2 by a lumped parameter system (LPS). Typical approaches to this problem have included the numerical techniques of orthogonal collocation and finite differences [15]. In the former technique, the reactor balances are discretized in both the radial and axial directions to result in a set of ODEs which scale in size directly with the number of interior collocation points. In the finite difference approach, the operating regime is also discretized; however, the individual regions now have uniform properties and difference equations result.

For illustration, the results of modeling studies performed on a laboratory methanation reactor [61] [90] are presented. In order to accurately model the observed behavior, an orthogonal collocation approach required one interior radial point, 12 interior axial points, and resulted in a $49th$-order LPS. Roughly the same CPU requirements were obtained in a finite difference approach with 100 internal mesh points. This led to a model with 401 ODEs.

There are two principal difficulties with these modeling techniques for nonlinear control applications. First, the measurement of the peak temperature in the reactor (the hot spot temperature) is often poorly represented by models with an inadequate number of interior collocation points or too coarse of a finite element mesh. This quantity (hot spot temperature) is typically one of the targeted variables for control as its regulation can assure acceptable temperature profiles, thus minimizing the possibility of catalyst deactivation or reactor damage. Quite often, the peak temperature location will vary greatly with the operating conditions.

Clearly this problem could be improved with a greater number of collocation points or a finer finite element mesh, but this leads to a second difficulty: high-order dynamic models. The proposed approaches for nonlinear control require very low-order models (typically fewer than six to ten states). Higher-order models lead to intractable problems, even with the aid of symbolic manipulation software. Subsequently, the

traditional approaches to packed bed reactor modeling of orthogonal collocation and finite differences are not directly useful for feedback linearizing control synthesis.

4.2.2 Model Reduction

The goals of the present work motivate the development of a reduced-order representation of the *essential* process dynamics for control purposes. In this context, essential refers to a minimal representation of the dynamics which affect the overall stability and performance of the reactor as a function of the controlled inputs. In this manner, the controller design problem is more tractable and the resultant control action is effective in as much as the model captures the appropriate dynamics.

In the context of linear dynamical systems, Hankel methods for model reduction have been widely used. Numerically stable algorithms are available for calculating balanced realizations of high-order linear systems. These simplified models retain their observability and controllability properties, but now in an irreducible structure. The shortcoming of this approach, from a control engineering perspective, is the fact that the new dynamical variables may have little physical meaning. By reducing the size of the system model, key engineering state variables and their associated dynamics may be lost.

More recently, there have been attempts at model reduction for general nonlinear systems of ODEs and algebraic equations. One approach involves a so-called optimal projection of the system trajectories onto a space of lower dimension than the original state space. The approach is reasonably systematic. Recent work has strengthened the theoretical results and general applicability of such techniques [59]. Using this approach, a packed bed reactor can be modeled by a nonlinear dynamical system of on the order of six differential equations; however a large number of additional states may be required for operation under conditions of high parametric sensitivity (*i.e.*, incipient thermal runaway). The results show great promise, but again, the principal

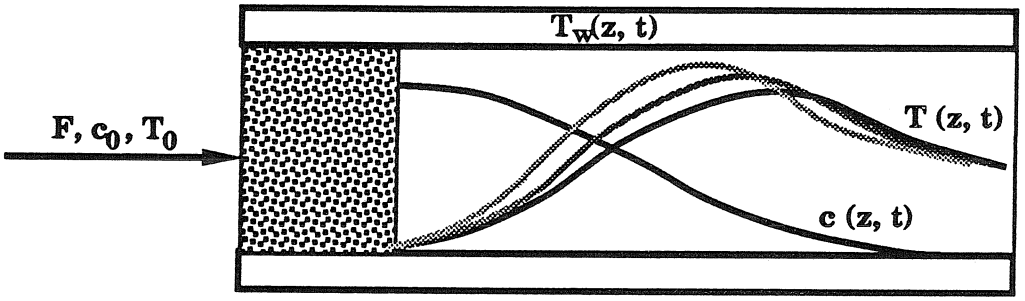

Figure 4.1. Packed Bed Reactor

weakness is the physical insignificance of the states in the reduced-order model.

4.2.3 Low-Order Physical Model - Wave Propagation

Background

An alternative approach for low-order modeling of packed bed reactors was put forth by Gilles and co-workers at Stuttgart in the early 1980s [32], [33], [34]. This approach has great intuitive appeal because it attempts to identify the key dynamical variables in the reactor from physical arguments and it results in lumped parameter nonlinear models of very low order (two to six dynamical states). The general idea is to treat the active transport processes in the reactor as a nonlinear wave which propagates along the reactor bed in response to changes in the operating conditions. The mathematical treatment of a number of chemical processes as propagating waves is described in [62]. In this section, a few of the details of wave propagation modeling are sketched, primarily the enhancements to the approach described in [34] for the present study.

The physical observation in packed bed reactors which suggests the wave propagation approach is the fact that temperature profiles respond to changes in operating conditions by *shifting position while retaining the same essential form.* This is shown in Figure 4.1 for a typical temperature response for a change in inlet flow rate. The temperature profile is modeled as a nonlinear wave which possesses a form stability, which can be characterized in precise mathematical terms [33]. From an engineering

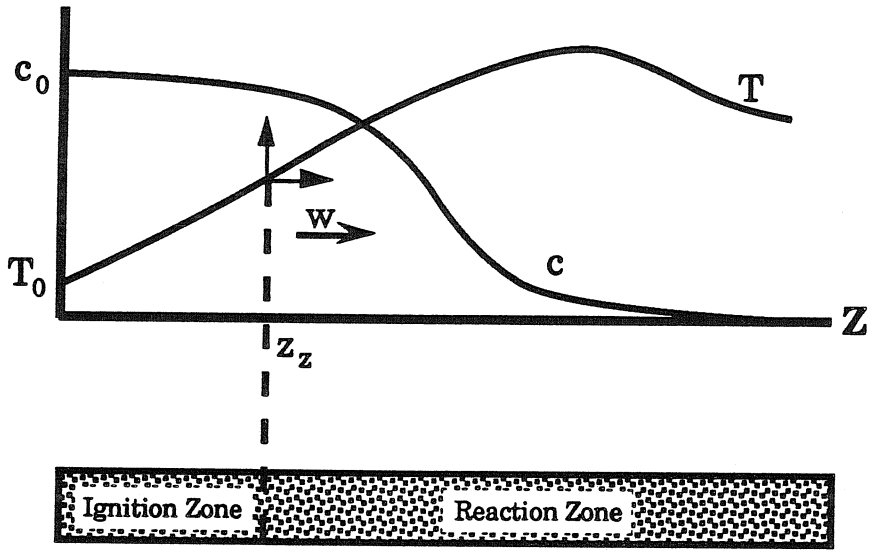

Figure 4.2. Wave Propagation Model Schematic

perspective, the bed is divided into two regions: an *ignition zone* in which the reactants begin to heat up and a semi-infinite *reaction zone* over which the reactions take place and a peak temperature is observed (if present). The dividing point between the two regions is called the ignition position, z_z, and represents the key dynamic state for this model. This is schematically depicted in Figure 4.2. If a coordinate system moving at velocity w is constructed at z_z, then the nonlinear wave can be treated as a quasi-stationary process with respect to this coordinate system. As the equilibrium of this system is perturbed (*e.g.*, by changing operating conditions), the ignition position moves (the nonlinear wave propagates) to restore the mathematical form stability of the profile. In engineering terms, this critical condition is given by the point where the heat production curve is tangent to the heat removal line. Thus, the dynamical processes in the bed are captured by a low-order, physically based nonlinear model.

The study in [34] focused on the open-loop (uncontrolled) dynamical properties of a packed bed reactor under various operating conditions. This formulation leads to great numerical sensitivity with respect to initial conditions, and more importantly,

the dynamic computations are unstable for large changes in the operating conditions. This limits the applicability of such an approach to closed-loop (controlled) studies. An additional complication is the relative inaccuracy of the hot spot temperature calculation for the approach in [34]. In this approach, the reaction rate is integrated over the length of the reactor in order to calculate the energy balances and this leads to an averaging or smoothing of the temperature profiles. Consequently, as in the case of orthogonal collocation, it is very difficult to accurately reproduce the steep profiles associated with certain reaction conditions. This, in turn, leads to large uncertainty between the modeled hot spot position and temperature versus the actual calculation from more detailed models and experimental results. As this variable, hot spot temperature, is a primary output variable from a control perspective, a more rigorous treatment of its behavior is required.

Present Model

The following attributes distinguish the present model from the previous approaches:

- Quasi-stationarity with respect to reaction zone.
- Neglection of conductivity.
- Integration/interpolation for hot spot calculation.

The first assumption results in fewer dynamical variables in the reaction domain. The second assumption simplified the computation of the wave dynamics and facilitated the use of Runge-Kutta integration for the temperature profile. The last feature results in a complex, implicit formulation of the hot spot temperature as a function of the dynamic variables. The resultant dynamical model is computationally stable over a wide operating range (including regions of parametric sensitivity), and yields hot spot temperature calculations which are relatively accurate.

The original mass and energy balances (Equation 4.2) can be rewritten in dimensionless form as:

$$\begin{gathered}
\frac{\partial y}{\partial z} = -\mathcal{D}a\, r(x,y) \\
y(0,t) = y_0(t) \\
\frac{\partial x}{\partial t'} + \frac{\partial x}{\partial z} - \epsilon\frac{\partial^2 x}{\partial z^2} + \mathrm{B}(x - x_w) = q\, \mathcal{D}a\, r(x,y) \\
x(0,t) = x_0(t) \\
\left(\frac{\partial x}{\partial z}\right)_{z=1} = 0
\end{gathered} \tag{4.3}$$

If a moving coordinate system (z', t) centered at the ignition point is defined as in Figure 4.2, the balances can be expressed:

$$\begin{gathered}
\frac{\partial y}{\partial z'} = \mathcal{D}a\, r(x,y) \\
y(z'=0) = y_z \\
\frac{\partial x}{\partial t'} + (1 - w_z)\frac{\partial x}{\partial z'} - \epsilon\frac{\partial^2 x}{\partial z'^2} + \mathrm{B}(x - x_w) = q\, \mathcal{D}a\, r(x,y) \\
x(z'=0) = x_z \\
\left(\frac{\partial x}{\partial z'}\right)_{z'=\Delta} = 0
\end{gathered} \tag{4.4}$$

where y_z, x_z are the values at the ignition position, and Δ defines the length of the reaction zone. w_z is the propagation velocity of the coordinate system. The remaining dimensionless variables are defined in Table 4.1.

The resultant numerical algorithm evaluates the critical energy balance for each time step in a simulation. Assuming an initial value for the ignition position, the temperature profile is integrated from Equation 4.4 for the reaction zone. The assumptions of neglected conductivity and quasistationarity allow this to be accomplished in a straightforward manner using the Runge-Kutta method. From this profile, it is possible to calculate the critical stability condition. Iterations continue until the condition is satisfied and the desired accuracy is achieved.

Table 4.1 Dimensionless Variables for Reactor Model

y	$\frac{c}{c_{ref}}$
x	$\frac{T}{T_{ref}}$
x_w	$\frac{T_w}{T_{ref}}$
t'	$\frac{t}{t_{ref}}$
c_{ref}	c_0
T_{ref}	T_0
t_{ref}	$\frac{L}{u}\frac{(\rho C_p)^*}{(\rho C_p)}$
$\mathcal{D}a$	$\frac{Lk_0(1-\epsilon)}{u}$
$\mathbf{B}$	$\frac{4hL}{u\rho C_p D}\left(\frac{F}{F_0}\right)^{\lambda}$
q	$\frac{-\Delta H c_0}{\rho C_p T_{ref}}$
γ	$\frac{E}{RT_{ref}}$
ϵ	$\frac{\lambda}{t_{ref}(\rho C_p)^*}$

This leads to a "critically stable" nonlinear wave representing the temperature profile in the new coordinate system. From this information, it is possible to calculate the peak temperature (hot spot), and the accuracy of this calculation can be improved by interpolation.

The two key calculations in this model, the energy balance and the integration of the temperature profile, lead to implicit formulations for the desired variables in the dynamic model. In terms of the numerical computations, this provides only a nominal obstacle. However, it will be seen that this implicit nonlinear model will prevent the mathematical formulation of a closed form control law for the reactor.

For control purposes, the nonlinear dynamical model is a single input-single output, second-order system. The regulated output is the hot spot temperature in the reactor, and the two dynamic variables are the ignition position and a fast lag on the controlled input. The latter state results from the requirement that the output function remain independent of the manipulated variable. This simplifies the nonlinear control synthesis and is justified by the physically finite propagation of changes in

Table 4.2 Reduced Model Variables	
x_1	Filtered Manipulated Variable
x_2	Ignition Position
y	Hot Spot Temperature
u	Manipulated Variable (F, c_0, or T_w)

the feed stream or cooling jacket. The candidate manipulated variables include inlet concentration, inlet flow rate, and jacket temperature. The model is described by the following equations:

$$\begin{aligned} \tau \dot{x_1} &= -x_1 + u \\ \dot{x_2} &= w(x_1, x_2) \\ y &= h(x_1, x_2) \end{aligned} \tag{4.5}$$

where the nonlinear functions w and h are complicated, implicit functions of the state variables. w is calculated from the critical energy balance and h is solved from the integrated temperature profile.

4.2.4 Open-Loop Simulations

Operating Conditions

The physical parameters and operating conditions chosen for this study are taken from a paper by Van Welsenaere and Froment [88] in which they studied the issues of parametric sensitivity and runaway for packed bed reactors. The rationale for choosing parametrically sensitive operating conditions is as follows: clearly, regions of mild, linear dynamical behavior can be optimally controlled with a linear controller. It stands to reason that any potential advantages to be gained from nonlinear control will be achieved over an operating range which exhibits highly nonlinear dynamical behavior. The values of the physical parameters which lead to parametrically sensitive behavior are as given in Table 4.3. In addition, the time constants shown in Table 4.4

Table 4.3 Physical Parameters for Packed Bed Reactor	
c_0	.208
T_0	$625K$
T_w	$625K$
ϵ	0.0
$\mathcal{D}_a$	$7.059E8$
B	11.38
q	1.0
$r(x,y)$	$e^{-\gamma/x}$
γ	21.82

Table 4.4 Time Constants for Manipulated Variables (Dimensionless)	
τ_{c_0}	0.025
τ_F	0.01
τ_{T_w}	0.1

are employed in the first state equation in Equation 4.5 for the lag applied to the respective manipulated variables.

Inlet Concentration

Inlet concentration is the first variable studied as a candidate for the manipulated variable in the reactor. In terms of the variables presented in the previous section, the nonlinear steady-state dependence of the hot spot temperature (y) and the ignition position (x_2) on the inlet concentration (x_{1ss}) is investigated. This is depicted in Figure 4.3, where the left hand vertical axis shows the peak reactor temperature and the right hand vertical axis shows the ignition position, both as a function of the steady-state inlet concentration. Several things are clear from this diagram:

- The peak temperature begins to run away as the concentration is increased above 1.2 (note that a dimensionless temperature of 1.2 corresponds to an actual

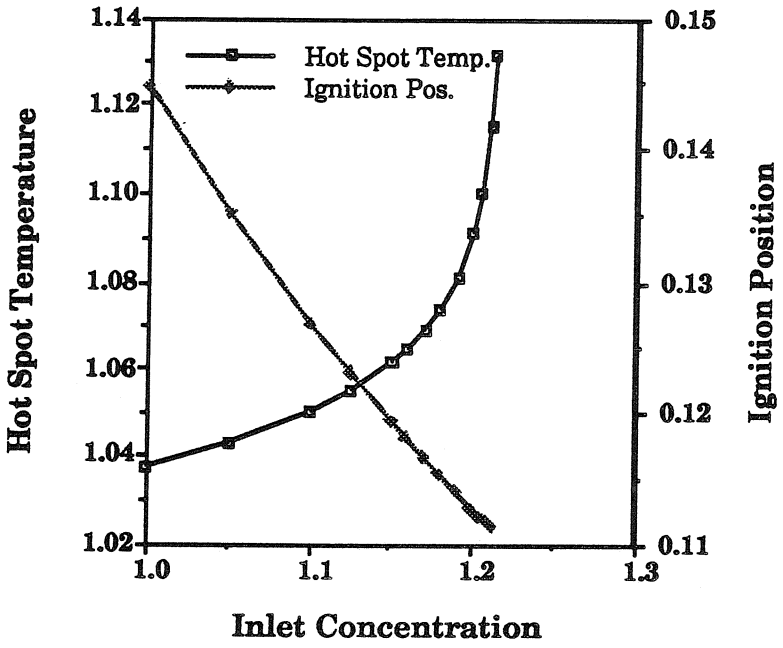

Figure 4.3. Steady-State Dependence of the Reactor Hot Spot Temperature and Ignition Position on the Inlet Concentration

temperature of $750K$).

- The ignition position exhibits a virtually linear dependence on the first model state, even into the region of reactor runaway.

- The wavefront propagates toward the reactor entrance as the concentration is increased and runaway is excited.

These effects correlate with the understanding that the increasing reaction rate leads to a steeper heat production curve. Thus, in order to satisfy the critical energy balance of the propagating wave, the ignition point migrates inward (toward the reactor entrance) to match the gradient of heat production to the gradient of heat removal.

Greater insights are obtained from a dynamical study of this system. Specifically, an open-loop simulation involving a step increase in the inlet concentration from 1.16 to 1.21 is investigated. In Figure 4.4, the time trajectories of the hot spot

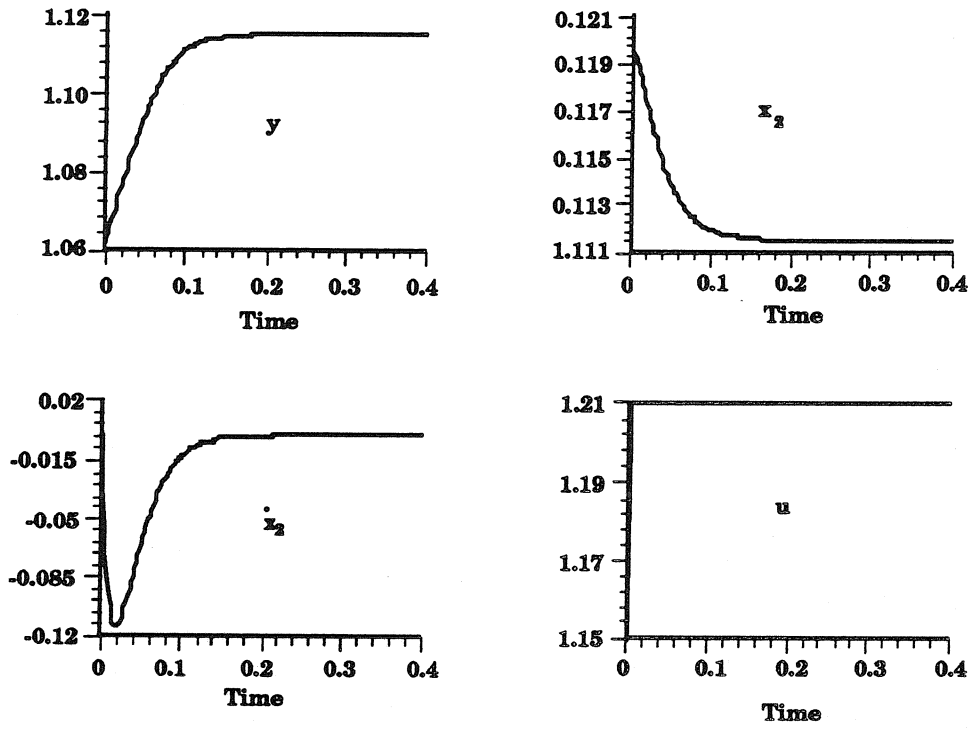

Figure 4.4. Open-Loop Response of Model Variables to a Step Change in Inlet Concentration

temperature (y), ignition position (x_2), wavefront propagation velocity ($\dot{x}_2$), and the inlet concentration (u) are shown. In addition, a plot of the full reactor profile showing the time history in the reactor is shown in Figure 4.5. As discussed earlier, the reactor is being pushed from a critically stable regime towards runaway. The plots show that, in response to the increase inlet concentration, the reactor temperature rises, causing the reaction rate to accelerate. This, in turn, induces a movement in the wavefront backwards (towards the front of the reactor).

Jacket Temperature

The choice of jacket temperature as a manipulated variable leads to even greater parametric sensitivity for the packed bed reactor than that demonstrated by c_0 in the last section. This is depicted in Figure 4.6. Again, the variables displayed are the steady state hot spot temperature (left vertical axis) and ignition position (right

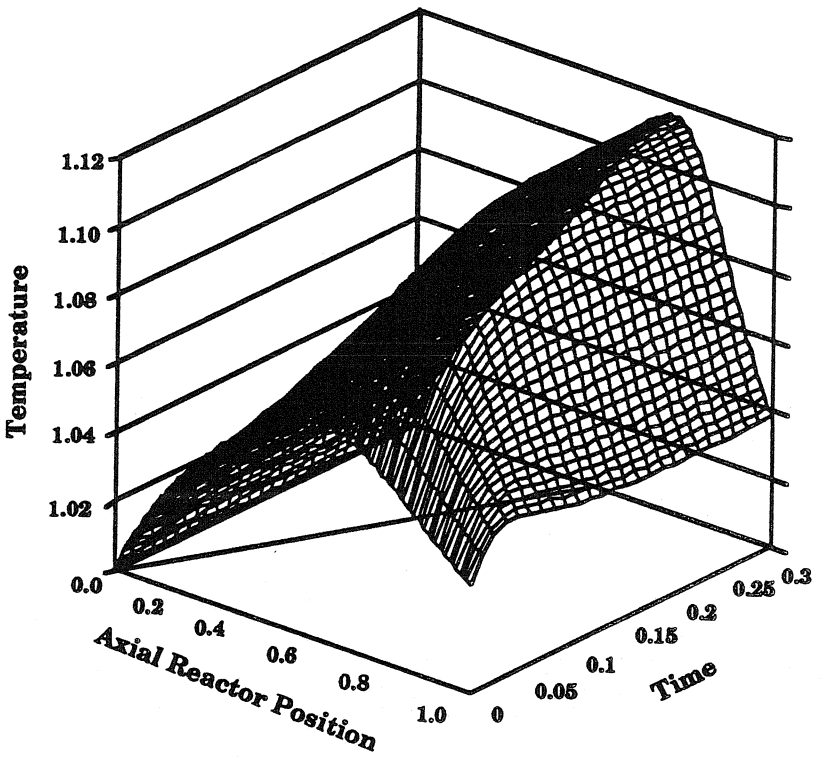

Figure 4.5. Open-Loop Response of Reactor Temperature Profile to a Step Change in Inlet Concentration

vertical axis) as a function of the jacket temperature. Observe that the same range in reactor temperature (20%) is represented here for a much smaller range in jacket temperature (3%) compared to the inlet concentration in Figure 4.3 (30%). The following observations are relevant:

- The peak temperature begins to run away as the cooling jacket temperature is increased above 1.01 ($631K$).
- The ignition position exhibits more nonlinearity in its dependence on the first model state; however the behavior is still very well behaved as the reactor begins to run away.
- The wavefront propagates toward the reactor entrance as the jacket temperature is increased and runaway occurs.

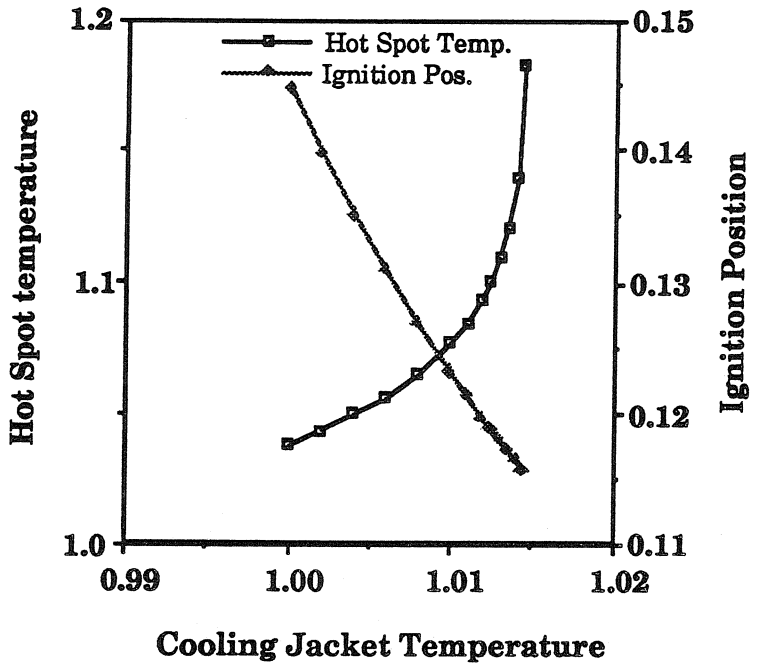

Figure 4.6. Steady-State Dependence of the Reactor Hot Spot Temperature and Ignition Position on the Jacket Temperature

As before, these phenomena are easily understood in terms of the dynamics of the propagating wavefront. As the jacket temperature is decreased, the heat removal line shifts towards the reactor inlet, forcing the wavefront to propagate backward to reestablish the critical energy balance.

These ideas are depicted in the open-loop simulation shown in Figures 4.7 and 4.8. Here is shown the response of the uncontrolled reactor to a step change in the jacket temperature from 1.0 to 1.013. Again, the variables plotted are hot spot temperature (y), ignition position (x_2), wavefront propagation velocity ($\dot{x}_2$), and jacket temperature (u). In Figure 4.8, the same simulation is shown in a depiction of the entire bed temperature profile.

Qualitatively, the behavior is very similar to that observed by increasing the inlet concentration. One very significant difference is the time scale over which changes occur. This is largely attributed to the choice of time constants chosen for the lagged input (Table 4.4). The selection of these variables is somewhat arbitrary; in this

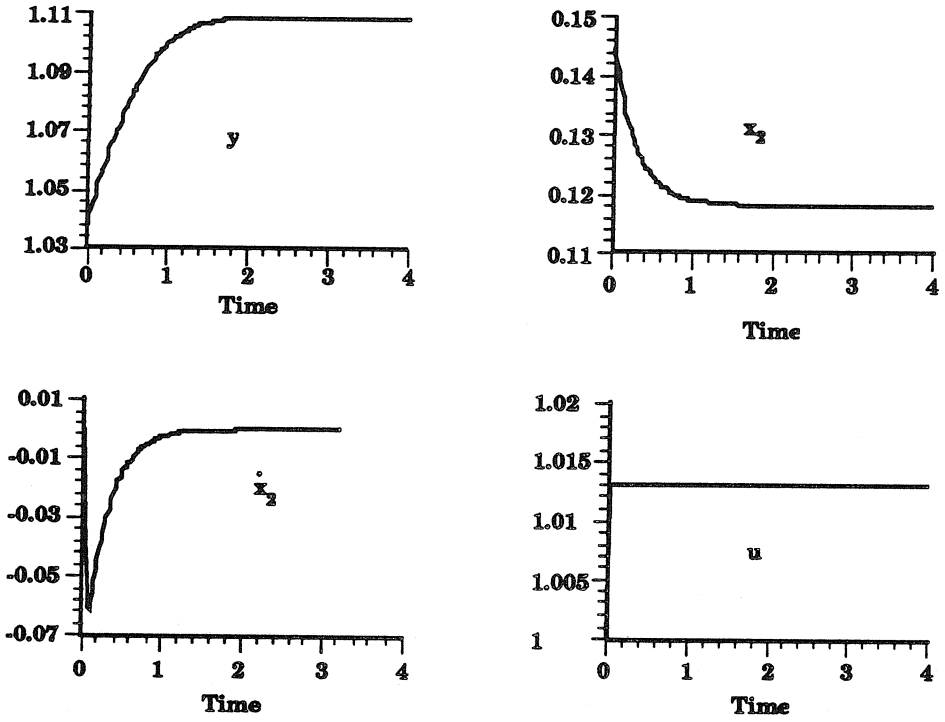

Figure 4.7. Open-Loop Response of Model Variables to a Step Change in Jacket Temperature

particular case, they reflect the experimentally observed difference in time scales for thermal versus mass effects in a pilot plant methanation reactor [90].

Flow

The final choice of manipulated variable, the inlet flow rate, leads to a fundamentally different dynamical system. It is well known that this choice of a manipulated variable leads to a nonminimum phase system which displays inverse response behavior, as opposed to the previous two simulations involving minimum phase systems.

As before, the nonlinear steady-state dependence of the peak reactor temperature and the wave ignition position on the manipulated variable (inlet flow rate) is investigated. This is shown in Figure 4.9 with hot spot temperature on the left vertical axis and ignition position on the right vertical axis. As in the previous two cases, the following phenomena are observed:

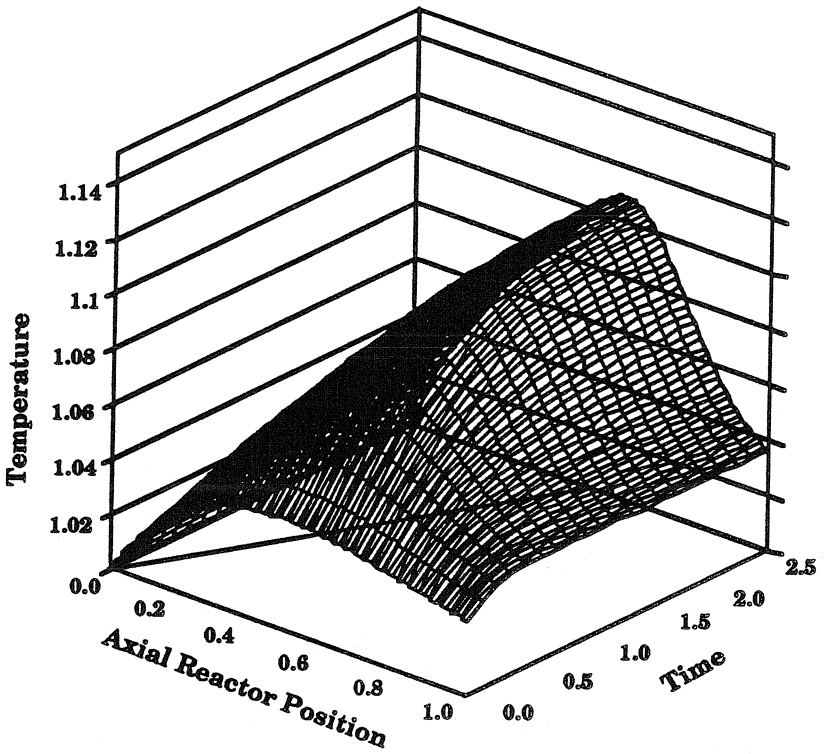

Figure 4.8. Open-Loop Response of Reactor Temperature Profile to a Step Change in Jacket Temperature

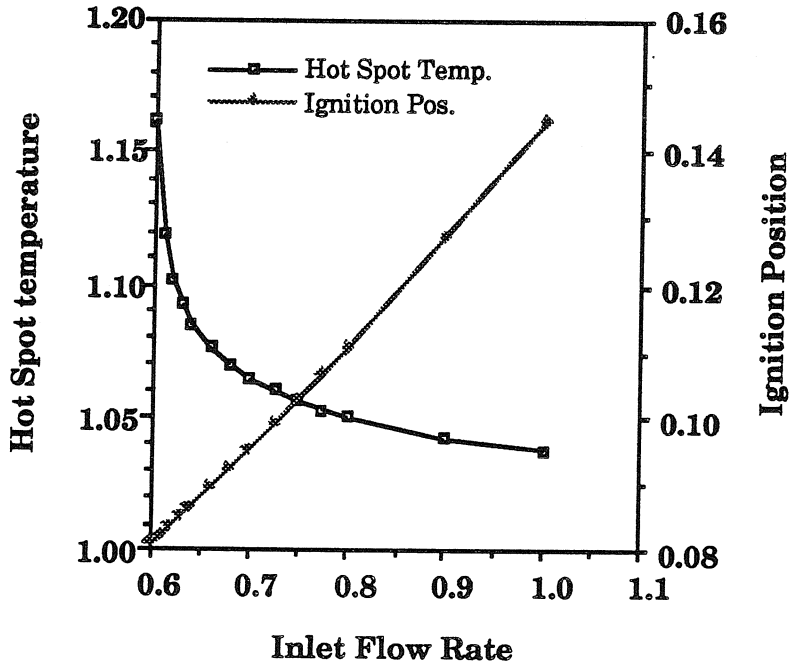

Figure 4.9. Steady-State Dependence of the Reactor Hot Spot Temperature and Ignition Position on the Inlet Flow Rate

- The peak temperature begins to run away as the inlet flow rate is decreased below 0.65.
- The ignition position is fairly linear in its dependence on the first model state, even through runaway.
- The wavefront propagates toward the reactor entrance as the flow rate is decreased and the temperature runs away.

These ideas are again in accordance with the proposed wavefront mechanism. As the flow rate decreases, the initial effect (mass action) is a deceleration of the reaction rate. However, this is offset by the slower thermal effects which lead to poorer heat transfer and, eventually, an overall increase in the reactor temperature. This leads to wavefront motion toward the reactor inlet to reestablish the critical energy balance.

This idea of inverse response or "wrong-way" behavior can be clearly seen in the dynamic open-loop simulation in Figures 4.10 and 4.11. This particular simulation shows the reactor's response to a step decrease in the flow rate from 0.70 to 0.60. As before, Figure 4.10 shows the hot spot temperature (y), ignition position (x_2), wavefront propagation velocity ($\dot{x}_2$), and jacket temperature (u). Figure 4.11 shows the complete reactor temperature profile evolution. In this diagram it is quite easy to observe both the inverse response effect (hyperbolic region of the surface) and the parametric sensitivity of the reactor at the onset of runaway.

Discussion

Two key points must be stressed about the previous open-loop simulations and the accuracy of the reduced nonlinear model in predicting the actual reactor dynamics:

- Qualitatively, the model is highly accurate. It shows the proper trends in the reactor variables and reproduces both inverse response and parametric sensitivity.

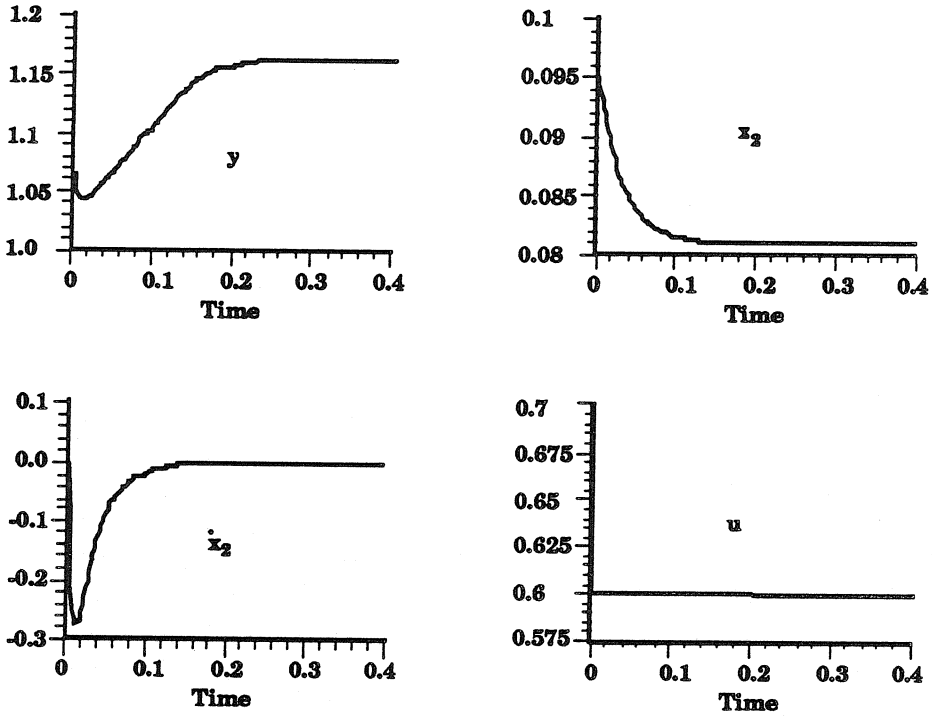

Figure 4.10. Open-Loop Response of Model Variables to a Step Change in Flow Rate

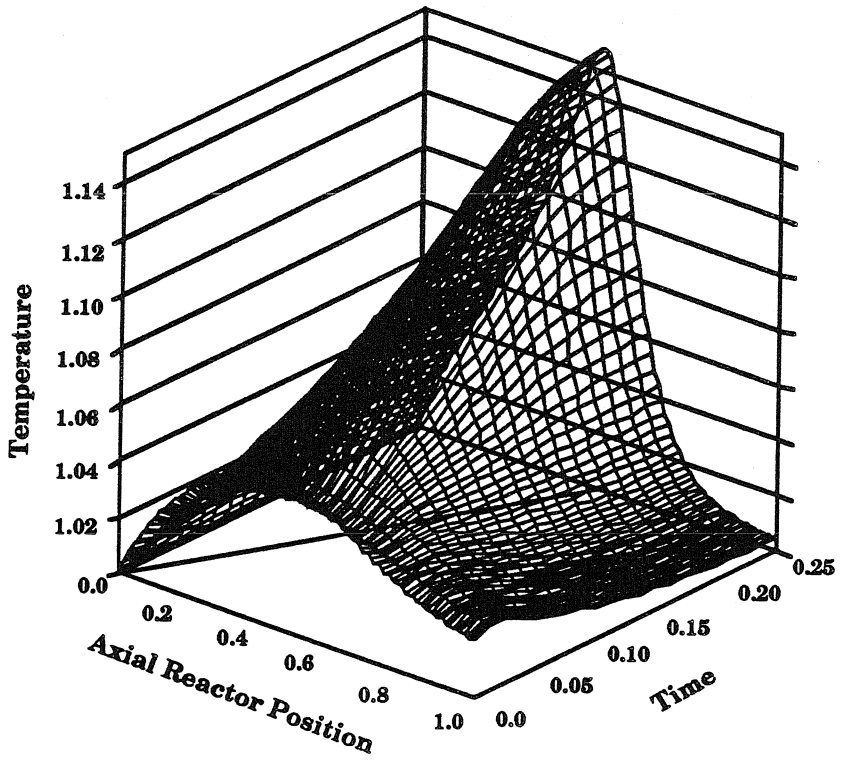

Figure 4.11. Open-Loop Response of Reactor Temperature Profile to a Step Change in Flow Rate

- Quantitatively, the model has been found to be reasonably close to the observed data. Inaccuracies can be "fine-tuned" using a number of simple parameters present in the model.

The qualitative behavior is clearly of critical importance in the endeavor to design a low-order model which captures the essential reactor dynamics for control purposes. This has been demonstrated in the preceding simulations where the pathological behavior of reactor runaway and the associated sensitivity with respect to reactor parameters is accurately displayed by the low-order model. In addition, the nonminimum phase properties associated with flow manipulation can severely reduce the attainable performance of the closed-loop system. This has also been captured by the model described in section 4.2.3.

The quantitative accuracy of the second-order nonlinear model presented in section 4.2.3 cannot realistically be expected to be absolutely precise in its description of an industrial packed bed reactor. However, it has been found that even this simple homogeneous model accurately reproduces regions of parametric sensitivity. As discussed in [68] and [88], this is a reasonable starting point for parametric sensitivity studies, but for a more detailed description, a heterogeneous model must be employed. Then, a more accurate description of the particle interactions is possible and the regions of multiplicity which are not observed in a homogeneous model [79] can be reproduced. Consequently, if tight control of a complex reaction mechanism which exhibits an optimum in a parametrically sensitive region (and may possibly involve the exploitation of multiplicities) is the objective, a heterogeneous model should be used. As a first step toward addressing this concern for the present model, it is suggested that treatment such as that in [70] be employed. This would introduce only two new algebraic states into the model.

The quantitative refining of the model against experimental data can be accomplished via the dimensionless groups in Table 4.3 or by tuning the time constants in

Table 4.4. Clearly the values in the latter table will only affect the speed of manipulated variable action. A more thorough correlation can be introduced by parametrizing the Damköhler number ($\mathcal{D}a$) over the operating region. This can be accomplished by fitting the value of $\mathcal{D}a$ in the proposed model to match experimental data at several operating points. This information can be utilized to propose a functional form for the Damköhler number : ($i.e.$ $\mathcal{D}a = f(x_1, x_2)$).

An evaluation of the quantitative accuracy of the model is provided in appendix B. There, experimental data collected from the Caltech methanation reactor [90] is used for parameter fitting and fine tuning of the low-order model. The model results show a very good match with the experimental data; however, the operating conditions in that reactor are not parametrically sensitive.

4.3 Nonlinear Control Synthesis

4.3.1 Theoretical Issues - Feedback Linearization

The differential geometric techniques of feedback linearization will be employed as a candidate synthesis method to be evaluated against standard linear approaches. The idea behind feedback linearization is a transformation of a complicated dynamical system into an equivalent but simpler (linear) dynamical system. The appeal to such an approach is clear; the nonlinearities are treated directly, and well-known linear techniques are applied to the transformed linear system. In the following discussion, attention is restricted to SISO control problems. All the presented results generalize to the MIMO case. A detailed theoretical discussion of the differential geometric techniques can be found in [44].

There are two alternative approaches to feedback linearization, global state linearization (GSL) [43], and input/output linearization (IOL) [17]. In GSL, a change of coordinates and nonlinear feedback is calculated to yield an equivalent system which now exhibits linear state dynamics (in the new coordinates). However, this technique

will not guarantee that the relationship between the input and output is linear. In IOL, a nonlinear feedback law is calculated which results in a dynamical system with a linear mapping from input to output, and some subset of the state dynamics are linear. If this subset has dimension less than the original system order, it is referred to as partial linearization; if it is equal, it is referred to as exact linearization. As the objective in this study is the maintenance of some performance specifications on the packed bed reactor output (hot spot temperature), the technique of IOL will be used.

The general form of a nonlinear dynamical system will be given by the control-linear structure:

$$\begin{aligned} \dot{x} &= f(x) + g(x)u \\ y &= h(x) \end{aligned} \tag{4.6}$$

where f, g, and h are vector functions of x. This formulation is not restrictive for most chemical engineering systems where the effect of a control variable on the state dynamics is often linear. If the machinery described in [44] is to be applied, the system must first be transformed to the so-called Byrnes-Isidori canonical form. This is accomplished by calculating the system's *relative degree.* Mathematically, the relative degree, r, is defined as the smallest integer for which $L_g L_f^{r-1} h$ is nonzero. This is also equal to the number of differentiations of the output variable required to obtain a direct dependence on the input variable. For linear systems, it can be easily shown to be equal to the pole-excess, *i.e.*, the number of poles minus the number of zeros, or equivalently, the number of zeros at infinity.

The normal form for system (4.6) is given by:

$$\begin{aligned} \dot{z_1} &= z_2 = L_f h \\ \dot{z_2} &= z_3 = L_f^2 h \end{aligned}$$

$$
\begin{aligned}
&\vdots \\
\dot{z_{r-1}} = \quad z_r = \quad & L_f^{r-1}h \\
\dot{z_r} = \quad & L_f^r h + uL_g L_f^{r-1}h \\
\dot{z_{r+1}} = \quad & q_{r+1}(z) \\
&\vdots \\
\dot{z_n} = \quad & q_n(z) \\
\\
y = \quad & z_1
\end{aligned}
\tag{4.7}
$$

This normal form clearly illustrates the input/output linearization approach along with its restrictions. Now a new input variable, v, is defined by

$$v = (\beta_r L_f^r h + \beta_{r-1} L_f^{r-1} h + \cdots + \beta_0 h) + u\beta_r L_g L_f^{r-1} h \tag{4.8}$$

and this quantity is set equal to $\dot{z_r}$. This can be solved for u, provided that the system has a well-defined relative degree:

$$u = \frac{v - (\beta_r L_f^r h + \beta_{r-1} L_f^{r-1} h + \cdots + \beta_0 h)}{\beta_r L_g L_f^{r-1} h} \tag{4.9}$$

Then the relationship between v and y can be calculated as:

$$y = \frac{v}{\beta_r s^r + \beta_{r-1} s^{r-1} + \cdots + \beta_1 s + \beta_0} \tag{4.10}$$

The system in Equation 4.7 is now partitioned into two subsystems:

- An r dimensional system with linear dynamics.
- A $n - r$ dimensional system with nonlinear dynamics.

Clearly, the latter is an unobservable subsystem of the original system. It is denoted

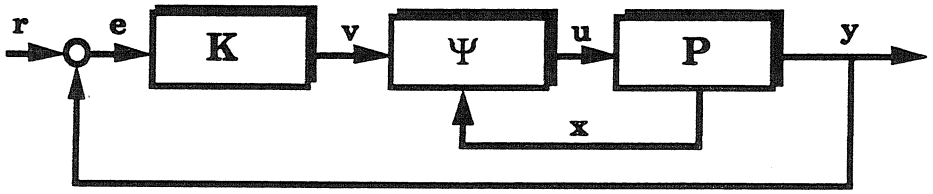

Figure 4.12. Schematic of Input-Output Linearization

the *zero dynamics*. These dynamics are the direct analog of zeros of a linear transfer function. The stability of these dynamics can be analyzed by setting $z_x = \eta_{x-r}$ (for $x > r$) and setting $z_x = \bar{u}_0$ (for $x \leq r$)

$$\begin{aligned} \dot{\eta}_1 &= q_{r+1}(\eta, \bar{u}_0) \\ \dot{\eta}_2 &= q_{r+2}(\eta, \bar{u}_0) \\ &\vdots \\ \dot{\eta}_{n-r} &= q_n(\eta, \bar{u}_0) \end{aligned} \tag{4.11}$$

where $\bar{u}_0$ is taken to be an exponentially decaying input to the system. A straightforward exercise reveals that the poles of the classical linearization of the zero dynamics are exactly equal to the finite zeros of the classical linearization of the original system (4.6). Consequently, the stability of these dynamics reflect the minimum or nonminimum phase properties of the nonlinear system in Equation 4.6.

Schematically, the IOL is described in Figure 4.12. Here P represents the nonlinear plant given in Equation 4.6 and Ψ is the nonlinear feedback law given in Equation 4.9. This controller requires the measurement of the system states. It is a straightforward exercise to show that the control law ψ represents a minimal order realization of the inverse of the nonlinear plant given by P. Consequently, Ψ is an *inverse-based nonlinear* controller. The internal stability of the closed loop can be guaranteed if and only if the original system has a stable inverse, *i.e.*, stable zero dynamics (see [17] for detailed proof). Now, the mapping from v to Y is given by Equation 4.10, so

an optimal linear controller, K, can be designed for this linear system.

In summary, the requirements for a system to yield an internally stable input/output linearizing controller are:

- Criterion #1 : The system must possess a finite relative degree.
- Criterion #2 : The system must have stable zero dynamics.

Many process systems will violate one or the other of the above criteria. Certain systems may satisfy the conditions locally but not over the global state space; thus there are imposed restrictions on the range of validity of this approach.

Packed Bed Reactor Model

The packed bed reactor model developed in the previous section is now considered. In order to apply IOL for a prescribed set of physical parameters and operating conditions, the above criteria must be satisfied. This first involves a calculation of the relative degree. Consider if $r = 1$:

$$L_g h = \frac{1}{\tau} \frac{\partial h}{\partial x_1} \neq 0 \tag{4.12}$$

It is found for the physical parameters and operating conditions used in this study that this condition is only satisfied locally. In other words, the classical linearization yields a C matrix in which the first element is nonzero. However, it is possible to describe a locus away from the operating curve for which this condition is not satisfied. Crossing this locus leads to a singularity in the control law (Equation 4.9), and this effect must be accounted for in closed-loop operation.

If the condition in Equation 4.12 is satisfied, then the following change of coordinates

$$z_1 = \quad h(x_1, x_2)$$

$$z_2 = \quad x_2 \tag{4.13}$$

leads to the subsequent Byrnes-Isidori canonical form for the packed bed reactor model:

$$\begin{aligned} \dot{z_1} &= \tfrac{1}{\tau}\tfrac{\partial h}{\partial x_1}[-h^{-1}(z_1, z_2) + u] + \tfrac{\partial h}{\partial x_2} w(h^{-1}(z_1, z_2), z_2) \\ \dot{z_2} &= w(h^{-1}(z_1, z_2), z_2) \end{aligned} \tag{4.14}$$

The second condition for admitting IOL requires that the packed bed reactor model is minimum phase. Clearly this limits the choice of manipulated variables to the inlet concentration and cooling jacket temperature. It is well known and clearly understood that flow control leads to a nonminimum phase system which exhibits so-called inverse response. Consequently, a preliminary investigation will focus on inlet concentration and jacket temperature as a manipulated variable. There are new results for nonlinear control of nonminimum phase dynamical systems, and the ramifications of these will be addressed for flow control in the reactor in a later section.

For global results, the nonlinear zero dynamics are calculated from the Byrnes-Isidori canonical form for the packed bed reactor. These are given by

$$\dot{\eta} = w(h^{-1}(\bar{u}_0, \eta), \eta) \equiv \hat{w}(\eta, \bar{u}_0) \tag{4.15}$$

where $\bar{u}_0$ is some exponentially decaying input [44] which could be arbitrarily taken to be zero. The stability of the zero dynamics for the reactor model will be guaranteed (locally) by checking the zeros of the classical linearization of the model (Equation 4.6). This yields the following condition for minimum phase (locally stable zero dynamics):

$$\frac{\partial w}{\partial x_2} - \frac{\frac{\partial h}{\partial x_2}}{\frac{\partial h}{\partial x_1}} \frac{\partial w}{\partial x_1} < 0 \tag{4.16}$$

or in the transformed coordinates:

$$\frac{\partial \hat{w}}{\partial \eta} < 0 \tag{4.17}$$

Theoretical Restrictions

In summary, feedback linearization can be theoretically applied to the packed bed reactor model, provided that the following conditions are satisfied:

- Measurements of the states x_1 and x_2 are available.
- The operating region yields a finite relative degree (Equation 4.12).
- The zero dynamics are stable (Equation 4.16).

If these conditions are met, the following nonlinear control law can be synthesized:

$$u = \frac{v - (\beta_1 L_f h + \beta_0 h)}{\beta_1 L_g h} \tag{4.18}$$

Substituting for the values of g and f leads to:

$$u = \frac{v + \beta_1 \tau^{-1} \frac{\partial h}{\partial x_1} - \beta_1 w \frac{\partial h}{\partial x_2} - \beta_0 h}{\beta_1 \tau^{-1} \frac{\partial h}{\partial x_1}} \tag{4.19}$$

If this law is implemented as indicated as in Figure 4.12, then the mapping from v to y will be given by:

$$y = \frac{v}{\beta_1 s + \beta_0} \tag{4.20}$$

where β_1 and β_0 are tuneable parameters of the nonlinear controller.

4.3.2 Practical Issues - Feedback Linearization

The study of feedback linearizing control and its implementation for a complex, *practical* system, like the packed bed reactor, has led to the identification of additional

constraints regarding the application of this technique. The first consideration arises from the sampling of a continuous-time nonlinear system for purposes of digital control implementation. It has been shown for global state linearization that sampling can destroy the linearizability properties of the original continuous-time system [36]. On the surface, these results would appear to inhibit a generalization of the presented ideas for a sampled data controlled reactor. The second consideration involves the implicit formulation of the nonlinear dynamic model for the packed bed reactor and the subsequent synthesis of a nonlinear control law.

Sampling Effects

In order to implement a control law with a digital computer, it is necessary to measure the process signals at discrete time intervals. The speed of this sampling is related to the microprocessor's capability and, more importantly, to the measurement device's ability to translate physical measurements into useful signals. Clearly, the higher the frequency of sampling, the closer the sampled data system will behave to its continuous-time counterpart.

For control applications, high-frequency sampling leads to complications with the dynamics of the discrete system. It is a well-known result in linear system theory [1] that sampled-data linear systems can exhibit finite zeros which are not observed in the original continuous-time system. The stability of these new zeros are directly correlated with the rate of sampling: small sampling times lead to destabilization of the zeros. The presence of unstable zeros clearly limits the achievable performance for a controlled system. Furthermore, inverse-based control algorithms which were designed for minimum phase continuous-time systems can become internally unstable by fast sampling.

These ideas translate directly for nonlinear systems. In this context, the stability of the *zero dynamics* for the sampled nonlinear system must be analyzed. In [66] it

is shown that the dimension of the zero dynamics for a discrete system, obtained by sampling a continuous-time system over a fixed-time interval, is always equal to $n-1$. This correlates directly with the linear result that a pulse transfer function has $n-1$ zeros. In effect, $r-1$ new dynamic states are introduced in the nonlinear zero dynamics by sampling, which correspond to the $r-1$ zeros which move in from infinity to finite measure for linear systems. And like the linear case, the resultant $n-1$ dimensional zero dynamics can have markedly changed stability properties. This is rigorously proved in [66] by showing that classical linearization and discretization by sampling commute and that classical linearization and feedback linearization commute. The main result from [66] is summarized here:

Theorem 4.1 *Discrete Input/Output Linearization*

For small enough sampling periods:

1. *If $r = 1$, then the zero dynamics for the sampled data discrete system are hyperbolically stable (minimum phase) if and only if the zero dynamics for the continuous-time system are hyperbolically stable (minimum phase).*
2. *If $r > 2$, then the zero dynamics for the sampled data discrete system are unstable (nonminimum phase).*

This result shows that the stability of the sampled-data reactor system under feedback linearization is guaranteed if and only if the original system is internally stable. This is due to the fact that the reactor model has relative degree 1 and no new zeros will be introduced by sampling this system. In general, however, this will not be true for more complex, higher-order models with relative degree greater than 2.

So, for the packed bed reactor problem, the system can be sampled as fast as the measurement devices will permit. This way, the performance properties of the continuous-time system can be reproduced while maintaining the internal stability of

the system.

Implicit Model Formulation

The nonlinear controller described by Equation 4.18 is a function of the quantities $w(x_1, x_2)$, $h(x_1, x_2)$, $\frac{\partial h}{\partial x_1}$, and $\frac{\partial h}{\partial x_2}$. As has been indicated in the discussion of the model, there are no explicit closed-form representations for the propagation velocity (w) or the hot spot temperature (h) and its derivatives as a function of the two states. Therefore, the control law must be implemented as an implicit function of the measured states and the appropriate control action will have to be calculated at each time step.

In order to simplify the calculations, the functions $w(x_1, x_2)$, $h(x_1, x_2)$, $\frac{\partial h}{\partial x_1}$, and $\frac{\partial h}{\partial x_2}$ will be evaluated *a priori* over a selected operating range. A sufficiently large number of points (small mesh) will be considered to guarantee the accuracy of the resultant control law calculations. Between mesh points, the functional values will be interpolated for mild operating conditions (low parametric sensitivity). For regions of high parametric sensitivity, the values (particularly h and its derivatives) will be fit with exponential functions to provide a highly accurate interpolation between points.

In effect, the control law is implemented in a "look-up" fashion as a function of the two measured states, x_1 and x_2. The validity of such an approach has been verified by closed-loop simulations in regions of high parametric sensitivity. Here it is found that errors on the order of 5% in the interpolated values lead to closed-loop simulations which were indistinguishable from those employing the exact values. In the subsequent studies, the mesh for interpolation is chosen to limit the interpolation error to under 1%.

It should be emphasized that such a look-up approach is, in general, a necessary method for the application of sophisticated nonlinear control to practical systems. In typical practical applications, the order of resultant implicit nonlinear equations

will preclude the possibility of on-line calculations for reasonable computer power. However, it should also be emphasized that this approach is fundamentally different from so-called linear gain scheduling. In the latter case, static control parameters are interpolated between the values computed for several linear plants along some operating locus. In the present case, there is a spectrum of values, both *along* the operating curve and *off* the locus to calculate the dynamic control action required for the transient conditions as well.

4.3.3 Advanced Control Schemes

Recent results in nonlinear control [16], [53], [91] have enabled the synthesis of more sophisticated nonlinear control approaches for the packed bed reactor. In particular, it can be shown that the packed bed reactor model presented in 4.2.3 is rather versatile and will admit solutions which overcome two of the previously discussed restrictions to feedback linearizing control:

- Nonminimum phase systems.
- Lack of state measurements.

In the following discussion, the importance of the results in [53] and [91] for the current study are briefly summarized.

Nonminimum Phase Control

The presence of right half plane zeros is known to impose limitations on the achievable performance of controlled linear systems. ISE-optimal systems can be found by decomposing the linear system into a stably invertible part and an all-pass. Control design is based upon the inversion of the former half. Such a systematic approach to system decomposition for nonlinear systems is not currently available. However, for a very restricted class of problems (second-order, relative degree one), there has

been a recent result describing such a nonlinear control formulation. As the packed bed reactor model presented in section 4.2.3 meets these requirements; the following control law (derived from [53]) will result in an ISE optimal nonlinear controller.

Assuming that the original model is nonminimum phase (*i.e.* $u = F$), it can be shown that the zero dynamics are unstable:

$$\frac{\partial \hat{w}}{\partial \eta} > 0 \text{ in some neighborhood of } \hat{w} = 0$$

Then the following control law can be utilized

$$u = \frac{v - \psi - \epsilon L_f \psi}{\epsilon L_g \psi} \tag{4.21}$$

where ψ is given by:

$$\psi = h(x_1, x_2) - 2\frac{\partial h}{\partial x_1}\frac{w}{\frac{\partial w}{\partial x_1}} \tag{4.22}$$

Substituting the value of ψ into Equation 4.21 yields

$$u = \frac{v - \psi - \epsilon\left(-\frac{1}{\tau}x_1\frac{\partial \psi}{\partial x_1}\right) - \epsilon\left(w\frac{\partial \psi}{\partial x_2}\right)}{\epsilon\frac{1}{\tau}\frac{\partial \psi}{\partial x_1}} \tag{4.23}$$

where:

$$\frac{\partial \psi}{\partial x_1} = -\frac{\partial h}{\partial x_1} - 2\frac{\partial^2 w}{\partial x_1^2} w \left(\frac{\partial w}{\partial x_1}\right)^{-1} + 2\frac{\partial h}{\partial x_1} w \left(\frac{\partial w}{\partial x_1}\right)^{-2} \frac{\partial^2 w}{\partial x_1^2} \tag{4.24}$$

$$\frac{\partial \psi}{\partial x_2} = \frac{\partial h}{\partial x_2} - 2\frac{\partial^2 h}{\partial x_1 \partial x_2} w \frac{\partial w}{\partial x_1} - 2\frac{\partial h}{\partial x_1}\frac{\partial w}{\partial x_2}\left(\frac{\partial w}{\partial x_1}\right)^{-1} + 2w\frac{\partial h}{\partial x_1}\left(\frac{\partial w}{\partial x_1}\right)^{-2} \frac{\partial^2 w}{\partial x_1 \partial x_2}$$

The resulting closed loop behaves like a first-order lag in series with a nonlinear all-pass:

$$\begin{aligned} \dot{z} &= -\tfrac{1}{\epsilon} z + \tfrac{1}{\epsilon} v \\ \dot{\eta} &= -F_1(z, \eta) \end{aligned} \tag{4.25}$$

$$y \quad = \psi(z, \eta) \tag{4.26}$$

This response is achieved by the replacement of the true output y by the approximate output Ψ (see equation 4.22). This new output has the useful property that it results in stable zero dynamics. More importantly, the new nonlinear controller has a classical linearization (Jacobian) along the operating locus which is exactly equal to the optimal linear control for a nonminimum phase system (all-pass plus lag). The properties of a nonlinear all-pass F_1 (as defined in [53]) are that it is stable, has zeros at the mirror images of poles across the imaginary axis, and has static gain equal to one. If the tuning parameter ϵ in Equation 4.21 is made infinitesimally small, then ISE optimal behavior is obtained from the closed loop.

This look-up table for this control law requires values for the new variables introduced in Equation 4.23. These derivatives of w ($\frac{\partial w}{\partial x_1}$, $\frac{\partial w}{\partial x_2}$, $\frac{\partial^2 w}{\partial x_1 \partial x_2}$,and$\frac{\partial^2 w}{\partial x_1^2}$) can be readily calculated from the existing values of w in the table.

Output Feedback Control

In many cases the state measurements required for the nonlinear feedback linearizing controllers are not available. In the case of the packed bed reactor, the filtered inlet and ignition position may be more difficult to obtain than more readily measurable quantities such as axially spaced thermocouple temperature readings. Such quantities would make it rather easy to calculate the hot spot temperature in the reactor (by interpolation or some inferential scheme). As this quantity is the output of the controlled process, it may be more desirable to synthesize a nonlinear control law which only requires measurement of the output (and possibly some higher order derivatives). Such an approach was described recently [16].

The dynamic output controller for the packed bed reactor is given by two parts,

an error feedback linear controller

$$\begin{aligned} \dot{\xi} &= (y_{sp} - y) \\ v &= \frac{\beta_0}{\epsilon}\xi + \frac{\beta_1}{\epsilon}(y_{sp} - y) \end{aligned} \tag{4.27}$$

and an output feedback nonlinear controller:

$$\begin{aligned} \dot{z_1} &= \hat{w}(z_1, y) \\ u &= \frac{\frac{1}{\epsilon}\beta_0\xi + \frac{\beta_1}{\epsilon}(y_{sp}-y) - (\beta_0 y + \beta_1 L_f h(z_1,y))}{\beta_1 L_g h(z_1,y)} \end{aligned} \tag{4.28}$$

This is equivalent to a PI controller with $K_p = \frac{\beta_1}{\epsilon}$ and $\tau_I = \frac{\beta_1}{\beta_0}$ in the outer (linear) loop, around an inner dynamic nonlinear controller which reconstructs the state. The resulting closed loop is given by:

$$\frac{y}{y_{sp}} = \frac{1}{(\epsilon s + 1)} \tag{4.29}$$

Thus, the linear input-output behavior has been achieved from solely measuring the hot spot temperature at the expense of an additional dynamic state in the controller. Though not explored in this work, this approach shows promise for use in applications with an actual experimental reactor where quantities such as lagged input and ignition position may not be as convenient to measure as the peak bed temperature.

4.4 Case Studies

4.4.1 Inlet Concentration Manipulation

The first variable selected for study as a manipulated variable in both a linear and nonlinear closed-loop configuration is the inlet concentration. Selecting c_0 as the manipulated variable in Equation 4.5 leads to the construction of the output function

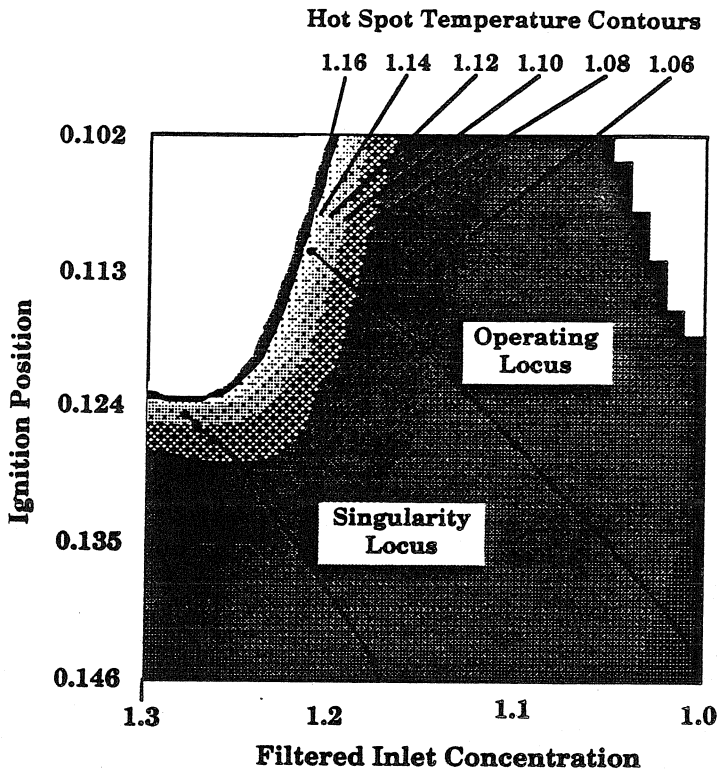

Figure 4.13. Region of Operation (u = Inlet Concentration)

$h(x_1, x_2)$ (hot spot temperature) which is depicted in Figure 4.13 and 4.14. (Note that x_1 corresponds to the *filtered inlet concentration*, that is, the value of the manipulated variable after a lag has been applied.) The values of the other variables are as follows: $F = 1.0, T_w = 1.0$, and the exponential dependence of the heat transfer coefficient on the flow rate is 0.05. Figure 4.13 shows a contour plot of the hot spot temperature in the $x_1 - x_2$ plane about a nominal state position of $(x_1, x_2) = (1.15, .124)$. Also shown are two loci: the operating locus and the singularity locus. The former is the steady-state solution of Equation 4.12. The implications for closed-loop operation under nonlinear (IOL) control are straightforward: this locus cannot be crossed. Thus the control action must be limited to the region around the operating curve away from the singularity locus. Experience in simulations with this system indicate that this is not a very restrictive condition.

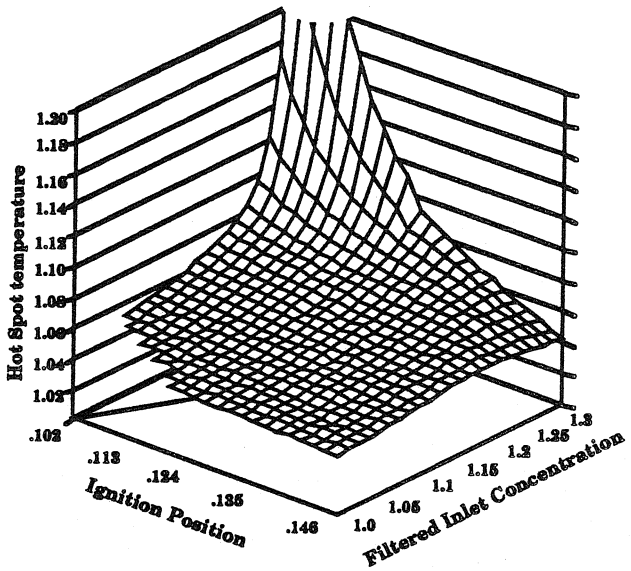

Figure 4.14. Hot Spot Temperature Profile (u = Inlet Concentration)

In Figure 4.14 is shown a three-dimensional portrait of the hot spot temperature over the operating regime. From this diagram it is clear that the chosen operating conditions correspond to parametrically sensitive reactor behavior. At lower concentrations (< 1.15), the temperature profile is fairly mild. However, as one moves along the operating curve in the direction of increasing concentration, the temperature quickly escalates as the sensitivity rapidly increases.

This diagram suggests three operating points for the comparative study of non-linear versus linear control. They are: $c_0 = 1.0$ (benign operation), $c_0 = 1.15$ (mild sensitivity), $c_0 = 1.20$ (high sensitivity). At each operating point, the closed-loop response of the system to a set point change in the hot spot temperature of .02 ($12.5K$) will be examined. To enrich the study, $\pm 1K$ of white noise will be added to the measured signal y.

In Figures 4.15 , 4.16, and 4.17 are shown the closed-loop response of the system

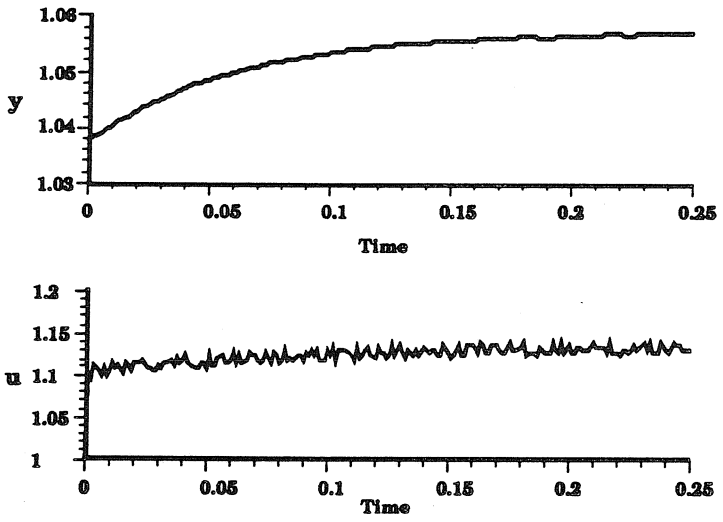

Figure 4.15. Set Point Response ($c_0 = 1.0$, Linear Controller)

under linear (PI) control. The control parameters ($K_p = 10.0, \tau_I = 20.0$) were selected as the values which drove the system bandwidth up to the point of instability at $c_0 = 1.2$. It can be observed that the speed of response accelerates as the inlet concentration is increased. This is clearly caused by the increasing gain of the reactor as it moves into a region of parametric sensitivity while the control gain remains constant. It is also seen that the attenuation of the measurement noise worsens

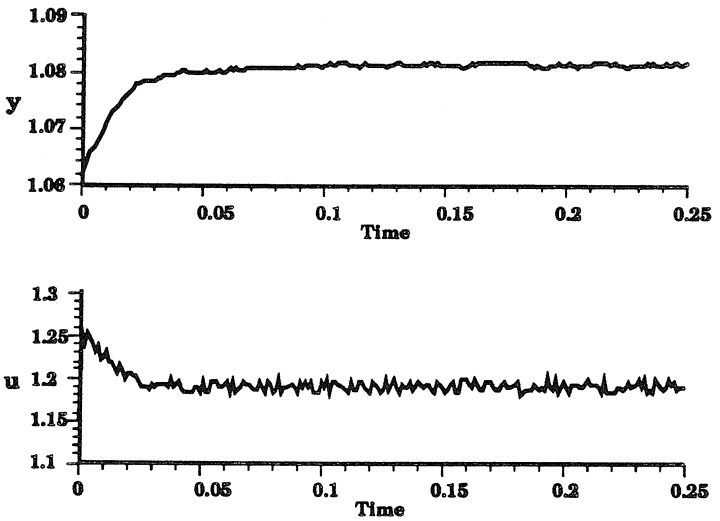

Figure 4.16. Set Point Response ($c_0 = 1.15$, Linear Controller)

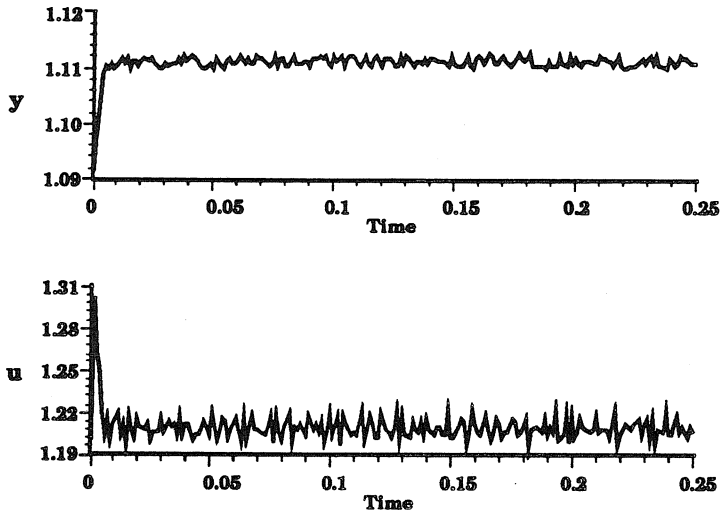

Figure 4.17. Set Point Response ($c_0 = 1.2$, Linear Controller)

as the speed of response increases. Again, this is a fairly intuitive idea, that the attenuation of noise in the output is traded off against speed of response by changing the system bandwidth.

In Figures 4.18, 4.19, and 4.20 are shown the closed-loop response of the system under nonlinear (IOL) control with an external PI controller. The control parameters ($\beta_1 = 1.0, \beta_0 = 0.1, K_p = 50.0, \tau_I = 20.0$) are chosen to roughly approximate the

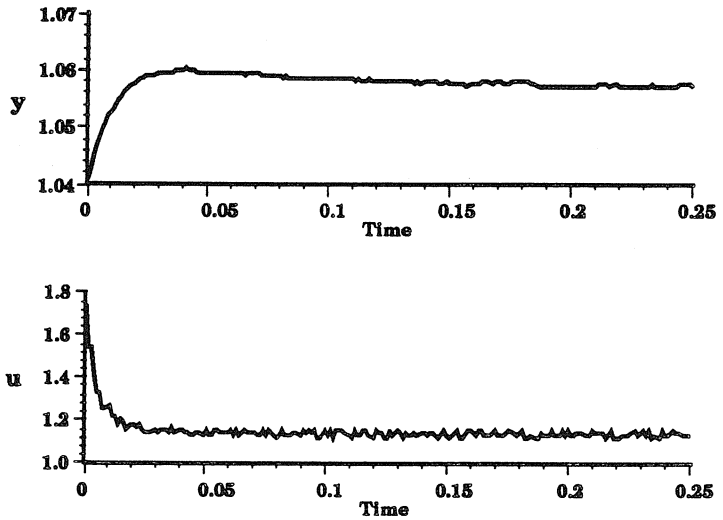

Figure 4.18. Set Point Response ($c_0 = 1.0$, Nonlinear Controller)

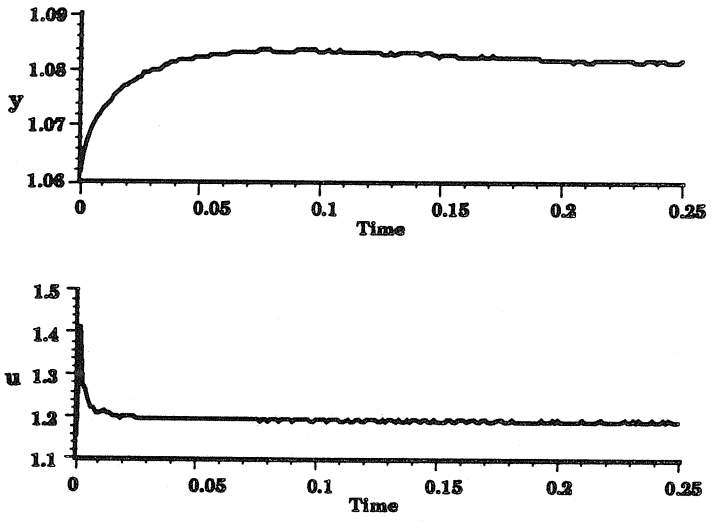

Figure 4.19. Set Point Response ($c_0 = 1.15$, Nonlinear Controller)

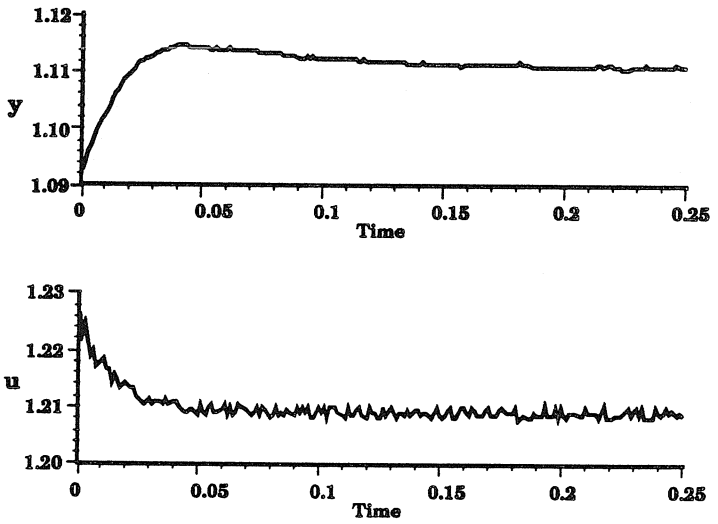

Figure 4.20. Set Point Response ($c_0 = 1.2$, Nonlinear Controller)

system behavior of the linearly controlled system at $c_0 = 1.15$. (Exact replication is not possible as the reactor is a second-order, relative degree 1 system, while the "linearized" plant in IOL is a first-order, relative degree 1 system.) As can be seen in Figures 4.18, 4.19, and 4.20, the response of the (noisy) hot spot temperature to the set point change is virtually identical in each case. This is as expected since the nonlinear controller "dynamically gain schedules" to account for the changing operating conditions so as to produce the same closed-loop input-output behavior at each operating point. The amount of control effort required is depicted in these three diagrams and, particularly in the third case ($c_0 = 1.2$), reveals the utility of nonlinear control. In this case, the reactor has, for whatever reason, drifted from the nominal operating point at $c_0 = 1.15$ into a region of higher parametric sensitivity. The nonlinear controller is self-tuning and reduces the controller gain to compensate, ensuring uniform closed-loop behavior over the whole operating region. By contrast, when the system drifts into a region of lower parametric sensitivity, the nonlinear controller gain is increased to compensate for the reduced reactor gain.

4.4.2 Jacket Temperature Manipulation

The second manipulated variable studied in a closed-loop configuration is the jacket temperature. From a practical perspective, this choice of u is far more logical than c_0 for manipulation, and industrial packed bed reactors traditionally rely on tight control of coolant temperatures in achieving optimal reactor operation. An additional modification from the previous case study is that the linear control algorithm employed will be IMC (Internal Model Control) [67]. This is expected to yield better comparative results as IMC is a direct linear generalization of the nonlinear model-inverse-based approach of IOL. Consequently, a direct comparison of "apples to apples" is possible with each system having identical nominal response.

Selecting the jacket temperature as the manipulated variable in Equation 4.5 leads

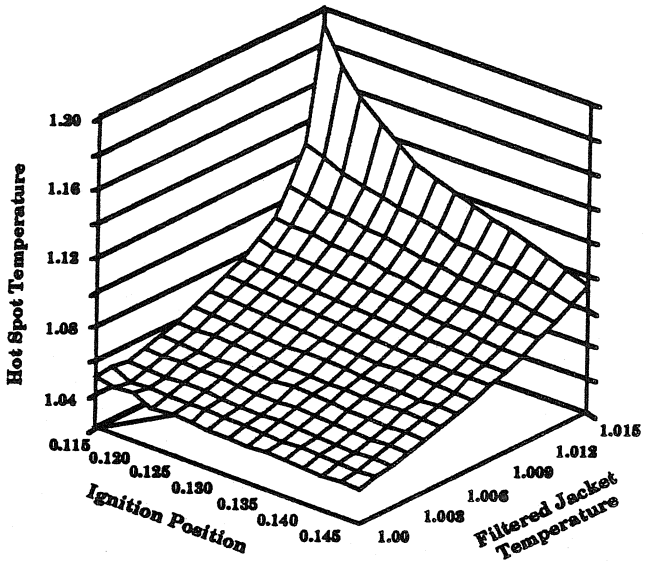

Figure 4.21. Hot Spot Temperature Profile (u = Jacket Temperature)

to the function $h(x_1, x_2)$ depicted in Figure 4.21. (Note that x_1 corresponds to the *filtered jacket temperature*, that is the value of the manipulated variable after a lag has been applied.) The values of the other variables are as follows: $c_0 = 1.0, F = 1.0$, and the exponential dependence of the heat transfer coefficient on the flow rate is 0.05. This three-dimensional diagram shows the operating neighborhood around $(x_1, x_2) = (1.0075, 0.13)$. Recalling Figure 4.6, the sensitivity of hot spot temperature on jacket temperature is much higher than on inlet concentration. Thus, a smaller region of the operating locus is selected in order to observe a wide range in dynamical behavior. As opposed to the previous case ($u = c_0$), there are no singularity constraints on this control law and the relative degree is well defined over the operating region. This diagram suggests three operating points for the comparative study of nonlinear versus linear control. They are: $T_w = 1.002$, $T_w = 1.008$, and $T_w = 1.0115$. At each operating point, the closed-loop response of the system to a set point change in the hot spot temperature of .03 ($18.75K$) will be examined. To enrich the study, $\pm 1.5K$ of white noise will be added to the measured signal y.

Figures 4.22, 4.23, and 4.24 show the closed-loop response of the system under

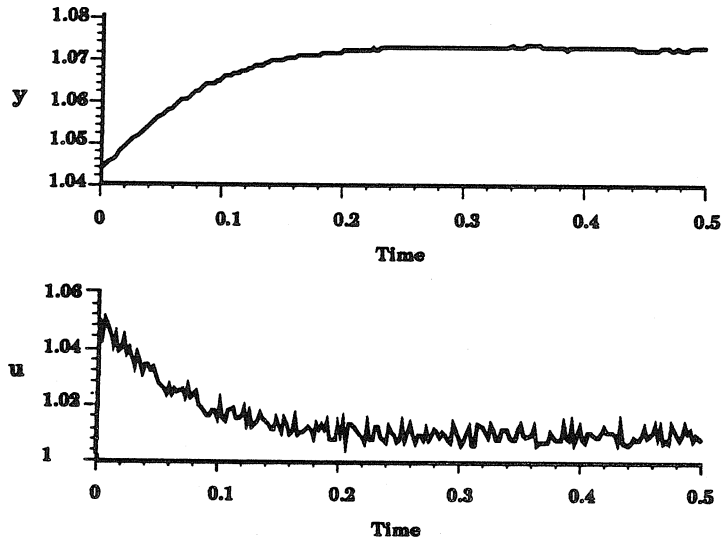

Figure 4.22. Set Point Response ($T_w = 1.002$, Linear Controller)

linear (IMC) control. The controller is designed with a first-order filter and a filter time constant equal to 0.1. It can be observed, as in the previous case study, that as the reactor is pushed into a region of greater parametric sensitivity, the open-loop gain increases, which leads to a faster closed-loop speed of response. In addition, the noise attenuation worsens as the reactor sensitivity increases.

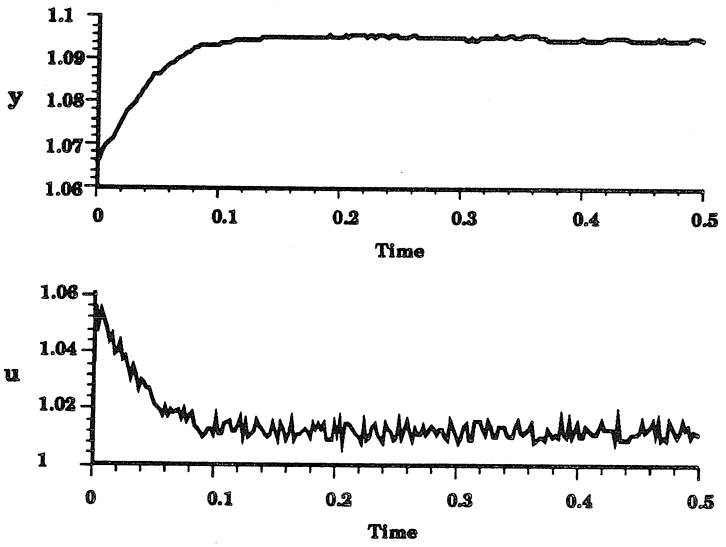

Figure 4.23. Set Point Response ($T_w = 1.008$, Linear Controller)

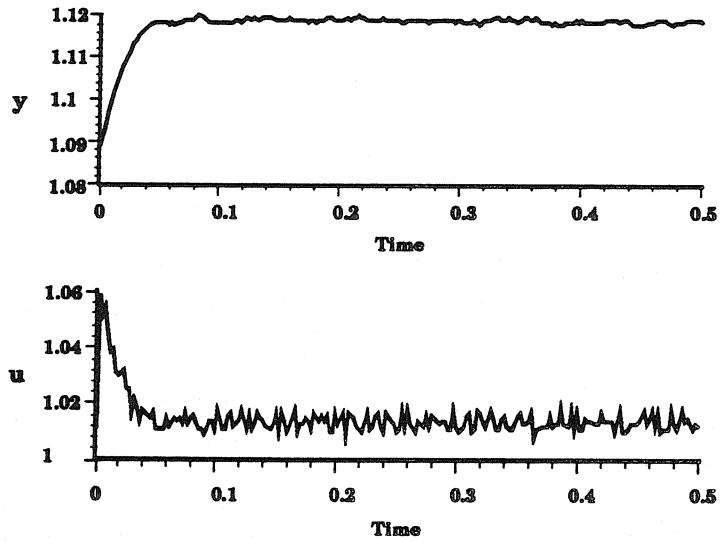

Figure 4.24. Set Point Response ($T_w = 1.0115$, Linear Controller)

By contrast, the nonlinearly controlled reactor results in uniform behavior over the operating envelope as seen in Figures 4.25, 4.26, and 4.27. The nonlinear controller is tuned with the parameters ($\beta_1 = 1.0, \beta_0 = 0.1$) and an external PI controller with parameters ($K_p = 0.1, \tau_I = 1.0$) to match the response of the linearly controlled system at the nominal operating point ($T_w = 1.002$). As the cooling jacket

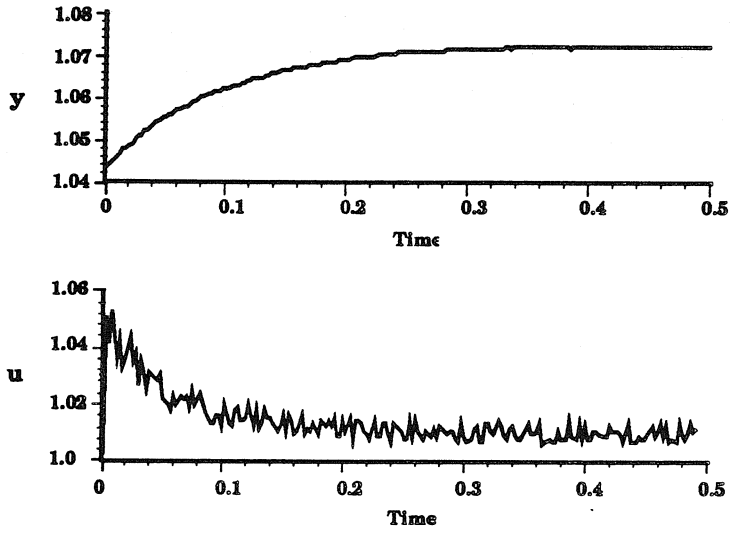

Figure 4.25. Set Point Response ($T_w = 1.002$, Nonlinear Controller)

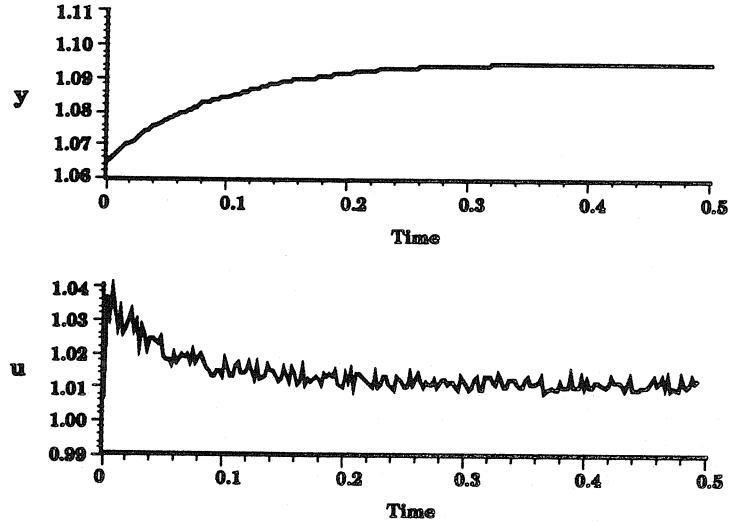

Figure 4.26. Set Point Response ($T_w = 1.008$, Nonlinear Controller)

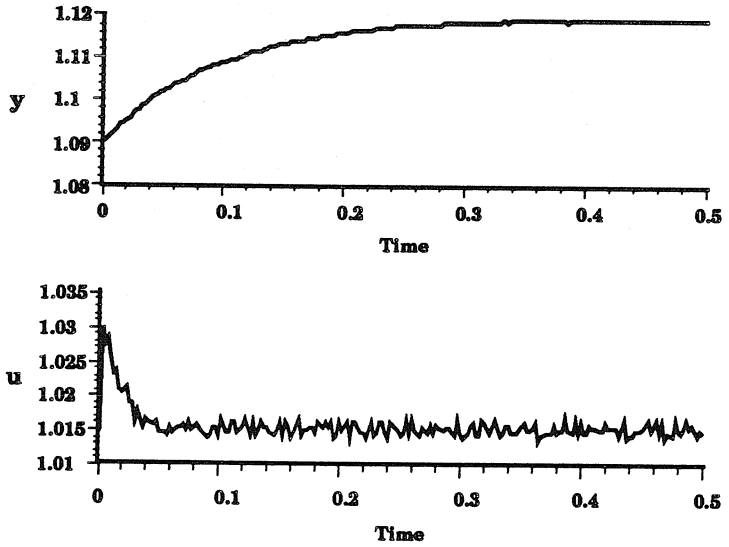

Figure 4.27. Set Point Response ($T_w = 1.0115$, Nonlinear Controller)

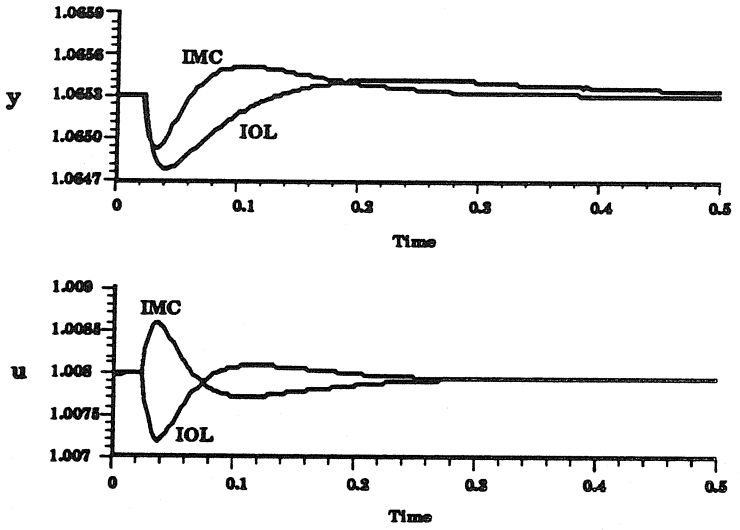

Figure 4.28. Flow Disturbance Response ($T_w = 1.008$)

temperature is increased and the gain of the reactor also increases, the nonlinear controller "schedules" the manipulated variable action so that the output behavior remains uniform (speed of response, noise attenuation).

The previous simulations all focused on nominal operating conditions. That is, the models were all assumed to be accurate and the influence of unmeasured disturbances is ignored. In the following two simulations, the impact of these two effects are further analyzed.

In the first case, consider a step disturbance in the inlet flow rate. The response of the linearly controlled reactor is shown in Figure 4.28. The controller parameters are as before and the temperature set point = 1.0653 (corresponding to a T_w value of 1.008). At time t=0.025, a 10% decrease in the flow rate is introduced (from 1.0 to 0.9). Several interesting trends are observed in Figure 4.28. The initial gain of the control action is opposite in sign for the linearly controlled versus the nonlinearly controlled reactor. The direction of the nonlinear control gain is correct because the decrease in flow rate must be offset by a decrease in cooling jacket temperature to maintain the same hot spot temperature. This gain directionality is attributed to the

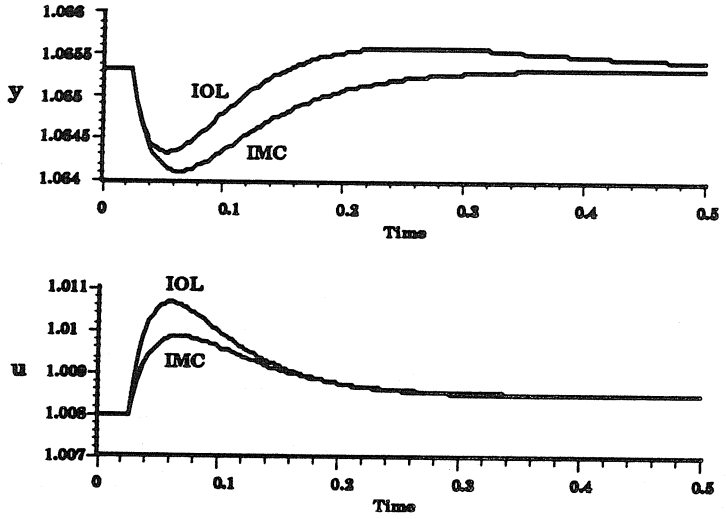

Figure 4.29. Concentration Disturbance Response ($T_w = 1.008$)

nonlinear dependence of the control action on the operating conditions. The resulting effect is that the nonlinearly controlled reactor has a larger undershoot but a smaller overshoot in the hot spot temperature response. Note that this change in the flow rate invalidates the nonlinear look-up control table which was designed for $F = 1.0$.

In Figure 4.29 is shown the closed-loop response of the system to a disturbance in the inlet concentration. The same operating conditions are chosen ($T_w = 1.008$) and at time t = 0.025, a decrease in inlet concentration (from 1.0 to 0.9) is introduced. Now, this represents a minimum phase disturbance and it is observed that both controllers have the same initial gain sign but the nonlinear control action is more aggressive and the resulting error trajectory shows less overshoot. As before, this disturbance may be interpreted as a perturbation in a model parameter which, strictly speaking, invalidates the exact linearization control law.

The final simulation is shown in Figure 4.30. The reactor is initialized at $T_w = 1.002$ and at time t = 0.025, the Damköhler number is reduced by 5%. In this case, an unfiltered model parameter has been directly perturbed and the response in both cases (linear and nonlinear control) is instantaneous. Note, however, that the nonlinear control action is much more aggressive and the speed of response in

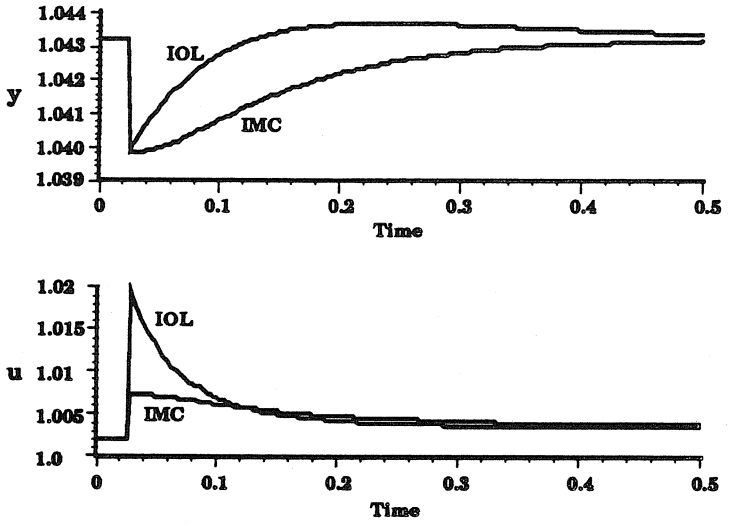

Figure 4.30. Robustness to Error in $\mathcal{D}a$ ($T_w = 1.002$)

returning to the original set point is much faster.

4.4.3 Flow Manipulation

A final closed-loop configuration is investigated in which the flow rate into the reactor is manipulated to control the hot spot temperature. Selecting F as the u in Equation 4.5 results in a nonminimum phase system and leads to the hot spot temperature profile ($h(x_1, x_2)$) depicted in Figure 4.31. (Note that x_1 corresponds to the *filtered flow rate*, that is the value of the manipulated variable after a lag has been applied.) The values of the other variables are as follows: $c_0 = 1.0, T_w = 1.0$, and the exponential dependence of the heat transfer coefficient on the flow rate is 0.5. The grid selected for the look-up table is centered around the nominal point $(0.7, 0.095)$. As in the previous case ($u = T_w$), there are no singularity constraints on this control law and the relative degree is well defined over the operating region. The control law in this case is complicated by the difficulties mentioned in section 4.3.3 and this is reflected in the complexity of the look-up table for this controller. As in the previous two cases, it is observed that the reactor has a mild profile at higher flow rates and

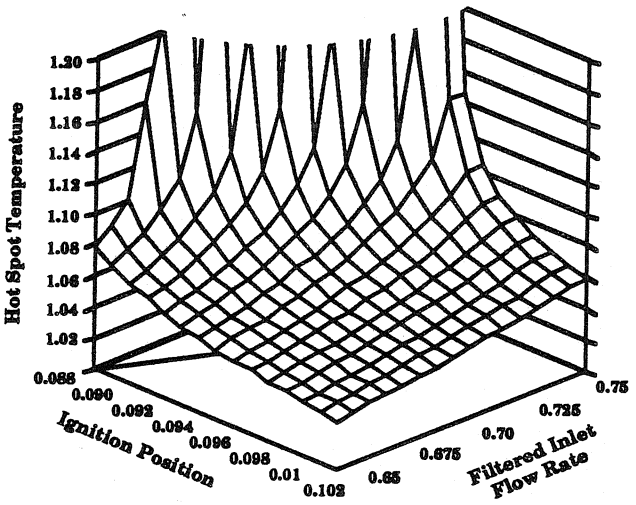

Figure 4.31. Hot Spot Temperature Profile (u = Flow Rate)

that the sensitivity of the reactor accelerates as the flow rate is reduced.

A simple set of simulations is presented to demonstrate the machinery introduced in section 4.3.3. Recall from that section that the presented approach to NMP control for nonlinear systems yields a system with linear optimal response in a close neighborhood of the operating locus. However, as opposed to the IOL for MP systems, the off-equilibrium behavior is not linear. This can be seen in the following figures. First, the inner nonlinear controller is synthesized from Equation 4.21 . If this inner loop is subjected to a step in the new manipulated variable, v, (from 0.0 to -0.03) the result is the trajectory shown in Figure 4.32. The resulting closed inner loop response behaves like a first-order lag in series with an allpass.

Now consider the synthesis of the outer loop. An IMC controller is designed

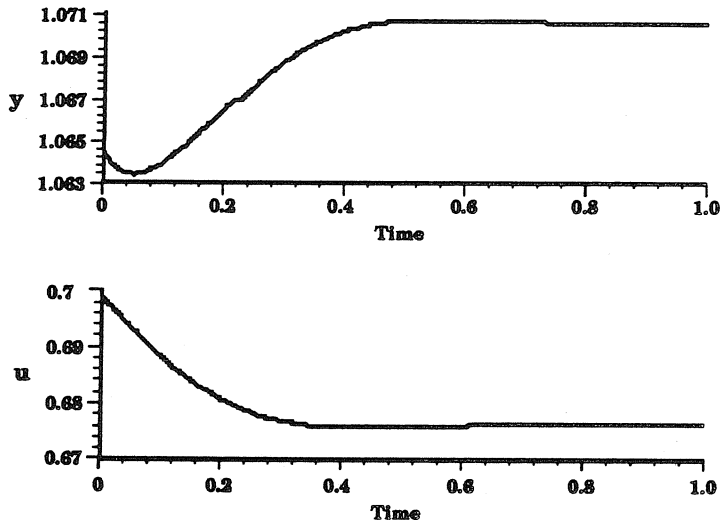

Figure 4.32. Open (Inner) Loop Response (Nonlinear Controller)

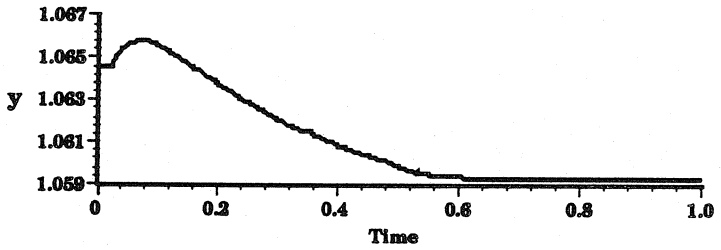

Figure 4.33. Set Point Response ($F = 0.7$, Linear Controller)

to result in an outer closed-loop response equal to an allpass in series with a first-order lag with time constant 0.1 (at least nominally, that is, along the operating curve). Similarly, as a basis for comparison, a linear IMC control law for the reactor is synthesized, which results in a closed-loop response (nominally, at the operating point) equal to an allpass in series with a first-order lag with time constant 0.1. The results of a set point change in hot spot temperature (from 1.0646 to 1.0706, $3.75K$) are shown in Figures 4.33 and 4.34. Note the characteristic inverse response of these NMP systems. It is also observed that the nonlinearly controlled reactor has a small overshoot and a mild oscillation which is quickly dampened. The source of this departure from both the ideal linear behavior and the linearly controlled nonlinear reactor is the nonlinear allpass configuration for the IOL. As the results discussed

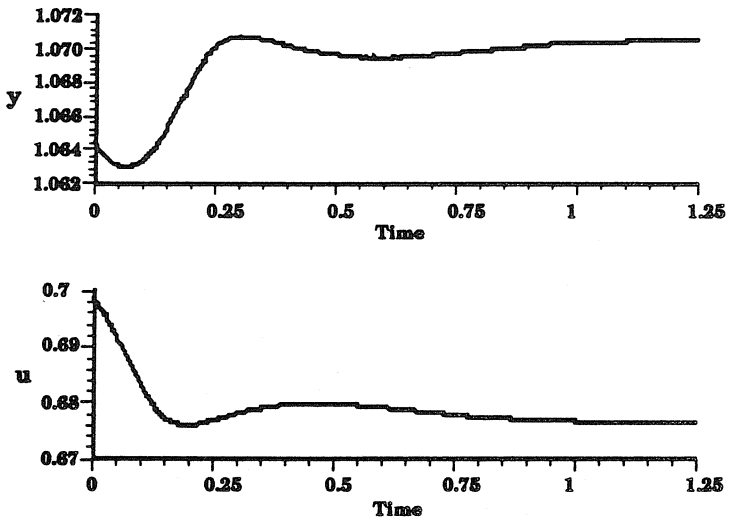

Figure 4.34. Set Point Response ($F = 0.7$, Linear Controller)

in section 4.3.3 from [16] have not been evaluated in closed-loop simulations, it is concluded that further investigations of the stability and performance of this approach must be undertaken. The results presented here demonstrate the viability of the approach for the IOL control of a packed bed reactor.

4.4.4 Discussion

A number of conclusions can be drawn from the preceding simulations about the viability of nonlinear (IOL) control for a packed bed reactor and its comparative advantages over linear control.

The dominant advantage of IOL over PI or IMC control is the ability of IOL to "dynamically gain schedule" the control law over a wide operating envelope. It is clear that operation in a region of high parametric sensitivity will lead to considerable variations in the parameters of a model which describes the reactor. A simple, single linear controller will result in a closed loop which has a varying bandwidth over the operating envelope. This will lead to widely varying speeds of response as well as fluctuations in the ability to attenuate measurement noise. Note that the self-tuning

mechanism in IOL prescribes in a systematic way the control action as a function of the reactor states. This is contrasted with so-called linear "gain scheduling," in which optimal linear control about a tiny neighborhood of an operating point is generalized in an ad-hoc way to cover the operating space.

It is observed that in order to obtain a uniform closed-loop response over a wide operating regime, the gain variations in the reactor must be offset by gain variations in the controller. If the reactor moves away from the nominal design point into a region of lower parametric sensitivity, the nonlinear control action must become more aggressive. This may present a problem if rate and magnitude constraints are violated. In contrast, if the reactor moves into a region of higher parametric sensitivity, the plant gain increases and the nonlinear controller detunes itself. The consequences may be catastrophic if the controller is not detuned as noise becomes amplified and thermal runaway occurs.

The closed-loop response of the packed bed reactor to disturbances in both flow and concentration indicate comparable performance by the linear and nonlinear controller. In the case of inlet concentration disturbances, the nonlinear control action is more aggressive and smaller overshoot is observed. Qualitatively, the behavior is very similar for the two systems. In the case of a NMP disturbance (flow rate), the qualitative behavior of the two systems is quite different. The linear controller moves initially in the wrong direction (relative to the final value) and displays an overshoot in y as a result. The nonlinear controller moves in the correct initial direction and displays minimal overshoot, but the price paid is large undershoot in the initial temperature transient. As before, it should be noted that the alteration of either flow rate or inlet concentration invalidates the exact IOL and the resulting behavior indicates the robustness of this approach.

A final measure of robustness is revealed by the change in the Damköhler number. Here the nonlinear controller proves to be very effective at returning the system to its

original set point. However, this response comes at the expense of fairly aggressive manipulated variable action which may be considered unacceptable.

Overall, the simulation results suggest that in the nominal case (no model uncertainty, no unmeasured disturbances), the nonlinear controller has a clear advantage in maintaining uniform reactor behavior over a region of parametric sensitivity. This behavior is exactly the performance demanded of industrial packed bed reactors: uniform operation over a wide region. IOL presents one approach to achieving this performance with a self-tuning algorithm.

In terms of robustness, it is clear that many more case studies must be considered. Presented here are some fairly representative case studies which suggest that the nonlinear controller is more robust to NMP disturbances and errors in the physical parameters of the reactor. However, extensive simulations must be performed with a variety of model errors, disturbances, and operating conditions before absolute conclusions can be drawn. A systematic, analytical approach to ascertaining the relative robustness of the linearly and nonlinearly controlled reactor is presented in the following section.

4.5 Robustness Considerations

This section presents the formal framework for analyzing the robust performance properties of the closed-loop packed bed reactor. First, the system is cast in the Byrnes-Isidori normal form (Equation 4.14), where z_1 is the hot spot temperature and z_2 is the ignition position. From this open-loop representation, it is straightforward to derive a closed-loop representation corresponding to the application of IOL (Equation 4.19):

$$\begin{aligned} \dot{z}_1 &= \frac{v}{\beta_1} - \frac{\beta_o z_1}{\beta_1} \\ \dot{z}_2 &= \hat{w}(z_1, z_2) \\ y &= z_1 \end{aligned} \tag{4.30}$$

(Note that this represents the inner loop of Figure 4.12.) This system is linear in the output, linear in the first state equation, and has a nonlinear, unobservable second state equation. This will be directly compared to the original nonlinear plant:

$$\begin{aligned} \dot{x}_1 &= -\tfrac{1}{\tau}x_1 + \tfrac{1}{\tau}u \\ \dot{x}_2 &= w(x_1, x_2) \\ y &= x_1 \end{aligned} \tag{4.31}$$

Each of these two plants will be closed with a linear controller in a feedback configuration and the resultant performance properties can be ascertained. In the subsequent analysis, the formulation of an uncertainty structure for each of the two plants is carried out.

Consider an error in the modeled hot spot temperature function ($h(x_1, x_2)$). This is easily plausible as the complicated packed bed reactor dynamics have been reduced to a second-order representation in which there is bound to be uncertainty. For the purposes of this example, consider the following simple deviation from the actual nonlinear output:

$$y = h(x_1, x_2) + [0.1(x_1 - x_{10}) + 1.2(x_2 - x_{20})] \equiv \tilde{h}(x_1, x_2) \tag{4.32}$$

This investigation of the robustness properties will consider an elliptic operating regime stretching from the operating point at ($x_{10} = 1.0982, x_{20} = .11174$) to ($x_{10} = 1.2018, x_{20} = .12726$). If this is perturbed output substituted for the value of h in the nonlinear control law in Equation 4.19, the original inner plant becomes

$$\begin{aligned} \dot{z}_1 &= \tfrac{v}{\beta_1}\Delta_1 - \tfrac{\beta_o z_1}{\beta_1}\Delta_2 + \tilde{w}\Delta_3 \\ \dot{\eta} &= \tilde{w}(z_1, z_2, \Delta_4, \Delta_5) \end{aligned} \tag{4.33}$$

where

$$\begin{aligned} \Delta_1 &= \frac{\frac{\partial h}{\partial x_1}}{\frac{\partial h}{\partial x_1}} \\ \Delta_2 &= \frac{\tilde{h}\frac{\partial h}{\partial x_1}}{h\frac{\partial h}{\partial x_1}} \\ \Delta_3 &= \frac{\frac{\partial h}{\partial x_2}}{\frac{\partial h}{\partial x_1}} - \frac{\frac{\partial \tilde{h}}{\partial x_2}}{\frac{\partial h}{\partial x_1}} \end{aligned} \tag{4.34}$$

and Δ_4 and Δ_5 are more complicated functions of w and h and $\tilde{h}$.

A first principles analysis of the output dynamics (z_1) reveals the following insights about the uncertainty elements Δ_1, Δ_2, and Δ_3:

1. Δ_3 is attenuated by the wave propagation velocity, which is zero on the operating locus.

2. Δ_2 corresponds to pole uncertainty in the first-order transfer function relating v to y.

3. Δ_1 corresponds to gain uncertainty in the first-order transfer function relating v to y.

From robust control theory [67], it is known that pole uncertainty in a first-order transfer function does not present a robustness problem and that high gain feedback will alleviate this problem while improving the overall system performance (speed of response). On the other hand, gain uncertainty will cause a tradeoff between the robust stability and robust performance of the system, leading to a sacrifice in performance to ensure stability.

A direct analysis of the impact of the model uncertainty (Equation 4.32) on the two candidate plants for linear control is now considered. This analysis was carried out in the framework of chapter 3, where conic sectors are utilized to arrive at a tight description of a linear nominal model and the associated uncertainty.

First consider the following linear uncertain representation for the IOL inner plant:

$$\begin{pmatrix} \dot{z}_1 \\ \dot{z}_2 \end{pmatrix} = \begin{pmatrix} -\frac{0.75\beta_0}{\beta_1} & 0.0 \\ -13.8 & -34.7 \end{pmatrix} \begin{pmatrix} z_1 \\ z_2 \end{pmatrix} + \begin{pmatrix} 0 & 0 \\ 1.92\delta_1 & 5.05\delta_1 \end{pmatrix} \begin{pmatrix} z_1 \\ z_2 \end{pmatrix}$$

$$+ \begin{pmatrix} \frac{0.75}{\beta_1} \\ 0 \end{pmatrix} v + \begin{pmatrix} 0.2\delta_2 \\ 0 \end{pmatrix} v \qquad (4.35)$$

$$y = z_1 + 0.01\delta_3 z_1$$

where δ_1, δ_2, and δ_3 represent uncorrelated, conic-sector bounded, unit norm, nonlinear operators. Now consider the original packed bed reactor and its associated linear uncertainty description :

$$\begin{pmatrix} \dot{x}_1 \\ \dot{x}_2 \end{pmatrix} = \begin{pmatrix} 0.0 & -\frac{1}{\tau} \\ -5.36 & -34.7 \end{pmatrix} \begin{pmatrix} x_1 \\ x_2 \end{pmatrix} + \begin{pmatrix} 0 & 0 \\ 1.192\delta_4 & 5.054\delta_4 \end{pmatrix} \begin{pmatrix} x_1 \\ x_2 \end{pmatrix} + \begin{pmatrix} \frac{1}{\tau} \\ 0 \end{pmatrix} u$$

$$y = (0.383 \quad 0.107) \begin{pmatrix} x_1 \\ x_2 \end{pmatrix} + \begin{pmatrix} -0.107\delta_5 & -0.287\delta_5 \\ 0.107\delta_6 & -0.320\delta_6 \end{pmatrix} \begin{pmatrix} x_1 \\ x_2 \end{pmatrix} \qquad (4.36)$$

The perturbation elements (δ_i) can be interpreted as the uncertain deviation from the nominal linear system description ($\delta_i = 0$). They include both the effect of uncertainty in the output function, h, and the effect of the nonlinearities in the nominal system description.

The purpose of this derivation is to show how in terms of the uncertainty formulation used for SSV calculations, lower overall deviation from nominal performance (*i.e.*, good robust performance) is achieved via IOL versus linear control.

Uncertainty in the hot spot temperature function leads to much larger variations from an ideal linear description for the original packed bed reactor compared with the IOL inner plant. Effectively, the IOL action has served a two-fold purpose:

- Eradication of the nonlinear nature of the model.
- Minimization of the perturbation from this model for plant uncertainty.

The result is less deviation from linear behavior for the nonlinearly controlled packed bed reactor and, consequently, a better overall level of robust performance.

Note that this analysis is somewhat informal and really gives only an indication of how linear the resulting closed loops are. Even the two nominal plants under scrutiny have different linear approximations. A full analysis using the SSV theory would be futile because of the complexity of the uncertainty structure coupled with the conservativeness of those results for nonlinear systems. As discussed in chapter 3 and [24], direct comparison is not possible because the results are only upper bounds on the attainable performance levels.

The intent here is to reveal, in a manner more formal than simulation, the impact of IOL versus linear control on the robustness properties of the closed-loop packed bed reactor.

4.6 Conclusions

This chapter outlines the development of a two-tier approach to synthesizing a nonlinear control law for a packed bed reactor

In the first stage, a low-order nonlinear model of the packed bed reactor is designed. This model relied on a treatment of active transport mechanisms in the bed as nonlinear waves which propagate up and down the reactor. The dynamics of the derived model were successfully validated against results found in the literature and results available from a laboratory methanation reactor.

The real strength of this modeling approach, for control studies, lies in its general applicability to a variety of chemical engineering systems. These include the basic unit operations of distillation, sedimentation, crystallization, heat exchange, adsorbtion,

and others described in [62]. It is envisioned that such low-order modeling of process systems will lead to a greater understanding of the control relevant dynamics and will serve as a firm foundation for advanced control studies.

The second tier of this design scheme is the actual synthesis of a nonlinear control law for the packed bed reactor. Using the tools of differential geometry, an input-output linearizing control law is successfully designed and implemented on the reactor model. Modifications to the basic control law are incorporated to facilitate the control of NMP systems and to handle the problem of unmeasured states.

A key contribution of this work is the definition of the implementational hurdles to utilizing these nonlinear control algorithms on an actual physical reactor. The primary obstacles identified were the discrete sampling issues and the treatment of implicit control laws. Although the practical side of the reactor problem has been emphasized, one acknowledged weakness of the present work is the lack of experimental verification of the presented results. This is one clear indication of necessary future direction for this work.

Another contribution of this work is an investigation of the comparative advantages of nonlinear control over linear control for a complicated system like the packed bed reactor. Through both simulation and analysis, the relative merits of the two closed-loop systems are evaluated with respect to nominal performance and robust performance (disturbance handling and model uncertainty). The results are not exhaustive, but strongly point towards IOL as a more effective means of controlling a packed bed reactor in a region of incipient runaway.

Further study of the comparative merits of nonlinear and linear control is vital to an understanding of the potential applications for nonlinear control. This will continue to be a focal point of this research. Some preliminary results for several systems are discussed in chapter 6.

Chapter 5

Design Considerations for Multitubular Packed Bed Reactors

Abstract

Practical guidelines are required for the design and operation of complicated catalytic packed bed reactors. Primary among design considerations is the avoidance of operating regions of high parametric sensitivity, in which small changes in operating conditions can lead to thermal runaway in the reactor. Existing criteria for predicting these regions rely on complex mathematical formulations for differential sensitivity between input and output variables. The present work centers on the development of practical design criteria for avoiding reactor instability and temperature sensitivity in multitubular packed bed reactors. A set of simple guidelines is proposed for the sizing of reactors and proper selection of operating conditions. The implications of these open-loop sensitivities for a controlled reactor are investigated. It is shown through simulation studies that violation of the proposed criteria leads to control problems and difficulty in operating at the design point.

5.1 Introduction

Multitubular packed bed reactors display a rich range of steady state and dynamic behavior. Often, there is an economic incentive to operate near a region of parametrically sensitive behavior. In these regions, small changes in inlet conditions and/or

physical parameters can lead to catastrophically large excursions in the bed temperature. Clearly it is important to establish guidelines for safe reactor operation and it is moreover advantageous to specify *a priori* the design of a reactor which avoids these dangerous operating conditions.

In this chapter, some simple design criteria for sizing a reactor and choosing reaction conditions are described. The usual uncertainties associated with catalyst properties and reaction kinetics suggest the formulation of conservative criteria. This conservatism might be reduced with more detailed modeling. However, the proposed criteria are far simpler to evaluate and provide reasonable bounds.

It is possible to formulate these design guidelines in terms of three straightforward criteria:

- The reactor should have a mild radial temperature profile. This protects against self-acceleration of the reaction at the center of the reactor.
- The reactor temperature profile should not exhibit sensitivity to small perturbations in the inlet conditions and physical parameters.
- The pressure drop must be kept at an acceptable level.

Initially it is assumed that the catalyst particle has a single steady state, but, as will be shown, it is possible to modify the parametric sensitivity criterion to predict the occurrence of multiple steady states.

Of particular interest in this study is the sensitivity criterion. This property has been described in great detail for a variety of reactors [30], [68], [69], [70], [78], [89]. These studies focus on the formulation of normalized differential sensitivities for describing conditions of runaway behavior. However, the direct implications of this sensitivity theory for reactor design are not apparent. Alternatively, extensive simulations can be used for predicting these conditions. However, there are often large uncertainties associated with the parameters in these models. A primary goal

of this work is the formulation of an incipient runaway condition in terms of *practical* design variables which are well known (diameter, length, catalyst properties, etc.) and can be directly incorporated into an efficient design scheme.

The preceding discussion focused on open-loop (uncontrolled) packed bed reactor operation. There are, however, several incentives for using feedback control in a chemical reactor (either tubular or continuous stirred tank):

- Stabilization of an unstable operation.
- Mitigation of open-loop sensitivity.
- Improvement of overall performance.

Unstable operation is characterized by the presence of multiple steady states with hysteresis between ignited and quenched states. In contrast, open loop sensitivity is characterized by a single stable steady state. In an ideal packed bed reactor or CSTR, open loop sensitivity is manifested at conditions where small perturbations in operating conditions lead to huge excursions in the single stable reactor temperature. In the ideal CSTR, the operating conditions can be further perturbed to lead to bifurcations in the steady state temperature; thus introducing steady state multiplicity and unstable modes of operation. In an *ideal* tubular reactor, the lack of a mechanism for thermal feedback within the reactor's contents precludes the possibility of multiple steady states. However, in practice, the conduction of heat backward through the tube wall, countercurrent cooling and feed preheating with the effluent, all contribute to thermal feedback and lead to steady state multiplicities in the tubular reactor. From a practical perspective, it is not important whether thermal runaway occurs from high parametric sensitivity or ignition to a new steady state. The overriding concern is tight control of such temperature excursions.

A number of academic studies have demonstrated that multiplicity and open-loop sensitivity in a CSTR are easily handled with simple proportional control action (see

[5] for earliest work in this area). The relatively straightforward design of industrial CSTRs suggests that these theoretical stabilizing properties should also work in practice (with proper mixing, etc.).

In principle, the same stabilization theory can be invoked for a packed bed reactor, and safe closed-loop operation can be attained in a region of open loop sensitivity (see, *e.g.*, [80]). A number of experimental studies have also focused on the stabilizing effects of feedback control in a *single* tube reactor [38], [41], [64], [85]. The interested reader is referred to a comprehensive survey by Jörgensen for additional studies on packed bed reactor control [45]. However, these ideas were never introduced into industrial practice. These theoretical and experimental studies have largely ignored some of the key industrial issues; in particular, the consideration of *multitubular* reactors. Furthermore, industrial control of tubular reactors has focused on the maintenance of cooling jacket temperatures at prescribed steady state values. During transient operation, key variable measurements are often unavailable. In addition, manipulated variables are constrained, thus limiting their effectiveness. These two considerations preclude the possibility of dynamic reactor stabilization.

This brings into question the validity of these theoretical stabilization studies and their relevance to industrial packed bed reactor control. As this article will demonstrate through analysis and simulation, the only recourse for safe reactor operation is strict adherence to design guidelines of the type presented here.

5.2 Tubular Reactor Design Criteria

5.2.1 Radial Temperature Profile

In an exothermic reaction taking place in a tubular reactor, the heat evolved at the center has to be transferred to the wall. If this radial temperature difference, ΔT_r, is too large, the reactions will self-accelerate at the center of the reactor. Consequently, the first design criterion will focus on the permissible size of ΔT_r, and the translation

of this specification into meaningful reactor parameters.

A good measure of the range of acceptable radial temperature difference is given by the parameter:

$$\Theta = \frac{RT_w^2}{E} \tag{5.1}$$

Consider a Taylor series expansion of the temperature profile from the wall to the center of the bed:

$$-\frac{1}{T_{center}} = -\frac{1}{T_w} + \frac{\Delta T_r}{T_w^2} + \cdots \tag{5.2}$$

Then, the reaction rate can be approximated as follows:

$$r = k_0 e^{\frac{-E}{RT}} f(C) \sim k_0 e^{\frac{E}{RT_w}} e^{\frac{\Delta T_r}{\Theta}} f(C) \tag{5.3}$$

From this equation, it is evident that Θ is a scaling parameter for ΔT_r. Furthermore, consider the following Taylor series expansion:

$$e^{\frac{\Delta T_r}{\Theta}} \sim 1 + \frac{\Delta T_r}{\Theta} + (\frac{\Delta T_r}{\Theta})^2 \frac{1}{2!} + \cdots \tag{5.4}$$

A reasonable criterion for avoiding self-acceleration at the reactor center is to require that the $\frac{\Delta T_r}{\Theta}$ term be less than unity. From Equation 5.4, it is clear that this will lead to a reaction rate which increases at most linearly with temperature along the radial direction in the bed. However, this criterion involves the calculation of the radial temperature difference and is therefore limited as a design tool. From a pragmatic viewpoint, we require a criterion which depends on such quantities as the physical dimensions of the reactor, the catalyst properties, and the overall conversion.

We can derive a similar result from engineering insights regarding heat balances in the reactor. In this case, however, the resulting criterion will be more useful for design purposes. Consider the following sources for heat generation (reaction) and

heat removal (convection, conduction) in the reactor:

$$\begin{aligned} \text{Reaction} \quad & r(T)\Delta H \\ \text{Convection} \quad & \frac{GC_p\Delta T}{D} \\ \text{Conduction} \quad & \frac{k_{eff}\Delta T}{D^2} \end{aligned}$$

Clearly, if self-acceleration at the center of the reactor is to be avoided, then the heat produced by the reaction must be quickly removed by convection and conduction (ignoring radiation effects). The ratio of convective forces to conductive forces is given by the Peclet number

$$\text{Pe} = \frac{GC_pD}{k_{eff}} \tag{5.5}$$

which approaches 11 for high flow rates. Consider a small section of the reactor tube in which no mixing occurs. Recall that a Peclet number of 11 implies that for a distance of about 5.5 diameters (or 11 radii), the heat from the center does not reach the wall (*i.e.*, for diffusion across r, the heat is convected across $11r$). Thus, if we consider a bed of length $5.5D$, no heat can reach the wall and operation is adiabatic. Clearly, to avoid acceleration of the reaction rate at the center of the reactor, the adiabatic temperature rise over this unmixed portion of the bed must be small. This problem was considered by Zchlowitch and applied by Pismen [92] to the specific problem of radial temperature uniformity in a tubular reactor. Their resulting criterion is:

$$\frac{1}{\Theta}\frac{\Delta Hr(T_w)D^2}{k_{eff}} < 2 \tag{5.6}$$

Rewriting this as

$$\frac{\Delta T_r}{\Theta}\frac{\Delta Hr(T_w)}{\Delta T_r k_{eff}/D^2} < 2 \tag{5.7}$$

shows that for a fixed ratio of heat produced by reaction to heat removed by diffusion, the Pismen criterion also results in a requirement on the tolerable size of $\frac{\Delta T_r}{\Theta}$.

Let us consider the translation of Equation 5.6 into variables which are more appropriate for reactor design. Using a Peclet number of 11 and inserting the resulting value for k_{eff} obtained from Equation 5.5 yields:

$$\frac{1}{\Theta}\frac{\Delta Hr(T_w)}{C_pG}\frac{11D}{2} < 1 \tag{5.8}$$

Note that $\frac{\Delta Hr(T_w)}{C_pG}$ is the temperature rise per unit length and at all conditions, including the maximum reaction rate, this inequality must be satisfied. Thus, in a simplified form, Equation 5.8 says that the adiabatic temperature rise in a bed of this length should be less than Θ.

Equation 5.8 can be further simplified for preliminary design. If the reactor is approximately isothermal, then basic design principles [31] for a first order reaction lead to:

$$r_{max}(T) = (-\ln(1-x))\frac{G}{L} \tag{5.9}$$

Now consider the adiabatic temperature rise over a distance $\ell = \frac{11D}{2}$ for a first order reaction with conversion x (based on isothermal reaction). The design equation [31] for an adiabatic bed yields:

$$\frac{\ell}{L}k_0\tau = \frac{C_p}{\Delta H}\int_T^{T(\ell)} \frac{e^{\frac{E}{RT}}d\tilde{T}}{(1+\frac{C_p}{\Delta H}T) - \frac{C_p}{\Delta H}\tilde{T}} \tag{5.10}$$

Assuming that $\frac{D}{L}$ is very small ($\frac{\ell}{L} << 1$), and thus the temperature rise $T(\ell) - T$ is small, we can approximate the integral as follows:

$$\frac{\ell}{L}k_0\tau \cong \frac{C_p}{\Delta H}e^{\frac{E}{RT}}(T(\ell)-T) \equiv \frac{C_p}{\Delta H}e^{\frac{E}{RT}}\Delta T_{ad}(\ell) \tag{5.11}$$

The adiabatic temperature rise over the full length of the reactor (for a conversion of

x) is given by:

$$\Delta T_{ad}(x) = \frac{x\Delta H}{C_p} \tag{5.12}$$

Therefore

$$\frac{\Delta T_{ad}(\ell = \frac{11D}{2})}{\Delta T_{ad}(x)} = -\frac{11D}{2L}\frac{\ln(1-x)}{x} \tag{5.13}$$

and the temperature gradient is given by:

$$\frac{\Delta T_{ad}(\ell = \frac{11D}{2})}{\frac{11D}{2}} = -\frac{\Delta T_{ad}(x)}{L}\frac{\ln(1-x)}{x} \tag{5.14}$$

This maximum temperature gradient is substituted for $\frac{\Delta H_r}{C_p G}$ in Equation 5.8 to yield the final result

$$-\frac{1}{\Theta}\frac{\Delta T_{ad}}{L}\frac{\ln(1-x)}{x}\frac{11D}{2} < 1 \tag{5.15}$$

or

$$\frac{L}{D} > 5.5\frac{\Delta T_{ad}}{\Theta}\left[\frac{-\ln(1-x)}{x}\right] \tag{5.16}$$

where ΔT_{ad} is the temperature rise of the total feed at conversion x. To be safe, one might want to start with an $\frac{L}{D}$ at least twice as large as the term on the right side. Note that the radial temperature criterion resulted in a requirement for a minimum $\frac{L}{D}$ which is independent of space velocity and catalyst activity. It is just a function of conversion and:

$$\frac{\Delta T_{ad}}{\Theta} = \frac{\Delta T E}{R T_w^2} \tag{5.17}$$

Up to this point it was assumed that the reactions taking place in the reactor are irreversible. We can modify this for reversible reactions if we know the maximum reaction rate. For a first order reversible reaction, we can simply substitute $-\ln(1-\frac{x}{x_e})$ for $-\ln(1-x)$. In a second order irreversible reaction we get

$$\frac{L}{D} > \frac{5.5\Delta T_{ad}}{\Theta}\frac{1}{1-x} \tag{5.18}$$

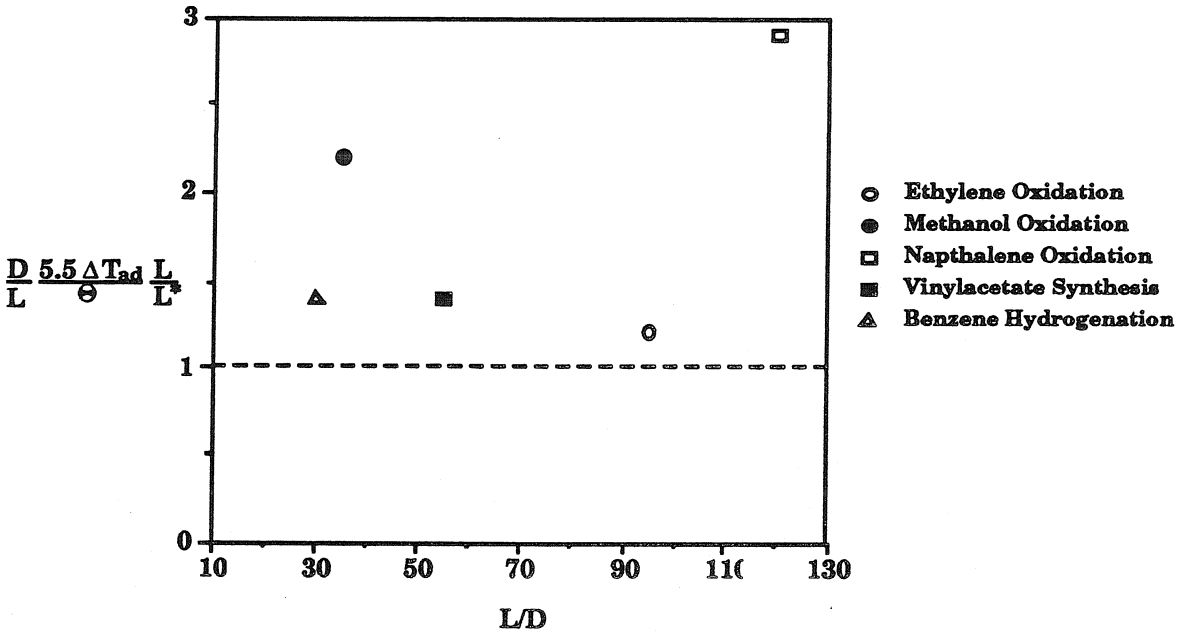

Figure 5.1. Verification of Radial Temperature Criterion

where again x is the fraction of reactant converted and ΔT_{ad} is the adiabatic temperature rise of the total feed at conversion x. For reversible reactions or any more complex reaction expression, Equation 5.18 becomes:

$$\frac{L}{D} > \frac{5.5\Delta T_{ad}}{\Theta}\frac{L}{L^*} \tag{5.19}$$

where $\frac{L^*}{L}$ is the normalized length of the reactor required to obtain the conversion in an isothermal reactor if the reaction rate would be at the maximum rate throughout the reactor. For practical considerations, this parameter can be measured on a microreactor or a small pilot plant.

In Figure 5.1 are plotted values for the quantity $\frac{D}{L}\frac{5.5\Delta T_{ad}}{\Theta}\frac{L}{L^*}$ versus the $\frac{L}{D}$ ratio for typical industrial reactor data [40]. The criterion in Equation 5.19 dictates that $\frac{D}{L}\frac{5.5\Delta T_{ad}}{\Theta}\frac{L}{L^*}$ should be less than 1 which is clearly violated for these reactors. A less restrictive condition on the radial temperature profile will be derived in the following section on parametric sensitivity.

5.2.2 Parametric Sensitivity

Barkelew [7] and others have formulated criteria for the temperature sensitivity of packed bed reactors to changes in operating conditions or physical parameters. However, these criteria are in terms of mathematical differential sensitivities which offer little insight for a practical design engineer. Using engineering judgement, we will show that these criteria can be reduced to a very simple form involving practical design parameters.

In order to transfer the heat through the wall, a driving force close to the inside of the wall is required. When the reaction rate changes, the temperature close to the wall has to rise to compensate for the higher heat transfer required. Exercising good engineering judgement, we require that the temperature difference $T - T_w$ is small compared to Θ. Again, referring back to Equations 5.2, 5.3, and 5.4, this is understood as requiring the reaction rate to accelerate at most linearly along the radial direction. In terms of the "forces" involved, we know that in a well-mixed reactor, the rate of heat generation is balanced by the rate of heat removed by cooling through the wall:

$$h_v(T - T_w) = r\Delta H \tag{5.20}$$

Thus our requirement becomes:

$$\frac{T - T_w}{\Theta} = \frac{r\Delta H}{h_v\Theta} < 1 \tag{5.21}$$

Substituting for the heat transfer coefficient (normalized to unit volume)

$$h_v = \frac{h\pi D}{\pi\frac{D^2}{4}} = \frac{4h}{D} \tag{5.22}$$

and using the relationship in Equations 5.9 and 5.12

$$r_{max}(T)\Delta H = GC_p\frac{\Delta T_{ad}}{L}[-\ln(1-x)] \tag{5.23}$$

we get

$$\frac{\frac{GC_p\Delta T_{ad}}{L}[-\ln(1-x)]}{\frac{4h}{D}\Theta} < 1 \tag{5.24}$$

where ΔT_{ad} is the adiabatic temperature rise for the complete feed at full conversion. As before, we can substitute $\frac{x}{1-x}$ for the quantity in brackets for a second order reaction. This equation can be interpreted as a limit on the reactor diameter

$$D < D_{max} = \frac{4}{v_s[-\ln(1-x)]}\frac{h\Theta}{C_p\Delta T_{ad}} \tag{5.25}$$

where v_s is the space velocity.

Compare this with the approach used by Barkelew. In his notation, the sensitivity criterion is given by

$$\frac{SC_pc_0k_0}{h_ve^{\frac{E}{RT_w}}} < \frac{1}{\Phi(S)} \tag{5.26}$$

where $\Phi(S)$ is given in Figure 5.2 and

$$S = \frac{\Delta HE}{C_pRT_w^2} \tag{5.27}$$

For large S, $\Phi(S)$ approaches a constant value of 2.5. In our notation, $S = \frac{\Delta T_{ad}}{\Theta}$ and $c_0k_0e^{\frac{-E}{RT_w}}$ is simply $r(T_w)$. Thus, Barkelew's criterion (5.26) becomes:

$$\frac{r(T_w)\Delta H}{h_v\Theta} < \frac{1}{\Phi(S)} \tag{5.28}$$

Following the same manipulations as before, the final design criterion can be expressed

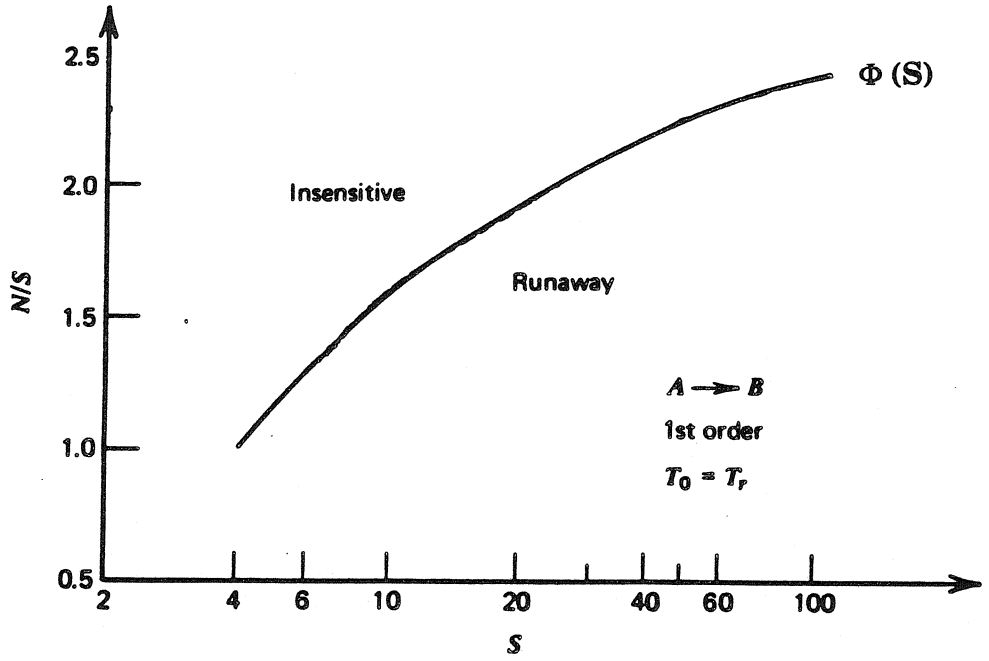

Figure 5.2. Barkelew's Sensitivity Criterion (from Froment and Bischoff, 1979)

as a maximum diameter for the tube:

$$D < D_{max} = \frac{1}{\Phi\left(\frac{\Delta T_{ad}}{\Theta}\right)} \frac{4}{v_s[-\ln(1-x)]} \frac{h\Theta}{C_p \Delta T_{ad}} \tag{5.29}$$

$\Phi(S)$ can be taken from Figure 5.2 and it changes from 1 to 2.5.

This result is very similar to our earlier result (Equation 5.25), which was based upon simple engineering rules of thumb. However, for large values of $\Phi(S)$, Equation 5.29 is more stringent than Equation 5.25. This result should be made more conservative by introducing a safety coefficient as we do not know our parameters very accurately and they may change during operation. A safety factor of 2 is rea-

sonable for both cases (*i.e.*, $D = 0.5D_{max}$).

Instead of a look-up table approach to solving for $\Phi(S)$, it is possible to actually calculate an explicit value from the following correlation proposed in [68]

$$\Phi = 2.718\Gamma\left[1 - \left(\frac{S_0}{S}\right)^{\frac{2}{3}}\right] \tag{5.30}$$

where Γ is an empirical parameter given by

$$\Gamma = \frac{8.7}{7.66 + n^{0.6}} \tag{5.31}$$

and for n (reaction order) equal to 1, the expression for S_0 is:

$$S_0 = \frac{4\gamma}{\gamma - 4} \tag{5.32}$$

where γ is the dimensionless activation energy, $\frac{E}{RT_w}$. The advantage of such an approach is clear; one can trivially rederive the critical $\Phi(S)$ curve for different reaction orders, feed temperatures, and activation energies. The correlation can be readily incorporated into Equation 5.29 and thus eliminate the use of Figure 5.2.

The accuracy of the two approaches (Barkelew's look-up table and the correlation in Equation 5.30) are examined against experimental data in the literature for vinyl-acetate synthesis [30] and from a university methanation reactor [90]. In Figure 5.3, we plot $\frac{D}{D_{max}}$ versus $\frac{\Delta T_{ad}}{\Theta}$, where D_{max} is taken from Equation 5.29. Four sets of data are plotted in the diagram:

- One datum point for the Caltech methanation reactor, not parametrically sensitive.
- Data for Emig's vinyl-acetate synthesis reactor, which displayed temperature sensitivity.

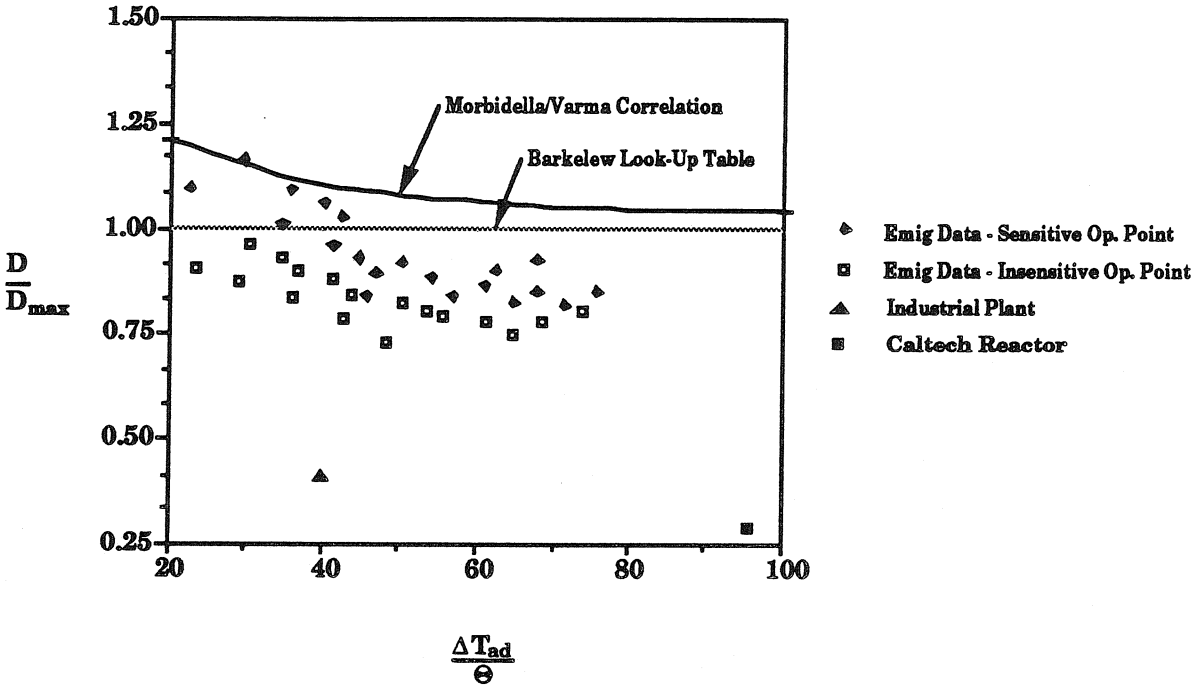

Figure 5.3. Verification of Sensitivity Criterion

- Data for Emig's vinyl-acetate synthesis reactor, which did not display temperature sensitivity.
- One datum point for an industrial vinyl-acetate synthesis reactor, not parametrically sensitive.

In addition, two loci are shown:

- The design criterion in Equation 5.29 using Barkelew's look-up for Φ.
- The design criterion in Equation 5.29 using the Morbidelli/Varma correlation in Equation 5.30 for Φ.

It can be seen that the agreement is quite good between the predicted regions for temperature sensitivity and the experimental data. The agreement for the Φ correlation from Equation 5.30 is better qualitatively than the one based upon Barkelew's look-up for Φ, although the former is slightly more conservative. The quantitative

error could be attributed to the fact that the true order for the vinyl-acetate synthesis has been reported to lie between zero and one. The utility of the correlation in Equation 5.30 is that such changes in reaction order (or activation energy or inlet temperature) can be readily incorporated in the computation of Φ. As before, a safety factor of 2 should be incorporated ($D = 0.5D_{max}$).

Finally, it should be pointed out that both the Caltech methanation reactor and the industrial reactor have been properly designed (or even overdesigned) and exhibit no temperature sensitivity.

More involved calculations are possible for $\Phi(S)$, depending on the desired complexity. For instance, the same criterion (Equation 5.29) can be used with a Φ which has been modified to incorporate particle effects. The resulting criterion can be used as in [70] to predict the occurrence of multiple steady states in the reactor. The drawback of this latter approach is that it is more computationally intensive than even the Barkelew calculations.

The criterion in Equation 5.29 has been derived by assuming a simple homogeneous model with only axial heat conduction. A mean heat transfer coefficient can be calculated for such a model by considering the sum of the resistances to heat transfer in the bed and at the wall (as in [31])

$$\frac{1}{h_{eff}} = \frac{1}{h_w} + \frac{D}{8k_e} \tag{5.33}$$

where k_e is the radial conductivity and a quadratic temperature profile has been assumed. The critical assumption in one-dimensional models for parametric sensitivity calculations is that the first term on the right hand side in the Equation 5.33 is larger than the second term. In other words, one assumes that the jacket effects are larger than radial conduction effects

$$\frac{h_w D}{2k_e} = Bi < 4 \tag{5.34}$$

where Bi is the dimensionless Biot number. Let us compare this result to our earlier criterion for a uniform radial temperature profile (Equation 5.6). Taking the ratio of the criterion given in Equation 5.6 to the sensitivity criterion given in Equation 5.26 gives a "modified" Biot number:

$$\left(\frac{\Delta Hr(T_w)}{\frac{2K_{eff}}{D^2}\Theta}\right)\left(\frac{\frac{4hD}{\Phi}\Theta}{\Delta Hr(T_w)}\right) = \frac{4h}{\Phi}\frac{D}{2k_{eff}} = \frac{4Bi}{\Phi} \tag{5.35}$$

We can interpret this equation in the following manner. Since $\Phi \sim 2$, then for $Bi <\sim 0.5$, the second criterion (Equation 5.28) implies the first (Equation 5.6). In other words, the first criterion is about an order of magnitude more conservative than the assumption given in Equation 5.34. This is easily understood since in the radial temperature criterion we require a *flat* radial temperature profile. But for the one-dimensional model used in the sensitivity criterion, we assume a mild parabolic profile and only require the Biot number to be less than 4.

Some typical values for the Biot number are plotted in Figure 5.4 for several typical industrial reactors [40] as well an academic laboratory reactor [30]. It is clear that the radial profiles are fairly mild for the presented industrial data. However, in the case of the data from Emig [30] in which they were attempting to induce parametric sensitivity, the radial profiles were very steep and suggest that radial effects play a significant role in the critically stable behavior observed in this case.

In light of these observations, we recommend that the requirement on the Biot number (< 4) serve as a verification that the parametric sensitivity analysis is correct. Violation of this specification suggests the need for a more involved sensitivity criterion which incorporates radial effects.

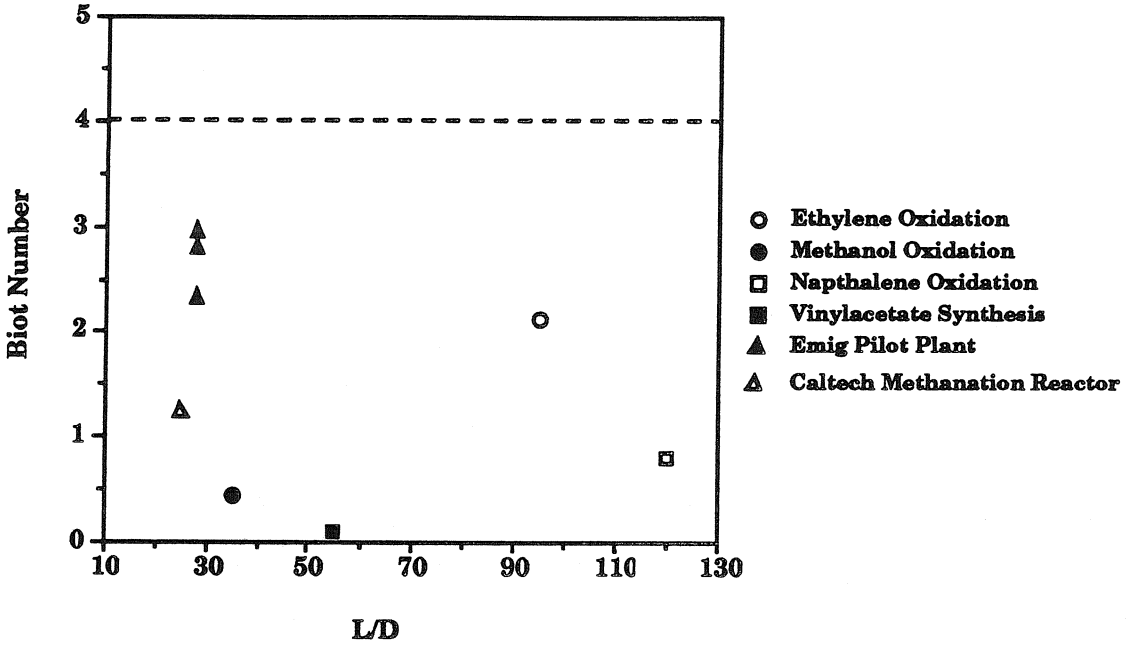

Figure 5.4. Verification of Biot Number Specification

5.2.3 Practical Considerations

Equations 5.16 and 5.29 give a reasonable first estimate for the physical dimensions of the reactor in terms of the parameters which are convenient for design purposes. The scaling parameter Θ depends on the activation energy and is thus determined by the nature of the reaction and the catalyst. The parameters which can be adjusted include ΔT_{ad}, v_s, L, and D. ΔT_{ad} can be lowered by adding a diluent to the feed. v_s is normally adjusted in coordination with the catalyst activity. If the activity is lowered, the maximum reaction rate is lowered which leads to a higher residence time in the reactor. The original conversion can be maintained by lowering v_s.

In terms of the diameter of the reactor, Equations 5.16 and 5.29 indicate that a smaller diameter yields better thermal stability in the bed. However, from an economic perspective, it is cheaper to produce tubes with larger diameters. Economic considerations also favor lower dilution rates and higher space velocities. Therefore, solving for an economically optimal set of conditions which also satisfy Equations 5.16

and 5.29 requires an iterative procedure. For instance, for fixed D, a reduction in v_s is traded off (via Equation 5.29) against less diluent and a higher ΔT_{ad}. Similarly, for fixed ΔT_{ad}, a reduction in v_s is traded off (via Equation 5.16) against a larger tube diameter and (via Equation 5.29) a longer reactor.

In the preceding analysis, it has been assumed that there is no recycle or dilution; however, it is straightforward to account for these effects. If the recycle is unconverted material, then it has no impact on Equations 5.16 and 5.29 as long as we remember that v_s is based on total feed to the reactor. v_s is often given in terms of fresh feed only, which is designated as v_{s0}. In this case, v_s has to be adjusted accordingly

$$v_s = v_{s0}(1 + R) \tag{5.36}$$

where R is mass recycle per mass feed. If the recycle contains a diluent, then this affects ΔT_{ad}. This requires iteration, but it is straightforward as long as we always use ΔT_{ad} and v_s based on total feed in Equations 5.16 and 5.29.

There are some practical considerations for choosing L and D. Normally, the smallest tube diameter for large scale reactors is one inch. Smaller diameters would be prohibitively expensive. There are also limitations placed on L by both shipping and transportation as well as the physical support of the tubes in the reactor. In addition, the tolerable pressure drop across the reactor limits the acceptable length (this will be discussed in the next section). On the other hand, it is seldom economical to have a tube length smaller than 40 feet, unless the catalyst volume required is very small. A larger L will give a larger maximum tube diameter and fewer tubes. For very large reactors, one can achieve this by connecting two reactors in series.

There is another aspect of the sensitivity criteria which is often overlooked. The criteria in the previous section relate to fixed operating conditions. In practice we have two deviations related to flow variations and maldistributions.

First, operating conditions rarely remain fixed at their designed settings. A reactor has to be able to operate at lower flow rates or throughputs than originally designed for. It will also be operated at higher throughputs, but there is often objection to provide for this in the design. An experienced designer does so but hides it in safety coefficients.

Second, the flow rates vary from tube to tube. We therefore have to look at the effect of variations in throughput on our criteria. If the reaction is not mass transfer controlled, r_{max} is independent of linear velocity and only depends on inlet composition and reactor temperature. Flow rate will impact the heat transfer coefficient in Equation 5.29 and the value of the mass flow rate G in Equation 5.8. In both cases, thermal sensitivity is reduced by increasing the flow rate. Therefore, the criteria must be evaluated at the lower bound on flow rates through the tubes. In this respect, Equation 5.8 is more sensitive than 5.29, as the criterion in Equation 5.8 is inversely proportional to flow rate, whereas in Equation 5.29, it is inversely proportional to a fractional power of the flow rate (typically $h_v = h_{v0}G^{\lambda}$ where $\lambda = 0.5-0.8$). If the criteria are conservative enough, they will protect against thermal sensitivity arising from flow variations.

In general, if the throughput is reduced, r_{max} should be reduced accordingly.

5.2.4 Acceptable Pressure Drop

The foregoing calculations are only concerned with the stability of the reactor and its sensitivity to disturbances. There is another important consideration, namely limiting the pressure drop to an acceptable limit.

For turbulent flow, which is a reasonable assumption for most tubular reactors, the total pressure drop is given by the Ergun Equation [31]

$$\Delta P = L\frac{\alpha}{D_p}\frac{G^2}{\rho} = \frac{v_s^2 L^3}{\rho}\frac{\alpha}{D_p} \tag{5.37}$$

where the friction factor, α, is equal to:

$$\alpha = \frac{(1-\varepsilon)}{\varepsilon^3}\left[\frac{150(1-\varepsilon)}{Re_p} + 1.75\right] \tag{5.38}$$

α can be directly measured in a pilot plant and experimental values are preferred.

The friction factor correlation in Equation 5.38 holds for spherical catalyst particles.

5.2.5 Summary

Summarizing the results of the previous sections, we have the following specifications on the reactor dimensions:

$$L > L_{min} = 5.5D\frac{\Delta T_{ad}}{\Theta}\left[\frac{-\ln(1-x)}{x}\right] \tag{5.39}$$

$$D < D_{max} = \frac{1}{\Phi\left(\frac{\Delta T_{ad}}{\Theta}\right)}\frac{4}{v_s[-\ln(1-x)]}\frac{h\Theta}{C_p\Delta T_{ad}} \tag{5.40}$$

$$L < L_{max} = \sqrt[3]{\frac{\Delta P_{max}\rho D_p}{\alpha v_s^2}} \tag{5.41}$$

The assumptions used in the derivation of these guidelines are as follows:

$$Pe = 11$$

First Order, Irreversible, Isothermal Reaction

$$\frac{L}{D} >> 1$$

Spherical Catalyst Pellets

Let us now look at the potential conflicts between these equations. Consider an undiluted feed and fixed conversion. This fixes ΔT_{ad} and we get $\frac{L}{D}$ from Equation 5.39. Turning to Equation 5.40, we can adjust v_s to get an acceptable diameter. These two results yield a reactor length, which can be verified against the acceptable pressure drop in Equation 5.41. If at the desired condition, both Equations 5.39 and 5.41 give satisfactory answers, then there is no problem. If either L or ΔP are not acceptable, we have to continue our iteration as long as Equation 5.39 conflicts with Equation 5.41.

Note that we have a separate criterion for L_{min} and for L_{max}. Each of these contain both independent and joint parameters. Since L_{min} increases with D, and L_{max} is independent of D, we can change their ratio by adjusting D. A reasonable guideline requires that L_{max} exceed L_{min} by a factor of 2. Otherwise, we have to modify other parameters. These modifications invariably affect the cost. For example, we can reduce L_{min} by lowering x (equivalently, reducing $\frac{L}{L^*}$). This is achieved at the expense of heat losses in recycling the unconverted feed.

Another way to modify the conditions is by diluting the inlet stream or by recycling the product stream. Assume we do it by keeping partial pressure constant. If the amount of diluent added per gram fresh feed is R, and C_p is constant, then:

$$\Delta T_{ad} = \frac{\Delta T_{ad}(0)}{1+R} \tag{5.42}$$

L_{min} in Equation 5.39 will decrease in proportion to $1+R$, but D_{max} in Equation 5.40 will not be affected as $\Delta T_{ad} v_s$ is independent of $1+R$. If we increase the pressure to keep partial pressure constant, then criterion 5.41 has the following dependence on R

$$\frac{\rho}{v_s^2} = \frac{\rho_0(1+R)}{v_{s0}^2(1+R)^2} \tag{5.43}$$

and L_{max} is proportional to $\frac{1}{\sqrt[3]{1+R}}$. If we keep total pressure constant

$$\frac{\rho}{v_s^2} = \frac{\rho_0}{v_{s0}^2(1+R)^2} \tag{5.44}$$

and L_{max} is proportional to $\frac{1}{\sqrt[3]{(1+R)^2}}$.

Therefore, increasing R with a recycle unit will improve the design feasibility by increasing the ratio of L_{max} to L_{min}.

In many cases, the pressure drop for a reactor of 40 feet or even 60 feet is acceptable. Thus, the pressure drop constraint applies only to reactors with very high flow rates, such as in the case of high recycle rates. Another situation in which these constraints apply is the case where the reactor is large enough that there is an economic incentive to go to larger tube diameters and build multiple reactors in series.

There are options to reduce pressure drop by choosing catalyst shapes with inherently lower pressure drops [31]. Equation 5.38 gives the friction factor for spherical catalyst particles. It is possible to select a differently shaped particle with better pressure drop properties but with nearly equivalent thermal properties (*e.g.*, ring shaped catalyst pellets).

We should also note that the care one has to apply to keep the reactor temperature uniform varies from case to case (*i.e.*, the penalty for large temperature excursions is different for each case). Higher temperatures may deactivate the catalyst, may cause side reactions, and may cause metallurgical problems. But in most cases it is advisable to look for conditions where temperature variations are small. This is discussed in more detail in [27], [28], and [29].

At last we should point out that, in the vast majority of cases, the design modifications required to achieve a very robust design with modest data are not expensive. Building a longer reactor (within the limits mentioned) has typically a very small impact on cost. If one has to severely limit productivity, this is an obvious penalty.

But in the experience of one of the authors (Reuel Shinnar), this happens because the designer has not fully taken into account all the measures that ensure robust performance.

5.3 Control Issues for Tubular Reactor Design

The sensitivity criterion (Equation 5.29) described in section 5.2.2 is appropriate for open-loop reactor operations. However, the application of a control law will in general significantly alter the dynamic properties of the system. This is the case for a simple CSTR in which open-loop bifurcations and pathologies are effectively eliminated by simple proportional control [5]. Similarly, theoretical studies suggest that accurate nonlinear model-based control can lead to safe operation near regions of parametric sensitivity [80]. However, as we will see in this section, there are certain complicating features of an industrial packed bed reactor which do not allow even an advanced control scheme to eradicate the sensitive open-loop behavior. We will focus on the particular control problems which arise when we try to operate the reactor near the critical values given in the design criteria.

Controlled operation of a multitubular packed bed reactor is complicated by the temporal and spatial variations inherent in a distributed parameter system. Additional difficulty is caused by flow variations between individual tubes. The combination of these effects pose a formidable task in the placement of sensors for measuring reactor conditions. An additional complication in control design is introduced by the presence of large, and often uncertain, time delays in the system.

These effects are considered in more detail in the subsequent analysis. In particular, their impact upon the proposed design criteria is investigated. In the final sections, a reduced order nonlinear model of a tubular reactor is presented for simulation purposes. The resultant case studies demonstrate the controllability problems which can arise when the reactor design criteria are violated.

5.3.1 Multitube Flow Variations

The flow dynamics of a multitubular reactor will, in general, be quite complicated. However, it is reasonably straightforward to show that maldistributions in the bulk feed flow can cause significant variations in the flow rates between the various tubes. In addition, it is likely that the packing in the tubes will be far from homogeneous, leading to varying resistances to flow in the individual tubes. A value of 30% has been reported in the literature recently [65], and will be used in the subsequent analysis to predict the peak variation from tube to tube. In some cases, all tubes are individually tested after filling, which can reduce variability of flow to ±10%.

Consider again the second criterion (Equation 5.29) for temperature sensitivity given in section 5.2.2. In the sensitivity diagram given in Figure 5.2, the ordinate $(\frac{N}{S})$ depends on the flow rate via the heat transfer coefficient between the wall and the bed (Equation 5.28). A reasonable empirical correlation (for high Re) is given by [93]:

$$h = Pr_f^{\frac{2}{3}} C_{pb} \left(\frac{1}{a\mu_f \psi} \right)^{(-0.41)} G^{0.59} \tag{5.45}$$

This expression gives a 0.59 power law dependence of h on flow rate (G). Consequently, flow variations in the tubes on the order of 30% will give rise to $\frac{N}{S}$ values which differ by as much as 16%. From Figure 5.2, it is clear that if our margin of safety in the reactor design is less than 16% of $\frac{N}{S}$, this flow perturbation will lead to a crossing of the sensitivity curve $(\Phi(S))$. Consequently, if the bulk of the tubes are at a higher flow rate (large $\frac{N}{S}$) and lower temperature, then the tubes with restricted flow (small $\frac{N}{S}$) may "ignite" and undergo thermal runaway.

The effect of this change in flow rate on the hot spot temperature is depicted in Figure 5.5. Plotted here are the values of the hot spot temperature for a condition of high parametric sensitivity [88]. The particular values of the physical parameters used here will be introduced with the closed loop simulations in section 5.4 (specifically

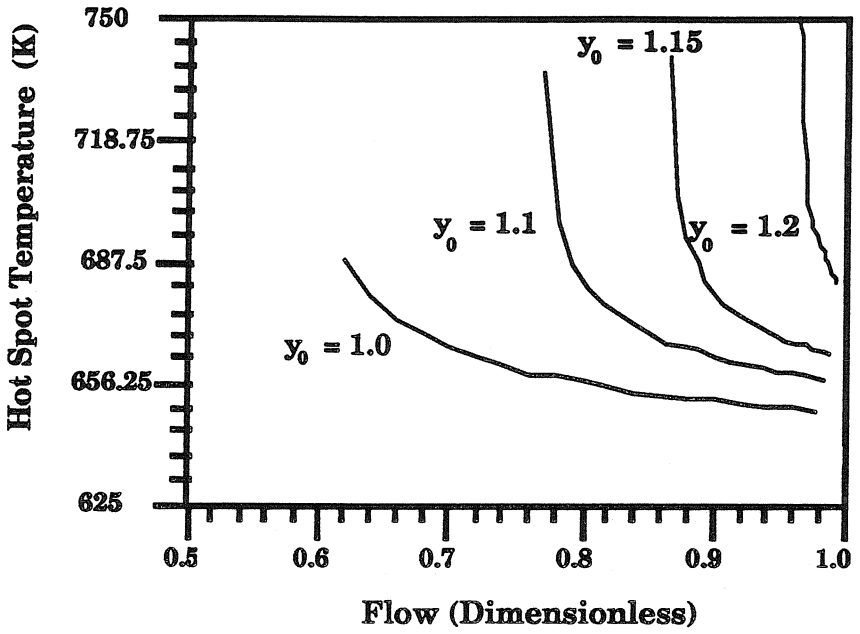

Figure 5.5. Steady State Dependence of Hot Spot Temperature on Flow Rate and Inlet Concentration (y_0)

in Table 5.3). It can be seen in the diagram, that as the flow rate is reduced, there is poorer heat transfer and, consequently, the hot spot temperature increases. The condition in Figure 5.5 corresponding to an extremely steep slope (for fixed inlet concentration and flow rate) corresponds to a point along the sensitivity curve in Figure 5.2 (incipient runaway). As expected, higher inlet concentration (y_0) leads to greater sensitivity as the reaction rate accelerates.

5.3.2 Measurement Set

For practical reasons, it is often necessary to use secondary measurements in the control of a tubular packed bed reactor to improve the performance of the system. For instance, temperature sensors located axially along the reactor can be used to "infer" the values of the other reactor variables. For multitubular reactors, one is not only concerned with a reasonable number of accurate measurements along the length of the tube, but one must collect measurements from enough tubes to assure

an accurate measurement of the true bulk temperature. There will be between 1000 to 5000 tubes in a multitubular reactor [31], but for control purposes, we want our measurement set to be much smaller. The practical implications are immediately clear: it will be impossible to monitor every tube in the reactor bundle. As was indicated earlier, this can be very dangerous when one operates near the cutoffs given for parametric sensitivity. There may be a few tubes which are not measured, have reduced flow rates, and consequently, ignite without being observed. Even if a measurement is made of a bulk property, such as the effluent temperature of the tubes, the diluted effect of the ignited behavior may still go unnoticed.

5.3.3 Nonminimum Phase Characteristics

An additional problem in packed bed reactor control is the presence of large, often poorly characterized, time delays in the system. Their causes include propagation rates in the bed, finite time required for actuator movement, and lags in measurement devices (*e.g.*, composition analyzers). The presence of these time delays will have a detrimental impact on the closed loop performance. As will be demonstrated in the subsequent case studies, there is a *dynamic sensitivity* associated with operation in regions of high parametric sensitivity. This also places certain limitations on the achievable performance of multitubular reactors operating in these regions. The combined effect of these two limitations can lead to unacceptable closed-loop behavior, such as large temperature transients.

Additional nonminimum phase (NMP) characteristics are associated with certain choices of the manipulated variable for reactor control. These include the inlet flow rate and inlet temperature. The selection of these variables for control inputs leads to right half plane zeros which are manifested in inverse-response behavior. This places severe limitations on the achievable system performance. It also precludes the application of advanced nonlinear techniques like input/output feedback linearization

[54]. In the subsequent case studies, the performance of a flow controlled reactor (NMP) and a jacket temperature controlled reactor (MP) will be investigated for conditions of both high and low parametric sensitivity.

5.4 Case Studies

5.4.1 Nonlinear Reduced Order Model

For simulation purposes, a simple pseudohomogeneous model is employed where all heat and mass transfer resistances between fluid and catalyst phase are neglected. In dimensionless form (see Table 5.1), the mass and heat balances are given by

$$\frac{\partial y}{\partial t'} + \frac{\partial y}{\partial z} = -\mathcal{D}a\, r(x,y) \tag{5.46}$$

$$\frac{\partial x}{\partial t'} + \frac{\partial x}{\partial z} = \mathrm{B}(x - x_w) - qDa\, r(x,y) \tag{5.47}$$

$$y(0,t) = y_0 \quad x(0,t) = x_0 \quad \left(\frac{\partial x}{\partial z}\right)_{z=1} = 0 \tag{5.48}$$

where x is the dimensionless temperature and y is the dimensionless concentration.

In developing a low-order model for this system, it is of critical importance to retain the *essential* nonlinear dynamics. By this, we refer to the relevant dynamics which accurately and succinctly reflect the stability of the reactor and the relationship between the control inputs, outputs, and the reactor's dynamic states. In this manner, a control algorithm based upon this model will provide suitable closed-loop performance. The approach adopted in this work is a treatment of transport mechanisms in the reactor as a nonlinear wave which propagates up and down the bed in response to changes in the operating conditions. The model will be summarized briefly here; the interested reader is referred to [22] for the full details of the model derivation.

Table 5.1 Dimensionless Variables for Reactor Model

y	$\frac{c}{c_{ref}}$
x	$\frac{T}{T_{ref}}$
x_w	$\frac{T_w}{T_{ref}}$
t'	$\frac{t}{t_{ref}}$
c_{ref}	c_0
T_{ref}	T_0
t_{ref}	$\frac{L}{u}\frac{(\rho C_p)^*}{(\rho C_p)}$
$\mathcal{D}a$	$\frac{Lk_0(1-\epsilon)}{u}$
$\mathbf{B}$	$\frac{4hL}{u\rho C_p D}\left(\frac{F}{F_0}\right)^{\lambda}$
q	$\frac{-\Delta H c_0}{\rho C_p T_{ref}}$
γ	$\frac{E}{RT_{ref}}$

The reactor bed is divided into two zones: an ignition zone and a reaction zone. Processes in the ignition zone are assumed to occur instantaneously compared to the relatively slower reaction zone. The front between these two zones propagates in response to changes in various reactor conditions. The dynamics of the front are considered to be the *essential* nonlinear dynamics of a packed bed reactor operating near ignition. The position of this wavefront is determined by a critical energy balance. Specifically, this condition requires that the heat removal line for the ignition zone is tangent to the heat production curve. Consequently, this zone is always at the "edge" of ignition.

This treatment leads to a simple second-order nonlinear model for the bed dynamics. The two states are the filtered input and the wavefront position. The former is a fast lag applied to the true manipulated variable, and the latter equation is given by the critical stability condition. Various choices are possible for the single manipulated variable: inlet concentration, inlet temperature, jacket temperature, and inlet flow rate. In the following case studies, we consider closed loop operation of a reactor

Table 5.2 Reactor Reduced Model Variables	
x_1	Filtered Input
x_2	Ignition Position
u	Manipulated Variable (Flow or Jacket Temperature)
y	Hot Spot Temperature
w	Wave Propagation Velocity
τ	Lag on Input

with flow manipulation, and separately, with jacket temperature manipulation. The logical choice for a controlled output is the peak temperature along the axial profile, the so-called hot spot temperature. As discussed earlier, this will minimize unwanted side reactions and catalyst deactivation which result from thermal runaway. The resultant SISO model structure is:

$$\begin{aligned} \tau \dot{x_1} &= -x_1 + u \\ \dot{x_2} &= w(x_1, x_2) \\ y &= h(x_1, x_2) \end{aligned} \tag{5.49}$$

The meaning of these variables is summarized in Table 5.2.

The numerical computations involve iterating on the ignition position until the critical energy balance is satisfied at a given time interval. In order to accomplish the energy calculations, it is necessary to perform an integration of the axial temperature profile. Once the ignition position has been determined, the wavefront velocity is calculated from the change in ignition position from the previous time interval.

5.4.2 Simulations

For the next four case studies, a set of operating conditions is selected which violated the proposed sensitivity criterion (Equation 5.29). In particular, the diameter

Table 5.3 Physical Parameters for Sensitive Simulations	
$\mathcal{D}a$	$7.059E8$
B	11.38
q	1.0
γ	21.82
λ	0.5
$r(x,y)$	$ye^{-\gamma/x}$

exceeded the recommended value (Equation 5.40) by 50% ($D = 1.5D_{max}$). In this manner, we will investigate the control problems associated with a parametrically sensitive packed bed. The particular choices of physical parameters are shown in Table 5.3; they correspond to parametrically sensitive behavior as studied in [88]. Note that the reaction under consideration has an irreversible first order rate law and is exothermic.

Case Study #1 (Steady State Sensitivity, Nonminimum Phase System)

The first phenomenon studied is the effect of multitubular flow variations. As was described earlier, flow rates from tube to tube will vary by as much as 30%. These variations affect the sensitivity through a power law dependence in the heat transfer coefficient. For this study, a nominal value of 0.5 is chosen for this coefficient.

In Figures 5.6 and 5.7 are shown the responses of the hot spot temperature for two reactor tubes to a step change in the set point of the bulk hot spot temperature. The particular simulation conditions are shown in Table 5.4. Note that the second tube has a restricted flow and has a throughput which is 8% lower than the first tube. The temperature in tube #1 is used as a measurement for a PI controller in an effort to control the hot spot temperature in the bed. This is accomplished by manipulating the bulk flow rate through the tubes. The control parameters ($K_p = 0.5$, $\tau_I = 0.05$) are selected for a reasonable speed of response. As the figures show, tube

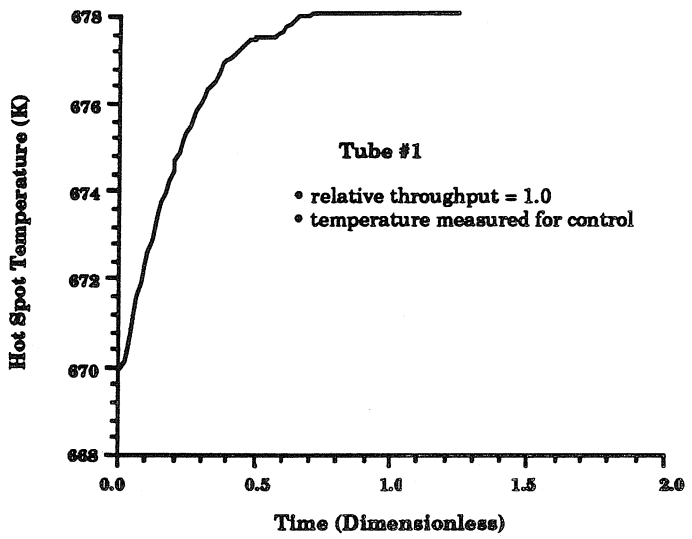

Figure 5.6. Closed-Loop Response (Case Study #1, Set Point Change, u= Flow Rate)

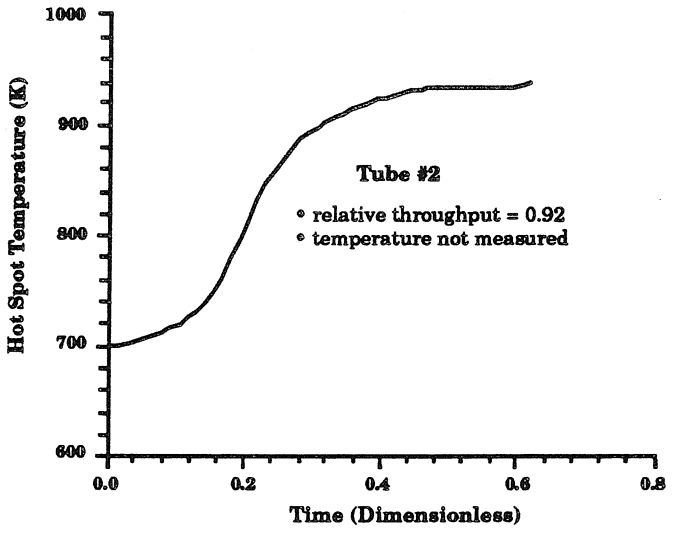

Figure 5.7. Closed-Loop Response (Case Study #1, Set Point Change, u= Flow Rate)

Table 5.4 Simulation Conditions (Case Study #1)		
Inlet Concentration (y_0)	1.1	
Flow Rate ($\frac{F}{F_0}$)	0.85	
Inlet Temperature (x_0)	1.00	
Jacket Temperature (x_w)	1.00	
Manipulated Variable (u)	Flow Rate	
Controlled Variable (y)	Hot Spot Temperature	
Disturbance	None	
Set Point Change	$8K$	
	Tube #1	Tube #2
Relative Throughput	1.0	0.92

#1 behaves as expected with an overdamped second-order response while tube #2 "ignites," reaching temperatures in excess of 900 K. It is clear that the restricted flow through the second tube leads to an unreasonably large excursion in the hot spot temperature. Using the information in Table 5.4 and Figure 5.5, it can be seen that the new steady state position of the second tube is in a region of ignition. Thus, we observe a *steady state sensitivity* with respect to operating conditions.

Note that the behavior depicted in Figures 5.6 and 5.7 is independent of the controller parameters. In fact, the response is independent of the controller employed (nonlinear, IMC, etc.) and all closed loop systems will exhibit the same steady state sensitivity for these simulation conditions.

Case Study #2 (Dynamic Sensitivity, Nonminimum Phase System)

Further insights are gained if a controlled response to a disturbance in inlet concentration is investigated. The simulation conditions for this example are displayed in Table 5.5. As before, the control configuration involves the manipulation of bulk flow rate to regulate the hot spot temperature. Measurements are only available from tube #1 and the controller is a PI controller with settings: $K_p = 0.5$, $\tau_I = 0.05$. Now the

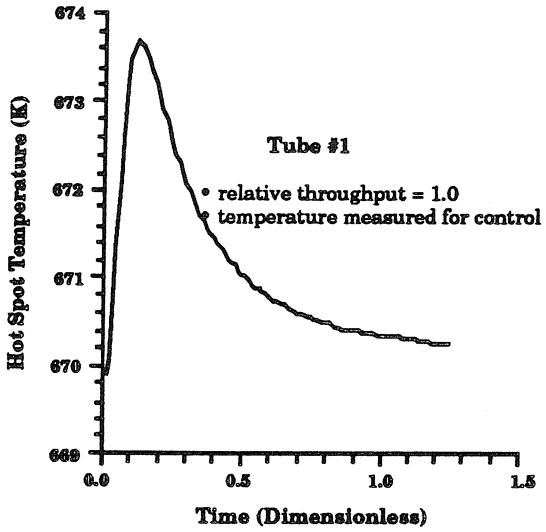

Figure 5.8. Closed-Loop Response (Case Study #2, Inlet Concentration Disturbance, u= Flow Rate)

controlled system is subjected to a 10% step increase in the inlet concentration. From the steady state values at the end of the simulations in Figures 5.8 and 5.9, we can see that both tubes have initial and final points which may be considered tolerable for the designed reactor. However, a large transient excursion of the temperature in tube

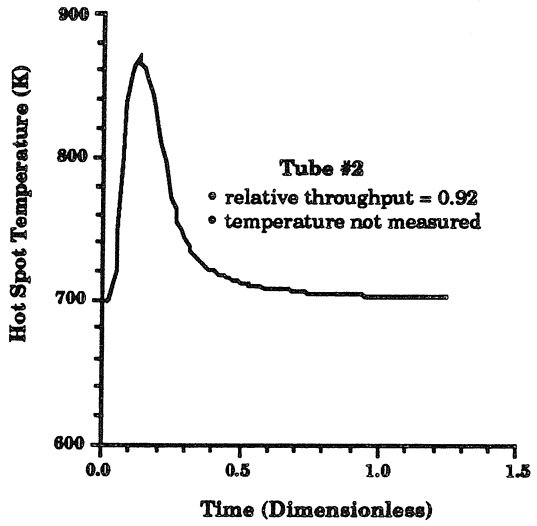

Figure 5.9. Closed-Loop Response (Case Study #2, Inlet Concentration Disturbance, u= Flow Rate)

Table 5.5 Simulation Conditions (Case Study #2)		
Inlet Concentration (y_0)	1.1	
Flow Rate ($\frac{F}{F_0}$)	0.85	
Inlet Temperature (x_0)	1.00	
Jacket Temperature (x_w)	1.00	
Manipulated Variable (u)	Flow Rate	
Controlled Variable (y)	Hot Spot Temperature	
Disturbance	+10% Step in y_0	
Set Point Change	$0K$	
	Tube #1	Tube #2
Relative Throughput	1.0	0.92

#2 is observed for the disturbance in concentration. The peak hot spot temperature observed is in excess of 150 K above the final steady state level. Such phenomenon could be accurately described as *dynamic sensitivity.*

In this case study, the controlled response is strongly dependent on the controller parameters. As the sensitivity exhibited in this in this case study is dynamic in nature, we can expect to minimize the size of the temperature excursion by optimizing the control parameters. Note, however, that the magnitude of the flow restriction also strongly affects this transient response.

Case Study #3 (Dynamic Sensitivity, Minimum Phase System)

The same sensitivities are evident in the closed loop for a *minimum phase* system. The control configuration is as before, with the replacement of bulk flow rate by jacket temperature as the manipulated variable. And as before, we only measure the temperature in tube #1 in an effort to control the hot spot temperature in the reactor. This effectively renders tube #2 off-line and no control action will be taken to handle disturbances in this tube. The control settings are as before ($K_p = 0.5$, $\tau_I = 0.05$). The remaining conditions for the simulation are shown in Table 5.6. In this case, we

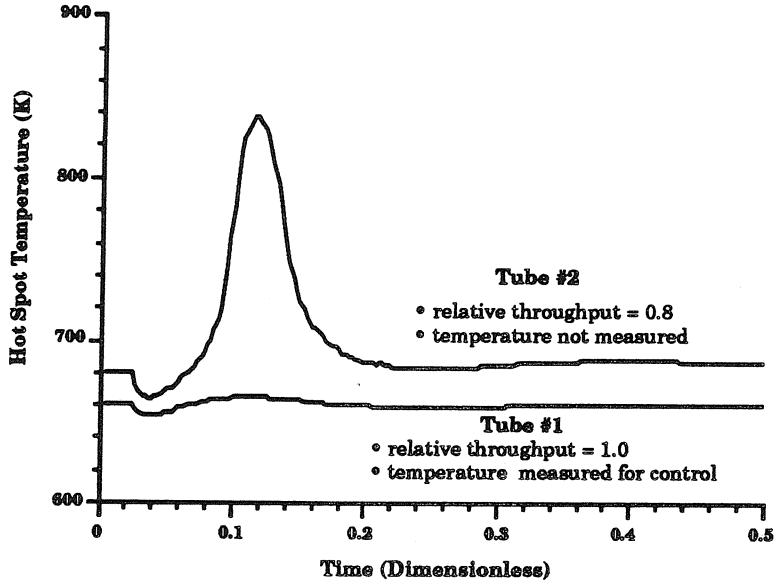

Figure 5.10. Closed-Loop Response (Case Study #3, Flow Rate Disturbance, u= Jacket Temperature)

consider a disturbance of a 10% step decrease in the flow rate for two tubes. The tubes chosen for this study differ by 20% in their flow throughput. The controlled response to this disturbance is depicted in Figure 5.10. Again, it is observed that there is a *dynamic sensitivity* associated with this operating condition as tube #2 experiences a 300 K overshoot in its response.

Table 5.6 Simulation Conditions (Case Study #3)		
Inlet Concentration (y_0)	1.1	
Flow Rate ($\frac{F}{F_0}$)	1.0	
Inlet Temperature (x_0)	1.0	
Jacket Temperature (x_w)	1.0	
Manipulated Variable (u)	Jacket Temperature	
Controlled Variable (y)	Hot Spot Temperature	
Disturbance	-10% Step in $\frac{F}{F_0}$	
Set Point Change	$0K$	
	Tube #1	Tube #2
Relative Throughput	1.0	0.8

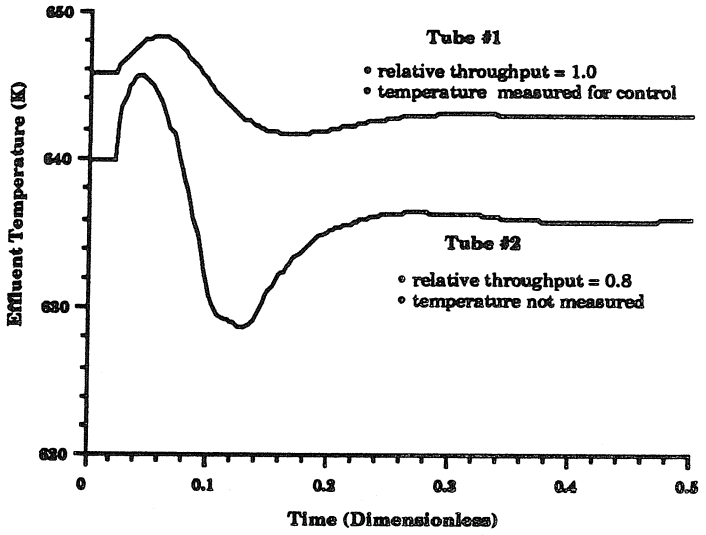

Figure 5.11. Closed-Loop Response (Case Study #4, Flow Rate Disturbance, u= Jacket Temperature)

As in case study #2, the size of this dynamic temperature excursion is a strong function of the control law and the magnitude of the flow restriction.

Remark (Case Studies #1, #2, #3)

As has been emphasized in the above three case studies, it is implicitly assumed that the flow-restricted tube (#2) represented an unobserved tube from the perspective of sensor measurement. Thus, it is effectively rendered off-line and no control action is taken to mitigate the effect of the disturbances.

Case Study #4 (Measurement Selection, Minimum Phase System)

An alternative sensor placement set might include some bulk measurements, such as the reactor effluent temperature. However, one can envision a reasonably representative flow distribution where tube #1 represents 99% of the tubes and 1% of the tubes are restricted to the flow levels given by tube #2. Recall the conditions in case study #3, and now consider the effect of the disturbance on the effluent streams from the two tubes. These results are shown in Figure 5.11. It is clear that the large hot spot temperature excursion is extremely localized and is only represented by a 15-degree

Table 5.7 Physical Parameters for Insensitive Simulations	
$\mathcal{D}a$	$7.059E8$
B	34.14
q	1.0
γ	21.82
λ	0.5
$r(x,y)$	$ye^{-\gamma/x}$

K range in the effluent temperature. Recalling our assumption that tube #1 represents 99% of the total flow, it is clear that the effect of the "hot tube" (#2) would be altogether lost by dilution effects in the mixed effluent stream. In this case, a mixed stream would show a profile which is indistinguishable from the profile exhibited by tube #1.

Case Study #5 (Insensitive Operation, Minimum Phase System)

Case studies #3 and #4 are repeated with a new set of operating conditions in which the reactor diameter is 50% smaller than that recommended by Equation 5.29 ($D = 0.5D_{max}$). This is accomplished by tripling the heat transfer coefficient. Now we have a reactor which is designed "safely" in accordance with the guidelines prescribed in this chapter. The physical parameters which lead to this condition are shown in Table 5.7. As before, we consider the manipulation of jacket temperature (using a PI controller with parameters: $K_p = 0.5$, $\tau_I = 0.05$) to regulate the hot spot temperature in the bed. We look at two different tubes, one of which has restricted flow rate and is not observed by the controller. Additional conditions for this simulation are shown in Table 5.8. The results for closed-loop operation are depicted in Figures 5.12 and 5.13.

We observe the effect of a 10% decrease in the feed-flow rate on the temperatures in the two tubes, which differ by 20% in their throughput. Figure 5.12 shows the

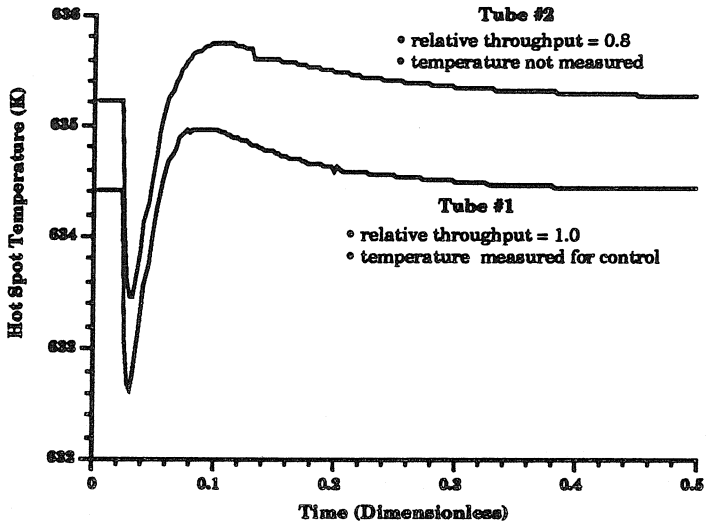

Figure 5.12. Closed-Loop Response (Case Study #5, Flow Rate Disturbance, u= Jacket Temperature)

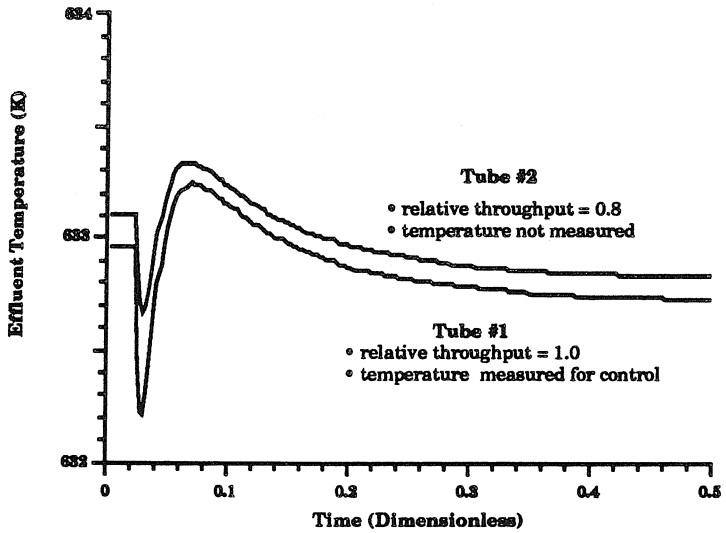

Figure 5.13. Closed-Loop Response (Case Study #5, Flow Rate Disturbance, u= Jacket Temperature)

Table 5.8 Simulation Conditions (Case Study #5)		
Inlet Concentration (y_0)	1.0	
Flow Rate ($\frac{F}{F_0}$)	1.0	
Inlet Temperature (x_0)	1.0	
Jacket Temperature (x_w)	1.006	
Manipulated Variable (u)	Jacket Temperature	
Controlled Variable (y)	Hot Spot Temperature	
Disturbance	-10% Step in $\frac{F}{F_0}$	
Set Point Change	$0K$	
	Tube #1	Tube #2
Relative Throughput	1.0	0.8

response of the hot spot temperatures; Figure 5.13 shows the response of the effluent temperatures. Clearly, the high sensitivity to operating conditions has been diminished, and the difference in temperature levels between the two tubes is negligible.

By designing a reactor which satisfies the proposed sensitivity criterion, we have considerably improved the controllability of the resultant system.

5.5 Practical Control of Tubular Reactors

The previous simulations demonstrate that it is advisable to design multitubular reactors such that they are inherently robust and insensitive to perturbations. While it is possible to operate a single CSTR by feedback stabilization, this is not advisable for a multitube reactor. The problem of designing a system such that it is robust and easy to control versus relying on advanced control methods for stabilization is one that often appears in practice [81], [82]. Regretfully, very often the problem of the impact of design on controllability is not sufficiently recognized both in practice and in the literature. If aware of the problem, most users will prefer an inherently robust design over one relying on control.

In the aerospace industries, there are cases where design of inherently unstable (or

sensitive) systems stabilized by control have demonstrated advantages. One clear example of this is the $X-29$ high performance aircraft (swept forward wing fighter) [3]. The design of this plane makes possible certain high performance combat flight maneuvers; however, its open-loop instability would lead to catastrophic circumstances in milliseconds if the feedback loop is turned off. There are also cases in process industries where such stabilization is essential ([57], [81], [82]), although the problem has not received sufficient attention.

For the specific case of the packed bed reactor, the design criteria proposed should allow safe robust design in most cases. Detailed computer modeling may sometimes allow relaxing these criteria provided detailed and reliable kinetic data are available. However, the cost of obtaining such data has to be weighed relative to the potential savings.

The proposed criteria can also be effectively utilized to update reactor operating conditions in response to a deactivating catalyst. The normal way to do so is to increase the temperature of the cooling bath. Several sets of thermocouples along the length of a tube allow the measurement of the maximum temperature difference between the bath and the tube. If this difference is maintained at the level prescribed by the sensitivity criterion (by adjusting cooling bath temperature), then the overall productivity of the reactor can be safely optimized. The problem is sometimes much more complex due to selective poisoning and deactivation of the front section in the reactor. Here, the temperature profiles can be used to diagnose the state of the catalyst. This allows one to predict in advance the need for catalyst regeneration.

A related approach involves profiling the catalyst activity [75]. It has been demonstrated that if less active catalyst is employed in the region of the reactor where the reaction driving force is greatest, then the parametric sensitivity of the bed is greatly reduced. In practice, this selective deactivation may occur unintentionally and lead to reduced sensitivity in a bed which may have originally been highly sensitive.

5.6 Summary

This chapter presents a set of *simple* and *practical* guidelines for the design of complex catalytic packed bed reactors. The design criteria are derived from requirements on the radial temperature profile, temperature sensitivity, and tolerable pressure drop. The specifications are formulated in terms of the practical reactor parameters of length and diameter, and illustrate the various tradeoffs involved in satisfying the three requirements on the temperature and pressure drop. Thus, the proposed criteria provide direct insights for the practical design engineer.

The stabilization of industrial multitubular packed bed reactors by feedback control is addressed. It is shown that multitubular variations and the lack of proper measurement signals precludes the dynamic stabilization of the reactor in regions of parametric sensitivity. Thus, stable closed-loop operation can only be accomplished with reactors which adhere to the proposed guidelines. These ideas are demonstrated by closed-loop simulations with a reduced order nonlinear packed bed reactor model. Operation of a reactor which violates the design criteria is shown to lead to steady state and dynamic sensitivity. This behavior is manifested as thermal runaway in reactor tubes with slightly restricted flow rates. It is also shown that for a reactor designed in accordance with the presented specifications, the behavior is stable, even for tubes with restricted flow rates. Thus, violation of the proposed criteria leads to unacceptable closed-loop performance.

Acknowledgements

A version of this chapter has been prepared for publication. The creative input of the co-author, Reuel Shinnar, is gratefully acknowledged.

Chapter 6

The Selection of Nonlinear "Linearizing" Control Versus Linear Control

Abstract

A comparative evaluation of the relative merits of linear versus nonlinear "linearizing" feedback control is carried out through a series of specific case studies. The issues of region of attraction, actuator penalties, and sensitivity to input disturbances are investigated for several physical and several purely mathematical dynamical systems. Based upon these results, specific recommendations are made for assessing the appropriate application of simple linear versus nonlinear "linearizing" control.

6.1 Introduction

The interest in nonlinear differential geometric control methods has grown considerably over the past five years. The applications of these so-called "linearizing" techniques have ranged from robotics to flight control to process control. However, many of these application studies have utilized straightforward models of the systems, and few studies have focused on the robustness issues and saturation effects. In addition, there has been little work done to evaluate the comparative performance of nonlinear and linear control structures.

In this chapter, we propose some simple guidelines for the assessment of which systems benefit from the more complex differential geometric control schemes as opposed

to simple optimal linear controllers. Consideration is given in this work to *realistic* performance weights, which include not only a penalty on tracking error but also a penalty on manipulated variable action. In general, the improved dynamical behavior of a "linearized" system is at the expense of large manipulated variable action. Clearly these actions may be excessive or may be limited by actuator constraints. Furthermore, a selection of *natural* performance weights, which vary from one operating point to another, is shown to require adaptive gain scheduling for the nonlinear schemes in order to achieve comparable performance to a single linear controller.

Through an analysis of phase portraits and regions of attraction, some of the robustness and performance tradeoffs are evaluated for various nonlinear systems. Case studies are documented which show an improvement in robustness properties with nonlinear control for certain classes of systems. A class of systems is outlined for which sensitivity in the zero dynamics leads to poor robustness properties. It is also shown that the control structure of "linearizing" techniques leads to increased sensitivity to input disturbances.

These case studies form the basis for a set of proposed guidelines for the judicious selection of nonlinear "linearizing" control **over** straightforward optimal linear control. Thus, we formulate qualitatively the *degree* of nonlinearity for a system, based upon the warranted control action to achieve a certain level of performance.

6.2 Performance Evaluation for General Closed Loop

6.2.1 Region of Attraction

The standard mathematical definition of a region of attraction for a point x_0 is the set for which all trajectories originating in that set eventually converge to the point x_0 [37]. Clearly, a large region of attraction around a process operating point enables the effective handling of perturbations in the system's physical parameters as well as external disturbances. Effective control action will preserve the asymptotic stability

of the point in some neighborhood despite the effects of these perturbations. Strictly speaking, this property is more closely associated with the overall robust stability of the dynamical system rather than its robust performance. However, the limitations imposed by the size of the region of attraction impact directly the tolerable range of operation, and consequently, the resulting performance. Thus, this measure will serve as a useful benchmark in evaluating competitive control structures (nonlinear versus linear).

In the following two case studies, the region of attraction about a nominal point in a dynamical system is investigated as a function of the feedback control law which is applied to the system. Two examples are considered: a purely mathematical system (though similar in structure to the van der Pol oscillator) which has a convenient phase portrait, and a simple process system (CSTR with Van de Vusse kinetics). The comparison is carried out in the phase plane for these second-order systems and consideration is given to the stability of various initial conditions. This is equivalent to considering impulse disturbances to the respective state equations.

van der Pol Oscillator

Consider the following dynamical model which is a slight modification of the equations describing a van der Pol oscillator [37]

$$\begin{aligned} \dot{x}_1 &= -x_1(\alpha^2 - x_1^2 - x_2^2) - x_2 \\ \dot{x}_2 &= u(\alpha^2 - x_1^2 - x_2^2) + x_1 \\ y &= x_2 \end{aligned} \tag{6.1}$$

where y represents the controlled output and u represents the manipulated variable. The two candidate control algorithms which will be investigated are input-output

linearization (IOL) with an external proportional controller

$$u = \frac{\frac{-1}{\beta_1} K_{NL} x_2 - x_1 - \frac{\beta_0}{\beta_1} x_2}{\alpha^2 - x_1^2 - x_2^2} \tag{6.2}$$

and proportional linear control:

$$u = -K_L x_2 \tag{6.3}$$

The choice of parameters ($\alpha = 1.0, \beta_1 = 1.0, K_L = 1.0$, and $K_{NL} = 1.0$) leads to the following two closed-loop systems:

$$\begin{aligned} \text{Linear} \quad \dot{x}_1 &= -x_1(\alpha^2 - x_1^2 - x_2^2) - x_2 \\ \dot{x}_2 &= -x_2(\alpha^2 - x_1^2 - x_2^2) + x_1 \qquad (6.4) \\ y &= x_2 \end{aligned}$$

$$\begin{aligned} \text{Nonlinear} \quad \dot{x}_1 &= -x_1(\alpha^2 - x_1^2 - x_2^2) - x_2 \\ \dot{x}_2 &= -(1 + \beta_0)x_2 \qquad (6.5) \\ y &= x_2 \end{aligned}$$

(6.6)

This particular system was chosen for the fact that both the open- and linear closed-loop dynamical systems have a region of attraction about $(0.0, 0.0)$ precisely equal to the unit circle. This can be seen in the phase portraits of Figures 6.1 and 6.2. If the gain of the linear controller is increased, this merely increases the speed of response as the system moves to the origin without changing the region of attraction.

Application of nonlinear control significantly alters this region of attraction as shown in Figures 6.3 and 6.4 for two different values of the parameter β_0. In the case where $\beta_0 = 0.2$ (Figure 6.3), it can be seen that the portions of the unit disk in two of the four quadrants are excluded from the region of attraction for the nonlinearly controlled system. If this gain is increased $\beta_0 = 1.0$ (Figure 6.4), the

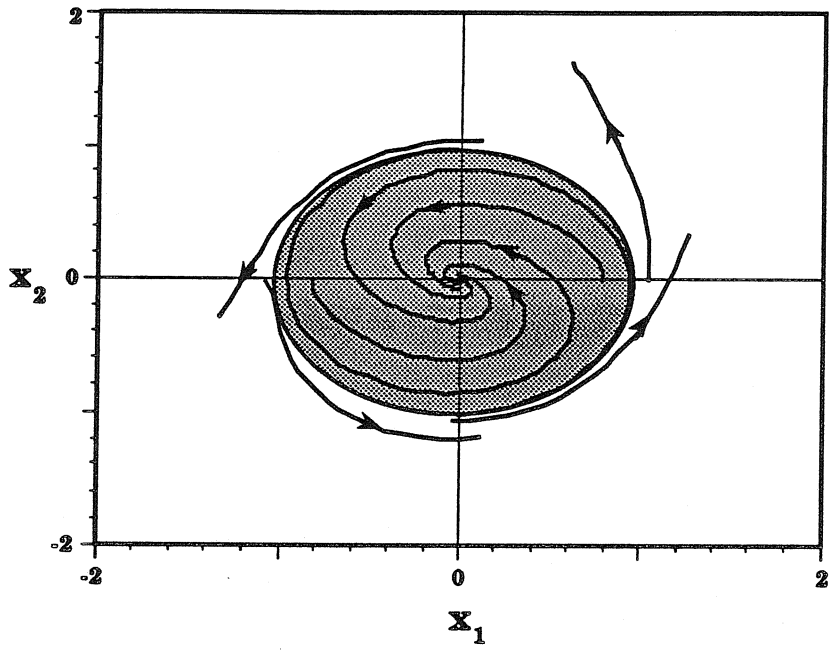

Figure 6.1. Phase Portrait for van der Pol Oscillator (Open Loop)

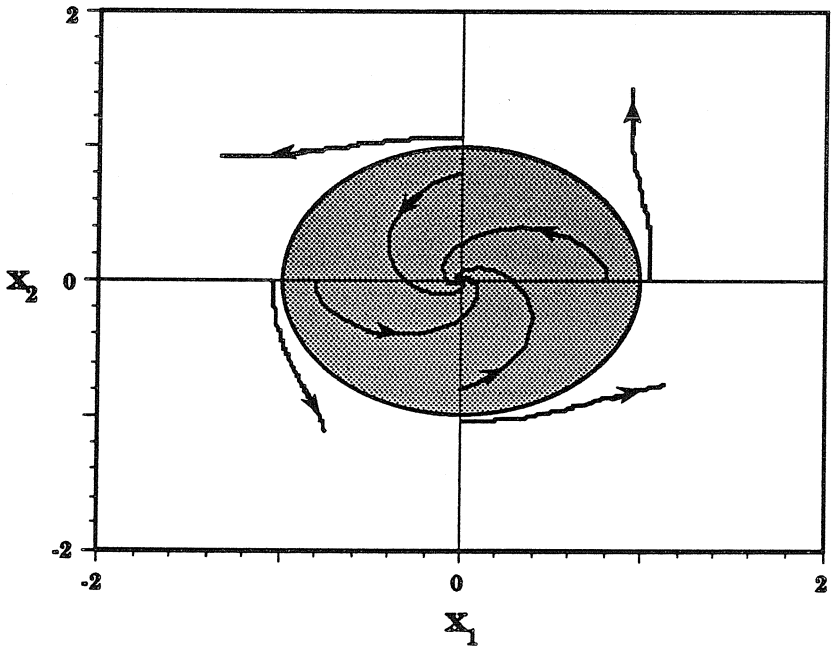

Figure 6.2. Phase Portrait for van der Pol Oscillator (Linear Control)

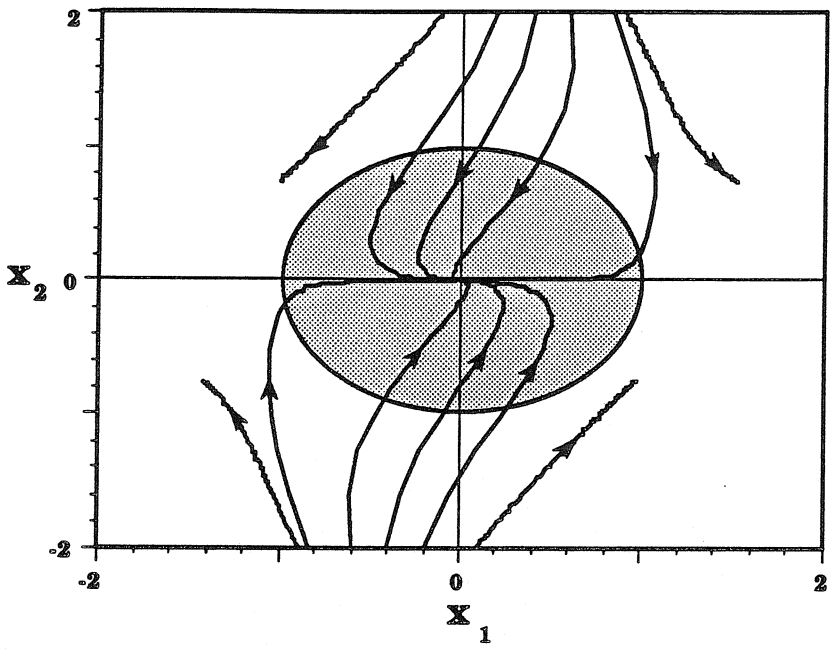

Figure 6.3. Phase Portrait for van der Pol Oscillator (Nonlinear Control, $\beta_0 = 0.2$)

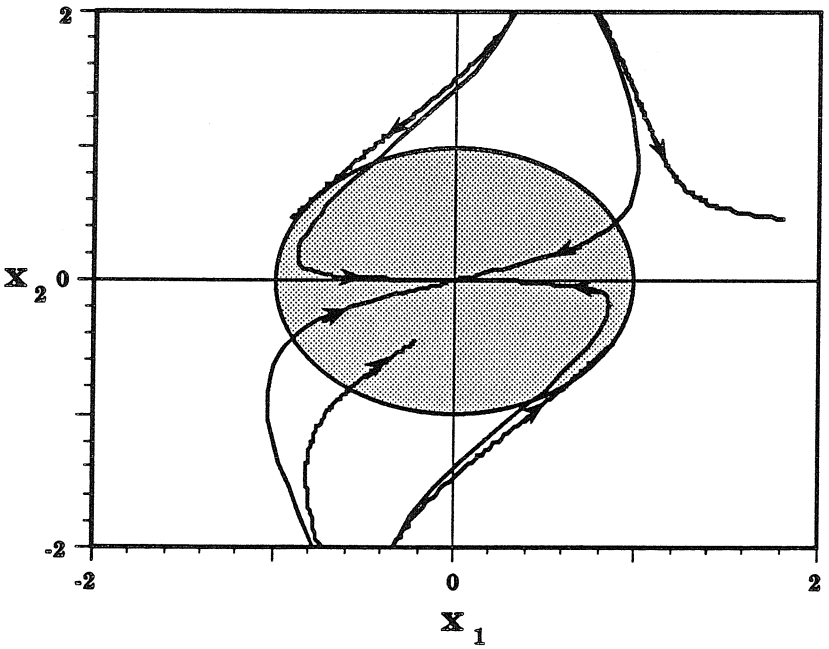

Figure 6.4. Phase Portrait for van der Pol Oscillator (Nonlinear Control, $\beta_0 = 1.0$)

region of attraction expands in the positive and negative x_1 direction and includes virtually all of the unit disk.

Clearly there is a tradeoff in the system between the occluded region of the unit disk and the increased region of attraction along the x-axis. In a physical plant, these considerations must be evaluated for a particular process. The point to be made here is that the two approaches result in different regions of attraction.

CSTR - Van de Vusse Kinetics

Consider the Van de Vusse reactions taking place in an isothermal CSTR (see Chapter 3) with physical parameters leading to the following dimensionless mass balances

$$\begin{aligned} \dot{x}_1 &= -2.5x_1 + 2.5x_1^2 - u \\ \dot{x}_2 &= -x_2 + x_1^2 + u \\ y &= x_2 \end{aligned} \tag{6.7}$$

where the output represents the concentration of the product and the manipulated variable is the dilution rate. Two control algorithms will be investigated, IOL with an external proportional controller

$$u = \frac{-K_{NL}x_2 - x_1^2 - \frac{\beta_0}{\beta_1}x_2}{\beta_1} \tag{6.8}$$

and proportional linear control:

$$u = -K_L x_2 \tag{6.9}$$

The choice of control parameters ($\beta_1 = 1.0, K_L = 1.0, \beta_0 = 0.5$,and$K_{NL} = 0.5$) leads to the following closed-loop systems:

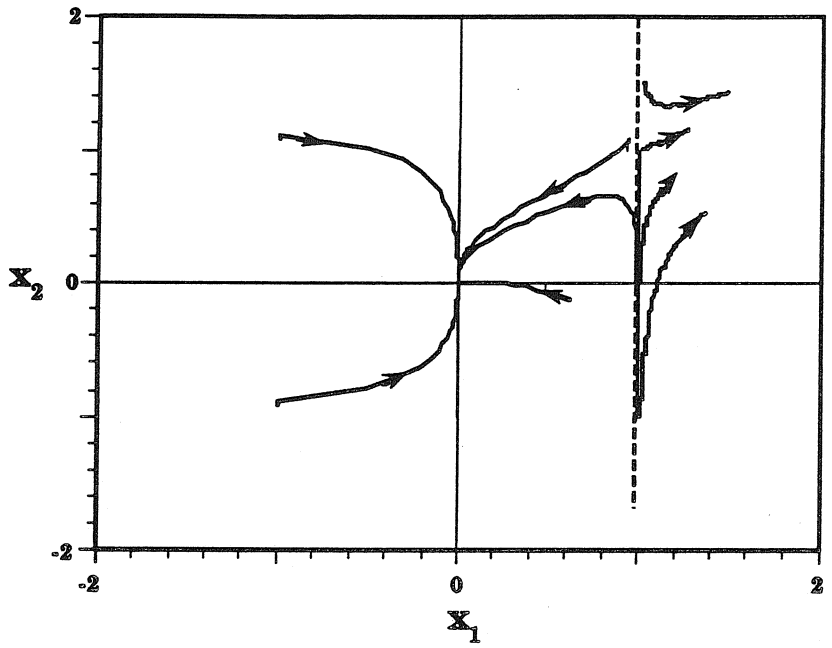

Figure 6.5. Phase Portrait for Van de Vusse Reactor (Open Loop)

$$\begin{aligned} \text{Linear} \quad \dot{x}_1 &= -2.5x_1 + 2.5x_1^2 + x_2 \\ \dot{x}_2 &= -2x_2 + x_1^2 \qquad (6.10) \\ y &= x_2 \\ \text{Nonlinear} \quad \dot{x}_1 &= -2.5x_1 + 3.5x_1^2 + x_2 \\ \dot{x}_2 &= -2x_2 \qquad (6.11) \\ y &= x_2 \end{aligned}$$

Consider the operation of the reactor at the origin and the surrounding region of attraction for each of the three cases (open loop, linear control, nonlinear control). In the open-loop case, Figure 6.5, we observe a stable manifold along the line $x_1 = 1$, which attracts all points along this manifold to the critically stable fixed point at $(x_1, x_2) = (1.0, 1.0)$. This manifold divides the state space into a region of attraction

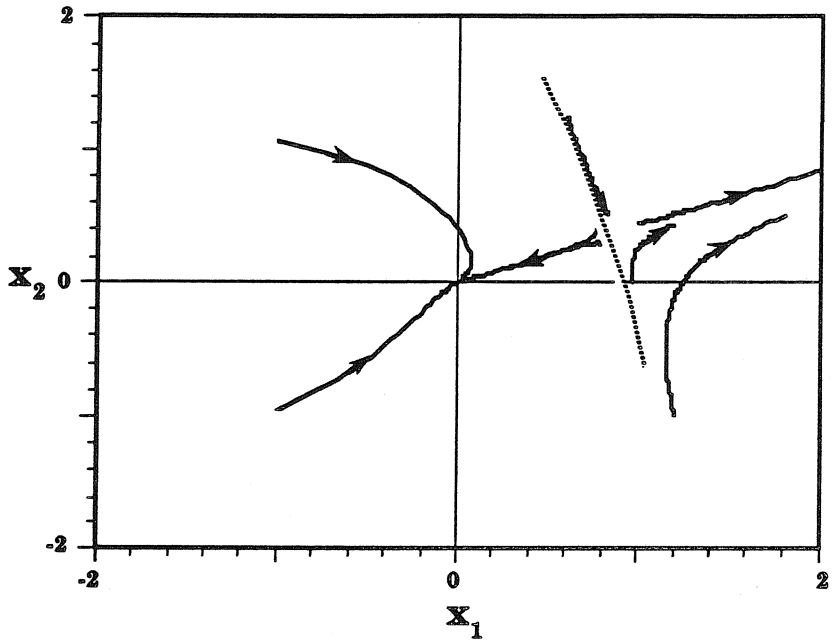

Figure 6.6. Phase Portrait for Van de Vusse Reactor (Linear Control)

to the origin and a region of repulsion. Thus, we will refer to this as the *dividing manifold.* All trajectories originating to the left of the manifold will be eventually attracted to the origin; those originating to the right will be repelled.

This dividing manifold for the linearly controlled reactor is sketched in Figure 6.6 by with a dotted curve. Points along this manifold now converge to the fixed point $(x_1, x_2) = (0.833, 0.347)$. As the control gain is reduced to zero, this manifold becomes the line at $x_1 = 1$. As the control gain is increased, the manifold folds and moves in the negative x_1 direction. The attracting point in the dividing manifold follows the family of parabolas $x_2 = \frac{1}{1+K_L} x_1^2$.

For nonlinear control, the situation is quite different. Now the dividing manifold passes through the fixed point $(x_1, x_2) = (0.714, 0.0)$ for *all values* of the controller gain, β_0. Varying the gain β_0 will fold the dividing manifold around this point; however, the manifold is fixed at this point. Consequently, the region $(x_1 > 0.714, x_2 \sim 0)$ will always be repelled from the origin. The dividing manifold for $\beta_0 = 0.5$ is shown

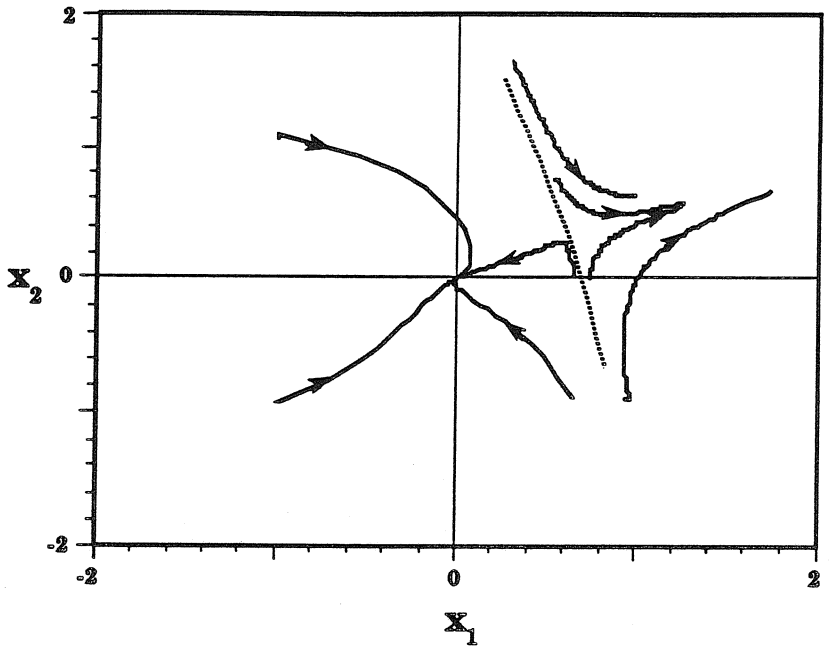

Figure 6.7. Phase Portrait for Van de Vusse Reactor (Nonlinear Control)

in Figure 6.7 as a dotted curve.

As in the previous case with the van der Pol oscillator, we observe two different regions of attraction corresponding to the selection of linear or nonlinear feedback control. In this case, linear control offers a more flexible tuning of the region of attraction through the controller gain.

It should be pointed out that there are several variables which could be tuned for the nonlinear controller (rather than β_0). In addition, one could consider more complex linear architectures such as PID or IMC. The point of this particular study was to demonstrate that the phase portrait behavior (as a function of a single tuning parameter) is fundamentally different for the nonlinear and linear control algorithms. The particular application of interest will determine if these trends favor the use of nonlinear or linear control.

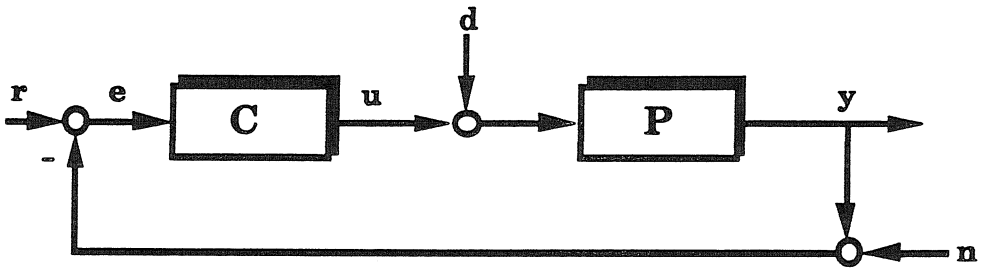

Figure 6.8. Block Diagram for Loopshaping

6.2.2 Loopshaping and Meaningful Performance Weights

A commonly cited fault of differential geometric linearization techniques is the excessive control action required to achieve the linear output response. The obvious question here is: what exactly is a meaningful performance specification for evaluating a closed-loop system? It stands to reason that merely weighting the output error function is not enough. In this section, it is shown that a reasonable performance measure which balances the tradeoffs between actuator movement and output error response has interesting ramifications for the relative merits of linear and nonlinear control.

Consider a performance specification which balances the tradeoffs between robust stability and robust performance by the following weights on the sensitivity (S) and complementary sensitivity (T) functions [20]:

$$\|(|W_1 S|^2 + |W_2 T|^2)^{\frac{1}{2}}\|_\infty \tag{6.12}$$

The infinity norm is chosen as an convenient measure for the manipulations which follow. Consider the block diagram in Figure 6.8, where d represents input disturbances, n represents measurement noise, r is the setpoint, e is the output error, and u and y are the usual manipulated and controlled variables, respectively. If e and u are selected as outputs, and d and n as inputs, then a reasonable performance criterion

would be to minimize a measure of the matrix (with weightings) which relates $(d, n)^T$ to $(e, u)^T$. A minimization of the norm of this matrix can be shown to be equivalent to the performance specification in Equation 6.12 with appropriately chosen weights. Putting a constant weight of 1.0 on d and n and a weight of 0.5 on e and u results in the following expressions for W_1 and W_2 (See [20] for details):

$$\begin{aligned} W_1 &= 0.5(|P|^2 + 1)^{\frac{1}{2}} \\ W_2 &= 0.5(|P|^{-2} + 1)^{\frac{1}{2}} \end{aligned} \tag{6.13}$$

By minimizing the specification in Equation 6.12 with respect to the controller and with the weights defined in Equation 6.13, an optimal controller is synthesized which achieves a reasonable balance between noise suppression, disturbance rejection, and actuator movement. It is easy to show that the controller which achieves the optimum has approximately unit norm.

In order to demonstrate this approach to loopshaping, consider the following simple nonlinear example:

$$\begin{aligned} \dot{x} &= e^x u \\ y &= x \end{aligned} \tag{6.14}$$

This system represents an integrator with a nonlinear gain. At a given operating point (x_0), the linear approximation of this plant is given by:

$$y = \frac{e^{x_0}}{s} u \tag{6.15}$$

The previously described loopshaping procedure will be evaluated for this system using both a linear and a nonlinear (IOL) control law. The linear controller and the outer linear loop in the IOL are chosen to be proportional controllers for simplicity.

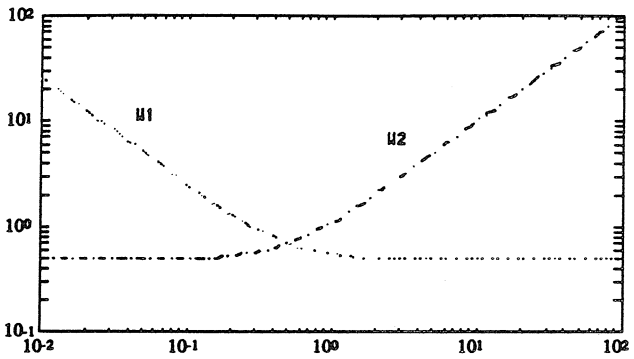

Figure 6.9. Weighting on Sensitivity (W_1), Complementary Sensitivity (W_2) ($x_0 = -0.693$)

The following control laws are selected:

$$\text{Linear} \quad u = [-K_L]\, e \tag{6.16}$$

$$\text{Nonlinear} \quad u = \left[\frac{K_{NL}}{\beta} e^{-x}\right] e \equiv \left[-(\tilde{K}_{NL} e^{-x})\right] e \tag{6.17}$$

The objective of this study will be to determine the optimal value of the respective gains, (K_L, K_{NL}), in a neighborhood of two operating points. Optimality here refers to a minimization of the performance specification given in Equation 6.12 for the linear approximation of each closed loop *around* the operating point. Locally, the nonlinear controller can be treated as a linear controller with gain $\hat{K}_{NL} = \tilde{K}_{NL} e^{-x_0}$.

The first operating point considered is ($x_0 = -0.693$). The weights on S and T (defined in Equation 6.13 as functions of P) are plotted in Figure 6.9. Adding the weighted S and T together, one can see the influence of controller gain on the overall performance specification (Figure 6.10). Plotted here are the values of the performance specification versus frequency for three different controller gains ($K = 0.5, 1.0$, and 2.0). It is easily seen that the optimal gain for the controller is 1.0. This can be understood as requiring the loop transfer function to have magnitude roughly equal to the plant magnitude. This means that the linear controller must have gain 1 and the outer linear controller for IOL must be tuned with gain equal to $e^{x_0} = 0.5$.

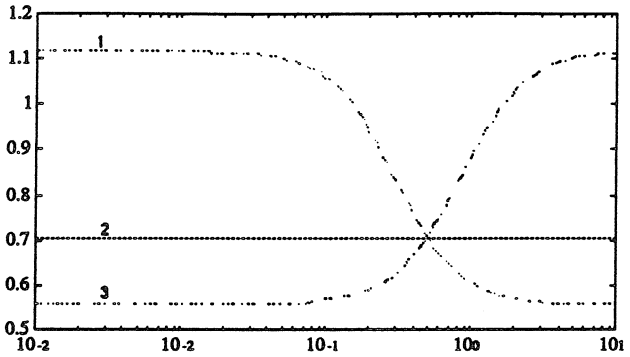

Figure 6.10. Performance Specification (Control Gain = (1) 0.5 (2) 1.0 and (3) 2.0, $x_0 = -0.693$)

Suppose the nonlinear controller has been improperly tuned with a higher or lower value than 0.5. The results are found in the simulations depicted in Figures 6.11 , 6.12, and 6.13. Figure 6.11 shows the response for a setpoint change of -0.5 (all variables are in deviation form). Both linearly and nonlinearly controlled systems show a balance between the error and the actuator movement required to reduce it. Also shown are the responses of the nonlinearly controlled system when the proportional

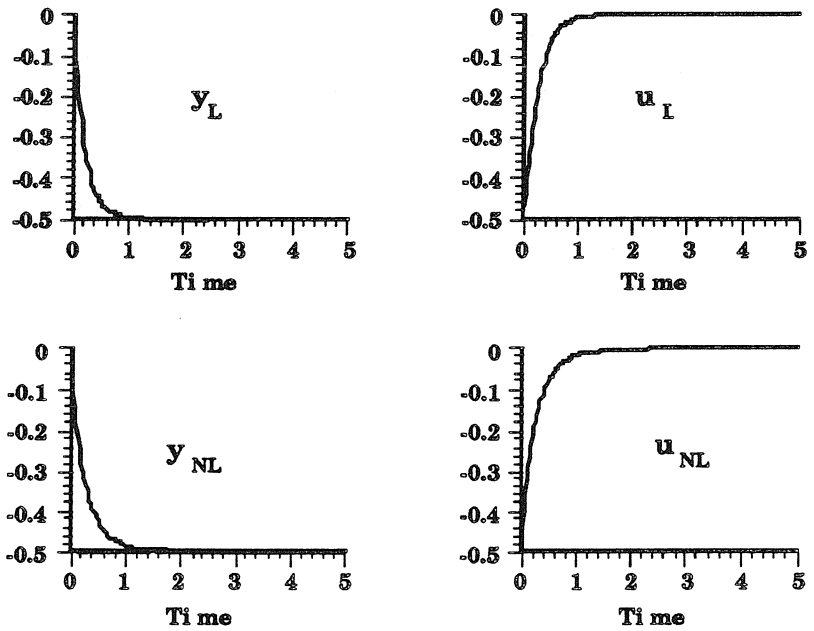

Figure 6.11. Set Point Response ($K_L = 1.0$, $\hat{K}_{NL} = 1.0$)

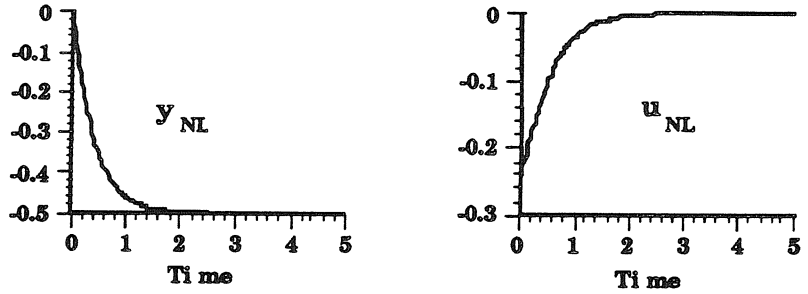

Figure 6.12. Set Point Response ($\hat{K}_{NL} = 0.5$)

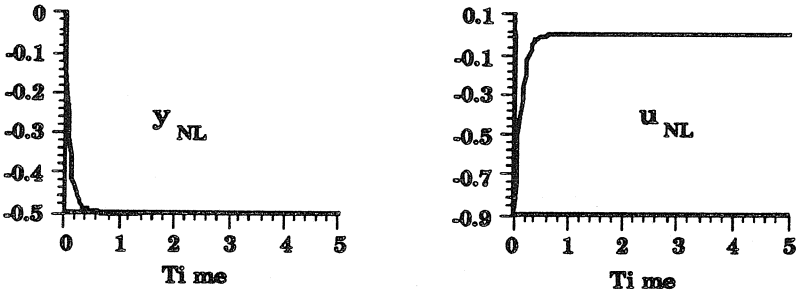

Figure 6.13. Set Point Response ($\hat{K}_{NL} = 2.0$)

gain in the outer loop is too low (Figure 6.12, $\hat{K}_{NL} = 0.5$) or too high (Figure 6.13, $\hat{K}_{NL} = 2.0$). In the former case, the speed of response is too sluggish because the system has been detuned. In the latter case, the control action is too aggressive and possibly excessive. These effects can also be clearly seen from a plot of the sensitivity (S) and complementary sensitivity (T) functions at this operating point for the different control gains (Figure 6.14). As the controller gain is reduced, the S function rolls off sooner, leading to less manipulated variable action but also to a slower response.

To understand how the two control approaches compare, we must investigate another operating point. Let us consider $x_0 = 1.609$. A completely analogous construction to the one above leads to the weightings on S and T in Figure 6.15. The control gains influence the overall performance specification as shown in Figure 6.16. Once again, as expected, the optimal proportional gain is one. This leads to a unity gain linear proportional controller and IOL with an outer linear loop having propor-

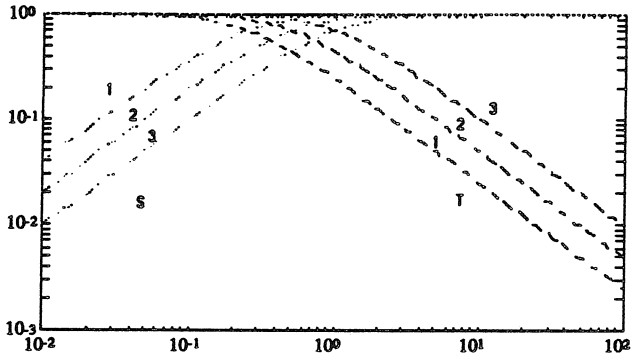

Figure 6.14. Sensitivity (S) and Complementary Sensitivity (T) Functions ($\hat{K}_{NL}$ = (1) 0.5 (2) 1.0 (3) 2.0)

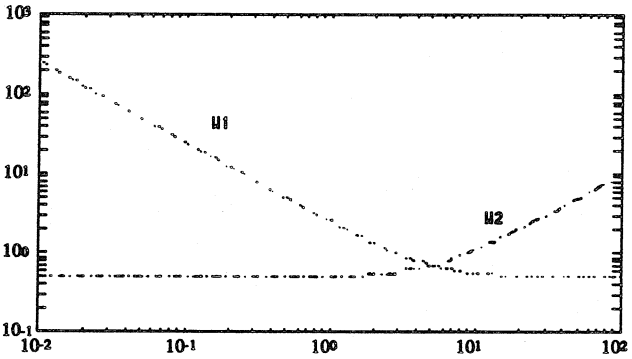

Figure 6.15. Weighting on Sensitivity (W_1), Complementary Sensitivity (W_2) ($x_0 = 1.609$)

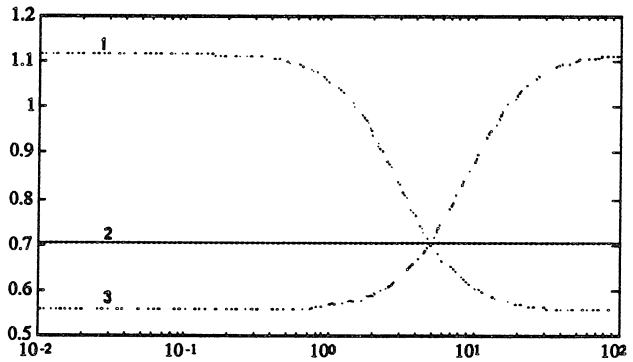

Figure 6.16. Performance Specification (Control Gain = (1) 0.5 (2) 1.0 and (3) 2.0, $x_0 = 1.609$)

tional gain $e^{x_0} = 5.0$. For brevity, we omit the simulations, but, it is possible to show how this gain in the outer loop optimally balances the tradeoff between manipulated variable action and error response.

This simple example has demonstrated that a perfectly reasonable performance specification (Equation 6.12) has led to either a single proportional linear controller, or to an IOL controller which must be gain scheduled in the outer loop to maintain a unit gain on the combined control action. This clearly diminishes the utility of the IOL approach (as measured by the proposed specification).

From a practical perspective, the idea of performance weights which are a function of the plant itself, and in the case of a nonlinear plant, the operating point, is quite relevant. In many process systems, the performance objectives will vary from operating condition to operating condition. One clear example of this is a variation in the disturbances which affect a unit operation differently at different conditions. The demand for an *operating-condition-dependent performance specification* necessitates a careful evaluation of the various tradeoffs present. An approach such as the one presented here logically compromises between system response and effort required to achieve it. The result of the present study is that a simple proportional controller with unity gain will outperform an IOL controller.

6.2.3 Input Disturbance Sensitivity

The sensitivity of closed-loop properties to disturbances in the manipulated variable is of equal concern for both linearly and nonlinearly controlled nonlinear dynamical systems. In the following section, the impact of step disturbances in the manipulated variable on the output will be investigated through an analysis of the steady-state behavior of the process.

Consider a general first-order nonlinear system subject to disturbances in the

manipulated variable:

$$\begin{aligned} \dot{x} &= f(x) + g(x)(u + d) \\ y &= h(x) \end{aligned} \tag{6.18}$$

Application of the following nonlinear control law (IOL with linear proportional control in the outer loop)

$$u = \frac{-K(y - y_{sp}) - \beta_1 \frac{\partial h}{\partial x} f(x) - \beta_0 h(x)}{\beta_1 \frac{\partial h}{\partial x} g(x)} \tag{6.19}$$

leads to the following closed-loop system dynamics:

$$\dot{y} = \frac{\partial h}{\partial x}\dot{x} = \frac{\partial h}{\partial x} g(x) d - \left(\frac{K}{\beta_1} + \frac{\beta_0}{\beta_1}\right)(y - y_{sp}) \tag{6.20}$$

At steady state, the following relationship is valid:

$$\frac{y_{ss} - y_{sp}}{\frac{\partial h}{\partial x} g(h^{-1}(y_{ss}))} = \frac{d_{ss}}{\left(\frac{K}{\beta_1} + \frac{\beta_0}{\beta_1}\right)} \tag{6.21}$$

In the case of simple linear control ($u = -Kh(x)$), the following closed-loop dynamics result

$$\dot{y} = \frac{\partial h}{\partial x}\left[(f(x) - g(x)K(y - y_{sp}) + g(x)d\right] \tag{6.22}$$

and at steady state, the following relationship holds:

$$\frac{-f(h^{-1}(y_{ss}))}{Kg(h^{-1}(y_{ss}))} + (y_{ss} - y_{sp}) = \frac{d_{ss}}{K} \tag{6.23}$$

The main point of this section is this: the solutions to Equations 6.21 and 6.23 for y_{ss}, given d_{ss} and functions f, g, and h, do not always exist. This means that for a fixed disturbance level, say a step disturbance, it may be possible to destabilize a

nominally stable plant.

For example, consider the case where $f(x) = x^2$, $g(x) = 1$, and $h(x) = x$. This leads to a quadratic function in Equation 6.23 with solutions that are functions of d_{ss} and K. For an improperly tuned controller, this could lead to physically unrealizable values for y_{ss} in response to a particular disturbance level.

Let us consider in greater depth another simple example, namely the variable gain integrator from the last section. Recall that for that system, $f(x) = 0$, $g(x) = e^x$, and $h(x) = x$. Consider the application of both linear and IOL as discussed above to yield the following steady state equations:

$$\text{Linear} \qquad (y_{ss} - y_{sp}) = \frac{d_{ss}}{K} \tag{6.24}$$

$$\text{Nonlinear} \quad \frac{(y_{ss}-y_{sp})}{e^{y_{ss}}} = \frac{d_{ss}}{\frac{K}{\beta_1}+\frac{\beta_0}{\beta_1}} \equiv \frac{d_{ss}}{K_{NL}} \tag{6.25}$$

As the control action on the error signal in each case is only proportional control, we must tolerate some offset ($y_{ss} - y_{sp} \equiv \Delta_{ss}$) in the final solution. Rewriting the two equations above, we get:

$$\text{Linear} \qquad \Delta_{ss} = \frac{d_{ss}}{K} \tag{6.26}$$

$$\text{Nonlinear} \quad \Delta_{ss} e^{-\Delta_{ss}} = \frac{e^{y_{sp}} d_{ss}}{K_{NL}} \tag{6.27}$$

The implication for linear control is straightforward: there will be an offset directly proportional to the disturbance magnitude and inversely proportional to the controller gain. So we can increase the gain to minimize the impact of disturbances.

For the nonlinear case, the situation is more complicated. Consider a plot of the function $y = xe^{-x}$ given in Figure 6.17. Clearly, for values of y greater than about 0.4, we cannot solve for x. Return now to Equation 6.27 and note the similarity. The implication is that for large enough values of the right hand side, there will be no solution for the steady state output variable.

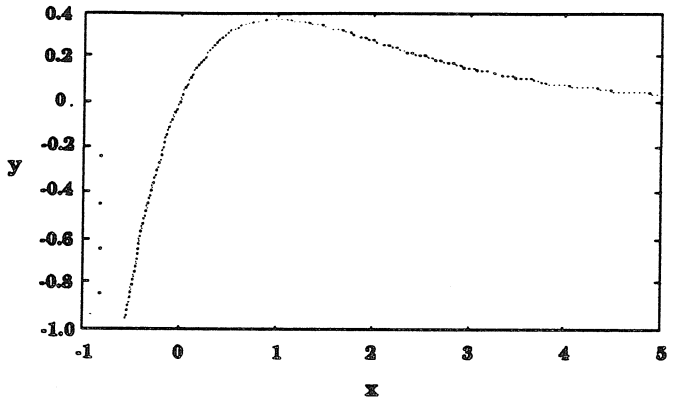

Figure 6.17. $y = xe^{-x}$

We will motivate this with the following series of simulations. Consider operation at $y = 1.609$ and controller parameters $K_L = 1.0, K_{NL} = 5.0$. Figures 6.18, 6.19, and 6.20 show the closed-loop response of the systems to increasing step disturbances in the input variable. Figure 6.18 depicts the response to $d = \frac{.05}{s}$. The systems show nearly equivalent behavior. In Figure 6.19, where $d = \frac{.25}{s}$, one observes that the offset for the nonlinear case is larger by about 40%, but both systems are stable. If we now

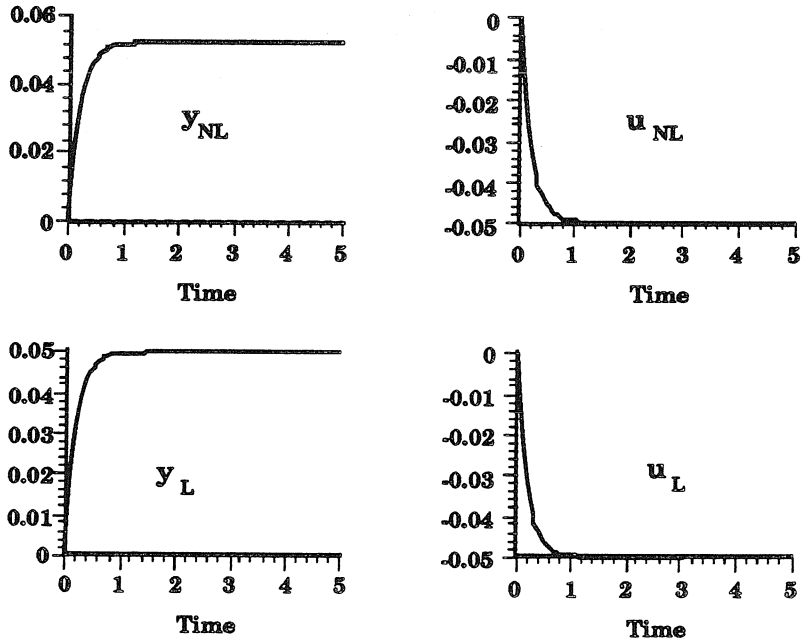

Figure 6.18. Disturbance Response ($x_0 = 1.609$, $d = \frac{.05}{s}$)

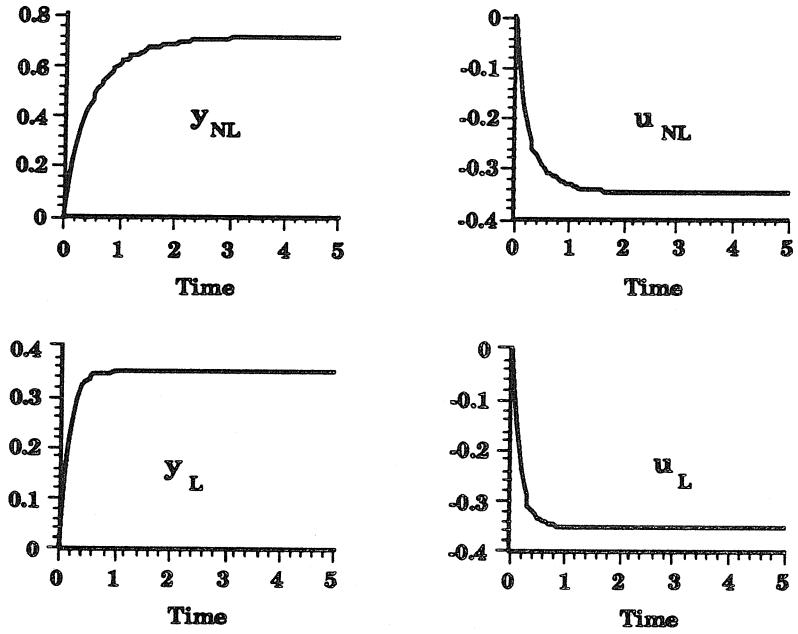

Figure 6.19. Disturbance Response ($x_0 = 1.609$, $d = \frac{.25}{s}$)

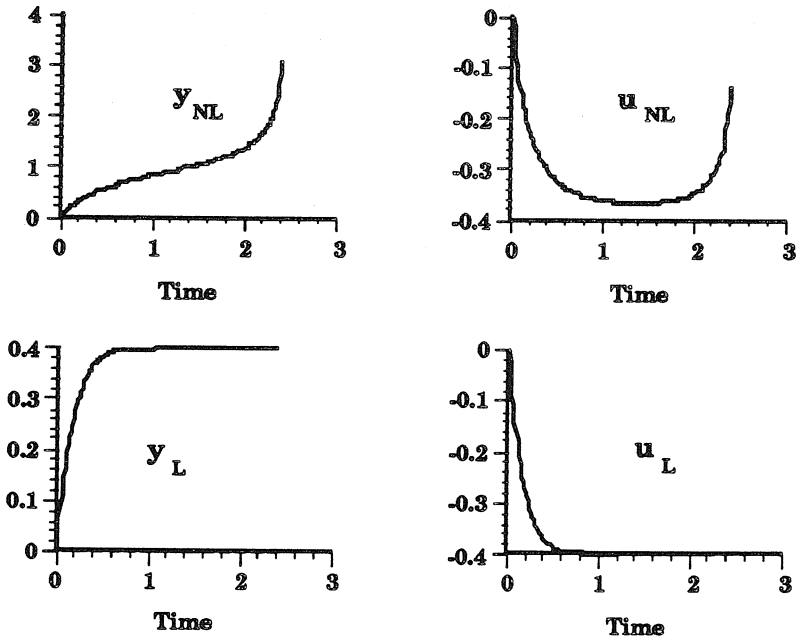

Figure 6.20. Disturbance Response ($x_0 = 1.609$, $d = \frac{.4}{s}$)

increase d to $\frac{4}{s}$ (Figure 6.20), it is seen that the linearly controlled system is stable but the nonlinearly controlled system goes unstable. This is due to the fact that there is no steady state value of y which will satisfy Equation 6.27.

We have underscored through this simple example the importance of input disturbances for nonlinear systems. While the chosen example was for a sensitive nonlinear control law, the form of Equations 6.21 and 6.23 suggest that both linearly and nonlinearly controlled nonlinear systems may suffer from sensitivity to input disturbances. In both cases, high proportional gain (K_L or K_{NL}) will help to minimize the sensitivity, but this can lead to other robust stability problems.

In the particular case of chemical reactor systems, typical $f(x)$ functions are polynomial (for mass law in kinetics) or exponential (Arrhenius temperature kinetics); $g(x)$ is either constant or linear in x (depending on the manipulated variable); and $h(x)$ is typically linear in x. Based upon these simplifications, one could conclude that input sensitivity for chemical reactors might be amplified by *linear* control. We need to be very careful about how this conclusion was drawn.

- This analysis only considers instability and not more benign deteriorated performance.

- This conclusion is based upon the broad generalizations for f, g, and h.

For a particular process system, it is very important to carefully examine the relevant process dynamics and the impact (both steady state and transient) of disturbances in the manipulated variable on the system behavior. This is clearly an area for fruitful research and can serve as a valuable benchmark for comparing the relative merits of nonlinear and linear control.

6.2.4 Actuator Constraints

This final case study incorporates both the effect of regions of attraction mentioned earlier with the imposition of hard constraints on the level of the actuator signal. As was discussed earlier, a common argument against differential geometric controllers is that the "perfect" output response (i.e. linear) is achieved at the (potentially) expensive cost of large excursions of the manipulated variable. Many of the academic examples published in the literature ignore this effect and result in closed-loop simulations which require physically unrealizable actuator signals. Through the case of a simple mathematical example, we will highlight this phenomena.

Consider the following mathematical system:

$$\begin{aligned}
\dot{x}_1 &= -x_1(4 - x_1^2 - x_2^2)(1 - x_1^2 - x_2^2) + x_2 \\
\dot{x}_2 &= -x_2(4 - x_1^2 - x_2^2)(1 - x_1^2 - x_2^2) - x_1 + 5u \\
\dot{x}_3 &= 20x_1x_2 - x_3 + u \\
y &= x_3
\end{aligned} \tag{6.28}$$

If the system is put in Byrnes-Isidori canonical form, the following zero dynamics are evident:

$$\begin{aligned}
\dot{\eta}_1 &= -\eta_1(4 - \eta_1^2 - \eta_2^2)(1 - \eta_1^2 - \eta_2^2) + \eta_2 \\
\dot{\eta}_2 &= -\eta_2(4 - \eta_1^2 - \eta_2^2)(1 - \eta_1^2 - \eta_2^2) - \eta_1 - 100\eta_1\eta_2
\end{aligned} \tag{6.29}$$

Removing the $100\eta_1\eta_2$ term results in a system with two concentric limit cycles: an attracting orbit at $r = 2.0$ and a repelling orbit at $r = 1.0$. Consequently, although the zero dynamics in Equation 6.29 are locally stable at the origin, they are "fragile" in the sense that perturbations would be expected to drive the system into a stable oscillating mode far from the operating point.

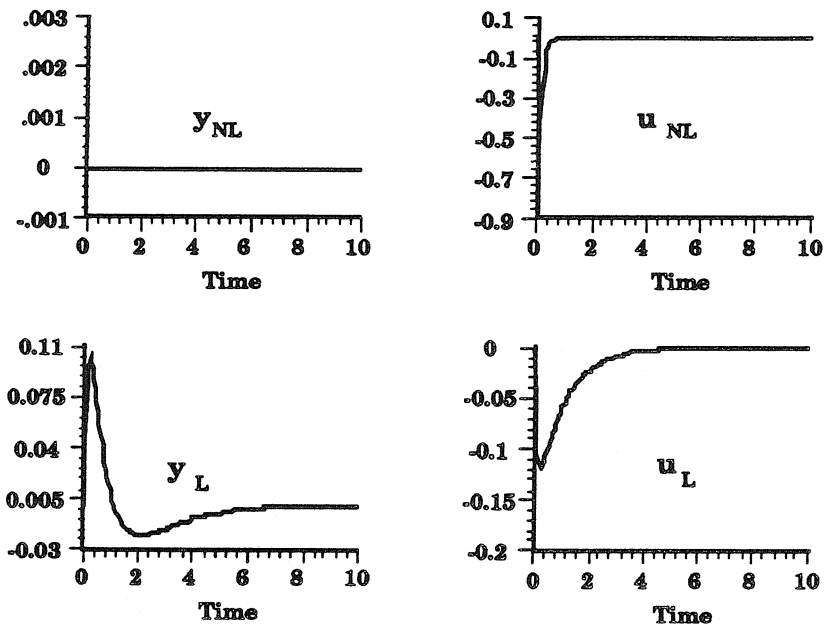

Figure 6.21. Closed-Loop Response (I.C.'s = $(0.25, 0.25, 0.0)$, No Constraints)

The linear approximation of the system in Equation 6.28 about the origin is given by the transfer function $\frac{1}{s+1}$ relating u to y. This suggests a nonlinear controller (for comparison purposes) with the following parameters

$$u = v - (20x_1x_2 - x_3) - x_3 \tag{6.30}$$

which yields an inner loop with the transfer function $\frac{1}{s+1}$ from v to y.

Now if we apply linear PI control to both the open loop and IOL inner loop (with $K_p = 1.0$ and $\tau_I = 1.0$), then the nominal responses would be expected to be similar. We consider the response of the system to a perturbation away from the nominal operating point. Initially, we ignore constraints.

In the first case (Figure 6.21), the system is started with the initial conditions $(0.25, 0.25, 0.0)$. It is observed that the nonlinearly controlled system shows no perturbation in the output, but requires a reasonably large actuator signal to drive the system to equilibrium. This is because the two perturbed states (x_1, x_2) are effectively

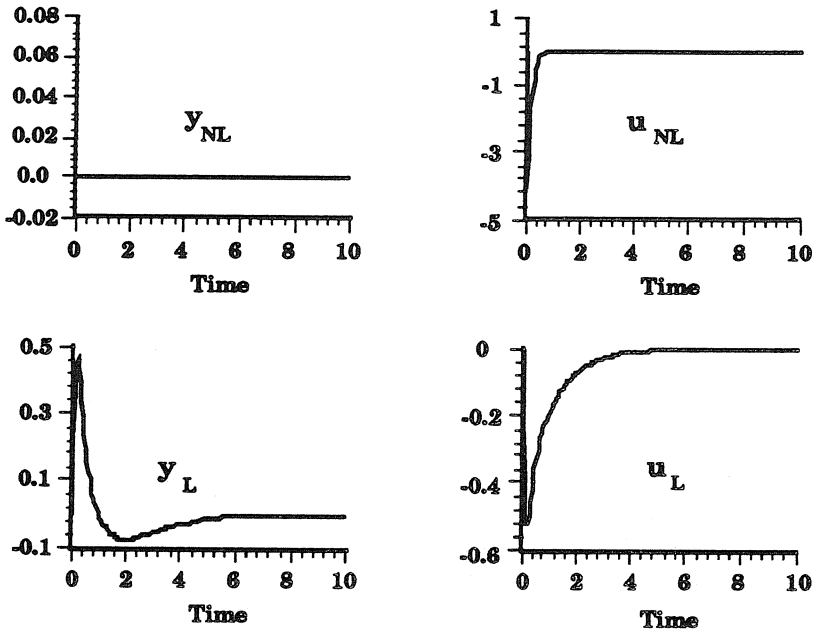

Figure 6.22. Closed-Loop Response (I.C.'s = $(0.5, 0.5, 0.0)$, No Constraints)

decoupled from the output via the nonlinear control law. The output only responds to changes in v. The dynamics of x_1 and x_2 are restricted to the unobservable zero dynamics.

The case is quite different for the linear controller. Here the output is disturbed as the controller works to restore equilibrium. However, the magnitude of the control effort is nearly an order of magnitude smaller.

Similar trends are apparent in Figure 6.22, where now the initial conditions are $(0.5, 0.5, 0.0)$. Once again, the perturbed states evolve back to equilibrium on the unobservable zero dynamics (IOL case).

Finally, in Figure 6.23, we observe that a sufficiently large perturbation in x_1 and x_2 away from the origin drives the unobserved states onto an oscillating trajectory. This is not manifested in the output, but the manipulated variable oscillates wildly in a clearly undesirable way. Because the linear controller is less aggressive (in a "nonlinear" way), the manipulated variable is able to drive the system back to its equilibrium point with mild actuator dynamics.

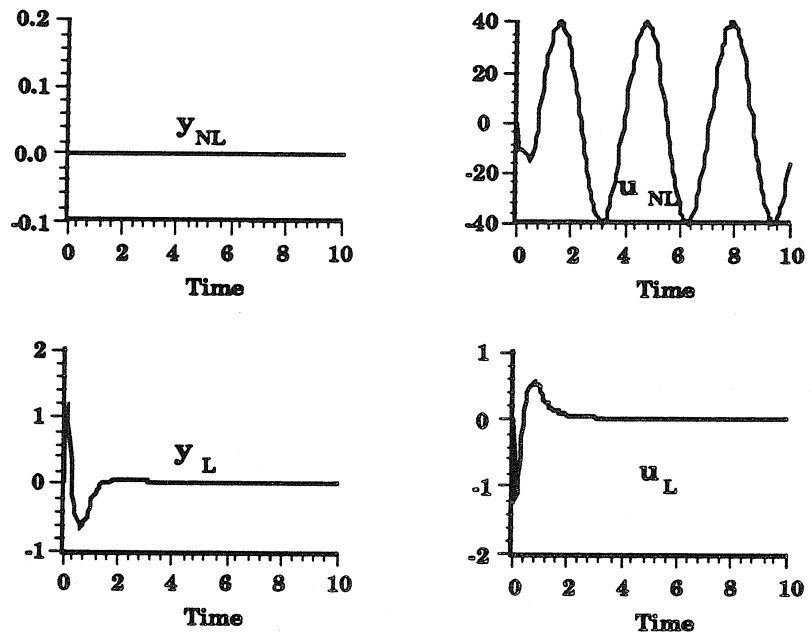

Figure 6.23. Closed-Loop Response (I.C.'s = $(0.725, 0.725, 0.0)$, No Constraints)

Now we consider the effect of magnitude constraints on the manipulated variable. Returning to the second example from above, we now apply a hard constraint of ± 0.5 on the manipulated variable and repeat the simulation (Figure 6.24). This constraint effectively recouples the nonlinearly controlled system with its zero dynamics and we now observe a perturbation in the output signal as the constrained dynamics are driven back to equilibrium. By comparison, the behavior of the two systems (nonlinear control, linear control) are virtually indistinguishable.

Similarly, we reexamine the third example from above (initial conditions of $(0.725, 0.725, 0.0)$ and apply a hard constraint of ± 1.0 on the manipulated variable (Figure 6.25). The coupling is observed once more between the output and the constrained system's zero dynamics as the output is perturbed. And once again, the performance level in the two systems (as measured by y and u) are very similar. Furthermore, the constraint on the manipulated variable has stabilized the fragile zero dynamics of the nonlinearly controlled system and the actuator is not driven to oscillate.

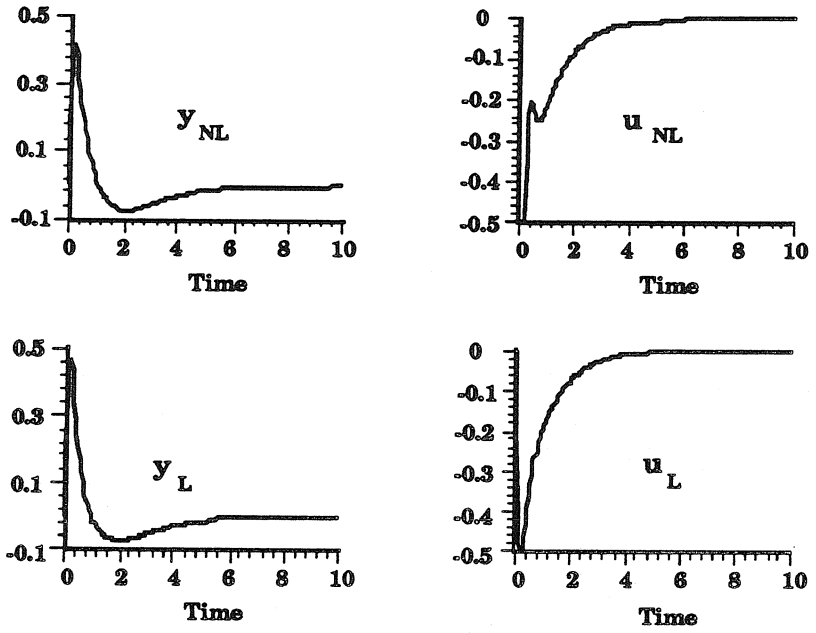

Figure 6.24. Closed-Loop Response (I.C.'s = $(0.5, 0.5, 0.0)$, $|u| \leq 0.5$)

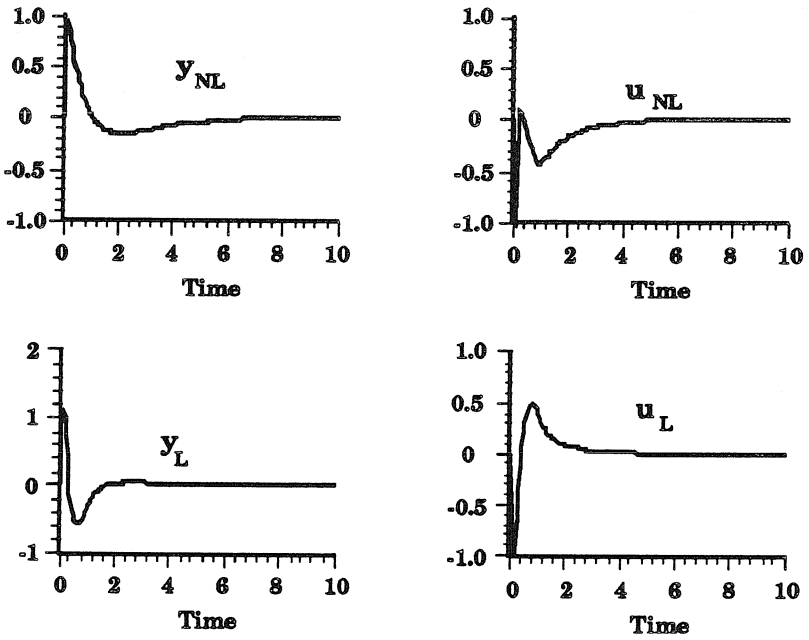

Figure 6.25. Closed-Loop Response (I.C.'s = $(0.725, 0.725, 0.0)$, $|u| \leq 1.0$)

Although this example is purely mathematical with little direct correlation to a process system, it highlights two important considerations in the selection of nonlinear versus linear control:

- Actuator constraints can erase the desirable properties of IOL (linear response, decoupled disturbances) and can make the behavior indistinguishable from a linearly controlled system.

- While the region of attraction property discussed earlier is important for the stability of a system's output, it is also important to evaluate regions of attraction for nonlinear systems zero dynamics and evaluate their global properties. Failure to do so may result in undesirable actuator dynamics.

6.3 Conclusions

The preceding case studies have highlighted several properties of a closed-loop system's behavior which are useful benchmarks for assessing the relative merits of competitive control strategies. These include region of attraction, actuator penalty, and input sensitivity. Unfortunately, many of the differential geometric control studies in the literature do not address these robustness issues. In this chapter, we take a careful look at some of the limitations and weaknesses of input-output linearization (IOL), and sketch some general guidelines for evaluating cases where its utilization is warranted.

There is a bias in this chapter in favor of linear approaches. The justification for this is simple: the meritorious use of "linearizing" control has been described in great detail in the literature (as well as earlier chapters in this work) in the fields of process control, flight control, and robot control. The work presented here represents an effort to balance the perspective on this subject. Clearly, there are systems which *require* nonlinear control for stabilization over an appreciable operating range. An

example of this, presented in [26], is a CSTR which exhibits a gain change at optimum levels. No linear controller can stabilize this region. IOL is also inappropriate for this application because of the singularity at the optimum. Work is underway in this group to investigate nonlinear approximate linearization (AL) solutions to this problem. Thus, the analysis presented in this chapter must be extended to include nonlinear controllers other than IOL.

The case studies in this chapter are by no means exhaustive and the guidelines presented are far from systematic. Nevertheless we consider this work to be a first and very important step in precisely defining meaningful criteria for control structure selection (linear, nonlinear) and effectively identifying the *degree of nonlinearity* of a dynamical system.

Chapter 7

Conclusions

7.1 Summary of Contributions

Novel tools are presented which facilitate the computation of bounds on the robust stability and robust performance of a general nonlinear system. These techniques precisely quantify regions in the operating space over which the robustness properties hold. This compares favorably to previous linear approaches which are valid over a vague neighborhood of the operating point in which a first-order approximation is accurate. Furthermore, conservative yet systematic approaches are presented for the calculation of bounds on the systems performance. While norms on linear operators allow the calculation of linear system performance, there has been no equivalent result for nonlinear operators and thus no previous nonlinear performance results. These new tools utilize conic sectors as approximations of the nonlinear operator. An algorithm is presented for calculating optimal conic-sector bounds on a general nonlinear operator. Optimality is measured by the conservativeness of the resulting performance result. The first application of these new advances in control theory are presented for several chemically reacting systems.

Formal criteria are defined and an objective comparison of exact linearization, approximate linearization, and linear control is carried out. Extensive simulations and case studies are carried out to support the theoretical results. This work is the first stage in the definition of meaningful performance criteria for the judicious

selection of nonlinear "linearizing" control versus linear control.

The application of input-output linearizing control to a packed bed reactor is reported in this thesis. In the design of this controller, a low order nonlinear model of the reactor has been developed for control purposes. The difficulties associated with the implementation of differential geometric techniques on a practical system are identified and comparisons are drawn between this approach and robust linear methods for packed bed reactor control.

Simple guidelines are formulated for the design of a packed bed reactor in terms of practical engineering variables. This represents an improvement over the mathematically formulated conditions for parametric sensitivity. Furthermore, the implications of the proposed guidelines for the control of multitubular industrial reactors are discussed.

7.2 Directions for Future Research

The tools presented here provide a meaningful, albeit conservative, measure of a nonlinear systems performance. The following improvements are recommended to reduce this conservatism:

- **More precise nonlinear uncertainty characterization** – The conic-sector bound presented here suffers from the fact that it includes many additional nonlinear operators in its uncertainty description. This is dramatically illustrated in the case of a saturation element which is bounded by a cone containing all operators from gain 0 (open loop) to gain 1. It may be possible to incorporate specific information about the nonlinearity into the D scalings used in the SSV calculations and thus increase the size of the class of D scalings and reduce the conservatism.

- **Real versus complex Δ structure** – As the nonlinearities treated in this work are real-valued (memoryless) perturbations, the current treatment of them as complex-valued is conservative. New software developed for real-μ problems should help reduce this conservatism.

The synthesis tools of exact and approximate linearization have been investigated and conclusions made about their utility in chemical process control. The following suggestions are made for continued research in the area of differential geometric control synthesis:

- **Approximate input-output linearization** – The technique of approximate linearization has been shown to have superior robustness properties to exact state linearization. However, it is also clear that input-output linearization is a more useful tool for process applications. As of yet, there is no systematic approach to the design of a controller which yields an approximate input-output linearization in some neighborhood of the operating locus. This promises to be a fruitful area of research for the design of robust nonlinear controllers.

- **Nonminimum phase systems** – Severely restrictive results are available in the literature for calculating a nonlinear input-output linearizing controller for a nonminimum phase system. Though no results exist to date, a systematic decomposition of the nonlinear system into an allpass and an invertible factor remains a goal of future research. One of the chief obstacles here seems to be a meaningful definition of a nonlinear allpass operator.

- **Robust synthesis** – Optimal linear methodologies for robust control synthesis are available (ℓ^1, H_∞), but no clear methodology has emerged as an optimally robust methodology for nonlinear systems. The method of sliding mode control shows promise as a robust synthesis technique for handling nonlinear parameter uncertainty.

- **Nonlinear identification** – The importance of identification for control purposes has been highlighted at a number of recent conferences. This is especially important for the presented technique of input-output linearization as it explicitly requires a nonlinear model for inversion. The case studies in the literature rely on first principles models for engineering systems. However, in many actual cases, there is also plant data available for analysis. As engineers, we are reluctant to discard either of these two pieces of information. It remains an ambitious task for future work to optimally integrate the actual data with the first principles model to identify a realistic model. A first step in this direction might focus on the identification of higher order terms in a series expansion for use with approximate linearization.

The target application in this work, the packed bed reactor, revealed the utility of nonlinear control approaches for very complicated, practical systems. The following ideas suggest improvements to the current work in this area of application:

- **Nonlinear model** – A fairly simple (second order) model has been derived to model this complex system. The assumptions of quasistationarity and homogeneous kinetics used in its derivation might be relaxed to improve its accuracy. The former will result in additional dynamic states while the latter could be treated through algebraic states. It seems reasonable that this improvement may yield improved dynamic accuracy at a modest computational expense.

- **Experimental work** – Although the work presented has focused on practical aspects, it remains untested in an actual reactor. Some of the key implementational issues have been addressed, but work remains to be done on the issues of measurement sensors which are appropriate for this control configuration. Furthermore, it is envisioned that an on-line optimization might be constructed for continuous updating of the wave-propagation model.

- **Other chemical engineering applications** – The utility of the differential geometric techniques has been investigated for a packed bed reactor as well as several CSTR configurations. The results show great promise for effective control of these highly nonlinear processes and suggest their application to other complex, nonlinear chemical engineering applications. One potential area of application is in the emerging area of microelectronics. The crystal growth processes in this area are characterized by highly nonlinear batch dynamics.

In the previous chapter, some informal guidelines were presented for comparison of nonlinear versus linear control systems. Although all chemical processes are nonlinear, it remains to be clearly defined as to what *degree* of plant nonlinearity warrants nonlinear control action. The work in chapter 6 makes some recommendations along these lines; however, this remains a particularly fruitful area of research with important practical ramifications.

Appendix A

ℓ^1 - Optimal Uncertainty Formulation

A.1 Introduction

In chapters 2 and 3, the conditions derived on the robustness performance of a nonlinear system are in the context of the structured singular value (SSV). The signals are bounded in energy or power and the resulting induced norm for the operator relating these signals is the infinity norm. The algorithm for computing robust performance in the H_∞ setting is discussed in detail in these chapters, as are the limitations and conservativeness of this approach.

An alternative approach involves the treatment of magnitude-bounded signals which lead to an ℓ^1-optimal structured uncertainty problem. Recent results in this area [50], [51] have shown a non-conservative (necessary and sufficient) result for the robust stability/performance of a general interconnection of a nominal discrete-time plant and controller together with structured, conic-sector bounded, nonlinear perturbations.

In this appendix, the relative merits of the two approaches are outlined in terms of the following properties:

- Performance description.
- Computational efficiency & resultant conservativeness.

The particular class of problems of interest is nonlinear process systems which contain static nonlinearities. Conic-sector bounds are employed to envelop the nonlinearities

and express the resulting system as an interconnection of a nominal linear closed loop together with structured, norm-bounded nonlinear perturbations. Once the problem has been formulated in this manner, it is possible to apply either H_∞ or ℓ^1-optimal performance objectives and utilize the respective software to calculate robust stability and robust performance properties.

In conclusion, a simple example is presented for a comparative investigation of the two approaches.

A.2 Performance Description

A quick review of the two relevant norms is presented. The operator norm induced by the 2-norm (power norm) is

$$\sup_{\substack{v\neq 0 \\ v\in\mathcal{L}_2(\mathcal{L}_p)}} \frac{\|Gv\|}{\|v\|} = \sup_{\omega} \bar{\sigma}(G(j\omega)) \triangleq \|G\|_\infty \tag{A.1}$$

where $\mathcal{L}_2$ ($\mathcal{L}_p$) is the space of functions with bounded 2-norm (power-norm). In discrete-time, ℓ_∞ space is defined as the set of all bounded sequences with associated signal norm:

$$\|\hat{v}\|_\infty = \sup_k |\hat{v}(k)| \tag{A.2}$$

The operator norm induced by the ℓ_∞-norm is

$$\sup_{\substack{v\neq 0 \\ v\in\ell_\infty}} \frac{\|Gv\|_\infty}{\|v\|_\infty} = \|g\|_1 \triangleq \|G\|_{\mathcal{A}} \tag{A.3}$$

where g is the pulse response of G. The resulting $\mathcal{A}$-norm will be used for subsequent computations.

In H_∞-optimization, the worst error resulting from an input signal of bounded energy (or power) is minimized. Modifications allow the treatment of steps and other signals of unbounded energy, provided the signals are well characterized. Conse-

quently, unknown, persistent disturbances cannot be treated in this framework. In general, performance weight specifications remain somewhat ad-hoc but can be used to shape the class of expected inputs and to express reasonable performance objectives. For instance, a frequency dependent weight of $\frac{as+b}{s}$ on the sensitivity function can be used to anticipate slowly varying inputs as well as to force the closed-loop sensitivity to be small when large inputs are expected [67].

In ℓ^1-optimization, the worst error resulting from an input of bounded magnitude is minimized. In this case, the treatment of unknown but persistent disturbances is possible, but signals of unbounded magnitude (such an impulses) cannot be handled. As before, the performance weight specification is not systematic. But engineering judgement can be loosely translated into performance weights. For instance, low frequency inputs can be modeled with low-pass FIR filters, and high-pass FIR filters can be applied to the plant uncertainty to emphasize high frequency uncertainty. Recent work [49] suggests that more flexible weights are possible in this framework, including magnitude and rate bounds.

It is clear that the application of interest will dictate the appropriate class of signals to be used. Traditional chemical engineering applications have focused on bounded-energy type performance specifications on the error signals. But time-domain magnitude bounds on variables like temperature and concentration are also quite relevant.

A.3 Computational Issues

The details of the numerical computations for the H_∞-optimal case have been described in chapter 2. The ℓ^1-optimal case involves the calculation of the $\mathcal{A}$-norm for the various transfer functions in pulse response of the matrix M in the general formulation (Figure 2.4). Given the z-transform of a certain sequence, the algorithm for approximating the $\mathcal{A}$-norm converges quite rapidly. Details of this algorithm can be

found in [51]. Both approaches require calculations in the discrete-time framework. The subsequent single calculation, ($\mathcal{A}$-norm or μ), for the discrete system is found to scale equally in difficulty for the two approaches over the limited range of applications investigated ($dim(\Delta) \leq 3$).

The present work addresses the analysis of closed-loop properties given a plant and a controller (both potentially nonlinear). As such, there has been little consideration given to the synthesis of optimal controllers in this framework (robust synthesis). Results in each area indicate continued improvement in the formulation of computationally efficient algorithms for calculating optimally robust controllers [21], [51]. Evaluation of the relative merits of these two approaches for robust synthesis remains as a topic for future research; however, preliminary results indicate the strength of ℓ^1-optimal synthesis [73].

The primary advantages of the ℓ^1-optimal approach for analysis is that the resultant calculations are necessary and sufficient for nonlinear perturbations. This is directly contrasted with the H_∞-optimal approach, which uses the Small Gain Theorem to derive conservative results. A point of caution is required here. The conservativeness of the results are for *all* the nonlinear operators contained within the conic-sector bounds. This introduces the most conservative step in the problem formulation. Whether in the H_∞ or ℓ^1 setting, the conic sector envelops a myriad of operators, many of which are potentially more pathological than the original nonlinearity. This point will be illustrated by an example in the next section.

A.4 Illustrative Example

Consider the following problem taken from [14]. The anti-reset windup problem (Figure A.1) is investigated with the plant:

$$P = \frac{1}{10s + 1}$$

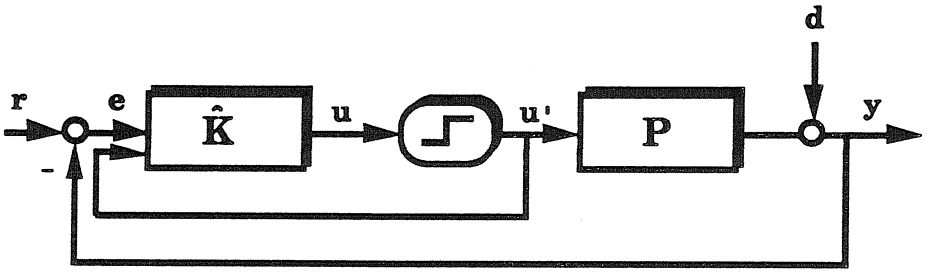

Figure A.1. Anti-Reset Example

and controller with the following state space representation:

$$\left[\begin{array}{c|cc} -\frac{1}{\tau_r} & K\left(\frac{1}{\tau_I}-\frac{1}{\tau_r}\right) & \frac{1}{\tau_r} \\ \hline 1 & K & 0 \end{array}\right]$$

corresponding to the PI controller with settings $(K, \frac{1}{\tau_I})$ in the absence of constraints $(u = u')$. The constraint $|u| \leq 2.0$ is applied, which means that $|u'| = max(|u|, 2.0)$. The problem involves solving for the optimal value of τ_r. The values $(K = 10.0, \tau_I = 10.0)$ are used in this study. It is shown in [14] that recent anti-windup theory yields an optimal value of τ_I equal to τ_r, and that this is in agreement with earlier work in constrained-control theory. Simulations of set-point change responses confirm that for $\tau_I > \tau_r$, the response is sluggish, and for $\tau_I < \tau_r$, the overshoot (from classic integrator windup) is excessive. However, all values of τ_r in the range from 2 to ∞ yield a stable closed-loop response.

Using a performance weight equal to a scalar (0.5) times the inverse of the sensitivity function at $\tau_r = 10.0$, the software for the $\mathcal{A}$-norm is used to compute the robust stability and robust performance for the closed loop as a function of the parameter τ_r. The perturbation element is the conic sector which envelops the nonlinear actuator constraint. The results are summarized in Table A.1. In interpreting these results, recall that the robust stability measure must be less than 1 to ensure stability. The nominal performance measure was arbitrarily selected to give a 0.5 nominal

Table A.1 Robustness Calculations			
τ_r	Nominal Performance Measure	Robust Stability Measure	Robust Performance Measure
2.0	2.0	0.334	48.5
10.0	0.5	0.819	48.8
∞	1.0	1.0	∞

performance measure at $\tau_r = 10.0$.

Several conclusions can be drawn from these results.

- The robust stability measure is very conservative as simulations have shown that this system is well-behaved for all values of τ_r.
- The robust performance measure is not very indicative of the performance trend observed in simulation.

Furthermore, if the SSV is used to calculate the same system properties, it is found that the robust stability measures are *identical !* Therefore the conservatism in this problem is concentrated in the conic-sector bounding of the actuator constraint, and the two algorithms yield the same result.

A.5 Concluding Comments

1. Direct comparison of the ℓ^1 approach and the H_∞ approach seems unlikely because of the very different physical interpretations of the two norms.
2. For a variety of chemical engineering problems, the ℓ_∞-norm is appropriate to bound uncertain compositions, temperatures, etc. However, energy-type performance objectives are also common (*i.e.*, ISE).
3. The chief limitation of both techniques for nonlinear systems is the very conservative casting of nonlinear static operators as conic sectors.

Our experience in this area is somewhat limited. However, the results for ℓ^1 analysis are very promising, and work will continue in this area and its applications for process systems. The conic-sector bounding of nonlinearities represents a significant hurdle for each approach. Future work must address modeling formulations which represent more precisely the specific nonlinearities.

Appendix B

Caltech Methanantion Reactor

B.1 Reactor Model

The Caltech methanation reactor, described in [61] and [90], is used for open-loop fitting of the wave propagation model introduced in chapter 4. Many of the design features in this pilot plant are also found in industrial fixed bed reactors, thus validating its use as a practical tool for control studies.

The primary reaction in this system is the methanation of carbon dioxide:

$$CO_2 + 4H_2 \rightleftharpoons CH_4 + 2H_2O \tag{B.1}$$

with the following expression for the rate of methane production:

$$\text{rate} = \frac{k_1 e^{\frac{-E_1}{RT}} C_{CO_2}}{1 + k_2 e^{\frac{E_2}{RT}}} \tag{B.2}$$

Using a crude approximation of this rate expression as a first-order rate law, and employing the physical parameters in [90], the following dimensionless balances hold:

$$\frac{\partial y}{\partial t'} + \frac{\partial y}{\partial z} = -\mathcal{D}a\, r(x,y) \tag{B.3}$$

$$\frac{\partial x}{\partial t'} + \frac{\partial x}{\partial z} = \mathrm{B}(x - x_w) - q\, \mathcal{D}a\, r(x,y) \tag{B.4}$$

Table B.1 Physical Parameters for Methanation Reactor	
$\mathcal{D}a$	$4.2E6$
$\mathbf{B}$	0.643
q	0.4
γ	18.36
λ	0.6
$r(x,y)$	$ye^{-\gamma/x}$

$$y(0,t) = y_0 \quad x(o,t) = x_0 \quad \left(\frac{\partial x}{\partial z}\right)_{z=1} = 0 \tag{B.5}$$

where the dimensionless groups have already been defined in chapter 4. For the methanation reactor, the values in Table B.1 are calculated for the dimensionless groups. The operating conditions under examination are as follows:

$$\begin{aligned} T_0 &= 256^oC \\ T_w &= 256^oC \\ F &= 13 - 15\text{slpm} \\ y_0 &= 0.0385 - 0.0173 \end{aligned}$$

At these conditions, the fixed bed is not parametrically sensitive and has a mild temperature profile which may exhibit a peak near the end of the reactor.

Insertion of the physical parameters in Table B.1 into the wave propagation model leads to a system with an ignition position which lies outside the reactor exit. Clearly, the crude linear approximation of the reactor leads to inaccurate values for the physical parameters; a fitting of the parameters is required. The exact details of the fitting procedure are not recorded here; instead, the "tuning" trends which affect the temperature profile are indicated in Table B.2. Finer tuning of the parameters against actual reactor data lead to the values depicted in Table B.3. The variables are not

Table B.2 Qualitative Trends for Model Tuning Variables		
$\mathcal{D}a$	$\uparrow$	Increased Temp. Sensitivity, Sharpened Temp. Profile
$\mathbf{B}$	$\uparrow$	Reduced Temp. Sensitivity, Lowered Temp. Profile
q	$\downarrow$	Reduced Temp. Sensitivity, Lowered Temp. Profile
γ	$\uparrow$	Increased Temp. Sensitivity, Raised Temp. Profile

Table B.3 Fitted Parameters for Methanation Reactor Model	
$\mathcal{D}a$	$4.0E6$
$\mathbf{B}$	0.6
q	0.27
γ	15.8
λ	0.6
$r(x,y)$	$ye^{-\gamma/x}$
$\tau_{\frac{F}{F_0}}$	.01
τ_{y_0}	.025
τ_{x_w}	.4

significantly different from the originally calculated values in Table B.1. The procedure for arriving at these values is somewhat ad-hoc, and a systematic identification scheme remains a challenge for future work.

B.2 Open-Loop Simulations

Using the parameters in Table B.3 and the wave propagation model described in chapter 4, several open-loop simulations were performed for evaluation against existing reactor data.

In the first simulation, a step decrease in the concentration of CO_2 was introduced in the feed stream. The exact operating conditions are summarized in Table B.4. The time profile of the actual reactor hot spot temperature is shown in Figure B.1; the model simulation is shown in Figure B.2. Clearly, the overall speed of response is

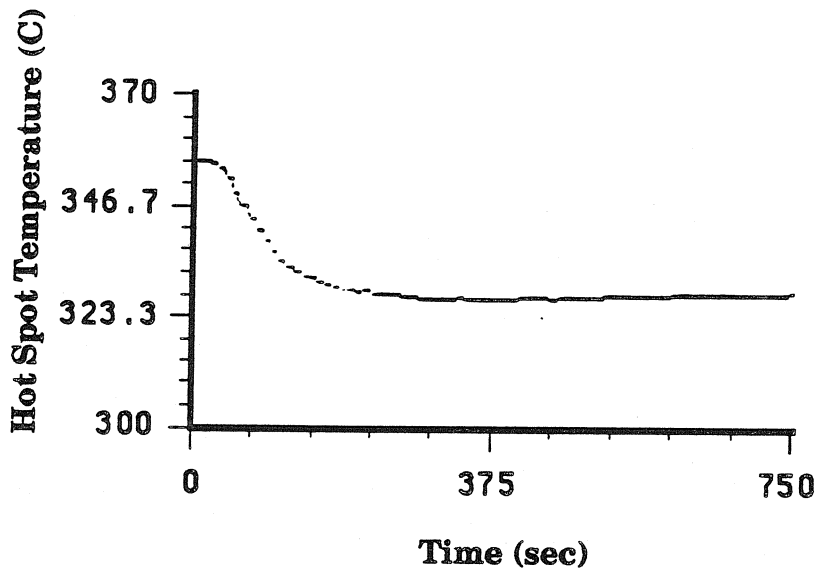

Figure B.1. Reactor Hot Spot Temperature Profile (Example #1)

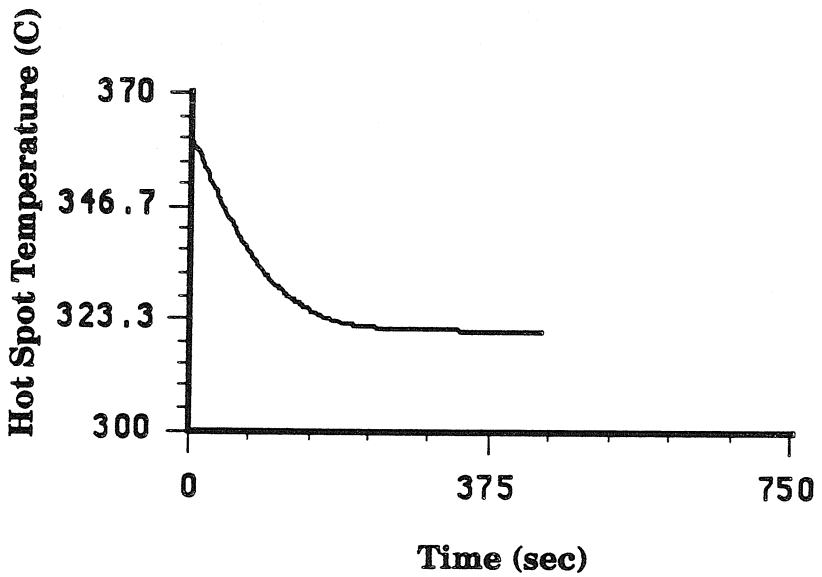

Figure B.2. Modeled Hot Spot Temperature Profile (Example #1)

Table B.4 Simulation Conditions (Example #1)	
Inlet Concentration (y_0)	1.0
Flow Rate ($\frac{F}{F_0}$)	1.0
Inlet Temperature (x_0)	1.0
Jacket Temperature (x_w)	1.0
Change in y_0	-0.240 Step
Change in $\frac{F}{F_0}$	0.0 Step

Table B.5 Simulation Conditions (Example #2)	
Inlet Concentration (y_0)	1.0
Flow Rate ($\frac{F}{F_0}$)	1.0
Inlet Temperature (x_0)	1.0
Jacket Temperature (x_w)	1.0
Change in y_0	-0.134 Step
Change in $\frac{F}{F_0}$	+0.154 Step

closely matched. The quantitative fit is also quite good, with the model predicting a final temperature that is $5°C$ too low (1.5% error).

A second simulation is investigated in which the flow rate of N_2 (diluent) in the feed is increased. The resulting effect is a decrease in y_0 and a simultaneous increase in total flow rate. The exact conditions are shown in Table B.5. The actual reactor hot spot temperature profile is shown in Figure B.3 and the modeled response is shown in Figure B.4. There are several features evident from these plots. First is the appreciable time delay present in the actual reactor. This is crudely modeled with the lag τ in the wave propagation model; however, in this case it is clear that a more accurate model requires explicit time delays. The inverse response for this nonminimum phase system is clearly evident, although the overshoot predicted by the model is higher than actually observed. This is most likely related to the time delay in the actual reactor, which leads to a less pronounced inverse response to the

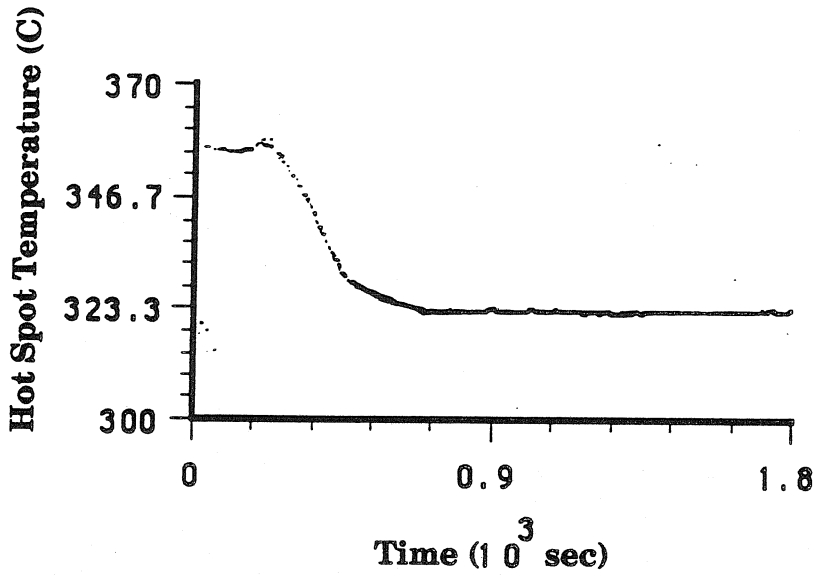

Figure B.3. Reactor Hot Spot Temperature Profile (Example #2)

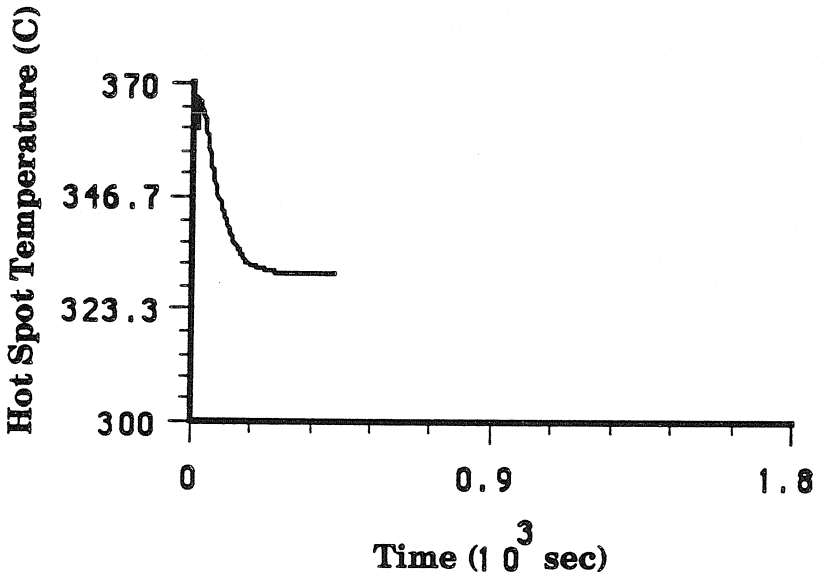

Figure B.4. Modeled Hot Spot Temperature Profile (Example #2)

Table B.6 Simulation Conditions (Example #3)	
Inlet Concentration (y_0)	0.866
Flow Rate ($\frac{F}{F_0}$)	1.154
Inlet Temperature (x_0)	1.0
Jacket Temperature (x_w)	1.0
Change in y_0	-0.208 Step
Change in $\frac{F}{F_0}$	0.0 Step

Table B.7 Simulation Conditions (Example #4)	
Inlet Concentration (y_0)	0.662
Flow Rate ($\frac{F}{F_0}$)	1.154
Inlet Temperature (x_0)	1.0
Jacket Temperature (x_w)	1.0
Change in y_0	-0.209 Step
Change in $\frac{F}{F_0}$	0.0 Step

disturbance.

The final three simulations are described in Tables B.6, B.7, and B.8. They correspond to two different step decreases in the inlet concentration of CO_2 at the higher flow rate, and a decrease in the inlet flow rate, respectively. The lack of accurate dynamic data precludes the possibility of a detailed analysis; however, in Table B.9, we compare the actual steady values for these runs against the simulated

Table B.8 Simulation Conditions (Example #5)	
Inlet Concentration (y_0)	0.453
Flow Rate ($\frac{F}{F_0}$)	1.154
Inlet Temperature (x_0)	1.0
Jacket Temperature (x_w)	1.0
Change in y_0	+0.091 Step
Change in $\frac{F}{F_0}$	-0.154 Step

Table B.9 Steady-State Results of Examples #3, #4, and #5				
	Actual Reactor Hot Spot Temperature		Reactor Model Hot Spot Temperature	
	Initial	Final	Initial	Final
Example #3	$325°C$	$311°C$	$333°C$	$301°C$
Example #4	$311°C$	$293°C$	$301°C$	$281°C$
Example #5	$293°C$	$299°C$	$281°C$	$293°C$

values. The discrepancy between the actual and modeled values for the steady state hot spot temperatures is primarily due to the fact that at these particular conditions, the ignition position has moved very close to the reactor exit and the propagating wave mechanism is not entirely accurate for describing transport properties at these conditions.

B.3 Comments

The wave propagation model provided a very accurate qualitative and quantitative depiction of the methanation reactor behavior at conditions where the temperature sensitivity was sufficiently high that a propagating wave mechanism was appropriate (Examples #1, #2). This sensitivity is considerably lower than the usual parametric sensitivity associated with thermal runaway. At the conditions where this sensitivity was low (Examples #3, #4, and #5), the accuracy of the model deteriorated.

Bibliography

[1] K. J. Åström and B. Wittenmark. *Computer Controlled Systems: Theory and Design.* Prentice-Hall, Englewood Cliffs, NJ, 1984.

[2] C. Alsop. *Nonlinear Chemical Process Control by Means of Linearizing State and Input Variable Transformations.* PhD thesis, The University of Texas at Austin, TX, 1987. Chemical Engineering.

[3] Ames Drysden Flight Research Facility. *X-29A High AOA Flight Control System: Preliminary Design Review Number One*, 1987. Internal Document # X-87-007.

[4] R. Aris and N.R. Amundson. An analysis of chemical reactor stability and control – I. The possibility of local control, with perfect or imperfect control mechanisms. *Chem. Eng. Sci.*, 7:121–131, 1958.

[5] R. Aris and N.R. Amundson. An analysis of chemical reactor stability and control – II. The evolution of proportional control. *Chem. Eng. Sci.*, 7:132–147, 1958.

[6] R. Aris and N.R. Amundson. An analysis of chemical reactor stability and control – III. The principles of programming reactor calculations. Some extensions. *Chem. Eng. Sci.*, 7:148–155, 1958.

[7] C.H. Barkelew. Stability of chemical reactors. *Chem. Prog. Symp. Ser.*, 55(25):37–46, 1959.

[8] E.G. Bauman and A. Varma. Parametric sensitivity and runaway in catalytic reactors: Experiments and theory using carbon monoxide oxidation. *Chem. Eng. Sci.*, 45(8):2133–2139, 1990.

[9] L.T. Biegler and J.B. Rawlings. Optimization approaches to nonlinear model predictive control. In *Proceedings of the 4th International Conference of Chemical Process Control*, 1991.

[10] S. Boyd and C.A. Desoer. Subharmonic functions and performance bounds on linear time invariant feedback systems. Technical Report ERL Memo M84/51, University of California, Berkeley, 1984.

[11] S. Boyd and Q. Yang. Structured and simultaneous Lyapunov functions for system stability problems. Technical Report Information Systems Laboratory Technical Report No. L-104-88-1, Stanford University, 1988.

[12] J.P. Calvet. *A Differential Geometric Approach for the Nominal and Robust Control of Nonlinear Chemical Processes.* PhD thesis, Georgia Institute of Technology, Atlanta, GA, 1989. Chemical Engineering.

[13] J.P. Calvet and Y. Arkun. Feedforward and feedback linearization of nonlinear systems and its implementation using IMC. *Ind. Eng. Chem. Res.*, 27(10):1822–1831, 1988.

[14] P.J. Campo. *Studies in Robust Control of Systems Subject to Constraints.* PhD thesis, California Institute of Technology, Pasadena, CA, 1989. Chemical Engineering.

[15] B. Carnahan, H.A. Luther, and J.O. Wilkes. *Applied Numerical Methods.* John Wiley & Sons, New York, 1969.

[16] P. Daoutidis and C. Kravaris. Synthesis of nonlinear dynamic feedback controllers. In *AIChE Annual Meeting*, 1990.

[17] P. Daoutidis, M. Soroush, and C. Kravaris. Feedforward/feedback control of multivariable nonlinear processes. *AIChE J.*, 36(10):1471–1484, 1990.

[18] J.C. Doyle. Analysis of feedback systems with structured uncertainties. *IEEE Proc., Part D*, 6:242–250, 1982.

[19] J.C. Doyle. *Lecture Notes in Advances in Multivariable Control.* ONR/Honeywell Workshop, Minneapolis, MN, 1984.

[20] J.C. Doyle, B. Francis, and A. Tannenbaum. *Feedback Control Theory.* Macmillan Publishing Co., 1990. In preparation.

[21] J.C. Doyle, K. Glover, P. Kharagonekar, and B.A. Francis. State-space solutions to standard H_2 and H_∞ control problems. *IEEE Trans. Autom. Control*, 34(8):831–847, 1989.

[22] F.J. Doyle III, H.M. Budman, and M. Morari. Theoretical and practical aspects of nonlinear packed bed reactor control. In *AIChE Annual Meeting*, 1990.

[23] F.J. Doyle III and M. Morari. Robust controller design for a nonlinear CSTR. In *Proceedings of American Control Conference*, pages 1087–1092, 1989.

[24] F.J. Doyle III and M. Morari. A conic sector-based methodology for nonlinear controller design. In *Proceedings of American Control Conference*, pages 2746–2751, 1990.

[25] F.J. Doyle III, A.P. Packard, and M. Morari. Robust controller design for a nonlinear CSTR. *Chem. Eng. Sci.*, 44:1929–1947, 1989.

[26] C. Economou and M. Morari. IMC. 5. Extension to nonlinear systems. *Ind. Eng. Chem. Process Des. Dev.*, 25:403–411, 1986.

[27] G. Eigenberger. Dynamics and stability of chemical engineering processes. *Int. Chem. Eng.*, 25(4):595–610, 1985.

[28] G. Eigenberger and W. Ruppel. Problems of mathematical modelling of industrial fixed-bed reactors. *Ger. Chem. Eng.*, 25:74–83, 1986.

[29] G. Eigenberger and H. Schuler. Reactor stability and safe reaction engineering. *Int. Chem. Eng.*, 29(1):12–25, 1989.

[30] C. Emig, H. Hofmann, U. Hoffmann, and U. Fiand. Experimental studies on runaway of catalytic fixed-bed reactors (vinyl-acetate-synthesis). *Chem. Eng. Sci.*, 35:249–257, 1980.

[31] G.F. Froment and K.B. Bischoff. *Chemical Reactor Analysis and Design.* John Wiley, New York, NY, 1979.

[32] E.D. Gilles. Application of modelling, estimation and control to chemical processes. In T.F. Edgar and D.E. Seborg, editors, *Proceedings of the 2nd International Conference of Chemical Process Control*, pages 311–337. Engineering Foundation, 1981.

[33] E.D. Gilles and U. Epple. Non-linear wave propagation and model reduction of the fixed-bed reactor. In *Modelling of Chemical Reaction Systems*, pages 312–336. Springer-Verlag, Berlin, 1981.

[34] E.D. Gilles and W. Ruppel. Model reduction of chemically reacting systems. In *Dynamics and Modelling of Reactive Systems*, pages 37–58. Academic Press, New York, NY, 1980.

[35] J. Gleick. *Chaos. Making a New Science.* Penguin Books, New York, NY, 1987.

[36] J.W. Grizzle and P.V. Kokotovic. Feedback linearization of sampled-data systems. *IEEE Trans. Autom. Control*, 33(9):857–859, 1988.

[37] J. Guckenheimer and P. Holmes. *Nonlinear Oscillations, Dynamical Systems, and Bifurcations of Vector Fields.* Springer-Verlag, New York, NY, 1986.

[38] K.W. Hansen and S.B. Jörgensen. Dynamic modeling of a gas phase catalytic fixed-bed reactor - I: Experimental apparatus and determination of reaction kinetics. *Chem. Eng. Sci.*, 31:579–586, 1976.

[39] J. Hauser, S. Sastry, and P. Kokotovic. Nonlinear control via approximate linearization: The ball and beam example. Technical Report UCB/ERL M89/95, University of California, Berkeley, 1989.

[40] V. Hlavacek. Aspects of design of packed catalytic reactors. *Ind. Eng. Chemistry*, 62:8–26, 1970.

[41] J.A. Hoiberg, B.C. Lyche, and A.S. Foss. Experimental evaluation of dynamic models for a fixed bed catalytic reactor. *AIChE J.*, 17:1434–1447, 1971.

[42] K.A. Hoo and J.C. Kantor. An exothermic continuous stirred tank reactor is feedback equivalent to a linear system. *Chem. Eng. Commun.*, 37:1–10, 1985.

[43] L.R. Hunt, R. Su, and G. Meyer. Global transformations of nonlinear systems. *IEEE Trans. Autom. Control*, 24:24–31, 1983.

[44] A. Isidori. *Nonlinear Control Systems - An Introduction.* Springer-Verlag, New York, NY, second edition, 1989.

[45] S.B. Jörgensen. Fixed bed reactor dynamics and control - a review. In *DYCORD 86*, pages 11–24. IFAC, 1986.

[46] S.B. Jörgensen and N. Jensen. Dynamics and control of chemical reactors - selectively surveyed. In *DYCORD 90*, pages 359–371. IFAC, 1990.

[47] J. Kantor. Global linearization and control of a mixed culture bioreactor with competition and external inhibition. *Math. Biosci.*, 82:43–62, 1986.

[48] S. Karahan. *Higher Degree Approximations to Nonlinear Systems.* PhD thesis, University of California, Davis, CA, 1988. Engineering.

[49] M.R. Keenan and J.C. Kantor. An ℓ_∞ optimal performance approach to robust feedback control. In *Proceedings of American Control Conference*, pages 549–553, 1989.

[50] M. Khammash and J.B. Pearson. Performance robustness of discrete-time systems with structured uncertainty. Technical Report # 9002, Rice University, 1990.

[51] M. Khammash and J.B. Pearson. Robust synthesis for discrete-time systems with structured uncertainty. In *Proceedings of American Control Conference*, 1991. preprint.

[52] C. Kravaris and C.B. Chung. Nonlinear state feedback synthesis by global input/output linearization. *AIChE J.*, 33:592–603, 1987.

[53] C. Kravaris and P. Daoutidis. Nonlinear state feedback control of second-order nonminimum phase systems. *Comput. Chem. Eng.*, 14(4/5):439–449, 1990.

[54] C. Kravaris and J.C. Kantor. Geometric methods for nonlinear process control. *Ind. Eng. Chem. Res.*, 29:2295–2323, 1990.

[55] C. Kravaris and S. Palanki. Robust nonlinear state feedback under structured uncertainty. *AIChE J.*, 7:1119–1127, 1988.

[56] A.J. Krener. Approximate linearization by state feedback and coordinate change. *Syst. Control Lett.*, 5:181–185, 1984.

[57] S. Lei, C. Katz, and R. Shinnar. The regulation of a continuous crystallizer with fines trap. *Symp. Ser. Crystallization from Solutions, Factors Influencing Size & Distribution*, 67(110), 1971.

[58] J. Lévine and P. Rouchon. Quality control of binary distillation columns based on nonlinear aggregated models. *Automatica*, 27(3), 1989.

[59] H.-P. Löffler and W. Marquardt. On order reduction of nonlinear differential-algebraic process models. In *Proceedings of American Control Conference*, pages 1546–1551, 1990.

[60] A.A. Lyapunov. Problèm général de la stabilté du mouvement. *Annals of Mathematical Society*, (17), 1892. Photoreproduction of the 1907 French translation from the original Russian version published in 1892.

[61] J.A. Mandler, M. Morari, and J.H. Seinfeld. Control system design for a fixed-bed methanation reactor. *Chem. Eng. Sci.*, 6:1577–1597, 1986.

[62] W. Marquardt. Traveling waves in chemical processes. *Int. Chem. Eng.*, 30(4):585–606, 1990.

[63] W. Marquardt and E.D. Gilles. Nonlinear wave phenomena as fundamentals for model based control system design in distillation. In *AIChE Annual Meeting*, 1990.

[64] P.E. McDermott, D.A. Mellichamp, and R.G. Rinker. Pole-placement self tuning control of a fixed-bed autothermal reactor, part II: Multivariable control. *AIChE J.*, 32:1015–1024, 1986.

[65] C. McGreavy and R.F. Maciel. Dynamic behavior of fixed bed catalytic reactors. In *DYCORD+ '89*, pages 95–100. IFAC, 1989.

[66] S. Monaco and D. Normand-Cyrot. Zero dynamics of sampled data nonlinear systems. *Syst. Control Lett.*, 11:229–234, 1988.

[67] M. Morari and E. Zafiriou. *Robust Process Control.* Prentice-Hall, Englewood Cliffs, NJ, 1989.

[68] M. Morbidelli and A. Varma. On parametric sensitivity and runaway criteria of pseudohomogeneous tubular reactors. *Chem. Eng. Sci.*, 40(11):2165–2168, 1985.

[69] M. Morbidelli and A. Varma. Parametric sensitivity and runaway in fixed-bed catalytic reactors. *Chem. Eng. Sci.*, 41(4):1063–1071, 1986.

[70] M. Morbidelli and A. Varma. Parametric sensitivity in fixed-bed catalytic reactors: The role of interparticle transfer resistances. *AIChE J.*, 32(2):297–306, 1986.

[71] A. Packard. *What's New with μ: Structured Uncertainty in Multivariable Control.* PhD thesis, University of California, Berkeley, CA, 1987. Engineering.

[72] A. Packard and J.C. Doyle. Structured singular value with repeated scalar blocks. In *Proceedings of American Control Conference*, pages 1213–1218, 1988.

[73] J.B. Pearson, 1990. Personal communication.

[74] D.D. Perlmutter. *Stability of Chemical Reactors.* Prentice-Hall, Englewood Cliffs, NJ, 1972.

[75] J. Pirkle Jr. and I.E. Wachs. Activity profiling in catalytic reactors. *Chem. Eng. Prog.*, pages 29–34, August 1987.

[76] H. Poincaré. *Oeuvres, Tome 1.* Gauthier-Villars, Paris, 1928.

[77] V.M. Popov. *Hyperstability of Automatic Control Systems.* Springer-Verlag, New York, NY, 1973.

[78] J. Puszynski, D. Snita, V. Klavacek, and H. Hofmann. A revision of multiplicity and parametric sensitivity concepts in nonisothermal nonadiabatic packed bed chemical reactors. *Chem. Eng. Sci.*, 36(10):1605–1609, 1981.

[79] D. Ramkrishna and P. Arce. Can pseudo-homogeneous reactor models be valid? *Chem. Eng. Sci.*, 44(9):1949–1966, 1989.

[80] W.D. Seider, D.B. Brengel, and A.M. Provost. Nonlinear analysis in process design. Why overdesign to avoid complex nonlinearities? *Ind. Eng. Chem. Res.*, 29:805–818, 1990.

[81] R. Shinnar. Impact of model uncertainties and nonlinearities on modern controller design. In M. Morari and T. McAvoy, editors, *Proceedings of the 3rd International Conference of Chemical Process Control.* Elsevier, 1986.

[82] J.L. Silverstein and R. Shinnar. Effect of design on the stability and control of fixed bed catalytic reactors with heat feedback. 1. Concepts. *Ind. Eng. Chem. Process Des. Dev.*, 21:241–256, 1982.

[83] J.-J. E. Slotine and W. Li. *Applied Nonlinear Control.* Prentice-Hall, Englewood Cliffs, NJ, 1991.

[84] R.S. Smith and J.C. Doyle. The two tank experiment: A benchmark control problem. In *Proceedings of American Control Conference*, pages 2026–2031, 1988.

[85] J.P. Tremblay and J.D. Wright. Computer control of a butane hydrogenolysis reactor. *Can. J. Chem. Eng.*, 52:845–847, 1974.

[86] A. Uppal, W.H. Ray, and A.B. Poore. On the dynamic behavior of continuous stirred tanks. *Chem. Eng. Sci.*, 29:967–985, 1974.

[87] J.G. Van de Vusse. Plug-flow type reactor versus tank reactor. *Chem. Eng. Sci.*, 19:994–997, 1964.

[88] R.J. Van Welsenaere and G.F. Froment. Parametric sensitivity and runaway in fixed bed catalytic reactors. *Chem. Eng. Sci.*, 25:1503–1516, 1970.

[89] A. Varma. Parametric sensitivity and runaway in chemical reactors. In *Recent Advances in Chemical Engineering*, pages 56–65. Tata McGraw-Hill, New Delhi, 1989.

[90] C.J. Webb. *Robust Control Strategies for a Fixed Bed Chemical Reactor.* PhD thesis, California Institute of Technology, Pasadena, CA, 1989. Chemical Engineering.

[91] R.A. Wright and C. Kravaris. Nonminimum phase compensation for nonlinear processes. In *AIChE Annual Meeting*, 1990.

[92] I.I. Yoffe and I.M. Pismen. *Heterogene Katalyse Chemie und Technik.* Akademe Verlag, Berlin, 1975.

[93] F. Yoshida, D. Ramaswami, and O. A. Hougen. Temperatures and partial pressures at the surface of catalyst particles. *AIChE J.*, 8:5–11, 1962.

[94] P.M. Young and J.C. Doyle. Computation of μ with real and complex uncertainties. In *29th Conference on Decision and Control*, pages 1230–1235, 1990.

[95] G. Zames. On the input-output stability of nonlinear time-varying feedback systems, parts i and ii. *IEEE Trans. Autom. Control*, AC-11:228–239, 465–476, 1966.